# INNOVATIVE APPROACHES FOR VENTRICULAR ARRHYTHMIA ABLATION: COMPARATIVE TREATMENTS, ADVANCED IMAGING, MACHINE LEARNING AND OTHER NOVEL TECHNOLOGIES

Kasun Jayaravi De Silva
BMed | MD | BSc (Med) Hons (Class 1) | FRACP

A thesis submitted in fulfilment of the requirements for the degree of Doctor of Philosophy

Faculty of Medicine and Health
University of Sydney
April 2025

Kasun De Silva

kasun.desilva@sydney.edu.au

ORCID iD:  0000-0002-3527-9289

# DECLARATION

This thesis is the sole work of the author, and the material contained herein has not been previously published or written by another person except where due reference has been made in the text. The work was performed by the candidate in Sydney at the Cardiology Department of the Westmead Hospital and the Westmead Applied Research Centre, University of Sydney for the express purpose of this thesis and no part thereof has previously been presented for the award of a degree at this or any other university. I certify that the writing of this thesis, the results, interpretations, opinions, and suggestions are entirely my work. This thesis does not exceed the length of 100,000 words, exclusive of the table, figures, appendices and bibliography.

Kasun De Silva

30th April 2025

A/Prof Saurabh Kumar

(Primary supervisor)

30th April 2025

# PREFACE

This work was performed in collaboration with several institutions, including:

1. Westmead Hospital (Department of Cardiology)
2. Westmead Applied Research Centre (University of Sydney)
3. Department of Animal Care, Vivarium (Western Sydney Local Health District)
4. Sydney Informatics Hub (University of Sydney)

All manuscripts and publications from this thesis were undertaken with the candidate as the principal author. Responsibilities included: protocol design, ethics and governance application, participant recruitment and follow-up, data collection, statistical analysis, and manuscript preparation. PhD supervisors performed revision and editing of submitted manuscripts only. In addition, co-authors listed in publications assisted in one or more of the above aspects and the critical revision of manuscripts, consistent with co-authorship requirements for the respective journals. However, no co-authors were responsible for drafting manuscripts and chapters contained herein (excluding critical revision). Those works do not form components of any other submitted body of work. Generative AI (Microsoft CoPilot) was used for correction of syntax and grammar only.

The candidate received funding from the National Health and Medical Research Council (NHMRC) in the form of a Postgraduate Research Scholarship (APP 2014261) for the duration of this PhD. This research was also supported by an Australian Government Research Training Program (RTP) offset scholarship Publications, published abstracts, prizes and grant funding emanating from this body of work are listed in the section entitled “Peer-reviewed publications.”

# ACKNOWLEDGEMENTS

First and foremost, I would like to thank my PhD supervisor, Associate Professor Saurabh Kumar. You have had untold impact upon my career, nurturing my passion for cardiac electrophysiology, ventricular arrhythmia and research, from even prior to my advanced training in cardiology. Thank you for your mentorship and guidance during this PhD journey, for the world class resources and team that you have put around me, your clinical training, career guidance and for your academic rigour. You taught us to our work on what would have clinical impact on the patients we treat. For all that you have done I will always be incredibly grateful. My thanks also to my co-supervisor Associate Professor Stuart Thomas for your training, guidance and advice.

Second my thanks to past and present members of the Complex Arrhythmia Program including Dr Yasuhito Kotake, Dr Chris Davey, Dr Kaimin Huang, Dr Kenji Hashimoto, Dr Juan Mundisugih and Mr Max Bickley for your collaboration and contributions to this thesis. I must especially thank Dr Timothy Campbell not only for leading the ovine animal experiment prior to my commencing this PhD that has directly contributed to Chapters 3-5 but equally so for your mentorship, and wisdom in all things electrophysiology. Learning from you, and working with you, was a privilege. I also mention Mr Samual Turnbull for your friendship, teaching and clinical advice. Our coffee runs discussing some aspects of our current projects were a highlight of the last three years. I wish you all success. Finally, Dr Ashwin Bhaskaran with whom I commenced internship in 2015, culminating in embarking on this PhD journey together. Thank you for being my friend, colleague and support many times during the last ten years and particularly so during this PhD. It has been with much pride that I have watched the (much deserved) accolades come

your way these last few years. Your intellect, kindness, humility and ethics make you one of the finest doctors that I know, and I wish you the very best.

I extend my gratitude to all collaborators in this thesis. To the clinicians, nurses and staff at the Westmead Cardiology Department and Westmead Vivarium where this research took place, I give thanks. Thanks to Professor James Chong, Professor Eddy Kizana and Dr Dinesh Selvakumar at The Westmead Institute for Medical Research for contributions and advice to the animal projects. Thanks Dr Schindeler and Dr O'Donohue for contribution to the histological experiments and to Dr Chi-Jen Hsu for your advice and wisdom in all things CMR. I thank Mr Kristian Maras, Dr Sebastian Haan, Dr Nathaniel Butterworth and Dr Tom Mauch, from the University of Sydney Informatics Hub for machine learning and coding contributing to Chapter 5 and Westmead Research and Education Network for funding these analyses. Thank you to Associate Professor Verity Ahern, Associate Professor Eric Hau and Associate Professor Pierre Qian for contributions to the RADIOABLATE-VT trial and to Dr Simone Marschner and the Westmead Applied Research Centre (Professor Clara Chow) for statistical and operational support.

I thank my many teachers and mentors during my Cardiology training, too numerous to mention in this acknowledgement. In particular, I thank Dr David Tanous who welcomed me into his team and has always been generous in his support, kindness and advice. I also thank my fellow advanced trainees; Dr Sumita Barua, Dr Tejas Deshmukh, Dr Samia Kazi, Dr Aaisha Ferkh, Dr Sally Kim and Dr Paul Geenty who provided much humour and wisdom these last few years. Dr Karan Rao, who commenced advanced training with Ashwin and me, I especially thank for your advice and friendship

Next, to my family without whom none of this would have been possible. To my father and mother, I extend my most heartfelt thanks. Thathi, you have taught me the joys of academic

pursuit and have been a role model in fatherhood. Any achievements that I have made I lay at your feet. Ammi you are the rock of our family, and you have shouldered an incredible burden looking after my father as well as caring for my two daughters when I could not due to this thesis. Thanks to my brother Udan and his wife Arpana for their love and companionship. To my father-in-law ("thatha") and mother-in-law ("amma") I also extend my sincerest thanks. You have gone above and beyond in caring for me and my family so that I could complete this work. I am truly blessed to have you in my life. In my eyes, you, as well as my parents, are unofficial co-authors for all these chapters, without you none of this would be possible.

I come at last to thank my kind-hearted, wonderful and loving wife Madhu. You have done much more than your fair share these last few years and done it with much sacrifice, love and strength. I thank you from the bottom of my heart for your companionship and support. It will always be a privilege to be your husband and I (and our daughters) would be lost without you. I love you. Last to my sweet daughters Annika and Amaya, who fill my heart with so much joy, I love you both. I can't wait to see the women that you grow into. Yes Annika, Thathi has finally "finished his PhD," and we can finally play as long as you want. It is to Madhu, Annika and Amaya that I dedicate this thesis.

# ABBREVIATIONS

**AAD** - Anti-arrhythmic drugs

**AF** - Atrial fibrillation

**AI** - Artificial intelligence

**AUC** - Area under the curve

**BZ** - Border zone

**CA** - Catheter ablation

**CCB** - Calcium channel blocker

**CI** - Confidence interval

**CMR** - Cardiac magnetic resonance imaging

**CMR-CCs** - Cardiac magnetic resonance imaging conducting channels

**CNN** - Convolutional neural network

**CRT** - Cardiac resynchronisation therapy

**DeEP –** Decrement evoked potential mapping

**DZ** - Deceleration zone

**EAM** - Electroanatomic mapping

**ECG** - Electrocardiogram

**EF** - Ejection fraction

**EQ5D** - EuroQol-5 dimension

**GDMT** - Guideline directed medical therapy

**HC-CC** - Histology confirmed-conducting channel

**HNS** - Half-normal saline

**ICD** - Implantable cardioverter defibrillator

**ICE** - Intracardiac echocardiography

**ICM** - Ischemic cardiomyopathy

**ILAM** - Isochronal late activation mapping

**IQR** - Interquartile range

**LAVA** - Local abnormal ventricular activities

**LGE** - Late gadolinium enhancement

**LP** - Late potential

**LV** - Left ventricle

**LVOT** - Left ventricular outflow tract

**LVp** - Left ventricular pacing

**MCC** - Matthews correlation coefficient

**MDCT** - Multidetector computed tomography

**MI** - Myocardial infarction

**NICM** - Non-ischaemic cardiomyopathy

**NS** - Not significant

**NSVT** - Non-sustained ventricular tachycardia

**NT-proBNP** - N-terminal pro-brain natriuretic peptide

**NYHA** - New York Heart Association

**OHCA** - Out-of-hospital cardiac arrest

**PES** - Programmed electrical stimulation

**PET** - Positron emission tomography

**PFA** - Pulsed field ablation

**PSI** - Pixel signal intensity

**PVC** - Premature ventricular complex

**QoL** - Quality of life

**RCT** - Randomised controlled trial

**RF** - Radiofrequency

**RFA** - Radiofrequency ablation

**RV** - Right ventricle

**RVOT** - Right ventricular outflow tract

**SBRT** - Stereotactic body radiation therapy

**SCD** - Sudden cardiac death

**SD** - Standard deviation

**SF-36** - Short Form-36 Health Survey Questionnaire

**SHD** - Structural heart disease

**SI** - Signal intensity

**VA** - Ventricular arrhythmias

**VF** - Ventricular fibrillation

**VM** - Viable myocardium

**VT** - Ventricular tachycardia

**WOI** - Window of Interest

# TABLE OF CONTENTS

# PEER-REVIEWED PUBLICATIONS

**Chapter 1**

Published manuscripts contributing to this chapter:

- De Silva K, Kumar S. Interelectrode spacing and ventricular scar. JACC: Clinical Electrophysiology. 2025 Jun 1;11(6):1142-4

**Chapter 2**

Published manuscript:

- De Silva K, Haqqani H, Mahajan R, Qian P, Chik W, Voskoboinik A, Kistler PM, Lee G, Jackson N, Kumar S. Catheter ablation vs antiarrhythmic drug therapy for treatment of premature ventricular complexes: a systematic review. *JACC: Clinical Electrophysiology*. 2023 Jun 1;9(6):873-85.

**Chapter 3**

Published manuscript:

- De Silva K, Campbell T, Bennett RG, Anderson RD, Davey C, O'Donohue AK, Schindeler A, Turnbull S, Selvakumar D, Bhaskaran A, Kotake Y, Hsu CJ, Chong JH, Kizana E, Kumar S. Whole-Heart Histological and Electroanatomic Assessment of Postinfarction Cardiac Magnetic Resonance Imaging Scar and Conducting Channels. Circulation: Arrhythmia and Electrophysiology. 2024 Sep;17(9):e012922. **Selected as Editors Choice**.

Prizes and Presentations

- Winner of the *Heart Rhythm* Prize session at the 73rd Annual Scientific Meeting of the Cardiac Society of Australia & New Zealand 2024 (Oral Presentation)

- Finalist for *Young Investigator Award* (Basic and Clinical Sciences) at the 17th Scientific Session of the Asia Pacific Heart Rhythm Society 2024. (Oral Presentation)
- Semi-Finalist for the Mark E Josephson Innovation in VT Abstract Award at the 18th Annual International VT Symposium (2023) (Abstract Presentation)

**Chapter 5**

Published Manuscript

- De Silva K, Campbell T, Bennett RG, Anderson RD, Davey C, O'Donohue AK, Schindeler A, Turnbull S, Selvakumar D, Bhaskaran A, Kotake Y, Hsu CJ, Chong JH, Kizana E, Kumar S. Feasibility of machine learned intracardiac electrograms to predict post-infarction ventricular scar topography. Circulation: Arrhythmia and Electrophysiology. 2025 Jul;18(7):e013611

Published Abstracts

- De Silva K, Campbell T, Bennett RG, Anderson RD, Davey C, O'Donohue AK, Schindeler A, Turnbull S, Selvakumar D, Bhaskaran A, Kotake Y, Hsu CJ, Chong JH, Kizana E, Kumar S. Machine learned intracardiac electrograms can accurately predict post-infarction ventricular scar topography. Accepted as a poster presentation for the 45th annual meeting of the Heart Rhythm Society (Heart Rhythm 2025).

**Chapter 6**

Published Manuscript

- De Silva K, So TC, Turnbull S, Bickley M, Hashimoto K, Bhaskaran A, & Kumar S. Pulsed field ablation of ventricular arrhythmias arising from intracavitary structures: insights from a clinical case series. Journal of Interventional Cardiac Electrophysiology. 2025 1-10.

**Chapter 7**

Registered trial protocol on Clinicaltrials.gov NCT06360939

**Other awards and grants arising during this thesis**

- NHMRC Postgraduate research scholarship (APP 2014261)
- Paulette Isabel Jones Career Award (University of Sydney) 2025
- Alan Young Australasian Fellowship (Western Sydney Local Health District) 2024
- TogetherVT Young EP travel grant for oral presentation at the TogetherVT Symposium in Leiden, Netherlands 2024
- WSLHD Research and Education Network Kickstarter Grant as chief investigator A - $50,000 to support AI approaches to optimise management of ventricular tachycardia 2023
- NHMRC Clinical Trials Committee Innovation Grant as chief investigator A - $50,000 in in-kind support for development of a clinical trial for management of premature ventricular complexes. 2023
- Royal Australian College of Physicians Research Entry Scholarship 2021 declined due to acceptance of NHMRC Postgraduate research scholarship

**Publications during this thesis candidature not contained within this thesis**

- De Silva K, Campbell T, Kumar S. PCI for Ischemic Left Ventricular Dysfunction. The New England Journal of Medicine. 2023 Jan;388(2):186-7. (letter to the editor)
- Turnbull, S., Garikapati, K., Bennett, R.G., Campbell, T.G., Kotake, Y., De Silva, K., Mahajan, R., Wong, M.S., Kazi, S., Marschner, S. and Byth, K., 2024. Accuracy of a Single-Lead ECG Device for Diagnosis of Cardiac Arrhythmias Compared Against Cardiac Electrophysiology Study. Heart, Lung and Circulation.
- Gupta, A., Danaila, V., De Silva, K., Bhaskaran, A., Turnbull, S., Wong, M.S., Campbell, T.G. and Kumar, S., 2024. The Current Landscape of Ventricular Tachycardia Trials: A Systematic Review of Registered Studies. Heart, Lung and Circulation.

Peer reviewed publications

- Liulu, X., Balaji, P., Barber, J., De Silva, K., Murray, T., Hickey, A., Campbell, T., Harris, J., Gee, H., Ahern, V.. Kumar, S. and Qian P, 2024. Radiation therapy for ventricular arrhythmias. Journal of Medical Imaging and Radiation Oncology.
- Bennett, R.G., Garikapati, K., Campbell, T.G., Kotake, Y., Turnbull, S., Bhaskaran, A., De Silva, K., Kanawati, J., Zhou, J., Wong, M.S. and Kumar, S., 2023. Mortality after catheter ablation of structural heart disease related ventricular tachycardia. International Journal of Cardiology, 386, 2023 pp.50-58.
- Bhaskaran A, De Silva K, Kumar S. Contemporary updates on ventricular arrhythmias: from mechanisms to management. Internal Medicine Journal, 2023 53 (6)
- Kanawati J, De Silva K, Bhaskaran A, Turnbull S, Zhou J, Kotake Y, Kumar S, Campbell T. Intracardiac echocardiography techniques to identify ventricular arrhythmia substrate. Heart Rhythm O2, 2022, 3(5) p602-612.
- Kotake Y, Huang K, Bennett R, De Silva K, Bhaskaran A, Kanawati J, Turnbull S, Zhou J, Campbell T, Kumar S. Efficacy and safety of catheter ablation as first-line therapy for the management of ventricular tachycardia. Journal of Interventional Cardiac Electrophysiology, 2023
- Kotake Y, Bennett R, De Silva K, Bhaskaran A, Kanawati J, Turnbull S, Zhou J, Kumar S, Campbell T. Correlation of spatial patterns of endocardial pace mapping to underlying scar topography in patients with scar-related ventricular tachycardia. Journal of Cardiovascular Electrophysiology, 2023.
- De Silva K, Kumar S. Catheter Ablation for Atrial Fibrillation: Are We Isolating Our Most Vulnerable Patients? Heart, Lung and Circulation, 2022, 31 (10) p1315-1317

# LIST OF TABLES

# LIST OF SUPPLEMENTAL TABLES

# LIST OF FIGURES

# LIST OF SUPPLEMENTAL FIGURES

# ABSTRACT

Over the past three decades, advancements in mapping technologies have significantly improved our understanding and treatment of ventricular arrhythmia (VA). Despite these advancements, long-term success rates for catheter ablation (CA) in structural heart disease (SHD) have plateaued, highlighting the need for mechanistic and translational studies to refine our understanding of arrhythmogenesis and improve current CA strategies. This thesis addresses the challenge of treating VA with catheter ablation, identifying knowledge gaps in the field and focusing on identifying and abolishing the arrhythmogenic substrate conducive to these arrhythmias.

In Chapter 2, we complete the first published systematic review of the evidence comparing antiarrhythmic drugs (AADs) and CA for premature ventricular contractions (PVCs), finding the need for improved patient centred randomised data incorporating currently used ablative technologies.

In Chapter 3, we validate image integration of cardiac magnetic resonance imaging (CMR) scar and CMR channels in an ovine model with meticulously co-registered whole heart histopathology, CMR and high density electroanatomic mapping. We found that CMR channels at sites of deceleration zones (DZs), which can be considered functional arrhythmogenic substrate, had higher intra channel adiposity but similar fibrosis than regions without DZs, suggesting that lipomatous metaplasia and not just fibrosis is an important driver of arrhythmogenicity of postinfarction scar.

Chapter 4 described an intervendor comparison of ADAS-3D and inHEART software for CMR image integration. We found that both are effective in identifying endocardial and intramural histological scar (with poorer performance in the epicardium). Nevertheless, both performed comparably to identify VT critical sites in human patients.

In Chapter 5, novel signal processing and machine learning algorithms are trained on endocardial intracardiac electrograms to determine histological scar and its depth. These strategies offer marked accuracy (greater than 95%) to identify intramural and epicardial scar substrate even from endocardial mapping offering significant improvements over voltage scar maps. These findings are leveraged to create an open-source code that can create readily importable into EAM scar depth maps from whole heart chamber mapping.

Chapter 6 turns our attention to ablation of VA, describing a pilot case series of pulsed field ablation (PFA) for treating intracavitary PVCs, showing promising results but requiring further validation.

Finally in chapter 7, this thesis discusses the design of a pragmatic randomised controlled trial (RCT) to compare stereotactic body radiotherapy (SBRT) against standard care for VA treatment, with patient recruitment underway.

Overall, this work offers incremental but important improvements in VA ablation, validating and developing new strategies for identifying and abolishing VA substrate. These contributions aim to advance the field towards control and hopefully cure of these deadly arrhythmias.

# Chapter 1

# 1 LITERATURE REVIEW

## 1.1 Introduction

Sudden cardiac death, which involves unexpected death or cardiac arrest from cardiovascular causes, is a leading cause of mortality in Australia, claiming 15,000 lives annually.[1] The common precursor to such deaths, often in the context of an underlying structural heart disease (SHD), are ventricular arrhythmias (VA) which arise from the lower chambers of the heart. VAs encompass a broad range of conditions including premature ventricular complexes (PVCs), ventricular tachycardia (VT) and ventricular fibrillation (VF) which often present as important clinical events in a patient's life and can portend significant morbidity and more devastatingly, premature death.[2]

Treatment for VA to prevent SCD includes implantable cardioverter defibrillators (ICDs).[3] These are invasive, have significant morbidity of their own[4-6] and can cause inappropriate shocks.[7,8] Further, ICDs are not infallible, with up to one-third of patients with ICDs dying from SCD despite the device and a further 17% having ICD related pro-arrhythmia, itself instigating SCD.[9] Another treatment modality is medications with anti-arrhythmic drugs, which themselves can have side-effects and variable efficacy.[10,11] Finally, catheter ablation (CA), an invasive electrophysiological procedure whereby the sites from which these VAs arise are identified and abolished, has been shown to improve morbidity and mortality in selected patients and in multiple randomised controlled trials (RCTs).[12] Unfortunately, despite numerous advances in our procedural toolkit and capabilities over the last thirty years to perform CA for VAs, meta-regression studies suggest no statistically significant incremental improvement in VA free survival

by publication time.[13] These surprising (and somewhat sobering) data suggest that improvements are needed to refine patient selection and CA techniques to advance care for patients suffering VAs.

Fundamentally the successful delivery of CA for VAs can be formulated into two separate but intrinsically linked clinical problems that the electrophysiologist must solve. These are (1) the identification of the complete arrhythmogenic substrate from which VAs arise and (2) adequate lesion formation at these sites such as to abolish this substrate. Indeed, studies of long-term CA failure suggest that in two-thirds of cases, VT sites identified on the subsequent procedure are at (or close to) sites previously targeted whilst one-third are in new sites, suggesting that both problems are inadequately addressed by current approaches and technologies.[14] A significant impediment to solving these problems are that VA substrate (and circuitry) are often located three-dimensionally within the myocardium.[15,16] That is, these VAs arise from variable components of the endocardium, intramural space and the epicardium. This makes identifying the entire arrhythmogenic substrate difficult and furthermore limits penetration of lesion delivery.[17] To address this problem, innovative approaches to VA CA are needed.

Such innovations can include addressing current limitations in invasive electroanatomic mapping (EAM) of the substrate that gives rise to VAs. Foundationally, our understanding of arrhythmogenic substrate has been developed from bipolar and unipolar electrograms generated through contact mapping of the ventricular myocardial surface.[18] Electrogram features including amplitude (voltage)[19] and fractionation[20], conduction velocity[21] and timing of the activating wavefront[22] and responses to pacing manoeuvres[23-26] can all be used to surmise the VA critical site. However often electrogram characteristics can depend on wall thickness of the ventricular myocardium, inter-electrode spacing, catheter contact quality, electrode orientation and direction

of the activating wavefront, all of which can obscure the underlying substrate.[27] It is to be determined if novel computational strategies applied to the intracardiac electrogram, including machine-learning approaches, can improve the ability of the EAM to identify substrate and sites of interest. Furthermore, recent advances in multi-modality imaging have allowed fusion of intracardiac echocardiography[28], cardiac magnetic resonance imaging (CMR)[29] and multi-detector computed tomography (MDCT)[30] with the EAM. The accuracy of such novel image-integration techniques, particularly with regards to their histological validation are unclear. Nevertheless, these innovative technologies offer potential to improve our understanding of the diseased myocardium (scar) in SHD and how such scar creates the arrhythmogenic milieu responsible for VA, potentially paving the way for improved procedural success. Finally, in terms of lesion delivery, traditional CA depends on radiofrequency (RF) ablation whereby heat energy is delivered to myocardial tissue to abolish and homogenise the underlying substrate. Cutting-edge technologies including pulsed field ablation (PFA)[31] and stereotactic body radiation therapy (SBRT)[32] offer promise in revolutionising lesion delivery, particularly to deeper arrhythmogenic substrate inaccessible to RF.

The aim of this literature review is to critically examine (1) the clinical problem and underlying mechanisms of VA; (2) the landscape of current management of VA; (3) strengths and limitations of current invasive electroanatomic assessment of ventricular arrhythmogenic substrate; (4) the role of non-invasive imaging in unveiling arrhythmogenic substrate and finally (5) current and emerging strategies in lesion delivery to abolish this substrate. Through this we hope to identify key knowledge gaps and possible innovative solutions that can be explored to advance the field of CA of VA.

## 1.2 Ventricular arrhythmias – understanding the problem

VA are defined by activation of the ventricles (lower chambers of the heart) independent of atrial conduction. This literature review has a specific focus on PVCs and VT, which are rhythms more commonly targeted for invasive EAM, non-invasive imaging and CA. These rhythms can also degenerate into VF, which in itself can be an arrhythmia targeted by CA.[33]

### *1.2.1 Cardiac conditions giving rise to ventricular arrhythmias*

VAs can be broadly distinguished into idiopathic arrhythmias or those arising from an underlying structural heart disease.

#### *1.2.1.1 Idiopathic ventricular arrhythmias*

Idiopathic VAs arise in patients who have structurally normal hearts, that is, arrhythmias arising in the absence of identifiable myocardial scar. They contribute to a minority (approximately 10%) of VA.[34] In a recent community snapshot encompassing the Rochester Epidemiology Project database, these VA had a crude incidence of 48 per 100,000, of which two-thirds were symptomatic PVCs, 29% idiopathic VT and 5% idiopathic VA associated cardiomyopathy.[35] In this same study, women had double the rates of symptomatic idiopathic PVCs than men, which may be a consequence of hormonal differences by sex[36] and how such sex hormones affect activation of potassium channel activity.[37] Conversely these differences could also be attributed to variable symptom perception and tendency to seek medical attention.[35] In this study, Sirichand et al. also found that idiopathic VA diagnoses seem to be increasing over time. This trend is likely due to greater awareness and recognition of idiopathic VA, facilitated by improved access to ambulatory heart rate and electrocardiographic (ECG) monitoring. Nonetheless, these data highlight the growing clinical challenge that such arrhythmias present to clinicians.

Idiopathic VAs typically originate from specific anatomical sites within the ventricles, including the outflow tracts, mitral and tricuspid annuli, the moderator band, the left ventricular summit, Purkinje fibres, and ventricular papillary muscles.[34,38] The predominant site of idiopathic VAs is the right ventricular outflow tract (RVOT), making up to 80% of encountered arrhythmias.[34,38] Their site of origin can often be inferred through careful analyses of the 12 lead ECG.[39] There are varied postulated mechanisms for idiopathic VA, ranging from cyclic adenosine monophosphate triggered activity dependent on delayed after depolarisations for outflow tract VAs[40] to automatic or triggered mechanisms for papillary muscle VAs.[41]

Most importantly, the diagnosis of "idiopathic" arrhythmia relies on exclusion of both overt and sub-clinical and/or microstructural abnormalities which can lead to misdiagnosis without adequate imaging and electrophysiological workup.[42,43] Nucifora et al. for example described that in a 120 patient cohort deemed to be "idiopathic" based on 12-lead ECG, exercise testing, angiography and transthoracic echocardiography (TTE), 23 had abnormalities on CMR (19/46 left ventricle (LV), 4/76 right ventricle (RV)).[44] Notably, CMR abnormalities significantly associated with a worse arrhythmic composite outcome of sudden cardiac death or need for ICD therapy. A recent systematic review supports these data, finding that the prevalence of concealed SHD revealed by CMR ranges from 11% to 84% of cases, again underscoring the importance of complete diagnostic workup in such patients with presumed idiopathic VA.[45]

#### *1.2.1.2 Ischaemic heart disease*

VA can occur in the context of coronary artery disease, both in the immediate phase of coronary ischaemia and because of the resultant myocardial scar. In the ischaemia phase, acute myocardial infarction can cause VF, leading to death within minutes if patients do not receive appropriate intervention. This is often the consequence of vulnerable substrate induced by

ischaemia (which causes heterogeneities in excitability, refractoriness, and/or conduction) as well as ectopic excitation of PVCs (often within the Purkinje system) that trigger lethal VF.[46-50] With time, myocardial scar is established whereby viable and healthy myocytes are lost as necrotic myocardium is replaced by fibrous tissue (collagen) and fat (lipomatous metaplasia). These patients are deemed to have a post myocardial infarction cardiomyopathy, which is more commonly though perhaps less accurately termed "ischaemic cardiomyopathy" (ICM).

The extent of myocardial damage post-infarction is determined by several interrelated factors, including the location of the coronary occlusion, the degree and duration of blood flow reduction to the ischemic area, and the heart's adaptive response to prior ischemic episodes.[51] Post-infarction, necrotic cardiomyocytes are cleared by macrophages with subsequent replacement fibrosis (consisting of collagen).[52] Fibrosis formation often occurs 3 to 10 days post infarct with the scar fibrosis maturing over 5 weeks.[53] This scar formation usually extends in a wavefront of ischemia from the subendocardium to epicardium dependant on duration of ischaemic injury[54] and leads to islands of surviving myocytes surrounded by scar. Importantly, cardiac remodelling post-infarction not only involves the infarcted tissue with collagen deposition and cross-linking during maturation of scar, but extends to remote myocardium whereby cardiomyocyte hypertrophy and fibrosis can occur due to wall stress, thereby affecting global cardiac contractility.[51] The result of such adverse (uncontrolled) remodelling is scar thinning, excessive fibrosis and cardiomyocyte hypertrophy leading to heart failure. Finally, it is important to remember the complexity of post-infarction scar which results not just in fibrosis but also lipomatous metaplasia (fatty intramyocardial infiltration)[55] which has recently been shown to be a key driver of arrhythmogenicity.[56]

Scar and composition of ICM has been evolving with changing and more emergent reperfusion of myocardial infarction (MI). Animal studies of non-reperfused subjects have demonstrated more homogenous, dense and transmural scar.[57,58] In contrast, whole-heart histological studies of ischaemia reperfusion animal models suggest that clinically encountered ICM in the modern era are more likely to have less confluent or transmural scar.[59] The changing nature of post-infarction scar has implications for arrhythmogenicity and susceptibility to VA. In an important mechanistic study of human ICM, Wijnmaalen *et al* [60] report a 36 patient cohort referred for VT ablation (14 early reperfusion, 22 referred late after MI) and found that VT cycle lengths were shorter in reperfused patients with patchy electroanatomic scar elicited in 71% of reperfused vs 14% of non-reperfused patients, confirming the above animal models. Histologically, bands of surviving myocardium were observed in the reperfused but not completed infarcts with more non-transmural and interstitial fibrosis, and greater areas of viable myocardium. These differences have also been shown to persist in chronic arrhythmogenic substrate with shorter VT cycle lengths in non-reperfused patients.[61]

#### *1.2.1.3 Non-ischaemic cardiomyopathy*

Non-ischaemic cardiomyopathies (NICM) encompass a broad range of myocardial diseases which are not the direct result of myocardial infarction. Classification of NICM has proven to be difficult. In 1980 (and then updated in 1995), the World Health Organisation classified NICM into dilated cardiomyopathy (characterised by impaired ventricular contraction which could be idiopathic, genetic, post-viral, substance induced or inflammatory), hypertrophic cardiomyopathy (with a predominant autosomal dominant inheritance pattern), restrictive cardiomyopathy (either idiopathic or associated with infiltrative diseases such as amyloidosis), arrhythmogenic right ventricular cardiomyopathy (ARVC) and unclassified cardiomyopathies.[62]

In contrast, the American Heart Association divides cardiomyopathy into two groups; "primary" (genetic, mixed and acquired) and "secondary" (such as infiltrative and inflammatory disorders), mainly depending on organ involvement and etiology.[63] The European Society of Cardiology guidelines separate NICM by structure and function into hypertrophic cardiomyopathies, dilated cardiomyopathies, restrictive cardiomyopathies, ARVC, and unclassified cardiomyopathies.[64] These groups are then further subdivided into familial and non-familial sub-groups.

Given NICM encompasses a broad range of myocardial diseases it is not surprising that the arrhythmogenic substrate of VA is incredibly varied. Despite this variability, electrophysiologists recognise that VA in NICM arise often from peri-valvular scar (seen in 63% of a 36 patient cohort).[65] More specifically, two dominant patterns of arrhythmogenic substrate have been described; the first, a basal anteroseptal subtype often arising from deep intramural substrate and the second, an epicardial dominant substrate in the inferolateral wall of the LV.[66] In contrast, genetic and imaging studies of 577 patient cohort with dilated cardiomyopathy demonstrated significant differences in late gadolinium enhancement (LGE) patterns between genes.[67] Patients with variants in Dystrophin, Desmoplakin, and Filamin-C genes showed predominantly subepicardial LGE scar. In contrast, scar patterns for Titin, BAG3, Lamin-A/C and Myosin binding protein C tend to be mid mural and/or endocardial. Regardless of distribution, another difference with ICM is that NICM scar may be more progressive, reflecting the underlying dynamic disease process.[68]

Our understanding of the development and character of arrhythmogenic substrate in NICM is limited by access to histopathologic studies or animal models. This is in contradistinction to ICM where animal models are more readily available for study. Opportunistic case reports and series provide some correlation between high density EAM and macropathology.[69] The most

definitive correlation of NICM electroanatomic and histopathologic substrate was performed by Glashan et al. in 2018 where the authors systematically co-registered whole histopathologic LVs in 8 NICM hearts (removed for transplant) with dense EAM.[70] They found that fibrosis patterns in NICM are highly variable and not just limited to the mid-wall and sub-epicardium. Further the fibrosis architecture was rarely compact (like in completed infarcts) but more typically patchy and diffuse, a finding which has implications for both invasive and non-invasive delineation of arrhythmogenic substrate.

#### *1.2.1.4 Mixed cardiomyopathy*

Finally, it is important to note that presence of ischaemic heart disease alone does not exclude NICM as a patient's predominant source of arrhythmia. Mixed cardiomyopathy can be present where myocardial scar is inconsistent with the distribution of coronary artery disease. Our lab has reported that mixed cardiomyopathy may form the underlying substrate in up to 14% of SHD VA ablations.[71]

### *1.2.2 Morbidity and mortality of ventricular arrhythmias*

#### *1.2.2.1 Sudden cardiac death*

The most feared complication of VA is sudden cardiac death (SCD) which can be defined as death within 1 hour after first symptom onset in the absence of known heart disease up to that time.[72] SCD can account for up to half of the years of potential life lost from heart disease. The aetiology of SCD varies by age. In a prospective study of children and young adults under the age of 35, Bagnall et al. described an annual incidence of SCD of 1.3 cases per 100,000 persons, three-quarters of which involved boys or young men. In this series, the most common cause of SCD was coronary artery disease (24% of cases) and inherited cardiomyopathies (16% of cases). In contrast,

in all-comers, the incidence of SCD is much higher, ranging from 14.9[73] to 147.8[74] per 100,000 persons, though reported rates vary due to definitions and data available in individual cohort studies.[1] In these all-comers, the most common cause SCD is coronary artery disease, purporting to approximately 70% in the western world, with NICM contributing to a further 15% and inherited channelopathies 2%.[1] Aside from age, prevalence of SCD further varies by sex (two-fold higher in men[75]) and ethnicity.[1] Though rates of SCD have tended to improve over time in the context of evolution of medical and device therapies, cardiopulmonary resuscitation and improved risk prediction,[76] recent data suggest that these improvements have plateaued. Ghajar et al. (2025) most recently described in the United States population that though the age adjusted mortality rate secondary to VA significantly decreased year on year from 1999–2010 (with an average annual percent change of − 6.6% [95%CI, −6.8, −6.3]), these rates have plateaued from 2010 to 2018 (average annual percent change of 0.7% [95%CI, −0.3,1.5]).[77] These data suggest the need for improved innovations in detection and treatment of VA to prevent sudden death.

VA in the form of VT or VF have previously been purported to be the first identifiable rhythm in up to 40% of cases.[78] More recent data suggest however a reduction in prevalence of these shockable rhythms. Analyses from the Aus-ROC Australian and New Zealand OHCA epidemiological registry  for example suggest that VA are the initial presenting rhythm for 28% of arrests,[79] though importantly, untreated VF can degenerate into asystole or electromechanical dissociation and hence the burden of these VA may be underestimated. A recent registry attributes 320,000 deaths in the United States to VT or VF[77] though again, such data can be biased by reliance on death certificates, incomplete data reporting and potential misclassification based on coding (or under coding missing information).

#### *1.2.2.2 Non-fatal morbidity of ventricular arrhythmias*

The non-fatal morbidity of VA is significant and underappreciated, with a relative paucity of research in this area compared to efforts to improve survival from these arrhythmias. There is a complex and bi-directional association between VA and congestive cardiac failure (heart failure).[80] VA arrhythmogenesis in acute heart failure can result from electrophysiological remodelling (including altered calcium re-uptake and potassium currents), structural and functional remodelling (with resultant fibrosis, chamber stretch, hypertrophy and ischaemia), altered neurohormonal mechanisms (including increased adrenergic tone, altered renin-aldosterone system activation and electrolyte abnormalities) and drug interactions (such as triggered activity from sympathomimetic drugs in acute decompensated heart failure).[81-84] In contrast, suppression of VA have been shown to improved heart function and heart failure in selected cohorts, particularly in patients with a PVC mediated cardiomyopathy.[85] RCTs are underway to ascertain the benefits of treatment of VT in end stage heart failure[86] and such results may establish CA as a "*fifth pillar*" of therapy in such patients.

Assessing quality of life QoL in patients experiencing VA or surviving sudden arrest is difficult, as such studies, which are generally targeted at measuring a patients " state of complete physical, mental and social well-being and not merely the absence of disease or infirmity,"[87] can necessarily encompass a wide variety of definitions or scales. Whilst in a study of sudden arrest, the overwhelming majority (49/50) of survivors judged their situation post resuscitation as "worth living,"[88] other studies describe that up to three-quarters of patients have low participation levels in society, with more than half having significant fatigue and one-third feelings of anxiety and depression.[89] PVCs are also associated with poorer QoL outcomes with cohort studies demonstrating improvement with CA,[90] though randomised data are lacking

Furthermore, the therapies utilised for management of VA can themselves have substantial impacts of QoL. In a recent patient-centred survey by the European Heart Rhythm Association of 1809 patients, device related complications were reported by 505 (22.4%), including one or more inappropriate shocks (11.6%).[91] Although most reported improved QoL (particularly with cardiac resynchronisation therapy), 1 in 10 experienced a significant decrease, driven mostly by complications such as ICD shocks. Other studies are not so reassuring, with one showing that more than 40% of patients with heart failure and defibrillators develop depressive symptoms with associated lower QoL and functional class.[92] AADs used to treat VA can themselves also be associated with reduced QoL, with adverse effects of these AADs causing worsening in physical functioning, vitality, and sleep and psychological distress.[93] Taken together these data underscore the need for innovative and novel solutions to treat VA and reduce their significant burden on morbidity and mortality.

## 1.3 Mechanisms of ventricular arrhythmias

The underlying mechanisms of VA can be separated into three categories: increased automaticity, triggered activity and re-entry. Multiple mechanisms can be responsible for VA in a single patient even in the presence of SHD where myocardial scar is predominantly thought to be responsible for re-entrant VA.[33,94] This review will first describe the roles of each mechanism in the initiation and propagation of VA before focussing on the re-entrant circuit which is the primary contributor to VT in SHD.

### *1.3.1 Automaticity, triggered activity and the re-entrant circuit*

#### *1.3.1.1 Automaticity*

Pacemaker cardiac myocytes have the ability to spontaneously generate action potentials without external stimuli, caused by a net inward current positive current during phase 4 of the action potential which progressively brings the membrane potential to the depolarisation threshold, termed automaticity.[95] Under normal conditions, ventricular myocytes do not exhibit spontaneous diastolic depolarisation but abnormal automaticity can arise under pathological conditions such as infarction, adrenergic stimulation or electrolyte derangement, which cause the resting membrane potential to becomes less negative, leading to PVCs or more sustained VA.[96] This may result from a decrease in the inward rectifier potassium current or increased calcium release from the sarcoplasmic reticulum.[97]

#### *1.3.1.2 Triggered activity*

The second mechanism of cardiac arrhythmogenesis is triggered activity whereby cardiac impulses are dependent on afterdepolarisations (membrane potential oscillations that occur during or immediately following the preceding action potential).[96] When the afterdepolarisation reaches a threshold potential, a new action potential is generated, which can, in turn, generate ongoing responses, leading to sustained VA. After depolarisations can be considered early, occurring in phase 2 and 3 of the action potential, or delayed, occurring in phase 4.

An early after depolarisation occurs when repolarisation is interrupted by a transient, positive shift of membrane potential.[97] It occurs in phase 2 and 3, prior to complete repolarisation. They are most often associated with prolonged action potential repolarisation (i.e. a longer action potential duration), perceptible as prolonging of the QT segment of the ECG and/or alterations in the T wave morphology. Congenital long QT syndromes result from genetic alterations in membrane currents that prolong this action potential duration, affecting; voltage dependant sodium

channels L-type calcium currents, the outward delayed and rapid rectifier potassium currents and the inward rectifier potassium current.[98] Acquired long QT due to electrolyte abnormalities and drug interactions can also manifest early depolarisations.

A delayed after depolarisation occurs can occur when calcium levels in the sarcoplasmic reticulum are pathologically elevated (calcium overload).[97] These delayed after depolarisations can be provoked by sympathetic stimulation or digitalis toxicity whereby calcium leaks from the sarcoplasmic reticulum into the intracellular space through calcium release channels, which themselves are controlled by ryanodine receptors. Mutations in the genes coding these receptors can themselves cause delayed after depolarisations (causing catecholaminergic polymorphic ventricular tachycardia). Further, ischemia and heart failure can also cause leak of calcium from the sarcoplasmic reticulum (even when it is not overloaded with calcium).[81]

#### *1.3.1.3 Re-entry*

The third mechanism of cardiac arrhythmia is re-entry, which is the primary cause of VT in SHD.[52] Re-entry involves continuous excitation of the ventricle throughout the entire cardiac cycle. This occurs due to a re-entrant circuit, an electrical pathway where the activation wavefront travels in a loop.[99] Several conditions are required for re-entry to occur. First, it requires an underlying substrate consisting of two connected pathways with differing electrophysiological properties (conduction velocity and refractoriness), surrounded by electrically inexcitable tissue. This inexcitable tissue can be due to anatomical boundaries (myocardial scar or valve annuli) or functional block (whereby an arc of conduction block occurs in some circumstances e.g. wavefront orientation and/or coupling interval but not all).[100] Second, re-entry necessitates an appropriately timed stimulus that causes unidirectional block in one pathway and subsequent slowed conduction in the alternative pathway. If conduction in this pathway is sufficiently slow, the impulse can return

to the initial region of unidirectional block once it has repolarised (i.e., the impulse arrives at the "excitable gap"), permitting conduction and facilitating the formation of a continuous re-entrant loop.

### *1.3.2 Re-entry in structural heart disease*

In SHD, re-entry within myocardial scar is the predominant mechanism for monomorphic ventricular tachycardia.[101] In 1972 Wellens et al. interrogated the initiation and termination of VT in 5 patients with recurrent VT, 4 of whom had old myocardial infarction and suggested that the causal mechanism of VT in these patients was most likely re-entry, which they postulated could be due to circuits within the bundle branch, Purkinje fibres and infarcted tissue.[102] Post-infarction, remodelling and fibrogenesis form islands of electrically conducting viable myocardial cells, often found in the infarction border zones, causing wavefront activation to take a zig-zag route with associated slowed conduction.[103] NICM scar can be even more diverse due to variance in their underlying pathophysiology, with variable patterns of fibrosis, myocardial cellular hypertrophy, adiposity and increased interstitial cellularity.[70,104] Regardless of aetiology, it is important to remember that this scar is metabolically, mechanically and electrically dynamic living tissue and not electrically inert.[52] This milieu of viable and functional myocytes, fibrotic cells, adipocytes and replacement fibrosis, all of which cause significant electrical and structural remodelling, contribute to the arrhythmogenic substrate responsible for re-entry. Post-infarction canine studies have established that unidirectional block can thus occur due to differences in activation wavefront propagation secondary to myocardial fibre orientation causing nonuniform anisotropy[103,105] as well as due to discontinuities in axial resistance causing decremental conduction,[106] heterogenous refractory periods,[107] intramural delay[108] and impedance mismatch.[100]

The re-entrant circuit in ventricular tachycardia can take different shapes, though most classically post-infarction re-entrant VT circuits in humans and swine are usually in the form of a double loop, as first described by El-sherif et al.[109] and confirmed in high density mapping studies by Anter et al.[110] In this double loop (or "figure of eight") circuit, propagation of the activating wavefront is during the diastolic interval of the ECG through the common central pathway, also known as the *isthmus*.[111] As the wavefront emerges from the central pathway, at the *exit*, it depolarises the larger mass of myocardium and thus generates the systolic phase (coinciding with the QRS onset). To return to the isthmus (vis the *entrance*), this activating wavefront can travel through *outer loops* in healthy myocardium or *inner loops* in scar. Macro-re-entrant single loops have also been described where the activating wavefront travels around the myocardial scar (often subtended by valve annuli),[101] and furthermore, to add to complexity, VT circuits can have multiple isthmii, entrances and exits.[99] Careful mapping in large animal studies have demonstrated that the entrance and exit sites of these circuits are associated with the greatest conduction slowing, with relatively preserved conduction through the central isthmus.[110]

There are several challenges in identifying and localising the re-entrant circuit in human VT. First, the circulating excitation wavefronts propagate through regions of scar in relatively small volumes of myocardial scar and hence these depolarisations are not usually detectable from the body surface ECG during VT,[111] thus necessitating intracardiac mapping. Second, many VTs are hemodynamically unstable, preventing entire mapping of the circuit.[112] Third, as described previously, the substrate can be functional limiting delineation of the re-entrant circuit in the absence of the tachycardia. Complicating this, even anatomic boundaries may not be apparent if the activating wavefront travels parallel to it during invasive mapping.[99] Fourth, many re-entrant

circuits have multiple entrances or exits, as well as blind loops and bystander regions,[101,110,111] and therefore clear delineation of the isthmus even when the tachycardia is mappable can be difficult.

Most importantly however, recent data refute the simple two-dimensional concept of the re-entrant circuit, which is now better appreciated in three-dimensions, underlining the complexity of delineation of the VT circuit. Our understanding of VT in post-infarction cardiomyopathy was developed first through endocardial mapping and then surgical resection of the endocardial tissue at the borderzone of post myocardial infarction aneurysms,[113] supporting the two-dimensional model of VT as being formulated in the sub-endocardium. Multiple studies since however have established that re-entry can occur at depth, that is, incorporating some combination of endocardial, intramural and/or epicardial myocardium. In 1991, Kaltenbrunner et al. performed intraoperative endocardial and epicardial mapping of post-infarction VT, demonstrating that the majority of VTs (76%) were not constrained to the sub-endocardium or sub-epicardium.[114] This was similarly shown by Tung et al. through sequential endocardial-epicardial mapping where 73% of VTs in post-infarction cardiomyopathy had three-dimensional involvement.[15] Bhaskaran et al. subsequently showed with intramural needle mapping of explanted ICM and NICM hearts that 42% of VTs co-localised to the intramural space.[16]

Given these challenges, there is a requirement for delineation of the entire substrate responsible for VT that addresses limitations in invasive assessment of re-entrant circuits. One such approach is substrate mapping, whereby inferences can be made as to the location of these re-entrant critical sites based on electrogram features without mapping the tachycardia itself.[18] Attempts to address the three-dimensionality of these circuits include non-invasive mapping techniques such as CMR and MDCT. Computational and machine learning analyses may offer further insights. These approaches will be evaluated in sections 1.5 and 1.6.

### *1.3.3 Mechanisms of arrhythmia in chronic post infarction scar*

There are multiple hypotheses regarding the unifying mechanisms of re-entry in chronic post-infarction myocardial scars. Seminal work by De Bakker et al. established the zig zag route of myocardial infarction through viable myocyte bundles separated by fibrosis with accompanying fractionated electrograms.[103] It is important to note however both De Bakker et al. and others[115,116] have found such myocytes bundles in regions of infarction both conducive to and also not conducive to VT, suggesting that fibrosis interrupted myocytes bundles alone are not enough to create conditions for re-entry. Impairments in cell-cell coupling due to pathologically impaired function of connexin proteins (responsible for gap junctions between cardiomyocytes) have been suggested to play a role in arrhythmogenesis of post-infarction scar. For example, quantitatively reduced and also lateralised connexin 43 expression has been implicated in conduction slowing and arrhythmogenesis in ICM and NICM.[117,118] Connexin 43 modulation via gene transfer has been shown to improve myocardial conduction and reduce VT inducibility by 60% in pre-clinical swine experiments.[119]

As suggested by Donahue et al. however, these fixed elements of tissue discontinuity and slowed conduction offer an unsatisfying explanation alone for the arrhythmogenicity of post-infarction scar.[120] If all that was required was slowed conduction then we would expect to see VT more often than we do in post-infarction patients. Pathological myocyte excitability, due to raised resting membrane potentials and abnormal upslope velocities in phase 4 of the action potential could be an alternative explanation Donahue et al. suggest that early afterdepolarisations from enhanced adrenergic tone or automaticity from unstable membrane potentials could generate the trigger (a PVC), which, if appropriately timed, arrives at two pathways with repolarisation heterogeneity leading to re-entry.[120]

Finally, development of VT in chronic post-infarction scar is dependent on the age of infarction. Older infarcts are more likely associated with VT inducibility as well as abnormal electrograms within the scar tissue.[121,122] An emerging concept that could explain the arrhythmogenic potential of such scar and it's evolution over time is the development of intramyocardial adipose tissue within scar (deemed lipomatous metaplasia).

#### *1.3.3.1 Lipomatous metaplasia*

In 1997, Baroldi et al. first described the presence of extensive adipose tissue in healed myocardial infarction in an autopsy study of 116 consecutive hearts excised for transplantation (68% ICM) and 24 aneurysmectomies.[55] The development of this lipomatous metaplasia correlated with infarction age and the degree of LV dilatation. This was confirmed in 2004 by Su et al. who demonstrated lipomatous metaplasia in 84% of hearts with healed myocardial infarction.[123] These findings have also been born out in more recent imaging studies reliant on CMR utilising water-fat separation imaging[124] or MDCT studies.[125] Human imaging studies suggest that it takes time to develop these intramyocardial adiposities, with no human hearts demonstrating lipomatous metaplasia at less than 10 months vs 89% with infarct age greater than 3 years.[125]

The aetiology of this remodelling however is unclear. Both Baroldi et al. and Su et al. hypothesised that these adipose tissues were derived from transformation of fibrocytes to adipocytes or transformation of uncommitted multipotent stem cells to adipocytes. Conversely, more recent data in a canine model 6 months post infarction suggest that lipomatous metaplasia in ICM is unique to haemorrhagic myocardial infarction, with it being observed exclusively at the confluence of iron and lipid remnants.[126] Validated models of lipomatous metaplasia resembling human disease are therefore required to further understand the mechanisms and possible therapies (such as iron chelation) for such remodelling.

This is particularly important as there is a rapidly developing appreciation of the role of this lipomatous metaplasia in re-entry. Pouliopoulos et al, at our centre, first established the role of fat in conduction slowing and VT propagation. Seventeen sheep with myocardial infarction and 5 controls (without infarction) underwent electrophysiological study between 3 and 172 weeks post infarction and intracardiac electrograms were matched to intramural biopsies where adiposity was computed.[56] They demonstrated that whilst unipolar electrogram amplitude correlated with viable myocardium, adiposity and fibrosis, abnormal conduction velocity only did so with fat and viable myocardium but not fibrosis. In nine infarcted sheep with inducible VT, they found more adiposity, myocyte discontinuity (with connexin lateralisation), reduced conduction velocity and unipolar electrogram amplitude compared to 4 sheep without inducible VT. Early sites of VT were associated with more adiposity. Together these data implicated fat and not fibrosis in the arrhythmogenesis of post-infarction VT. In a follow up study by the Westmead group, Samanta et al.[127] found that intramyocardial adiposity correlated better with unipolar electrogram amplitude than fibrosis. These authors however did not describe intracardiac electrogram signatures of this intramyocardial scar beyond amplitude, which may better help the electrophysiologist identify and target the most arrhythmogenic sites conducive to VT. We also do not yet understand the relationship of fat to functional substrate.

With improving multimodality imaging to identify lipomatous metaplasia as well as image integration techniques to co-localise these with intracardiac electrograms further interesting insights have been made. First, Sasaki et al. demonstrated that beyond voltage, other electrogram characteristics such as electrogram duration also associated with lipomatous metaplasia.[128] Furthermore three quarters of identified critical sites either co-localised to lipomatous metaplasia or the border zone of this remodelled area. Second Sung et al. have demonstrated that the lowest

electrogram voltages associated with fat and fibrosis admixture rather than fibrosis alone.[129] Finally, these findings have been further explored in a seminal human series of post-infarct (and later NICM) patients with VT by Xu et al. who demonstrated that when the EAM is co-registered with both CMR and MDCT, 99% of borderzone channels that were electroanatomically proven to harbour VT (critical channels) co-localised to lipomatous metaplasia.[130] This compared to 92% of borderzone channels that did not give rise to VT (non-critical channels) which were distant from fat. In ICM, these critical channels co-localising with lipomatous metaplasia were shown to have lower conduction velocity compared with non-critical channels that did not,[131] with prolonged repolarisation and increased repolarisation dispersion.[132] Importantly (though perhaps not surprisingly given the work of Baroldi et al.), this same group (Xu et al) demonstrated a higher prevalence and volume of lipomatous metaplasia co-localising to borderzone channels that harboured VT compared to those that did not.

Interestingly, lipomatous metaplasia has been shown to also contribute to conduction slowing and re-entry in NICM. In a subsequent study, Xu *et al* performed the same correlation of invasive EAM with multimodality cardiac imaging in 49 patients with various NICM phenotypes.[133] They again demonstrated a higher prevalence and volume of lipomatous metaplasia co-localising to borderzone channels that harboured VT compared to those that did not, with less current variation along critical channels.[133,134] Together these data establish the role of fat in ventricular re-entry and suggest that further work to understand the arrhythmogenic potential of lipomatous metaplasia in VA as well as better technologies to identify it beyond MDCT may be useful.

## 1.4 Management of ventricular arrhythmias

As alluded to earlier, there are multiple facets to management of VA, ranging from implantable cardiac device therapy to prevent tragic sudden death, anti-arrhythmic medications with varied pharmacological mechanisms and abolition of VA substrate, primarily with radiofrequency CA.

### *1.4.1 Implantable cardiac device therapy*

#### *1.4.1.1 Implantable cardioverter defibrillators*

The development of ICDs to prevent SCD were pioneered by Michel Mirowski and Morton Mower who first showed the efficacy of intravenous ventricular defibrillation for VF in man during coronary artery bypass grafting[135], then subsequently for treatment of a canine model of VF[136] and finally, first-in-man studies in a highly selected cohort of 3 patients.[137] The development of this technology was not without controversy, including early scepticism that the morbidity of such a device would justify the potential lives saved.[138] Subsequent observational studies in sudden cardiac death survivors established the role of ICDs in secondary prevention.[139,140] The first (and largest) RCT for ICD use in secondary prevention (for patients who were resuscitated from VF or required cardioversion for VT – with either syncope or other cardiac symptoms, and also an ejection fraction (EF) less than 40%) found a significant absolute risk reduction in mortality (75.4% survival versus 64.1% survival at three years ($P<0.02$), numbers needed to treat 8.8) with ICD use compared to amiodarone.[141] Two subsequent studies (with lower patient recruitment) found similarly numerically improved survival though both did not achieve statistical significance.[142,143] A subsequent meta-analysis of all three studies confirmed mortality reduction in this patient cohort (with hazard ratio of 0.72, confidence interval 0.60-0.87, $P=0.0006$) and

therefore ICD therapy is standard of care in patients with sustained VA in the absence of an identifiable and treated reversible cause.[144]

The role of ICDs in primary prevention of sudden death in patients at risk of VA is less clear and dependant on underlying aetiology of structural heart disease, patient age and competing risk of death (such as risk of non-arrhythmic death from heart pump failure). ICD therapy for prevention of death in ischaemic heart disease has been investigated in multiple RCTs. The first, MADIT in 1996 found that in 196 patients with ICM (EF less than 35%, with either spontaneous non-sustained VT or sustained VT inducible by electrophysiological study (EPS), ICDs compared to medical therapy saw a reduction in all-cause mortality (hazard ration 0.46, confidence interval 0.26-0.82, P=0.009).[145] The follow up study, MADIT-II, in 2002 extended the role of ICD in ICM to encompass ICM patients with an EF less than 30% but without need for positive electrophysiological study nor spontaneous VT and found that ICD therapy compared to medical therapy associated with an absolute reduction in all-cause mortality of 5.6% (14.2% with ICD therapy vs 19.8% without, P=0.016),[146] and this benefit has been born out with longer term follow up of the same cohort out to 8 years.[147] In contrast, the use of ICD therapy early after myocardial infarction (less than 40 days) does not seem to improve overall survival, as the treatment of life-threatening VA by ICD therapy seems to be balanced by the competing risk of pump failure in this cohort.[148] More recently, the role of ICD in primary prevention in a mixed group of patients with SHD (48% NICM) was investigated in the SCD-HeFT study which found lower mortality in the ICD group compared with no ICD (hazard ratio 0.77, 97.5% confidence interval 0.62-0.96, P=0.007, absolute risk reduction 7.2%, numbers needed to treat 13.9).[149] Sub-analysis by cause of cardiomyopathy found significant reductions in all-cause mortality in ICM (HR 0.79, 97.5% CI

0.60-1.04, P=0.05). Although not significant, there was a trend towards significance in NICM there (HR 0.73, 97.5% CI 0.50-1.07, P=0.06).

Data for the role of ICD therapy in pure NICM is more heterogenous. The first two studies of ICD therapy in this cohort were terminated early due to futility.[150,151] Subsequently, the DEFINITE trial (n=458 patients with NICM, EF less than 35% and either non-sustained VT or PVCs)[152] and the DANISH trial (n=1116 patients, EF less than 35%) showed no reduction in mortality with ICD therapy (with mean follow up of 2.4 years in DEFINITE and median follow up 5.6 years in DANISH).[153] Both studies demonstrated reductions in risk of sudden arrhythmic death suggesting once more the role of competing risks of death (pump failure vs arrhythmic) in these cardiomyopathies. Despite these findings, closer examination of study methodology suggests against discarding ICD use off-hand in NICM. In the DANISH study for example, more than half of patients received cardiac resynchronisation therapy, and therefore it is not conclusive whether ICD therapy would be beneficial in patients who do not qualify for this therapy. Furthermore, sub-analysis by age in DANISH suggests that patients younger than 70 did derive benefit from ICD therapy for survival (hazard ratio 0.70, confidence interval 0.51-0.96, P=0.03) vs older patients who were less at risk of sudden arrhythmic death. It remains to be seen if ICD therapy in NICM targeting particular phenotypes (or aided by additional risk stratification tools) may show more conclusive survival benefits in this cohort.

#### *1.4.1.2 Cardiac resynchronisation therapy*

Cardiac resynchronisation therapy (CRT) is another invasive device based technology for heart failure, which beyond its initially postulated improvement in mechanical and electrical synchrony between ventricles also seems to have direct impact on global LV function, modulation of heterogenous gene expression in the failing left ventricle, improvement in the mitochondrial

subproteome and beta adrenoceptor regulation.[154] Following multiple cohort studies, the first RCT for use of CRT, the COMPANION trial demonstrated in 1520 patients randomised 1:2:2 to guideline directed medical therapy (GDMT) vs GDMT plus CRT (pacemaker function only) vs GDMT plus CRT (including defibrillator), that CRT pacing (CRT-P) non-significantly but numerically improves overall survival by 24% (P=0.059) and CRT defibrillators (CRT-D) improve survival by 36% (P=0.003).[155] Subsequently, the MADIT-CRT RCT randomised 1820 patients with any cardiomyopathy and ejection fraction less than 30% and QRS duration more than 130ms to either CRT-D or ICD, finding that CRT itself improved a composite outcome of all-cause death and non-fatal heart failure, predominantly driven by the latter and with a more pronounced effect when QRS duration was more than 150ms.[156] Finally in the RAFT study, 1798 patients with EF less than 30% and QRS more than 120ms (or 200ms if paced) were followed to a median 40 months after randomisation to ICD or CRT-D. In this study, in contrast to MADIT-CRT, there was a significant reduction not just in heart failure but in death,[157] a finding that has been confirmed in subsequent long term follow up of the same study.[158] Despite discrepant results, sub-analyses of both trials have demonstrated reduction of VA with CRT, suggesting that this therapy might modulate the arrhythmogenic substrate conducive to these arrhythmias.[159,160]

### *1.4.2 Anti-arrhythmic drug therapies*

AADs are an important (and often primary) therapeutic strategy used for treatment of patients with VA (both in idiopathic VA and in patients with an underlying SHD). Seminal work by Miles Vaughan Williams in the 1970s established four main modes of action of AADs, variously modifying sodium, potassium, and calcium channel function or intracellular mechanisms regulated by adrenergic activity, and resultant effects on the cardiac action potential.[161]

Class 1 AADs are postulated to act on phase 0 of the action potential through sodium channel blocking effects, divided into 1a, 1b and 1c sub-classes based on the specific channel targeted. Of note for VT, Class Ib drugs, which modulate inactivated sodium channels during depolarisation of the action potential, include lignocaine and mexiletine. Lignocaine can be used for emergent cessation of VA electrical storm or monomorphic VT, though conversion rates in reported literature are low (8-20%),[162-165] with head-to-head randomised trials in monomorphic VT suggesting superiority of intravenous amiodarone[166] or sotalol[162] for achieving chemical cardioversion. For chronic therapy of VT, though there is some observational data on role of mexiletine in addition to amiodarone therapy,[167] a randomised controlled trial comparing CA vs escalation of AADs (including use of mexiletine) found this strategy inferior for treatment of VT.[168] Side-effects of lignocaine and mexiletine which affect the gastrointestinal and central nervous system can limit long term use. Class 1c agents block the fast sodium channels, blunting the overall phase 0 curve of the action potential. The quintessential clinical class 1c AAD is flecainide. In an important paradigm shifting RCT, the Cardiac Arrhythmia Suppression Trial (CAST) demonstrated excess deaths in patients treated with flecainide for ventricular ectopy suppression post myocardial infarction.[169] Therefore it is contraindicated in patients post myocardial infarction (though more recent pilot data suggests a potential role for flecainide in treating PVCs in NICM patients protected by ICD).[170] It can be used with effect for suppression of idiopathic PVCs.[171]

Class 2 AADs are beta-blockers, and they affect phase 4 of the action potential through blockade of beta-adrenergic receptors with resultant negative chronotropic and inotropic activity. They are often used as first line agents for treatment of idiopathic PVCs and VT.[172,173] They seem to have a synergistic effect in VA suppression when combined with amiodarone in SHD.[174] They

also seem to improve the efficacy of anti-tachycardia pacing (ATP) through ICD therapy with a dose-dependent effect.[175]

Class 3 AADs predominantly affect phase 3 of the action potential through blockade of potassium channels resulting in longer repolarisation and an increase in myocyte refractory period. Amiodarone is the most ubiquitous class 3 agent, and this drug also has class 1,2 and 4 effects. Multiple randomised studies have shown reduction in anti-arrhythmic death or sudden cardiac arrest with use of amiodarone in high risk post-infarction patients (before the era of modern GDMT), though at the expense of adverse events in up to a third of patients.[176-178] In fact, in the 11 year follow up of patients enrolled in the Canadian Implantable Defibrillator Study, comparing ICD to amiodarone, at just over 8 years follow-up, all patients randomised to amiodarone had either died, had recurrence of arrhythmia or were required to discontinue amiodarone due to side effects.[179] Sotalol is another commonly used class 3 agent (though it also has primarily beta-blocking properties below dosage of 160mg/day). In a study of 421 patients who had recently received an ICD for spontaneous or inducible VT/VF, randomised to amiodarone plus beta blocker, sotalol or beta-blocker alone, amiodarone plus beta blocker reduced risk of subsequent ICD shock compared to beta blocker alone (hazard ratio 0.27, 95% confidence interval 0.14-0.52, P<.001).[180] There was a trend towards less shocks with sotalol compared to beta blocker alone (hazard ratio 0.61, 95% confidence interval 0.37-1.01, P = .055). Concerningly, this study again reinforced the risk of adverse effects with drug therapy, as these class 3 agents were stopped at 1 year in 18.2% of cases (amiodarone) and 23.5% cases (sotalol).

Finally, class 4 AADs act on blockade of calcium channel blockers, affecting phase 2 of the action potential with reduction of calcium ion influx. These agents are often used in idiopathic PVCs or in verapamil sensitive fascicular re-entrant VT.

### *1.4.3 Catheter ablation of ventricular arrhythmias*

Ablation of VA is aimed at destroying the myocardial tissue responsible for initiation and/or propagation of the arrhythmia. Prior to CA, initial control of VA (and specifically, monomorphic VT secondary to myocardial infarction) was with open-chest surgical excision of aneurysm or sub-endocardial excision guided by intraoperative endocardial and epicardial mapping.[113,181,182] Due to significant morbidity from open-chest treatment, percutaneous CA was developed, initially with use of direct current shock,[183-185] and then subsequently, the delivery of RF energy.[186] Novel energy sources and alternative strategies to ablate and abolish arrhythmogenic substrate will be reviewed in later sections.

#### *1.4.3.1 Outcomes of catheter ablation of premature ventricular complexes*

There are multiple case series and observational cohort studies describing CA of PVCs, sometimes compared to non-randomised control groups treated with drug therapy.[187-192] These studies demonstrate improvement in the frequency and burden of PVCs (with burden defined as percentage of heart beats which are PVCs)[187,191] as well as demonstrating improvements in ventricular function in the context of PVC induced cardiomyopathy.[188,190] Observational cohort studies have also demonstrated some benefit in overall quality of life with CA of PVCs, though the scales used are varied and not often arrhythmia specific.[90,193] In these studies, there was no comparison with an AAD drug arm.

Outcomes in PVC ablation tend to differ based on the site of origin of the PVCs. In a large multi-centre series of 1185 patients (55% female) who underwent ablation between 2004 and 2013, acute procedural success was 84% in the total cohort, however when stratified by PVC location, the highest success rate was in RVOT PVCs at 93% with much lower success rates for papillary muscle and epicardial PVCs (67%).[187] These sites are often more challenging due to intramural

PVC origin, difficult catheter contact of intracavitary moving structures and irritant ectopy during catheter ablation. In this same study, ablation of PVCs from papillary muscles and the epicardium demonstrated longer procedure times (249 ± 109 min and 249 ± 117 min, respectively) and fluoroscopy times (40 ± 21 min and 48 ± 27 min, respectively) when compared to ablation in patients with PVCs from the outflow tracts ($p < 0.01$).

Unfortunately, the only randomised controlled study to rigorously compare CA and AADs for PVC management only recruited patients with RVOT PVCs.[194] Ling et al. (2014) randomised 330 patients with RVOT PVCs to CA or AAD (metoprolol or propafenone) and followed up these patients with serial echocardiography out to 12 months. At final 1 year follow up, recurrence of PVCs was significantly lower in patients randomized to CA (32 patients, 19.4%) versus AADs group (146 patients, 88.6%; P<0.001). In the CA group, 1 patient required cardioversion for VF induction during ablation in the RVOT septum and there was 1 arteriovenous fistula with 2 haematoma complications. All patients with complications recovered without residual symptoms before discharge. In the AAD group, 17 patients were troubled by adverse events including symptomatic bradycardia and/or hypotension, fatigue and headaches.

Taken together these data suggest that further RCTs are required to establish the role of CA in the management of PVCs, especially encompassing the diverse origins of PVCs in idiopathic as well as structural heart disease. Prior to design of these trials, a systematic review of evidence comparing AADs vs CA for treatment of PVCs are required. No such published review is available in the literature to date. Such a study would inform essential power calculations as well as identifying optimal primary and secondary outcomes in the management of PVCs.

#### *1.4.3.2 Outcomes of catheter ablation of ventricular tachycardia*

When describing the outcomes of CA for monomorphic VT it is important to define what "success" means. Typically, CA of VT is defined in terms of acute procedural success ("complete success" where no VA is inducible, "partial success" where the clinical VT is abolished but other VTs may remain inducible, or "procedural failure" where both the clinical and/or non-clinical VTs are inducible) as well as by long term arrhythmia free survival. These definitions are accepted due to data suggesting that absence of VT inducibility by programmed electrical stimulation (PES) can predict longer term arrhythmia free survival.[195] There is however contention as to the protocol for PES and whether conventional (up to 3 extra-stimuli) or extensive (up to 4 extra-stimuli) induction better predicts future recurrence. Campbell et al. (2020) demonstrated that between 11% and 17% of inducible VTs may be missed if PES with 4 extra-stimuli and/or burst pacing are not performed and further, that patients who were non-inducible for any VT using the conventional induction protocol had worse VA-free survival (12 months, 43% vs. 82%; p = .03) compared to patients who were noninducible for any VT using induction up to 4 extra-stimuli.[196] Nevertheless, there are also other limitations to using non-inducibility to define procedural success including effects of background AAD treatment and dependence on anaesthesia. In high risk patients, non-inducibility post ablation does not seem to portend good prognosis for arrhythmia free survival.[197] Alternative end-points such as in-excitability of scar, elimination of surrogates of critical isthmii such as late potentials or local abnormal ventricular activities, elimination of imaging defined substrate or elimination of functional substrate by EAM have all been suggested.[198]

With regards to longer term outcomes, traditionally VT free survival, as well as freedom from anti-tachycardia pacing (ATP) or ICD shocks are reported, as well as composite outcomes of mortality, heart failure hospitalisation and heart transplantation. Our centre has suggested that,

similar to atrial fibrillation outcomes, "VT burden" represents a more real-world therapeutic endpoint for VA ablation as a representative metric of long term procedural success.[199] This was initially reported in the THERMOCOOL VT trial where 249 patients with post-infarction VT were recruited for irrigated CA and for whom VT burden was reported in 139 patients.[200] In this study, 82% of patients benefitted from ≥75% reduction in VT and the proportion of patients with ICD shocks decreased from 81.25% to 26.8%, ($p<0.001$), over a 6-month period after ablation. VT burden is increasingly reported in modern trials of VT ablation including those most studies describing outcomes after SBRT.

There are 10 published RCTs that have compared catheter ablation with other therapies (usually AADs). These are, in order of publication, SMASH VT,[201] V-TACH,[202] CALYPSO,[203] VANISH,[168] SMS,[204] BERLIN-VT,[205] PARTITA,[206] SURVIVE,[207] PAUSE-SCD[208] and VANISH 2.[209] This review will not describe each individual study in turn as they have been extensively described and reviewed in the literature to date. In fact, in the last 5 years, there have been more published systematic reviews and meta-analyses of these trials than the number of trials themselves.[12,13,210-216] These studies have broadly established that CA for monomorphic VT reduces risk of recurrent VT, ICD shocks and cardiac hospitalisation.

Given (1) improving technologies and safety of CA with periprocedural mortality rates less than 1%,[217] (2) evidence that VT and ICD shocks can themselves worsen cardiac function and (3) known toxicities of AADs, it is biologically plausible that CA would improve survival in selected patients. Unfortunately, however, trials have broadly failed to show a survival benefit from CA versus AAD therapy for SHD. This is partly because these studies were not powered to detect a mortality difference between therapies. Another posited reason for was that CA for VT was historically seen as a treatment of last resort and therefore potentially employed as a palliative

procedure for arrhythmic control in advanced cardiomyopathy. In the VANISH trial for example, CA was offered for patients with post infarction VT who had failed an AAD and this found no difference in total mortality (approximately 27% in both groups during a 2.3-year median follow-up).[209] Four recent studies, PAUSE-SCD, SURVIVE, PARTITA and VANISH 2 all challenged this concept by offering CA early to patients at risk of VA or after initial ICD shock. PARTITA was the only study to find a mortality benefit with CA of VT vs AAD therapy in patients who experienced their first ICD shock, however this was driven by numerically higher non-cardiac deaths in the AAD arm, which may suggest a Type 2 statistical error due to low sample size (n=47 patients randomised).[206] Nevertheless all four such studies establish the role of early CA finding that this strategy leads to improved arrhythmic control and less ICD shocks at acceptable tolerability.

There are many important caveats to interpreting the currently published trial evidence for CA of VT. Firstly, most trials have recruited purely or majority of patients with post-infarction cardiomyopathy. Only two studies have recruited NICM; PARTITA, for whom 19% of patients had a dilated cardiomyopathy and PAUSE-SCD where 30.6% had a NICM and a further 34.6% specifically had arrhythmogenic ventricular cardiomyopathy. In their meta-analysis of both RCTs and observational studies stratifying by ICM vs NICM, Kanagaratnam et al found that NICM patients were younger, with higher EF. Despite this, there were no differences in mortality and indeed VT recurrence was higher in NICM vs ICM patients (26.3 vs. 18.7 per 100 patient-years).[13] The second observation from these trials is that in general, RCTs investigating management of VT are difficult to complete, with an average duration of trial from initial enrolment to publication being in excess of 9 years, which may be one reason why such trials have been in general underpowered to demonstrate mortality benefits for VT. Third, there are few high quality trial level

data on patient-centred outcomes for VT ablation such as those reporting on improvement in symptom burden, functional capacity or quality of life. Finally, and somewhat concerningly, as we have described previously, despite numerous advances in our procedural toolkit and capabilities over the last thirty years to perform CA for VAs, meta-regression studies of these, and observational studies suggest no statistically significant incremental improvement in VA free survival by publication time.[13] In fact, if we were to compare outcomes of CA in an early report of linear ablation of low voltage scar by Marchlinski et al. published in 2000,[19] which established the role of three-dimensional EAM for CA of VT in a mixed cohort of 16 patients (44% of whom had NICM) to a modern RCT PAUSE-SCD (75% NICM)[208] where CA was guided by endocardial-epicardial mapping where needed, modern multielectrode catheters and functional substrate delineation techniques, there were similar rates of VT recurrence between the two studies at 8 months (approximately 80% freedom from recurrence). Further innovations may be the key to improving these outcomes, whether it be in substrate delineation or in better technologies to abolish the arrhythmogenic substrate, but such innovations will need future validation in representative RCTs which are often very difficult to design and complete.

## 1.5 Invasive assessment of ventricular arrhythmogenic substrate

Invasive assessment of the ventricular arrhythmogenic substrate can be divided into two strategies; mapping of the induced arrhythmia to delineate its precise circuitry, which is herein referred to as arrhythmia mapping and identification of surrogates of these circuits, referred to as substrate mapping. The latter is often required as many VTs are haemodynamically unstable and do not encompass a single mapped ventricular surface, preventing delineation of the entire VT circuit. Prior to modern EAM, these procedures were first performed during open heart surgery with direct visualisation of scar[113,182] and then subsequently guided by fluoroscopy. These

procedures were facilitated by recording of intracardiac electrograms using catheters tipped with electrodes which allowed direct sampling of the myocardial electrical activity directly below the recording electrodes.

### *1.5.1 Electroanatomic mapping*

Three-dimensional (3D) EAM has been a transformative technology to guide VA CA, which allows non-fluoroscopic depiction of the electrical myocardial activation of the heart in 3D space using either magnetic fields or tissue impedance. Ben-Haim described this innovation, which lead to the CARTO mapping system (Biosense-Webster) in his seminal publication in1996, which allowed mapping of an intracardiac chamber with as little as 40-60 points.[218] This technology uses magnetic fields generated by coils placed around the supine patient that can track the location sensor embedded within the tip of the mapping catheter, so as to triangulate its position in 3D space. Multiple vendor technologies now allow tracking of both mapping and ablation catheters, which allow linking of electrical information with their exact anatomical location. More recently, intracardiac echocardiography[219] and pre-procedural imaging with CMR or MDCT[220] can also be integrated into these systems such that electrical, functional and anatomical data can be precisely integrated to delineate VA circuits and substrate. Advances in catheter technologies including multielectrode mapping, contact force sensing, and automated EAM point collection have further revolutionised the invasive assessment of VA substrate and now many thousands of electrograms are acquired at ultra-high density during routine VA CA. Despite these enormous data, it is important still to remember the fundamental electrophysiological concepts guiding generation and interpretation of these electrograms and the important limitations and assumptions guiding their use which we will review below.

### *1.5.2 Intracardiac electrograms*

Intracardiac electrograms are generated by the potential difference in voltage between two recording electrodes, clinically defined as the difference between the positive anodal and negative cathodal input. Unipolar electrograms describe potential difference between the catheter electrode which is in contact with the myocardium and an indifferent remote electrode which has no cardiac signal.[221] This can be virtual (Wilson central terminal) or an electrode placed in the inferior vena cava. As, by convention, the recording electrode is connected to the recorder as the positive electrode (anode), a wavefront of depolarisation travelling towards this electrode generates a positive deflection, which then becomes steeply negative as the wavefront reaches and then travels away. In this way, the maximum negative slope (−dV/dt) of the electrogram signal can be considered to coincide with the arrival of wavefront directly beneath the catheter electrode (though this assumes uniform conduction through the tissue). Unipolar electrogram are deemed to have a larger field of view (that is, sample myocardium and increased depth and width from the recording electrogram). Recent co-registered CMR studies of infarcted swine suggest that conventional unipolar electrogram amplitude alone can have a field of view of 10mm for correlation of viable myocardium with voltage,[222] though it remains to be seen if alternate electrogram characteristics beyond voltage may improve this performance. There are however several caveats to interpretation of unipolar electrograms which include that they are sensitive to artefact on the indifferent electrode as well as respiratory and cardiac motion, localised current of injury and can be obscured by cardiac repolarisation. Importantly, because of their field of view, they contain substantial far-field signal from tissue remote from the recording electrode which can obscure localised wavefront activation within scar.[221] Although conventional wisdom suggests that electrode size can also influence the unipolar electrogram field of view, more recent data suggest little difference between conventional and micro-electrodes using the QDOT catheter,[222] probably because both electrodes

are orders of magnitude larger than the depolarising myocytes. Finally, filtering can also dramatically alter the shape of the unipolar electrogram.[223]

Bipolar electrograms depict the potential voltage difference between two electrodes on the myocardial surface, which are determined by subtracting the unipolar electrogram of one electrode from another. As the far field signal is theoretically similar in both unipolar electrograms of the two closely spaced recording electrodes, their subtraction is thought to depict the local signal at the site of the intracardiac catheter. This leads to improved near-far field resolution (lower signal-noise ratio) though at the expense of obscuring far field substrate.[59,70,224] The field of view of modern multi-electrode catheters with close inter-electrode spacing is approximately 5mm when validated by MDCT scar.[224] A further important caveat of these bipolar recordings is the concept of bipolar blindness as these electrograms are dependent on wavefront direction when compared to unipolar signals.[225] A wavefront of activation parallel to recording electrodes may for example result in no recorded signal, discrepant to the voltage recorded if the wavefront was oblique or perpendicular.[226] This thesis will review the fundamental assumptions and caveats to mapping bipolar electrograms within this section, which include dependence on electrode size, shape and spacing, contact force and angle between recording electrograms and the myocardial surface and myocardial wall thickness.

### *1.5.3 Arrhythmia mapping*

Arrhythmia mapping to identify either the circuitry of re-entrant VT or the focal origin of an automatic or triggered activity can help to precisely localise critical sites and targets for CA. It is the conventional strategy for CA of VA with purported benefits of limiting ablation lesions, identifying VT substrate where substrate mapping in sinus rhythm may underappreciate functional lines of block and finally helping to confirm that the targeted tissue is clinically relevant (when

arrhythmia terminates during ablation). Indeed, many of the original studies that established substrate mapping (an alternative approach), still relied upon arrhythmia mapping in the first instance after which surrogates of arrhythmogenic substrate such as late or fractionated potentials were targeted.[20,227] Newer technologies have improved our ability to map these arrhythmias with multi-electrode catheters, more accurate time annotation of multi-component electrograms and automated point acquisition at high density. Regardless of these technologies however, many VTs are not haemodynamically tolerated, and may not be inducible in the setting of background AAD use. Hence substrate mapping has become a major component of modern VT ablation. Recent data suggests superiority of extensive substrate ablation in comparison to limiting CA to well characterised VT circuits.[228] A randomised study in a mixed cohort with SHD found that VT arrhythmia mapping prior to substrate homogenisation prolongs procedural and fluoroscopy duration and the need for electrical cardioversion without improving acute success or long-term outcomes. [229]

#### *1.5.3.1 Entrainment mapping*

Entrainment mapping of re-entrant VT can help to define components of the VT circuit including the entrance, common isthmus pathway and exit. It can be performed complimentary to other forms of arrhythmia mapping or to confirm the tachycardia circuit at sites of interest identified during substrate mapping. Outside of rare exceptions, entrainment, which is continuous resetting of a re-entrant circuit, is proven by fixed fusion of paced complexes at a constant pacing rate, progressive fusion at different pacing rates (more liked pure paced configuration at shorter cycle lengths) or conduction block to an orthodromic site that terminates tachycardia followed by activation of that site by a paced wavefront from a different direction.[230] Responses of the tachycardia to entrainment in the form of the post-pacing interval, QRS configuration during

entrainment (manifest or concealed fusion) and the stimulus to QRS interval (as well as this intervals relationship to the intracardiac electrogram to QRS interval during tachycardia and the tachycardia cycle length) can all be used to predict the position of the pacing site to the re-entrant circuit anatomy (which includes critical isthmus, entrance, exit, outer and inner loops and remote and adjacent bystanders) which has been proven formatively in post infarction VT by Stevenson and colleagues.[25] More recent data with high-density mapping however suggest that the isthmus as defined by entrainment may be overestimated (particularly at the exit sites).[110] Furthermore there are other well-recognised pitfalls to entrainment mapping including mistaking re-entry as the VA mechanism, assumptions of circuit capture, concealment of isthmus electrograms due to low voltage and filtering and oscillations in the tachycardia cycle length.[231]

#### *1.5.3.2 Activation mapping*

Activation mapping is performed by recording the timing of intracardiac electrograms at various sites of the chamber(s) of interest with respect to a fiducial timing reference. Often this is represented on a three-dimensional EAM by binning these activation timings to colour-coded reconstructions which subsequently helps to delineate the mechanisms and site of origin of these arrhythmias. The pattern of activation can help to suggest both mechanism and arrhythmia location. Focal activation patterns with a central early region and then radial spread could suggest an automatic or triggered activity focus or micro-re-entry, though a focal breakout of a VT re-entrant circuit from deeper within the myocardium could also be responsible. In contrast, re-entrant circuits completely captured on the mapped surface will demonstrate activation across the entire tachycardia cycle length.[110] As we have described, activation mapping of both endocardial and epicardial surfaces of re-entrant VT have demonstrated that many such circuits are three-

dimensional in nature,[15,69] which can be appreciated when there is a lack of activation timing points to cover the entire tachycardia cycle length (suggesting intramural involvement).

Despite its utility, several caveats for activation mapping need to be acknowledged. The first is uncertainty on annotation of timing on each electrogram. When using unipolar electrograms, the local activation timing (LAT) is defined as the point of maximal negative slope (−dV/dt) of the initial downstroke, correlating with the depolarisation of the cardiac action potential.[106] In activation mapping of re-entrant VT circuits however, to disregard far-field activation, bipolar electrograms are conventionally used to annotate LAT, if which maximal signal peak, maximal signal slope or electrogram onset can be tagged. In a comparison of differing strategies, identification of the maximal negative slope of unipolar electrogram within a predefined bipolar window seems to afford best automatic delineation of LAT.[232] In the event of an abnormal electrograms however with multiple components or significantly delayed components, such as seen in complex ventricular scar, correct annotation can be challenging.

#### *1.5.3.3 Pace-mapping*

Pace mapping involves the replication of clinical VA QRS morphology by pacing from different sites in the ventricle. This can be represented by a pace score or correlation value that quantifies how much the paced QRS beat matches the VA QRS morphology. In re-entrant VT, theoretically, pace mapping at the exit of the isthmus will produce a similar QRS to the VA whilst pace-mapping more proximally at the isthmus will produce a similar QRS complex but with a longer stimulus (stim)-QRS interval.[23] Induction of VA during pace-mapping, or multiple QRS morphologies, suggesting multiple exits from a pace-mapped site are functional pace-mapping phenomena that can identify sites critical for re-entry,[24] and ablation at these sites can portend good arrhythmia free survival. Furthermore, in post-infarction VT, De Chillou and colleagues have

demonstrated that an abrupt change in QRS morphology can identify the critical isthmus, as the pacing stimulus activates the isthmus in an orthodromic and then antidromic direction.[233,234] We have also shown that endocardial pace mapping patterns, which can be divided into an abrupt change (as suggested by De Chillou) versus centrifugal attenuation pattern can identify whether the VT isthmus is on the surface mapped by the catheter (abrupt change) or deeper (centrifugal attenuation).[235] The cycle length of the pace-mapping stimulus, as well as strength of the stimulus can also affect the pace-mapping response, with the most optimal match observed closest to the VT cycle length.[236] Importantly, Nayyar et al performed meticulous pace-mapping to interrogate channels conducive to versus with no evidence of re-entrant VT, demonstrating an almost 6 times higher likelihood of having a prolonged stimulus to QRS delay of >80 msec in VT channels (with such channels being longer and with faster conductive properties).[237] Outside of re-entrant VA, pace-mapping can also allow reasonable arrhythmia free survival during PVC ablation procedures where there is a paucity of spontaneous PVCs for activation mapping.[238]

### *1.5.4 Substrate mapping*

Given the limitations of arrhythmia mapping, substrate mapping is an important toolkit in CA of VA in SHD. The development of substrate mapping was predicated on early studies in both human and animals post-infarction. Fractionation of sinus rhythm electrograms was observed in canines after coronary artery occlusion in 1975[239] which was confirmed in human studies by Josephson et al. who observed fractionation and prolonged electrogram duration exceeding 100ms during sinus rhythm at sites conducive to VT.[240] Subsequently Fontaine et al described delayed sinus rhythm electrograms, which we now know as late potentials correlating with the earliest recorded activation of VT.[241] Observations that these abnormal electrograms were more frequently seen in patients post-infarction with inducible VT versus in patients without,[242] as well as that

these abnormal electrograms tended to co-localise with infarction border-zones[243] further suggested that these electrograms may be abnormal substrate conducive to catheter ablation. CA of the substrate responsible for VT using three-dimensional EAM was first proposed by Marchlinski et al. in their seminal paper in 2000 whereby linear ablation lesions were performed in areas of scar with low voltage for patients with haemodynamically unstable VA.[19] Since, there has been rapid accumulation of data and studies establishing the role of substrate guided CA of VT.

The first RCT to compare limited ablation guided by traditional arrhythmia mapping versus substrate homogenisation that targeted all abnormal electrograms in scar was published in 2015.[244] In the VISTA trial, 118 patients were randomised to clinical ablation guided by entrainment, activation and pace-mapping for clinical and stable induced VTs vs identification of abnormal electrograms including low voltage regions with subsequent extensive ablation for complete homogenisation. In this study, there was a higher rate of VT recurrence in the clinical arrhythmia ablation arm versus scar homogenisation (48.3% vs 15.5%). A follow up study randomised 48 patients to substrate ablation with scar de-channelling (without upfront VT induction) compared with traditional VT induction, arrhythmia mapping and then subsequent scar de-channelling, and demonstrated that ablation guided primarily by substrate mapping can reduce procedural duration and radiation exposure without cost to acute or long term success.[229] In the following section we will describe the various approaches, strengths and caveats of substrate mapping for VT.

#### *1.5.4.1 Peak to peak voltage*

Three-dimensional EAM to identify ventricular scar through abnormal bipolar peak to peak voltage was established by seminal work by Marchlinski and colleagues 25 years ago, where healthy human ventricles were mapped with a standard 4mm electrode tipped ablation catheter

(with a 2mm ring electrode and 1mm interelectrode spacing).[19] A healthy bipolar voltage cutoff (> 1.5mV) was established as the 5th percentile of all sampled healthy subject electrograms. An ablation strategy targeting low bipolar voltage areas (<1.5mV) as defined by this cutoff in a cohort of patients with SHD (44% of enrolled patients had non-ischaemic cardiomyopathy) using linear ablation lesions within the scar resulted in an impressive 75% VT free survival at median 8 month follow up. Subsequently, this technique was also used to define abnormal LV unipolar voltage (< 8.3mV),[245] endocardial RV voltage (<5.5mV),[246] and epicardial voltage (<1.0mV) by the same group.[247]

#### *1.5.4.1.1 Validation in of voltage mapping and scar – the role of whole heart histology*

Attempts to validate these voltage thresholds in large-animal studies have been met with variable results. In an early study, endocardial and epicardial low voltage scar as collected by a 4mm tipped ablation catheter seemed to correlate well with macropathologic scar area assessment in swine with healed myocardial infarction.[57] Tschabrunn et al. performed a histological and CMR validation of voltage mapping using both standard 4mm ablation catheters and a modern multi-electrode catheter (Pentaray) in a swine study, finding that the total area of low bipolar voltage scar (defined as <1.5 mV) was 22.5% smaller using the 1-mm multielectrode catheters (21.7 versus 28.0 $cm^2$; P=0.003), suggesting the impact of electrode size and spacing on voltage.[248] When there was discordance between the conventional and multi-electrode voltage maps, CMR and histology tended to demonstrate less transmural scar and more heterogenous sub-endocardial scar, suggesting the complex interplay between scar substrate, scar depth, catheter characteristics and peak-peak voltage. The limitation of these micropathological assessments however is that precise co-registration of intracardiac electrograms with abnormal tissue, as well as understanding the underlying composition of this tissue is limited with gross scar area measurements. Glashan et al.

describe a technique of whole-heart histological co-registration whereby excised animal or human hearts are filled to maintain chamber dimension, fixed and then sectioned.[249] Photographs of the pathological sections can then be reconstructed using custom software into three-dimensional histology maps which can then be re-integrated into imaging and EAM studies. Further staining of these sections can then be used to identify viable myocardium, fibrosis and adipose tissue.

Using this technique, Glashan et al. demonstrated that bipolar voltage amplitudes are dependent on the amount of viable myocardium present and further, that the ideal bipolar voltage cutoff for abnormal viable myocardium is 1.27mV (rather than 1.5) for conventional electrode configurations, and then 2.84mV for closely space micro-electrodes on the QDOT catheter.[59] These micro-electrodes (0.167mm$^2$) tended to generate larger bipolar voltage amplitudes with the ability to detect discrete local activation separate from the far-field EGM. These techniques have also been applied in NICM, whereby Glashan et al. co-registered 8 NICM hearts (obtained either after death or transplantation) with EAM.[70] They found a wide variety of NICM scar patterns and furthermore, demonstrated the impact of wall thickness on both endocardial bipolar and unipolar voltage with an increase of 0.23mV (P=0.009) and 0.28mV (P=0.010) for every 1mm increase in wall thickness in transmural biopsies. Indeed, viable myocardium in the intramural or epicardial layers was shown to obscure bipolar voltage detection, with a 1mm$^2$ increase in the amount of viable myocardium beyond the 4mm sub-endocardium on transmural biopsy associating with a 0.05mV increase in bipolar voltage of 0.05mV (P=0.046). In a more recent post-infarction swine study, this group have also investigated whether there is a correlation between bipolar and unipolar voltage and scar geometric patterns, demonstrating in an ischaemia reperfusion model that unipolar voltage tends to better associate with transmural viable myocardium quantity than bipolar voltage when using a modern Octaray catheter.[250] Here, in contrast to previous validated thresholds for a

standard tipped ablation catheter, cutoff values of 3.7 mV (unipolar) and 1.0 mV (bipolar) in the LV tended to best associate with viable myocardium, suggesting the need for catheter specific voltage cutoffs. Most interestingly, bipolar electrogram morphology, frequently identified transmural biopsies with 2 layers of surviving myocardium (with interspersed scar).

EAM-CMR correlation studies further demonstrate the complexity of interplay between voltage and ventricular scar. Wijnmaalen et al have further demonstrated the limitations of traditional voltage thresholds in a cohort of 15 post-infarct patients with co-registered CMR and EAM.[251] They found that a median bipolar voltage <1.5mV obtained with a 3.5mm tip ablation catheter was only seen in scar that had more than 75% transmurality (which may be of less clinical applicability in modern early reperfused infarcts and NICM). Most importantly, Tung et al. demonstrated in a porcine infarct study with co-registered ex-vivo cardiac magnetic resonance imaging (CMR) that post-infarction scar is not only endocardial but has mid-myocardial and epicardial components.[252] They found modest sensitivity and specificity of voltage amplitudes to CMR-defined scar (57% sensitivity, 79% specificity for endocardial bipolar voltage < 1.5mV (2mm electrode spacing) and 81% sensitivity, 58% specificity for unipolar voltage <8.3mV). This was attributed to three dimensional spatial averaging, whereby low voltage may be the result of scar at a greater depth vs adjacent scar on the same surface. Furthermore, even within post infarction scar, the underlying cardiomyopathy can affect voltage. Sramko et al correlated EAM with a 4mm tip ablation catheter in 27 post-infarct patients, approximately half of whom had evidence of ventricular remodelling (abnormal left ventricular EF or volume).[253] The 5th percentile endocardial bipolar and unipolar voltage values in non-infarcted myocardial segments in non-remodelled patients were 3.0mV and 6.7mV respectively. In contrast, patients with remodelled LVs had lower bipolar and unipolar threshold values of 2.1mV and 6.4mV.

Given these data, which taken together demonstrate the impact of multi-electrode catheter composition, underlying scar substrate and cardiomyopathy and validation methodology (e.g. whole heart histology, macropathology or CMR), Campbell et al. investigated in an ovine infarct model with whole-heart histopathological and CMR correlation the accuracy of unipolar and bipolar voltage recorded on various multielectrode mapping catheters.[254] This study found that although grid array, multi-spline and linear electrode arrangements all have similar accuracy for the detection of viable myocardium, each catheter had unique voltage thresholds to best identify viable myocardium and compared with traditional voltage thresholds, use of catheter-specific thresholds significantly improved each catheter's accuracy for correctly identifying underlying viable myocardium on both LGE-CMR and histology by up to 20% for bipolar voltage and 75% for unipolar voltage.

It is still unknown how voltage or other bipolar or unipolar electrogram characteristics may perform to better describe histological post-infarction scar patterns and depth. Improved demarcation of ventricular scar topography (including its depth and location) would be advantageous, and it is plausible that electrogram features beyond voltage (given the complexity of interaction) may be useful to identify this topography.

#### *1.5.4.1.2 Voltage channels*

Given multiple studies that suggested that zones of slow conduction are frequently located within abnormal myocardium in dense scar,[103,255] Arenal et al. hypothesised that "conducting channels" of surviving bundles must have a larger voltage than the surrounding "dense" scar tissue and that careful step by step adjustment of the upper and lower bounds of 3D EAM bipolar voltage cutoffs for scar and dense scar could identify such bundles.[256] These authors correlated such voltage channels, which required a reduction of the dense scar voltage threshold from ≤0.5mV to

≤0.1mV with late potentials and VT circuits identified by pace-mapping. In a similar study, Hsia et al. soon afterwards interrogated voltage channels in humans with monomorphic VT and SHD, finding that VT isthmus sites reside predominately in the "dense scar," with voltage <0.5mV whereas most exit sites are located in the border zone (0.5-1.5mV).[257] Conducting channels colocalised with 56% of VTs with entrainment data, and again, hand-raking of voltage thresholds were required to identify these channels, whereby the optimal voltages used ranged from 0.1-0.7mV. Subsequently, in an important study mapping, Haqqani et al. demonstrated that ventricular substrate mapping of patients with sustained monomorphic VT demonstrated a 100% chance of identifying voltage conducting channels versus 59% chance of channels in patients without VT (P=0.015).[258] Based on these data, Berruezo and colleagues have demonstrated that CA targeting these voltage conducting channels, which they deemed "scar de-channelling," can lead to VT non-inducibility of VT in 54.5% of patients, with acute success increasing to 78% when combined with traditional arrhythmia mapping, with long term VT free survival of 80%.[259] Identification and ablation of CMR LGE channels have largely been predicated on the findings of these scar-de-channelling approaches.

#### *1.5.4.2 Local abnormal ventricular activities*

We have described foundational studies that established abnormal electrogram characteristics beyond voltage (described variously as "fragmentation" or "fractionation") as key markers of arrhythmogenesis,[239-243] and postulated to be caused by heterogenous activation of myocardial fibres interspersed amongst fibrosis[103,226] and fat.[128] Cassidy et al. established the bipolar electrogram characteristics of structurally normal hearts with endocardial mapping of 15 patients without evidence of SHD (3 of whom had idiopathic VT), showing that normal electrogram duration is less than 70 milliseconds with amplitude more than 3mV and no evidence

of splitting, fractionation or late potentials.[260] In comparison, in canine infarction studies Dillon et al. demonstrated that these fractionated electrograms are associated with sites of turning points at the entrance or exit of an isthmus during VT.[261] This concept, that fractionated, long electrograms in sinus rhythm correlate well with the isthmus barriers has also been shown by others,[262] though it should be noted that isthmus borders can just as often by functional rather than fixed, and hence obscured by only sinus rhythm mapping.[27] Furthermore, de Bakker et al. confirmed the co-localisation of late and/or fractionated electrograms with the diastolic pathway of induced VTs[255] and Stevenson et al. have demonstrated with pace-mapping in human post-infarction patients that sites with fractionation associated with slowed conduction (longer stimulus to QRS duration).[263]

Given these translational and mechanistic studies, it could be asked how often fractionated or late electrograms co-localise with critical sites of VT. Miller et al. demonstrated in human intraoperative studies that most abnormal electrograms at the site of mapped VTs were eliminated by resection of 2 to 3 mm of subendocardial tissue, with subsequent normalisation of half of nearby electrograms.[264] In 2006, Bogun et al. showed in a cohort of 19 patients with post-infarction VT that isolated late potentials were seen during sinus rhythm to co-localise with 40/41 distinct VT isthmii.[265] Follow up studies have demonstrated that these late potentials tend to co-localise with the mid-isthmus (89%) compared to entrance (57%) and exit (20%) sites.[266] In contrast however, Harada et al. found that these late potentials could also co-localise with bystander sites in the re-entrant circuit and that further, late potentials are found in only half of sites with successful termination of VT during ablation.[267] This is probably partially attributable to activation wave-front dependence of bipolar electrograms, as substrate mapping in this study was only performed in sinus rhythm. In contrast, in a mixed cohort of SHD patients with VT, Arenal et al. demonstrated that late potentials were uncovered in 96% of patients with pacing from the right ventricular apex,

compared with 55% with sinus rhythm mapping (P<0.01).[268] We also now know that abnormal electrograms can be unmasked not only with differing wavefronts of activation but also with earlier coupled extrastimuli, which will be covered in a later section.

A universal description of fractionated electrograms and late potentials was established by Jaïs et al who described them with the overarching term of local abnormal ventricular activities (LAVA).[20] Importantly in their description of fractionation, they also incorporated sharp buried potentials within otherwise normal large amplitude far field activation and further clarified their presence when there was uncertainty with pacing to separate the local and far field components. In this non-randomised study, complete elimination of LAVA in addition to abolishment of inducible VT demonstrated improved arrhythmia free survival (adjusted hazard ratio 0.49, 95% confidence interval 0.26-0.95, *P*=0.035).

#### *1.5.4.3 Functional mapping*

Given re-entry is the mechanism for the majority of VTs in SHD, and this phenomenon is predicated on regions of slowed conduction susceptible to unidirectional block, mapping of this "functional" substrate by characterising the underlying conductive properties of the myocardial tissue offers potential to improve VT CA.[208,269] This can be performed either through interpretation of sinus or paced rhythm activation maps or through assessing response of the myocardium to extra-stimulus pacing manoeuvres. From these strategies, multiple functional mapping techniques have been described which include identification of zones of slowed conduction (deceleration zones – DZ),[270-272] regions with wavefront discontinuities,[273] repolarisation and re-entry vulnerability mapping,[274,275] regions with cumulative activation slowing in multiple wavefronts,[276] measures of electrogram duration[277] and finally identification of decrement,[26] hidden slow conduction,[278] or hidden substrate[279] with extra-stimulus pacing manoeuvres.

#### *1.5.4.3.1 Isochronal late activation mapping to identify deceleration zones*

In 2015, Irie et al. (2015) challenged the assumption that the latest potentials during activation mapping in sinus or paced rhythm marked areas with the slowest conduction or with highest specificity for re-entry.[270] In a mixed cohort of 33 patients (with 47 critical sites of VT where VT termination could be appreciated during ablation), they created retrospective isochronal late activation maps (ILAM). Here they annotated the local activation time on the EAM system to the *offset* of the bipolar EGM, chosen to represent completion of local activation by encompassing late potentials, and due to inter-observer reliability. Hawson et al. (2024) very recently compared ILAM maps with annotation at the earliest bipolar electrogram, peak of the bipolar electrogram voltage, latest bipolar electrogram and steepest −dV/dt (with or without a dynamic window of interest to better identify latest potentials) and demonstrated the validity of the Irie et al. approach (though annotating to earliest and peak had similar performance).[280] For the Irie et al. study, the activation map was binned into 8 coloured isochrones (whereby 12.5% of the activation map was encompassed by a single isochrone).[270] They found that only 11% of critical sites were localised to the latest isochrone of activation, whilst the majority were in the second and third latest isochrones (36% and 28% respectively). Isochronal crowding with 3 or more isochrones within a 1cm distance (deemed DZs) were found at critical VT sites.

This preliminary work was then validated by this group in a prospective cohort of 128 patients with SHD where the definition of DZs was further refined to require presence of LAVA or split electrograms in addition to isochronal crowding.[271] In almost half of cases, 3 or more discrete DZs were observed. Ablation of this functional substrate in addition to targeting clinically induced VT resulted in long term freedom from recurrence in 70% of patients in this mixed cohort of NICM and ICM. More recently, this group has demonstrated with differential pacing at sites of

DZs that most VT isthmus boundaries have lines of block identifiable in baseline rhythm, primarily supporting a predominantly fixed rather than functional nature of circuit boundaries.[272] When combined with simultaneous endocardial and epicardial mapping, the authors demonstrated that these elicited lines of block act as depth boundaries for intramural isthmi in cases of three-dimensional VT. Based on these data, the two-dimensional concept of the re-entrant VT circuit was revised into a three-dimensional hyperboloid shape.

ILAM has been rapidly adopted into clinical practice and was used in the PAUSE-SCD clinical trial,[208] which has helped to establish the role of early VT ablation in SHD. It has been adopted into mechanistic work to understand the drivers of atrial arrhythmias.[281,282] Our understanding of the interplay between anatomy and physiology for establishment of arrhythmogenic substrate for VA has also been further advanced with multiple imaging studies, which have shown co-localisation of DZ with CT wall-thinning[283] and LGE-CMR channels.[284] In the latter study, Vázquez-Calvo et al. demonstrated that DZs are highly correlated with CMR conducting channels, and that further, remapping of the ventricle after ablation of primary DZs can unveil new, hidden zones, the abolishment of which offers improved VT free survival.[284] These authors have also demonstrated that this same annotation technique can be applied to extra-stimuli maps (both a first and second extrastimulus) with further unmasking of DZs co-localising with CMR channels.[285]

There are still some unanswered questions with regards to the ILAM approach. First, in the establishment of this methodology, the authors described 13 cases where ILAM was performed with two distinct wavefronts, and in these cases, there was concordance of DZ locations in 86%. A systematic comparison of the effect of sinus rhythm, RV pacing and LV pacing on DZ identification has not been performed. Second, there has been no histopathological assessment of

tissue characteristics at sites with DZs. In the context of multiple hypotheses for the driver of slowed conduction (myocyte disarray due to fibrosis, or lipomatous metaplasia), a co-registered EAM to histopathological model would further advance our knowledge of this knowledge gap.

#### *1.5.4.3.2 Wavefront discontinuities*

Canine and human non-contact and contact mapping studies by Ciaccio et al. have demonstrated that discontinuities in the sinus rhythm activation map co-localise to VT isthmus boundaries.[286-288] This is readily appreciable on the CARTO proprietary mapping system with the early meets late module, which has been deemed to allow wavefront discontinuity line (WADL) mapping.[273] The automated module can be used to visually delineates regions where adjacent points are separated by a custom annotated timing difference, which in their validation study Maher et al, set as 25-35% of the total mapped activation time. Similar to DZs, 74% of critical VT sites co-localised with WADL, the ablation of which afforded freedom from VT recurrence in 69% of patients at 12 months of follow-up.

#### *1.5.4.3.3 Extrastimulus pace-mapping*

Beyond examining activation wavefront, an alternative physiological functional substrate mapping approach can be to assess myocardial tissue response to electrophysiological stress with closely coupled extrastimuli, which can identify regions with decrement and conduction block. In an early study of superfused rabbit atria, Lammers et al. demonstrated that a single premature stimulus with significant decrement could correlate with initiation of tachyarrhythmia.[289] In a study of patients with hypertrophic cardiomyopathy, Saumarez et al. found prolongation of the ventricular electrogram with increased prematurity of the extra-stimulus beat, associating with tendency for clinical VF.[290] Subsequently Jaïs et al. demonstrated that with pacing, local sharp

potentials could be separated from the far-field ventricular electrogram and that abolishing such sites improved VT free survival.[20] This method was further refined by work by Jackson et al. who leveraged intraoperative post-infarction mapping in 6 patients to demonstrate in elegant electrophysiological studies progressive delay of late potentials with delivery of an earlier coupled extra-stimulus, until block, reversal of the activation wavefront and then initiation of re-entrant sustained monomorphic VT.[26] These were deemed decrement-evoked potentials (DeEP) and regions with DeEP had higher specificity for the VT diastolic pathway than late potentials, with a specificity of 95% when assessing points with greatest decrement. In a prospective clinical validation study of 20 patients with ICM, this team showed DeEP guided ablation led to a 75% freedom from VT recurrence at 6 months.[291] Most recently, Bhaskaran et al. have demonstrated in an ischaemia reperfusion swine model with whole chamber DeEP mapping that DeEP sites co-localise with CMR channels early post-infarction (58 days), with significantly greater decrement within vs outside channels (115 ± 31 ms vs 83 ± 29 ms; $P < 0.001$).[292] Alternative approaches to extra-stimulus functional mapping have been described including introducing an extrastimulus 20-60ms above ventricular refractoriness after an RV paced drive train to assess for conduction delay greater than 10ms or block, deemed evoked delayed potentials.[279] Finally, early coupled extra-stimulii during sinus rhythm have also been interrogated, which may avoid priming of the myocardium with the RV drive train.[278,293]

### *1.5.5 Intracardiac echocardiography*

A creative approach to substrate mapping is the use of intracardiac echocardiography (ICE), which was traditionally used for assessment of cardiac anatomy live during CA as well as to monitor catheter location/contact and ablation lesions. Certain proprietary softwares allow integration of ICE created model anatomy into the EAM. In post-infarction swine models, ICE has

been used to delineate infarction scar.[294] Echogenicity, wall-thinning and regional wall motion abnormalities can be used in ICE to determine scar[219] and its depth.[235] Hussein et al. demonstrated in a mixed cohort of 22 patients that scar by voltage criteria had increased signal intensities compared to border zones (149 signal intensity units vs 104, $P < 0.0001$) and normal myocardium (88 signal intensity units, $P < 0.0001$).[295] Signal intensity ≥137 SIU differentiated scar from non-scar zones (area under curve 0.91, $P < 0.0001$). Further, in a cohort of 38 ICM patients in the SOUNDSCAR study, ICE-defined scar parameters such as end-diastolic and end-systolic wall diameter, end-systolic wall thickening, slope (end-diastolic to end-systolic wall thickening), and wall motion scoring all correlated strongly with EAM-defined scar (voltage <1.5 mV).[296] These authors showed in a further prospective cohort of 21 patients, ICE-guided ablation was associated with shorter procedure times and comparable VT-free survival.

### *1.5.6 Computational analyses of the intracardiac electrogram*

With improved computational speed, accuracy and cost, our understanding of mechanisms of VA with in-silico modelling and the ability to process electrograms and integrate these analyses live into the EAM have improved. Some examples of such techniques include omnipolar mapping, multipolar mapping and peak frequency analyses. These techniques help to address some of the current limitations to invasive EAM.

#### *1.5.6.1 Omnipolar mapping*

We have discussed the impact of wavefront on conventional bipolar mapping previously. Masse et al. (2016) established an alternative computational technique of calculating an "omnipolar" electrogram. Local unipolar electrograms are obtained from a group of 3 electrodes (cliques) from which the myocardial electric field is derived along the myocardial surface.[297,298] This technology allows for determination of the wavefront direction and conduction velocity under

the recording electrodes (without need for isochronal activation maps). Further, omnipolar voltage is not susceptible to wavefront direction like bipolar mapping. The utility of omnipolar mapping versus conventional bipolar mapping for VT substrate identification during clinical CA has been assessed recently.[299] These authors found that omnipolar technology unveiled higher voltages in both ventricular chambers and in the epicardium, with significantly smaller low voltage areas (<1.5mV). Importantly, without histological validation, it is difficult to know what the optimal voltage thresholds should be for omnipolar mapping. Furthermore, omnipolar mapping performed better to identify abnormal electrograms, with less false positive automatic annotation of omnipolar electrograms (21.9% bipolar vs 6.8% omnipolar) and greater specificity of omnipolar late potentials to diastolic VT pathways (79% vs 63% bipolar). Functional mapping of DZ was also better to identify VT critical sites compared to the same mapping with bipolar electrograms.

#### *1.5.6.2 Multipolar mapping*

A novel computational approach to improve signal resolution and attenuate far-field electrograms is multipolar mapping. This strategy leverages the concept that with multi-electrode catheter mapping, each activation beat gives multiple electrograms recorded at relatively close yet unique locations. Theoretically near field local potentials will demonstrate spatiotemporal propagation whilst the far-field activated myocardium will be detected by all closely spaced electrodes at a relatively similar time. Using principal component analysis, a dimensionality reduction and machine-learned method, unipolar electrograms from adjacent electrode clusters are compared, with far field components subtracted such that the multipolar electrogram demonstrates the local unipolar waveform. This also allows assessment of wavefront direction. Using a grid catheter, Anter et al. demonstrated better annotation of electrograms to local activation and

histopathology compared to bipolar electrograms. This technique has not been validated in any large clinical cohorts of VA CA.[300]

#### *1.5.6.3 Peak frequency analyses*

Recent clinical studies have highlighted the importance of frequency analyses in identifying VT regions of interest using the Ensite X Omnipolar technology's near-field algorithm, which employs wavelet transform to automatically identify peak frequency. Using this algorithm, low voltage area peak frequency >220Hz has been shown to have 91% sensitivity and 85% specificity for detecting late potentials and LAVA and could predict deceleration zones in 9 out of 10 patients.[301] However, a further study by Mayer et al. demonstrated that low voltage area peak frequency >200Hz showed lower performance in identifying the VT isthmus (sensitivity 69%; specificity 64%).[302] Further, peak frequency analyses of VT activation maps indicated that sites with peak frequency >405Hz during VT predicted VT termination within 5 seconds during ablation (AUC 0.811), likely due to higher peak frequencies identifying near-field VT circuitry.[303] Given these conflicting results, likely more study is needed to identify the role of frequency analyses in understanding VA substrate. In fact a recent study by Tonko et al. (2024) found that peak frequency analyses alone could not differentiate the dominant VT site from low-voltage bystander sites.[304]

### *1.5.7 Artificial intelligence and machine learning*

Throughout this review, the complexity of the cardiac electrophysiological mechanisms underpinning ventricular arrhythmogenesis are clear. Also important to understand is the volume and variety of multi-modality data that is available to the cardiac ablationist treating VA. EAM, pre-procedural imaging (including MDCT, CMR and echocardiography), ECGs and the electronic health record generate many gigabytes worth of data for a single patient which must be readily interpreted to identify who is suitable for which treatment and determine, live, where and how the

electrophysiologist wants to treat VA with CA. There is a rapidly evolving recognition that with improved computational power, novel strategies can be used to answer these fundamental questions. Excitingly, artificial intelligence (AI) offers a new frontier in understanding and delineating the arrhythmogenic substrate responsible for VA.

AI despite its current exponential popularity, is not a novel concept, and defines the capability of computational systems to solve and perform cognitive tasks originally deemed to require human minds (such as learning, reasoning, problem-solving, perception, communication and decision making).[305] Within this broad field of AI, machine learning is a sub-field aimed at the study of statistical algorithms and models that can independently learn to make predictions on new data based on data it has previously analysed.[306] Machine learning allows systems to improve their performance on tasks without being explicitly programmed for each specific task. More specialised still is deep-learning, whereby specialised neural networks (inspired in part by biological neural networks) can process data to perform classification, regression and generative tasks from either labelled (supervised) or raw unstructured (unsupervised) data. Here, features of interest are learned directly by the algorithm and are not defined by the computer scientist.

The role of these approaches in addressing the fundamental problems of cardiac electrophysiology have been extensively reviewed,[306-309] including in a recent state of the art scientific statement co-authored by the European Heart Rhythm Association, Heart Rhythm Society and European Society of Cardiology working group in e-Cardiology [310] As it is not feasible in this review to extensively document advances in AI approaches to cardiac electrophysiology, here we will review the role of AI, machine learning and deep learning in ECG analyses, electroanatomic mapping and VA management and finally in imaging studies pertinent to VA.

#### *1.5.7.1 Machine learning of 12 lead electrocardiograms*

Many applications of AI have been applied to processing of ECGs including single lead rhythm strips, multi-channel telemetry recordings and formal 12 lead ECGS.[307] In a landmark study in 2019, Attia et al. demonstrated using a convolutional neural network (CNN) trained on 8 ECG leads (lead I, II, V1-V6) in 180,922 patients with 649,931 normal sinus rhythm ECGs to predict atrial fibrillation from the normal sinus rhythm ECG (with an AUC of 0.87).[311] Subsequent studies demonstrated that ECGs could also predict mortality at 1 year.[312] Yao et al. demonstrated in a cluster RCT that AI enabled processing of 12 lead ECGs would lead to earlier diagnosis of reduced ejection fraction compared to standard screening.[313] Pertinent to VA, Lampert et al. demonstrated in a 14,241 patient cohort using a pretrained ResNet neural network machine learning model (ResNet-152) that the 12-lead ECG alone can accurately predict new-onset cardiomyopathy in patients with PVCs independent of PVC burden.[314] Importantly, explainability analyses of this model using GradCAM showed that the QRS complex and ST-segment in sinus rhythm rather than the PVC morphology itself was most useful for model performance, suggesting that abnormal excitation-contraction coupling, calcium handling, or autonomic dysregulation preceding the PVC may portend cardiomyopathy development.

Despite these exciting results, there are important caveats to AI assisted ECG technologies that need mention. First, for generalisability, these models should best be validated in external datasets in diverse populations.[310] Second, prediction for predictions sake will not improve patient outcomes and these translational discoveries need to be linked to actionable changes in management that are shown, preferably in RCTs to improve patient outcomes. Third, risk of perpetuating bias with such technologies needs to be remembered.[315]

#### *1.5.7.2 Machine learning for treatment of ventricular arrhythmias*

Machine-learning approaches offer an avenue to better understand and predict risk of sudden cardiac death,[316] which may be abrogated with use of an ICD. Through the use of multiple custom neural sub-networks incorporating CMR and clinical covariates such as age, sex, EF, cardiovascular risk factors, medication use and ECG measurements, Popescu et al. demonstrated that individualised patient survival curves could be generated, with a concordance index of 0.74 in an independent test set.[317] This same group has demonstrated the efficacy of using multimodality imaging (positron emission tomography and CMR) and clinical biomarkers in a supervised multivariable classifier to predict sudden cardiac test with testing results of 60% sensitivity [95% confidence interval 57-63%], 72% specificity [95% confidence interval 70-74%], and 0.754 AUC [95% confidence interval 0.710-0.797] in a cohort of 45 patients with cardiac sarcoidosis.[318] Alternatively, Rogers et al. have tackled the prediction of sudden cardiac death with machine learning interpretation of invasively obtained ventricular monophasic action potentials. These signals were processed using the tsfresh (Time Series FeatuRe Extraction on basis of Scalable Hypothesis, version 0.20.3) Python package to identify features that could be processed by support vector machine and CNN algorithms to predict sudden death.[319] They found in patient level predictions in independent test cohorts an AUC of 0.90 for sustained VT/VF (95% confidence interval 0.76-1.00) and 0.91 for mortality (95% confidence interval 0.83-1.00). This process to date has not been applied to intracardiac electrograms.

An obvious application of machine learning techniques for management of VA is to help localise the VT isthmus and sites of origin of PVCs. Yokokawa et al. attempted to solve this problem in post-infarction VT, with input of 12 lead ECG pace-mapping in low voltage scar to correctly identify VT exit in a 10 segment model.[320] Performance of this model was only moderate

with validation in 33 patients demonstrating an accuracy of 71% for localising a VT exit site to a 15cm$^2$ region, which may have been due to small input data size and the complexity of post-infarction ventricular scar. More recently, Sapp et al. created a software platform to intraprocedurally process endocardial LV pace-mapping to localise exit of scar-related VT, validating prospectively that such a model could localise a VT exit site with a mean error of approximately 9 mm.[321,322]

As these approaches can be applied to ECG and monophasic action potentials, it is plausible to consider the application of similar strategies to bipolar and unipolar electrograms to identify arrhythmogenic substrate. Wavelet and Fast Fourier transformation of epicardial unipolar electrograms derived from multielectrode plunge needles in an ovine model suggest that higher frequency spectra are associated with myocardial tissue heterogeneity and increased propensity to ventricular tachycardia.[323] Machine learning aided frequency analyses of unipolar electrograms derived from an ablation catheter had an average within patient AUC of 0.841 for mid-myocardial fibrosis in non-ischaemic cardiomyopathy (0.591 for unipolar voltage alone).[324] It is therefore plausible that a CNN applied to electrogram time series could further extract hidden features to better delineate substrate. The only study to assess individual intracardiac electrograms using deep learning was performed by Ntagiantas et al. [325] They applied a feed forward CNN with an Encoder-Decoder architecture to assess the performance of computer-simulated atrial electrograms to identify tissue conductivity and fibrosis and showed that an array of concurrent simulated unipolar electrograms can identify underlying atrial scar, supporting, the plausibility that deep learning networks can infer the structural properties of tissues (albeit in an in-silico model). Importantly, these analyses did not incorporate bipolar electrograms, and further, did not utilise biologically

obtained electrograms with ground-truth histology. Whole-heart histological reconstructions in animal and human hearts with co-registered EAM offers the potential to extend this work.

## 1.6 Non-invasive assessment of ventricular arrhythmogenic substrate

Whilst invasive EAM allows for detailed electrophysiologic assessment of the substrate that can give rise to VA, in the previous section we have identified significant limitations and caveats that need to be acknowledged including the impact of electrode size and spacing, angle of wavefront to recording electrodes, catheter contact, filtering and wall-thinning.[27] The integration of cardiac imaging with EAM allows for the opportunity to co-register anatomic and imaging defined scar substrate live during the case (image integration) to guide substrate delineation. Multi-modality imaging can be harnessed to this end including CMR, MDCT, positron emission tomography (PET) and echocardiography.

### *1.6.1 Cardiac magnetic resonance imaging*

#### *1.6.1.1 Late gadolinium enhancement*

Early animal and human studies have established that in post-infarction cardiomyopathy, late gadolinium enhancement (LGE) in CMR can be used to identify the "peri-infarction" or border zone of myocardial scar which has been deemed to contain viable myocardium[326,327] and predict the presence of inducible VT.[328] In 2006, Yan et al. found that in post-infarction patients, the extent of the peri-infarct zone characterised by LGE CMR provides incremental prognostic value for survival beyond left ventricular systolic volume index or EF.[329] Early studies validating LGE-CMR were performed with side-by-side comparison to gross macropathological scar area with the LGE CMR segmented into binary (scar, no scar)[330-332] definitions based on various full-width half maximum, percentage signal intensity or standard deviation segmentation methods. Though there

can be differences in scar areas based on the quantification method to identify enhancing vs non-enhancing myocardium,[333] differences in their performances to identify functional tissue have not been shown to be significantly different.[334] More recently, Pop et al compared ex vivo LGE and diffusion-weighted imaging CMR in an infarct swine model (n=5) with picrosirius red stain-identified collagenous fibrosis.[335] Using n=9 short-axis slices, they found that a ternary classification of LGE into scar, borderzone, and normal tissue demonstrated a good correlation between imaging-defined scar and borderzone area with histology. Unfortunately, this study was performed with ex-vivo CMR limiting generalisability to clinical cases and without whole-heart histological co-registration. Taken together these data establish the possibility that LGE scar could be of use in VT CA for SHD.

Ashikaga et al. were the first to integrate ex-vivo and in-vivo LGE CMR obtained on a 1.5T machine with invasive EAM (activation maps of VT).[336] Hyper-enhanced regions on the ex-vivo CMR (which had sub millimetre slice thickness) were identified as regions with LGE signal intensity more than 6 times the standard deviation and then extracted using custom software. These studies showed that epicardial re-entry isthmii were characterised by a small channel of viable myocardium bound by the scar tissue at the infarct border zone or over the infarct.

Based on their work describing voltage conducting channels,[256] Perez-David et al. hypothesised that LGE-CMR conducting channels (CMR-CCs) could be identified non-invasively by thresholding LGE signal intensity (SI). 18 post-infarction patients with sustained VT and without ICD were recruited and LGE-CMR performed on a 1.5 Tesla scanner. Delayed enhancement imaging was performed 10-15 minutes after gadolinium administration at 5mm slice thickness. Dense scar was quantified to have SI greater than 3 standard deviations and borderzone (which authors deemed heterogenous tissue) 2-3 standard deviations. In this prototypical study,

CMR channels were identified by expert operators on visual inspection and defined as corridor of borderzone tissue in consecutives slices surrounded by scar and connected to normal myocardium by at least one side. Perez-David found that compared to a matched control group, a significantly higher proportion of patients with VT had these channels (88% vs 33%, $P$=0.0006). Within CMR-CCs fractionated potentials were noted, with more delayed activation in the centre of these channels compared with the entrances (167±33 msec vs 118±28 msec, $P$<0.0001).

Concurrently, Andreu et al. published their experience with CMR integration in 10 patients (again without ICD implantation) with post-infarction cardiomyopathy and sustained VT who underwent LGE CMR in a 3 Tesla machine a mean 3 days prior to VT CA. The CMRs were performed at very fine slice thickness (1.4mm). The scar was segmented with custom software (that eventually led to the development of the proprietary ADAS 3D software (Barcelona, Spain) ,which is now used clinically for VT CA). The authors post-processed LGE sequences using the full-width, half-maximum method and compared dense scar voltage area against voltage scar, finding that a 60% threshold of the peak SI to denote core scar and 40% threshold for borderzone yielded the highest correlation to traditional voltage scar definitions ($r^2$=0.827, $P$<0.001) and the best agreement, when compared with 50% and 70% thresholds. These thresholds have since become the conventional markers for dense scar and border-zone, though they have not been validated by histology. In fact, more recent studies have demonstrated large variability in scar patterns with adjustment of dense scar and borderzone thresholds,[337] emphasising further the need for systematic histologically co-registered data to establish the validity of image integrated scar and channels.

Despite these concerns, soon after these findings, this same group validated their approach to identifying CMR-CCs, demonstrating in a 21 patients with ICM that CMR-CCs identified 74%

of the critical isthmii of clinical VTs and 50% of all the conducting channels identified in EAM.[338] Follow-up observational clinical studies in larger cohorts have demonstrated that ablation targeting CMR-CCs could be a valid substrate homogenisation technique. In a larger cohort of 159 patients with scar related VT, a substrate homogenisation approach of "de-channelling" scar aided by CMR-CC ADAS 3D image integration had lower VT recurrence over a mean follow-up of 20±19 months compared to standard ablation (18.5% vs 43.8%, $P$=0.017).[339] In a more provocative study, this same group went on to demonstrate that a "CMR-guided" approach where upfront ablation of CMR-CCs was performed with subsequent traditional mapping and ablation if required led to lower VT recurrence rates with associated shorter procedural time and less fluoroscopy.[340] Both of these studies unfortunately are not randomised and further data is needed to establish clinical evidence for image integration with LGE CMR in VT CA.

Image integration of LGE-CMR can also be performed using custom or other proprietary software. Another solution is inHEART (Bordeaux, France), where CMR are shared on a cloud-based platform for segmentation by the commercial product team. Previous inHEART publications have reported a similar trilinear algorithm to ADAS-3D, (35% and 55% of maximum intensity for border-zone and dense scar respectively).[341] In an early validation of inHEART, Yamashita et al. found that 89% of VT termination sites co-localised to image defined scar.[342] There are no translational or clinical data that compares the two commercially available vendors that are commonly used for image integration.

Finally, some limitations of LGE-CMR image integration need to be acknowledged. Firstly, many patients undergoing LGE CMR have ICDs in situ which can cause significant artefact, particularly if they have concurrent CRT. Roca-Luque et al. have addressed this with the application of wideband cardiac magnetic resonance sequences, which allow adequate VT

substrate characterization to guide VT ablation with similar accuracy than conventional LGE-CMR in patients without an ICD.[343] Second these studies cannot be performed in patients with significant renal impairment due to risk of adverse events from the gadolinium injection. Third, though there are studies which have co-localised functional substrate including extra-stimuli mapping with 1 or 2 extrastimulii to CMR-CCs,[285] there are no RCTs that have established there role as improving VT CA. Voyage (NCT04694079) is a multi-centre study (principal site in Italy) seeking to recruit 103 patients. Recruited patients with VT from left ventricular structural heart disease with good CMR imaging will be randomized to either CMR guided or CMR aided ablation. Patients without CMR or with poor CMR imaging will be included in a third group (standard ablation arm). Primary outcome will be VT recurrence at 12 months. The trial protocol for this study has been published,[344] however, the status of the study is unknown as per ClinicalTrials.gov (no updates after expected completion). Finally, studies comparing whole-heart histological scar to CMR in NICM have shown that LGE-CMR can easily miss non-confluent scar even in areas where there is low amounts of viable myocardium.[70]

#### *1.6.1.2 T1 mapping*

Given the above limitations of LGE, an alternative mapping strategy to identify ventricular scar and substrate is mapping the T1 relaxation time. Here, extracellular volumes can be determined by comparing pre and post contrast T1 times, which can be used to indicate interstitial fibrosis.[345] Quantitative T1 mapping of the intraventricular septum has been shown to be an independent predictor of ventricular arrhythmia in both ICM and NICM in a cohort of 130 patients, a finding independent of LGE metrics.[346] Similarly T1 mapping has been shown to have excellent correlation with endomyocardial biopsy.[347] Most recently, Sramko et al. demonstrated in a cohort of 18 patients (8 NICM) that whole heart pre and post-contrast T1 mapping to determine

extracellular volume, had an inverse relationship with LV endocardial voltage.[348] Whilst in this study whole heart T1 maps could be registered with the EAM, further validation is required to see whether this could lead to more rapid, accurate or complete identification of critical sites of VT.

### *1.6.2 Cardiac multidetector computed tomography*

An alternative technology to CMR is contrast-enhanced MDCT which allows multi-parametric mapping of scar as well as accurate delineation of chamber anatomy, cardiac arterial and venous anatomy and extracardiac structures such as the phrenic nerve and oesophagus.

The first parameter that can be used with MDCT is wall-thinning. Due to submillimeter spatial resolution of MDCT (at less than 0.4 second acquisition time), this technology can identify wall thinning at high fidelity.[349] In their seminal study, Komatsu et al. established that wall thinning (in end diastole) less than 5mm had good correlation to endocardial low voltage.[350] Further, 87% of LAVA location within wall thinning regions. Ablation aided by MDCT identified wall thinning has been shown to improve acute procedural success and VT free survival, though the relative contribution of MDCT vs CMR is difficult to tease out.[342] More recently, Maher et al. tempered expectations for MDCT assessment of scar in a mixed cohort of SHD, finding that wall thinning is sensitive for functional substrate (DZs) in ICM (94.1% of primary DZs were located on areas of wall thinning) but not NICM (20% of DZs in NICM). Unfortunately, wall thinning channels had modest sensitivity for DZs (59% and 56% co-localisation with ICM and NICM DZs). This finding is supported by a study by Jáuregui et al who compared LGE CMR-CCs with wall thinning channels which they defined as thicker ridges of myocardial tissue surrounding thinner scar.[351] The sensitivity of CT wall thickness channels to identify CMR-CCs was 72% in transmural scar but fell to 36.4% in non-transmural scar ($P$=0.004), with CT failing to detect any channels in 36% of patients with only subendocardial scar. One way to overcome these limitations is to employ

computational post-processing of the CT maps to estimate conduction velocity and action potential duration.[352] Cedilnik et al. describe converting MDCT wall thickness maps into a patient specific digital heart twin from which virtual programmed electrical stimulation can be performed to simulate VT activation maps. In a cohort of ICM patients they found that 6 of 42 in-silico VTs matched patient mapped VT activation patterns. Taken together, these data suggest that wall thinning and wall thinning channels in MDCT can be used to guide CA mapping but are not sufficient alone for substrate mapping. Results of the InEurHeart RCT (NCT05225935) are anticipated soon. In this inHEART study, 119 patients with post-infarction VT have been randomised to either MDCT guided or standard no image integration ablation. MDCT image integration will be used to identify ablation targets (wall thinning channels and/or simulated VTs). The primary outcome is procedure duration. The study has completed enrolment with results expected May 2025.

The second parameter than can be used is hypoenhancement of the cardiac myocardium during the CT coronary angiogram phase. Ustunkaya et al demonstrated in a small cohort of patients with the aid of ADAS-3D that myocardial conduction velocity (estimated with endocardial mapping comparing the mapped point to 5 adjacent point) was associated with myocardial attenuation (2.9% decrease in conduction velocity per 10 Hounsfield unit decrease in attenuation; 95% confidence interval 2.3%–3.5%; $P < 0.001$). Hypoattenuated signals were more likely to associate with LAVA (odds ratio 0.89 per 10 Hounsfield unit increase; 95% confidence interval 0.85–0.93; $P <0.001$). Lead artefact and myocardial calcification limited assessment of the entire myocardium. Also, multi-electrode mapping was not used in this study which can affect near field resolution and detection of LAVA. Hypoenhancement on MDCT has not been validated in large

ablation cohorts. Furthermore, hypoenhancement can be used to identify lipomatous metaplasia which has been discussed at length in section 1.3.3.1.

The third parameter of use with MDCT is delayed hyperenhancement (similar to that seen with LGE in CMR). Esposito et al have shown reasonable concordance with hyperenhancement (derived from custom software) with low voltage areas on EAM, with better performance compared to wall thinning alone (sensitivity 84% vs 41%).[30] Further, abnormal electrograms localised to CT hyperenhancement scar segments in 79% of patients. More recently, Englert et al. have demonstrated a large observational cohort of patients with ablation guided by MDCT wall thinning and late enhancement using inHeart proprietary software vs EAM directed arrhythmia and substrate mapping. Within the usual caveats of a non-randomised study, they found a trend towards lower VT recurrence in the CT guided inHEART group (27% vs. 42%, $p < 0.06$).

### *1.6.3 Positron Emission Tomography*

Positron emission tomography (PET) studies offer the potential to allow functional metabolic characterisation of myocardial scar tissue, including identification of metabolically active tissue,[353] active inflammation in cardiac sarcoidosis[354] and sympathetic innervation,[355] depending on patient preparation and scanning protocol. Image integration of PET scar assessment has been assessed by Ghzally et al. in post-infarction cardiomyopathy patients.[356] This group identified "metabolic channels" which they defined as corridors of abnormal metabolic activity traversing myocardium with less preserved activity (more than 10% lower than the channel itself), a similar concept to CMR-CCs and wall thinning channels. Though these channels were observable in all patients, only one third corresponded to VT isthmus or exits via EAM. Alternatively, areas with significant transition in metabolic activity (more than 50% uptake in PET

activity within 15mm) localised well to VT isthmus or exits. More data in larger cohorts are needed however to establish the use of this technique in VT CA beyond understanding mechanism.

## 1.7 Strategies to abolish ventricular arrhythmogenic substrate

### *1.7.1 Radiofrequency catheter ablation*

RF ablation is the main energy source for CA of VA, with delivery of electrical energy to targeted myocardial tissue inducing tissue heating and myocardial necrosis.[357] Energy is delivered as an alternating current oscillating at 500 kHz. The anode for delivery is a metal electrode located at the distal tip of an ablation catheter whilst the cathode is the skin patch which functions as a distal grounding electrode for unipolar ablation. This results in direct resistive heating at the tissue and electrode interface and progressive conductive heating at deeper myocardial layers. Lesion size has been shown to depend on the amount of power, duration and contact force with the myocardium. Multiple strategies have been employed to target deeper intramural scar substrate responsible for VA.

#### *1.7.1.1 Saline irrigation*

The multi-centre, Thermocool VT ablation trial evaluated the safety and efficacy of an externally irrigated RF ablation catheter, combined with an EAM system, for ablation of recurrent VT in post-MI patients.[200] In this study acute procedural success was 49% and freedom from recurrent VT at 6 months was achieved in 53% of patients. VT episode burden was assessed in ICD patients and showed marked improvement after ablation.[200] These results were replicated in the smaller multi-centre Euro-VT study where in a 66 patient cohort, similar VT recurrence rates of 49% were seen at 12-month follow-up.[358] Since these studies, irrigated ablation catheters are

widely used in CA of VA which tackle the issue of heating at the catheter-myocardial tissue interface, leading to char formation with attendant risk of thromboembolism.

Even though open irrigation catheters offer larger and deeper lesions than solid tip ablation, arrhythmogenic substrate critical for re-entry may still be deeper within myocardium and still difficult to reach with standard saline irrigated ablation catheters. Half-normal saline (HNS) is a higher impedance irrigant compared with the lower impedance blood pool allowing current to be further diverted into the myocardial tissue, allowing deeper lesion formation, though at the expense of "steam pops" where accumulation of steam bubbles trapped within or nearby myocardial tissue can culminate in an explosion with resultant cardiac perforation and damage.[359] This strategy was investigated in a multi-centre trial by Nguyen et al who used HNS to treat VA refractory to both standard unipolar and bipolar ablation.[360] Most VAs targeted in this study were in the septum, LV summit or intracavitary structures such as papillary muscles. HNS ablation achieved acute non-inducibility in 83% of patients and 1-year VA-free survival was 89%. In a recent evaluation of HNS where lesion delivery was strictly monitored for impedance change and by ICE, Hasegawa confirmed that this strategy could have acceptable rates of complication (4 patients with stroke and 2 steam pops requiring surgical repair).[361] Randomised data comparing normal and half normal saline would be beneficial.

#### *1.7.1.2 Simultaneous unipolar RFA*

Simultaneous unipolar ablation can be performed with separate RF generators and ablation catheters to allow a bridged heating effect.[362] Yang et al. describe the performance of this approach in a small cohort of 6 patients with NICM with septal substrate. Compared to failed sequential unipolar ablation, simultaneous ablation resulted in VT non-inducibility in all 6 patients with 67% VT free recurrence at 20 months and no acute procedural complications.[362]

#### *1.7.1.3 Bipolar ablation*

An alternative method for deeper lesion delivery is bipolar ablation which can be used after failed standard sequential unipolar ablation techniques.[363] This technique uses two catheters on opposite sides of the myocardium (such as endocardial and epicardially placed catheters, or across the intraventricular septum). The first catheter (cathode) delivers RF energy whilst the second (anode) functions as the return electrode, allowing focussed energy between the two catheters and creating deeper lesions.[364] This has been studied clinically in small series of patients. For example, Della Bella et al. found in a cohort study of 21 complex NICM patients with drug refractory VT from the septum, bipolar ablation resulted in termination of the clinical VT in 95% of cases and acute procedural success in 71%.[365] One patient had tamponade, and no steam pops were reported. Recurrence was seen in one third of patients at follow up but these VTs were not from the ablated septum.

#### *1.7.1.4 Intramural needle ablation*

Intramural mapping and ablation with a needle tipped catheter is another alternative to standard RF ablation to target deep substrate. RF energy can be delivered through a heparinised saline irrigated 27-gauge needle which can be extended between 8–10mm from the dome electrode of an ablation catheter.[366,367] A recent report of all patients who have been treated by this technique has been published by Tedrow et al. who described a total of 114 procedures including 3 second procedures was performed in 111 patients.[368] Needle ablation abolished the targeted PVC in 33 of 37 patients (89%), and reduced frequency to less than 5000 in 29 patients (78%). For patients with VT, in this complex cohort, improvement or abolition of VT occurred in 47%. One quarter of patients required additional RF ablation in addition to needle ablation. Adverse events included 4 pericardial effusions (3.5%), 3 cases of (anticipated) atrioventricular block (2.6%), and 3 heart

failure exacerbations (2.6%). 5 deaths occurred at follow up, but none were procedurally driven. Modest success with this approach, though granted in a complex cohort, drives the need for further innovation in CA of VA.

### *1.7.2 Pulsed field ablation*

Pulsed field ablation (PFA) is an emerging technology designed to cause irreversible electroporation of cell membranes, leading to cell death and lesion formation in both healthy and diseased myocardium.[369,370] Whilst designed to target cardiomyocytes, PFA has also been shown to affect the electrical conduction system and eliminate Purkinje fibre potentials, which can reduce vulnerability to ventricular fibrillation (VF).[371]

Important pre-clinical studies have established the ability for PFA to delivery good quality lesions in the ventricle. No significant differences were seen in lesion depth between the focal and basket Farapulse catheters during bipolar PFA in both healthy and infarcted myocardium, though the larger footprint catheter invariably led to increased lesion width.[369] Depth of lesion formation is still dependant on catheter contact in PFA.[370] Recently, Nies et al. (2024) delivered lesions to intracavitary structures including the papillary muscles and moderator band with ICE guidance using a large footprint monopolar lattice tipped catheter, crucially with ICE, fluoroscopy and electroanatomic mapping guidance.[372] Papillary muscle lesions with good catheter contact had greater lesion dimensions (18.3mm x 15.3mm x 5.8mm deep) whilst lesions with intermittent contact had similar length and width but significantly less depth (3.9mm, p=0.014).

There are only small case series or case reports to describe PFA applications for VT. A recent review of these cases demonstrated that eight (88.8%) procedures were acutely successful with no recurrence on longer term follow up in all cases.[373] Further reports of experience with PFA

in the ventricle, including description of manoeuvrability of these larger footprint catheters are required.

### *1.7.3 Stereotactic body radiation therapy*

Stereotactic body radiation therapy (SBRT), widely used in oncology to treat tumours, has been innovatively used as a therapeutic modality for VT refractory to CA. After first in-human use in 2015,[374] a small case series (n=5) demonstrated 99.9% reduction in VT burden after 6-week blanking.[375] Localised inflammatory lung changes were noted, resolving at 12 months. One patient experienced a fatal stroke (although is unclear if SBRT caused the same). Subsequently, a Phase 1/II clinical trial (n=19 patients) has demonstrated a reduction in VT burden of 94% at 6 months.[376] Longer term, 2-year overall survival was 58%.[377] A retrospective case series (n=10) in Ostrava, Czech Republic demonstrated a VT burden reduction by 87.5% at 12 months.[378] Multiple further case series but no randomised studies have been published.[379-381] Recently, Das et al. published the first Australian experience with SBRT.[382] They enrolled 12 patients with drug-refractory VT for whom catheter ablation had failed or who were unsuitable for SBRT in 2 Australian centres, and found a significant reduction (64.5%; P = 0.011) in VT burden and VT storm (71.7%; P = 0.027) at 6-month follow-up. Unfortunately, 66.7% (6/9) of these patients experienced VT recurrence. There is an urgent and unmet need for randomisation of patients eligible for SBRT to establish its role in the toolkit for CA of VA.

## 1.8 Conclusion

In this review we have described the considerable advancements and achievements made in our understanding of the pathophysiology and treatment of VA. Many of these achievements were made during the birth of cardiac electrophysiology, with (relatively) simpler tools and computational ability at hand but by true pioneers in the field. More recently, electroanatomic

mapping with novel catheters and systems complimented by multi-modality imaging have allowed the acquisition of vast quantities of data which, hand in hand with improved computational processing, AI and machine learning techniques and novel ablative technologies offers to address the urgent need for improved outcomes for patients suffering from VAs.

Multiple knowledge gaps have been identified in this review. First, comparative data and evidence for CA vs AAD therapy for PVCs are scarce, with only one randomised trial which enrolled only PVCs arising from a single site of origin (the right ventricular outflow tract). Second, though there has been rapid accumulation of image integration of LGE-CMR into clinical VA CA, the optimal thresholding to identify scar and CMR channels are unclear and have not been validated by co-registered histology. Further, the tissue histopathology of functional substrate as identified by isochronal late activation mapping have not been well characterised. This understanding would help to advance our knowledge of the underlying mechanisms of arrhythmogenesis in post-infarction scar. Third, multiple vendor platforms (ADAS 3D and inHEART) are available for use but no intervendor comparisons have been published to date. Fourth, multiple studies have demonstrated the disconnect between voltage and traditional electrogram feature analysis (such as LAVA and electrogram duration) against scar depth and pattern. Signal processing and machine learning of these intracardiac electrograms offers a solution that may better allow the clinician to understand scar geometry, pattern and composition but are yet to be systematically applied to biologically obtained electrograms. Fifth, novel ablative technologies to abolish VA substrate are needed including further pilot descriptions of PFA in the ventricle as well as randomised data for the use of SBRT to treat patients with VA and advanced SHD.

## 1.9 Thesis aims

It is in the context of these knowledge gaps that this thesis has been formulated. The overall intent of this doctoral work is to advance the treatment of VA with CA with a particular focus on innovative approaches to identify and abolish arrhythmogenic substrate. The specific aims of this thesis and the chapters that support them include:

1. To perform a systematic review of the evidence for CA versus AAD therapy for treatment of PVCs which will inform design of future randomised controlled trials (Chapter 2, published manuscript)
2. To validate CMR scar, channels and functional substrate with co-registered tissue histopathology and high-density electrophysiological mapping in an in vivo ovine model. (Chapter 3, published manuscript)
3. To perform a clinicopathological intervendor comparison of LGE CMR image integration technologies with co-registered ovine histopathology as well as in a pilot clinical case series (Chapter 4, submitted manuscript)
4. To identify scar depth and pattern with endocardial substrate mapping using signal processing and machine learning which can then be used to create three-dimensional scar depth maps readily importable into current CA EAM software (Chapter 5, accepted manuscript)
5. To describe procedural characteristics and outcomes in a pilot case series of novel PFA delivery to target difficult to treat intracavitary PVCs (Chapter 6, submitted manuscript)
6. To design, establish and commence a feasible and pragmatic randomised controlled trial of SBRT to treat patients with advanced SHD and VT (Chapter 7, operational trial protocol).

# Chapter 2

## 2 CATHETER ABLATION VS ANTIARRHYTHMIC DRUG THERAPY FOR TREATMENT OF PREMATURE VENTRICULAR COMPLEXES: A SYSTEMATIC REVIEW

Author attribution statement

| **Title of published work** | **Catheter ablation versus anti-arrhythmic drug therapy for treatment of premature ventricular complexes: a systematic review** |
|---|---|
| **Nature of the candidate's contribution** | Design of study, data collection and analysis, manuscript writing and submission to journal |
| **Co-Authors** | **Nature of contribution** |
| Haris Haqqani | Contributed comments on manuscript |
| Rajiv Mahajan | Contributed comments on manuscript |
| Pierre Qian | Contributed comments on manuscript |
| William Chik | Contributed comments on manuscript |
| Aleksandr Voskoboinik | Contributed comments on manuscript |
| Peter M. Kistler | Contributed comments on manuscript |
| Geoffrey Lee | Contributed comments on manuscript |
| Nicholas Jackson | Contributed comments on manuscript |
| Saurabh Kumar | Discussion of methodology and results. Comments on manuscript. Overall supervision. |
| Signature of candidate<br>Kasun De Silva | |
| Signature of supervisor (signed on behalf of all co-authors)<br>Saurabh Kumar | |

## 2.1 Introduction

Premature ventricular complexes (PVCs) are the most common ventricular arrhythmia.[383] When screened by electrocardiogram (ECG) they occur in 1-4% of the general population, however prevalence of PVCs can increase to 50-70% when screened by ambulatory monitoring.[384] Whilst PVCs are generally benign in a structurally normal heart, in some patients they may cause ventricular systolic dysfunction (termed PVC-mediated cardiomyopathy),[385] may signify underlying structural heart disease,[386] or may herald life-threatening cardiac arrhythmias (PVC-medicated ventricular fibrillation [VF]).[387] Further, many patients suffer from debilitating symptoms including palpitations, chest pain, dyspnoea, dizziness and fatigue.

There are three pathophysiological mechanisms of PVCs.[388] An automatic focus with subsequent parasystole is one such cause. Propensity for PVCs to arise from well-established anatomical sites (such as outflow-tracts) may be secondary to embryological development and localization of specialized conduction tissue capable of increased automaticity at these sites. A second mechanism is triggered activity due to increased intracellular calcium load causing early or delayed afterdepolarizations. Finally, re-entry (within the bundle branches or scar) can also give rise to PVCs.

PVCs can cause PVC mediated cardiomyopathy and incident heart failure. A putative mechanism for this is left ventricular dyssynchrony caused by PVCs causing adverse remodelling and worsening systolic function.[389] Animal data suggest that high burden PVCs lead to increased interstitial fibrosis with LV dyssynchrony and fibrosis persisting even after resolution of left ventricular function.[390] Furthermore, cellular studies in animal models have demonstrated electrical remodelling (increased dispersion of action potential duration, altered calcium signalling and changes in ionic currents) in PVC cardiomyopathy.[391]

Alternatively, PVCs may be a sequalae rather than the primary cause of cardiomyopathy. PVCs triggering malignant arrhythmia have been described in patients after myocardial infarction, possibly due to surviving Purkinje fibres within infarcted borderzone tissue.[392,393] Cardiomyopathy as the cause for PVCs may often be missed clinically. Cardiac magnetic resonance imaging (CMR) of patients with frequent PVCs but normal screening echocardiography found concealed myocardial abnormalities (such as late gadolinium enhancement) in 16% of patients, with these patients having worse clinical outcomes (sudden cardiac death, resuscitated cardiac arrest and sustained ventricular arrhythmias).[394]

These varied presentations of PVCs may explain why the presence and increased burden of PVCs in the community portends worse prognosis. Dukes et al. have demonstrated that increased frequency of PVCs associate with a 5-year reduction in left ventricular systolic function, higher risk of heart failure and lower survival.[395] Given the variable morbidity of PVCs, from benign to life-threatening complications, risk stratification is complex, particularly as most available data is from patients already selected for electrophysiological studies rather than the general population. Within these limitations, high burden PVCs, increased PVC QRS duration, cardiac abnormalities on cMRI, a family history of sudden cardiac death or cardiomyopathy as well as multifocal PVCs without a classic outflow-tract morphology warrant specialized risk stratification (with consideration of advanced imaging and/or electrophysiological studies).[394,396,397] In contrast, recent data and expert consensus suggests that patients with PVCs who have been extensively investigated to rule out structural heart disease or cardiomyopathy have a prognosis similar to the general population.[383,398]

Given this variable patient morbidity, it is unsurprising that management of PVCs in routine clinical practice varies considerably. A randomized non-drug lifestyle interventional trial

involving abstinence of smoking and caffeine, reduced alcohol and increased physical exercise did not reduce the frequency of PVCs at rest or exercise as determined by 24-hour Holter monitoring.[399] In fact, commonly given clinical advice to reduce caffeine consumption is likely incorrect with recent studies incorporating mendelian randomization within the UK Biobank refuting the hypothesis that caffeine contributes substantially to increased PVC burden.[400] Standard anti-arrhythmic drug (AAD) therapy include beta-blockers and calcium channel blockers as well as class I (flecainide) and III agents (amiodarone, sotalol). When prospectively compared, class I and III AADs had superior efficacy to beta blockers, calcium channel blockers or conservative therapy though only achieved complete PVC suppression in one-third of patients.[401] Finally, radiofrequency catheter ablation (CA) for PVCs has procedural success rates of 80-95% but these approaches are invasive and complications are observed in up to 5% of cases.[187]

Recent international guidelines from the Heart Rhythm Society indicate CA as a class I recommendation for treatment of frequent symptomatic PVCs originating from the right ventricular outflow tract (RVOT) in an otherwise structurally normal heart. Guidelines recommend CA is preferable to metoprolol or propafenone and also suggest that CA can be considered when other AADs are ineffective, not tolerated or not preferred by patients (22). For PVCs from other sites of origin, there are class II recommendations driven by non-randomized studies for CA when AADs are similarly ineffective, not tolerated or not preferred.[402]

Despite these recommendations, there is limited evidence comparing CA vs AADs. Here, we performed a systematic review of the literature comparing AAD and CA strategies for the treatment of PVCs of any origin. We subsequently reviewed existing registered trial protocols comparing these two strategies to ascertain expected outcomes and insights from upcoming studies. This review aims to clarify the evidence base for the role of CA for the treatment of PVCs.

## 2.2 Methods

For current literature, Medline, Embase and Cochrane Library were searched on 27/04/2022. Keywords for PVC ("premature ventricular complex" OR "premature ventricular contraction" OR "ventricular ectopic") were combined with keywords for catheter ablation ("catheter ablation" or "radiofrequency catheter ablation" or "radiofrequency ablation" or "ablation techniques") or drugs ("drugs" or "medications"). To find registered but yet unpublished clinical trials, Australian and New Zealand Clinical Trials Registry, United States National Library of Medicine ClinicalTrials database and the European Union Clinical Trials Register were searched for "premature ventricular contraction" or "ventricular ectopic" or "ventricular arrhythmia" on 27/04/2022. Studies were only included if they described original research data where CA and AAD (or control) were directly compared with regards to pre-specified outcomes (PVC recurrence, PVC frequency (number of PVCs in 24-hours) or burden (percentage of PVCs in 24-hours), left ventricular function as measured by left ventricular ejection fraction (LVEF), complications, quality of life (QoL) and/or symptoms or cost effectiveness). Data extracted from each study included the study period, centre, demographic characteristics, details of medical and procedural therapy, follow-up and outcomes. Where data was only available in figures but not in text, it was extrapolated from the provided figure using WebPlotDigitizer (Pacifica, California, USA).[403] Study quality and risk of bias was assessed by the RoB 2 tool[404] for randomized studies and ROBINS-I[405] for non-randomized studies.

## 2.3 Results

718 records were identified by the primary and secondary search. After excluding 712 articles (as detailed in the flow sheet, Figure 1), a total of 6 studies[188,194,406-409] were identified however 2 studies presented retrospective data comparing CA and AADs from the same registry

(Rochester Medical Index database of the Mayo Clinic). As such, the study by Yang et al. (2016)[409] which compared outcomes specifically in PVCs associated with mitral valve prolapse was excluded leaving a total of five final studies. Further, four prospectively registered and randomized clinical trials were identified by the literature search [410-413].

Of the included completed studies (summarized in Table 1), one study, Ling et al., was a randomized controlled trial of CA vs AAD for symptomatic RVOT PVCs.[194] There were two retrospective studies. Bogun et al. compared 60 consecutive patients who had CA for symptomatic PVCs refractory to AADs with a control group of 11 patients with PVC mediated left ventricular (LV) dysfunction.[188] Zhong et al. presented retrospective data comparing CA and AADs from the Rochester Medical Index database of the Mayo Clinic.[408] Stec et al. performed a prospective open label crossover trial which initially treated patients with three AADs (metoprolol, verapamil and propafenone with wash-out in between) and then subsequently offered CA if patient preferred or if there was AAD intolerance or inefficacy.[406] Finally, Fang et al. performed a prospective observational study allocating CA, AAD or control (no treatment) according to patient preference.[407] Across all studies, there were significant differences in primary outcomes and measures of procedural success (with PVC frequency, PVC burden, PVC recurrence and LVEF nominated as outcomes of interest in different studies).

These studies included a total of 1113 patients. The mean age (± standard deviation [SD]) of patients in the included studies ranged from 45±11 years to 55±18 years (Table 2) and 58% of patients were female. Patients tended to have preserved left ventricular systolic function and the mean baseline LVEF of included patients ranged from 52.5%±10.1% to 64.3%±5%. Two of the studies included only patients with RVOT PVCs.[194,407] Two other studies recruited primarily patients with RVOT PVCs (>50% of included patients had RVOT PVCs).[188,406] Only one study

had a majority of patients with non-outflow tract PVCs.[408] Mean patient follow up was 6.3±2.4 months to 49±39 months. Mean duration of symptoms ranged from 3-8 years.

The randomized controlled trial that was included in this analysis was assessed to have low overall risk of bias (Table 3). There were serious concerns of bias in all other included studies related to confounding, intervention classification, deviation from intervention and missing data (Table 3).

### *2.3.1 AAD choice and techniques*

There was significant heterogeneity in choice of AADs including class I agents, beta blockers, calcium channel blockers and class III agents (Table 2). In the only randomized controlled trial (RCT) comparing AADs and CA, metoprolol (n=50) and propafenone (n=115) were used in an open-label fashion, with selection of either drug not randomized.[194] Metoprolol, verapamil and propafenone were compared head to head in one study.[406] In the retrospective study by Zhong et al. of all-comers with PVCs, the most used AAD class was beta-blockers (46%) followed by sodium channel blockers such as flecainide, propafenone and mexiletine (18%).[408] Other agents included amiodarone (14%), calcium channel blockers (7%) and sotalol (4%).

There was also significant heterogeneity in CA techniques (Table 2). Pace-mapping was employed in all studies and activation mapping where possible was used in all but one. Electroanatomic mapping was used in three of the five studies (60%). There was no documentation of use of intracardiac echocardiography (ICE). Irrigated catheters were used in the two most recent studies.[194,408] Contact-force sensing catheters were not used. Procedural endpoints also varied - non-recurrence and non-inducibility of all PVCs were required for two of the five studies[188,408] whilst for the other three, elimination of the clinical PVC only was acceptable.

### *2.3.2 PVC recurrence, burden and frequency*

In available studies, CA was superior to AADs in reducing PVC recurrence, frequency and burden (Table 4). PVC recurrence was reported in only one study,[194] and recurrence of >300 PVCs in 24-hours at 1 year was 88.6% (confidence interval [CI] 82.5-92.8) with AADs and 19.4% (CI 13.9-26.5) with CA ($P$<0.001). PVC frequency was similarly lower after treatment with CA compared to AADs with Zhong et al. reporting a reduction in mean 24-hour PVC frequency by 93% (from 23554±18448 to 1755±3375, $P$<0.001) when treated with CA versus 49% (from 17259±14512 to 8883±11734, $P$<0.001) when treated with AADs.[408] Finally PVC burden was the most commonly reported outcome metric (reported in 3 of 5 studies). Mean PVC burden was reported by two studies with superior outcomes for CA (Fang et al.: 19.19%±7.41% to 0.05%±0.12%, $P$<0.001 for CA versus 18.89%±5.16% to 6.72%±5.09%, $P$<0.05 for AAD, Zhong et al.: 18.4%±15.2% to 2.8%±5.3%, $P$<0.001 for CA versus 12.1%±12.8% to 7.2%±10.1%, $P$<0.001 for AAD). Median PVC burden was reported by Ling et al. which similarly showed CA improved burden from baseline 14% (interquartile range [IQR] 12-21) to 0.11% (IQR 0.05-0.20) ($P$<0.001) versus 14% (IQR 12-21) to 7% (IQR 6-9) for AADs. Finally, though direct comparisons between AADs and CA should not be made for Stec et al. as patients were initially treated with AADs prior to offer of CA if AADs failed or were not tolerated, there was a similarly high reduction in burden (>90% reduction in burden) in the CA arm (88%) versus only 37% who achieved this same reduction with acceptable drug tolerability in the AAD arm. Importantly, in this study, metoprolol, verapamil and propafenone were compared head-to-head. Propafenone was the most efficacious drug with 90% reduction in burden achieved in 42% of patients, compared to 15% of patients treated with verapamil and 10% of patients with metoprolol.

### *2.3.3 Effect of AADs and CA on ventricular function*

With regards to ventricular function, Ling et al. demonstrated that PVC burden was negatively associated with LVEF and that LVEF tended to increase after treatment in both groups though was not influenced by group allocation. In the only study that recruited patients with low LVEF (Bogun et al), there was a significant increase in ventricular function after CA with LVEF increasing from 34% to 53% ($P$<0.0001). In contrast there was no change in LVEF in the control patients. For the other included studies, where LVEF was preserved prior to recruitment, there was at most mild increases in ventricular function after CA compared to AAD (Table 4).

### *2.3.4 Adverse effects of AADs versus complications of CA*

With regards to complications, there were no reported mortalities with treatment from CA or AADs. Complication rate for CA ranged from 0% to 5.6% (see Table 4), and included vascular complications, cardiac tamponade, heart block and allergic reaction to anaesthetic drugs. There were approximately 9.5%-21% AAD related adverse events or AAD intolerance in the included studies (see Table 4). These adverse events included pro-arrhythmia, general intolerability, sinus bradycardia and symptomatic hypotension.

### *2.3.5 Symptom management, QoL and health-care cost*

Symptoms at long term follow up was assessed by only one of the five studies and none reported data on QoL using a rigorous arrhythmia specific scale. Of the study that reported symptom outcomes at long term follow up (Stec et al), 88% of CA patients were symptom free after CA (including 8 patients who had repeat procedures). In comparison, 82% of patients who chose not to proceed with CA were symptom free. Although symptom severity as assessed by a visual analogue scale did not associate with baseline PVC frequency, a greater than 90% reduction in PVC frequency due to AAD therapy was shown to associate with a significant reduction in

symptom severity as measured by a visual analogue scale. Cost effectiveness analysis was not performed in any study included in this analysis.

## 2.4 Discussion

### *2.4.1 Limited data for non-outflow tract PVCs*

We found that the only available RCT comparing CA and AADs has been for RVOT PVCs. For idiopathic outflow tract VAs, recent trends in successful ablation sites suggests that non-RVOT sites now form the majority of ablations (56%).[414] Furthermore, non-outflow tract PVCs are associated with poorer outcomes including adverse left ventricular remodelling when untreated.[415] Both PVC QRS duration and non-outflow tract site of origin have been shown to be independent risk factors for left ventricular dysfunction.[397] CA of PVCs from non-outflow tract left ventricular and epicardial sites were associated with higher complications and further, epicardial origin of these PVCs were a predictor of procedural failure.[416] From the studies included in this systematic review, Stec et al. assessed the efficacy of AADs and CA stratified by outflow tract versus non-outflow tract origin and efficacy was similar in either location.[406] In contrast, whilst there was a similar increase in LVEF between AAD and CA for outflow tract PVCs in the observational study by Zhong et al. (the only study to include a majority of patients with non-outflow tract PVCs), LVEF improved after CA for non-outflow tract PVCs, however it declined with AAD therapy suggesting that CA may be an especially superior option for treatment of non-outflow tract PVCs.[408]

### *2.4.2 What are optimal outcome to define efficacy of AADs and CA?*

The role of AAD and CA have not yet been defined in the treatment of PVCs, particularly as the natural progression of PVCs can be variable in patients. In fact, a recent prospective registry

examining the natural history of PVCs demonstrated that up to 44% of patients with PVCs had a mean reduction to less than 1% after a median of 15-months follow-up without any intervention at all, and only 4% of patients developed PVC induced cardiomyopathy (defined as an LVEF less than 50%).[417] Despite these findings, other studies have shown more clear associations between PVCs and systolic dysfunction or symptoms. For example, frequent PVCs (greater than 20%) associate with patient fatigue and markers of LV pressure load including increased N-terminal pro-B-type natriuretic factor and increased circumferential end-systolic wall stress.[418] Furthermore subtle (and early) markers of left ventricular dysfunction as defined by speckle tracking strain imaging are reduced by high burden of PVCs and improve after CA.[419] Hence consensus opinion on patient selection, optimal measures of efficacy of AADs and CA and goals of therapy for treatment of PVCs are yet to be accepted.

Of the analysed studies, all included a primary outcome of acute procedural success or PVC frequency, burden or recurrence, however few assessed the subsequent consequences of reduction in these numbers. Concerningly, only one study reported long-term symptoms and no study to date has assessed the role of AAD versus CA for improving QoL with rigorous arrhythmia specific QoL scales nor have they assessed the cost burden of either strategy to the healthcare system

### *2.4.3 Techniques for catheter ablation of PVCs are rapidly evolving*

The studies included in this review recruited patients from 1992 to 2012 and techniques employed for CA are different from modern practice. Notably, three dimensional electroanatomic mapping was only employed in 3 of the 5 studies, and ICE or contact force sensing catheters were not used in any study. These techniques could improve the safety and efficacy of CA for PVCs, particularly from non-outflow tract sites of origin. For example, for ventricular arrhythmias

originating from the papillary muscles, use of contact force sensing catheters and ICE have been shown to improve procedural success and reduce risk of recurrence.[420,421]

### *2.4.4 Upcoming clinical trials compared CA and AADs for PVCs*

Upcoming registered clinical trials are summarized in Table 5 and the Central Illustration (Figure 2). Of these four studies, all are registered with the Clinical Trials registry of the United States National Library of Medicine and only one of the trials (ECTOPIA) has a detailed published protocol.[422] They were registered between 2013 and 2019 and seek to enrol 80-180 patients with a follow up of 6-12 months.

ECTOPIA is an RCT comparing CA with two different AAD strategies (sotalol or flecainide + verapamil) in a 1:1:1 ratio with a cross-over design in the AAD arm. It aims to recruit patients with a PVC (outflow-tract or non-outflow tract) or non-sustained ventricular tachycardia (NSVT) burden of ≥5% on 24-hour Holter monitoring, without structural or coronary disease. Activation and pace-mapping with an electroanatomic mapping (EAM) system will be performed with ablation using a non-contact force sensing catheter (MIFI catheter). Procedural endpoint will be abolition of target PVC or all PVCs. The primary outcome of interest is >80% reduction in PVC/ventricular tachycardia (VT) burden with secondary outcomes including burden, change in burden and QoL as identified by the University of Toronto atrial fibrillation (AF) severity scale.

PAPS Pilot is randomized open label prospective trial comparing CA or AAD (without mandating AAD choice though amiodarone use is encouraged) in patients with a PVC burden of ≥10% burden and underlying impaired LV function (LVEF ≤45%). Both outflow and non-outflow tract PVCs will be recruited. CA will be performed using activation and pace-mapping using an EAM system. Procedural endpoint will be abolition of all PVCs. ICE will be used as needed. Primary outcome will be LVEF and number of patients with an LVEF increase greater than 10%.

Secondary outcomes will be a greater than 80% reduction in PVC burden, adverse events and a composite arrhythmia burden score (characterized by PVC recurrence, VT and arrhythmic sudden cardiac death).

CAT-PVC is a randomized open label parallel assignment trial comparing CA and amiodarone in patients with structural heart disease with or without reduced LVEF and PVC frequency greater than 10,000 in 24-hours or biventricular pacing less than 92%. Both outflow and non-outflow tract PVCs will be recruited. Technical information of CA strategies is not available. Primary outcome will be a change in PVC burden at 6 weeks. Secondary outcomes will include QoL scores (EuroQol-5 Dimension [EQ5D] questionnaire), LVEF, six-minute walk test (6MWT), New York Heart Association (NYHA) class, N-terminal pro-brain natriuretic peptide (NT-proBNP), hospitalizations and adverse events at 12-months.

AVATAR was a randomized parallel open label study comparing CA and AAD (flecainide or propafenone or sotalol). This trial was registered in 2013 and terminated due to poor enrolment (personal correspondence with primary author).

### *2.4.5 Future directions and clinical gaps*

The challenge of trial design for PVCs arises from deciding management of a disease which has a high prevalence in the general population but diverse causes, manifestations and patient outcomes. Multiple trials in diverse populations are required to establish the role of CA in treatment of PVCs. Whilst CAT-PVC and PAPS-Pilot will offer invaluable data on treatment of PVCs in the context of cardiomyopathy where treatment goals include reduction in PVC burden and improvement in left ventricular function, there will likely remain gaps in our knowledge of management of idiopathic PVCs without manifest or concealed cardiomyopathy. In this cohort with good long-term prognosis treatment is probably aimed at improving QoL and symptom

burden. Given data suggesting resolution of PVC burden to <1% in up to 44% of patients,[417] we suggest that comparator groups of reassurance and observation or even a surgical-placebo catheter ablation control group would be insightful for a future clinical trial. Such a trial would first require pilot data on recruitment barriers and feasibility of adequate blinding of a surgical placebo.

## 2.5 Conclusion

To our knowledge this is the first systematic review of published and ongoing clinical trials comparing AAD and CA for the treatment of PVCs. We have made several key findings. Firstly, there is limited evidence comparing AADs and CA for non-RVOT PVCs with all such available studies having serious concerns of bias. Secondly, from the available published evidence, it appears that CA is superior to AAD in reducing the burden or frequency of PVCs however, the head-to-head impact of either strategy on patient quality of life, symptoms or cost to the health system is unclear. Thirdly, modern technologies that could potentially improve the efficacy and safety of CA (including ICE and contact force sensing catheters) have not been used in published studies to date and thus safety and efficacy of CA may be under-estimated. Finally, we anticipate important insights from upcoming registered trials including the role of CA for low burden PVCs (>5%), for PVC-mediated cardiomyopathy and for PVCs associated with structural heart disease.

## 2.6 Figures

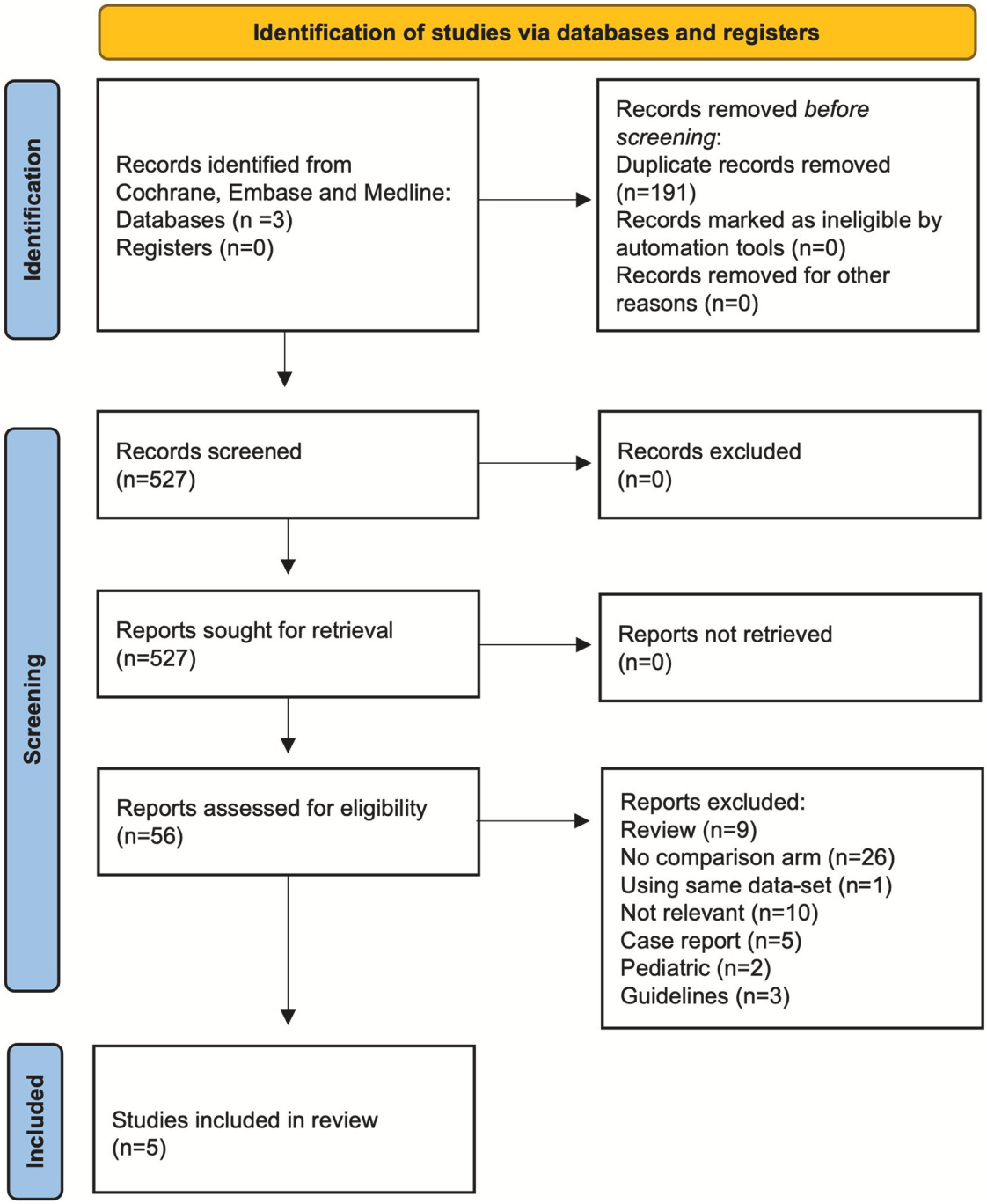


**Figure 2-1 PRISMA flowchart**

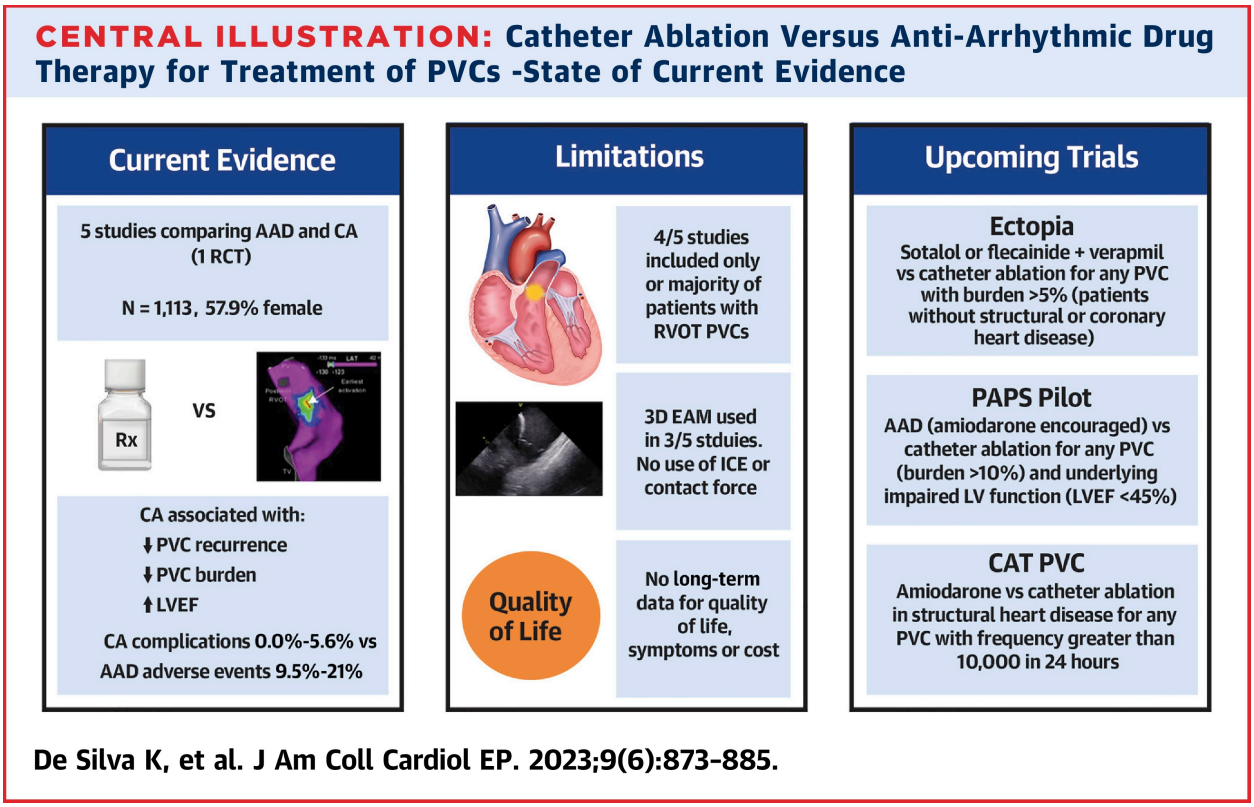


**Figure 2-2 Central Illustration**

Abbreviations: AAD – anti-arrhythmic drugs, CA – catheter ablation, ICE – intracardiac echocardiography, LVEF – left ventricular ejection fraction, PVC – premature ventricular complexes, QoL – quality of life, RVOT – right ventricular outflow tract

## 2.7 Tables

### Table 2-1 Baseline description of selected studies

| Study | Study type | AAD (n) | CA (n) | Inclusion criteria | Exclusion criteria | Outcomes measured | Mean follow-up (months) | Comments |
|---|---|---|---|---|---|---|---|---|
| Bogun (2007) | Retrospective | 11 | 60 | CA: symptomatic PVCs (>10/hr on 24-hr Holter) refractory to AAD AAD/control: PVC burden >20% and LVEF <50% | Coronary, valvular or congenital disease, LV hypertrophy, tachycardia induced cardiomyopathy, VT (including >1% burden NSVT) | 1. LVEF<br>2. Acute procedural success<br>3. LV end systolic/diastolic measurements | 49±39 | 60 consecutive patients with symptomatic PVCs refractory to mean 2±1 AADs offered CA. Control group of 11 patients with PVC mediated LV dysfunction |
| Stec (2012) | Cross-over open label trial | 84 | 50 | Symptomatic monomorphic PVCs (>2500 / 24-hr Holter) or severe symptoms clearly associated with PVCs Normal ECG and normal echocardiogram | Injury associated with syncope, NSVT or sustained VT, Significant cardiac disease or cardiomyopathy, Asymptomatic patients | 1. PVC frequency (24-hr Holter)<br>2. Symptoms as determined by detailed questionnaire using visual analogue scale | 48±10 | Randomised open label trial of metoprolol vs verapamil vs propafenone. After pharmacological testing, CA performed (if patient preference, AAD intolerance or AAD refractoriness) - n=50 of original 84 patients. Data on PVC frequency post CA not available. |
| Fang (2013) | Prospective non-randomised study | 44 | 24 | RVOT PVCs with or without symptoms (PVC burden 10% or >5% + ten episodes of VT/day) | Structural heart disease, endocrine disease, arrhythmogenic drug intake | 1. PVC burden<br>2. Cardiac chamber diameters<br>3. Ejection fraction | 6 | Three arms (AAD n=26, CA n=24 or no treatment=18) up to patient preference. 2 patients had unsuccessful CA and were transferred into AAD arm. |
| Ling (2014) | Randomised controlled trial | 165 | 165 | Symptomatic RVOT PVCs >6000 / 24-hr | Non-RVOT VT, previous AAD use, structural heart disease, Hyperthyroidism, electrolyte disturbance, diabetes, hypertension SBP >165, significant renal dysfunction, significant conduction disease | 1. Recurrence of RVOT PVCs >300 beats per day<br>2. PVC frequency<br>3. PVC burden<br>4. LVEF | 12 | |
| Zhong (2014) | Retrospective | 295 | 215 | PVC frequency >1000 / 24-Hr Holter | Inability to tolerate AADs and discontinued their use prior to 3-months | 1. PVC frequency<br>2. PVC burden<br>3. LVEF<br>4. Complications | 6.3±2.4 | Patients unable to tolerate 3-months of AADs excluded from study. |

Abbreviations: AAD – anti-arrhythmic drugs, CA – catheter ablation, LVEF – left ventricular ejection fraction, NSVT – non sustained ventricular tachycardia, PVC – premature ventricular complexes, RVOT – right ventricular outflow tract, VT ventricular tachycardia

**Table 2-2 Baseline patient and procedural characteristics**

| Study | Mean age (years) | Female (%) | Mean symptom duration (years) | PVC morphology | Baseline PVC frequency[1] / burden[2] | Baseline LVEF | AAD used | Activation mapping | Pace mapping | 3D EAM | ICE | Irrigated catheter | Contact force sensing catheter | Procedural endpoint |
|---|---|---|---|---|---|---|---|---|---|---|---|---|---|---|
| Bogun (2007) | 45±11 | 63.3% | 8±9 | RVOT 52%, LVOT 15%, non-outflow tract 33%. | 21%±17% (range 0.2-64%) | N/A [3] | N/A | Yes | Yes | Yes | No | No | No | Non-recurrence and non-inducibility of all PVCs |
| Stec (2012) | 47±15 | 71.4% | 4.3±6.9 | RVOT 51%, non-RVOT 49% | 13768±9424 | 61±7 | Metoprolol tartrate, verapamil or propafenone | Yes | Yes | No | No | No | No | Non-recurrence and non-inducibility of target PVC |
| Fang (2013) | 46.2±14.7 | 53% | 3.1±2.6 | RVOT 100% | 19.19%±7.41% | 64.1±4.9[4] | Amiodarone or metoprolol succinate | No | Yes | No | No | No | No | Non-recurrence and non-inducibility of target PVC |
| Ling (2014) | 51.61±11 | 73.6% | N/A | RVOT 100% | 14% (IQR 12-21) | 64.27±5.0 | Metoprolol tartrate or propafenone | Yes | Yes | Yes | No | Yes | No | Non-recurrence and non-inducibility of target PVC |
| Zhong (2014) | 55±18 | 44% | N/A | RVOT 21% LVOT 16.1% Non-outflow 48%, unavailable 14.9% | 19913±16565 (14.8%±14.2%) | 52.5±10.1 | B-blocker, CCB, mexiletine, flecainide, sotalol, amiodarone, propafenone | Yes | Yes | Yes | No | Yes | No | Non-recurrence and non-inducibility of all PVCs |

1. PVC frequency: Number of PVCs in 24-hours
2. PVC burden: percentage of PVCs of total QRS complexes
3. 22 in CA group had mean EF 34±13, 11 control patients mean EF 28±13. Mean EF for all CA patients not given.
4. Combination of mean LVEF given for AAD, CA and control arms. Where paired data is available, mean ± SD combined via method described by: Altman DG, Machin D, Bryant TN and Gardner MJ. (2000) Statistics with Confidence Second Edition. BMJ Books ISBN 0 7279 1375 1. p. 28-31.

Abbreviations: 3D EAM – three dimensional electroanatomical mapping, AAD – anti-arrhythmic drugs, CA – catheter ablation, CCB – calcium channel blocker, ICE – intracardiac echocardiography, LVEF – left ventricular ejection fraction, LVOT – left ventricular outflow tract, NSVT – non sustained ventricular tachycardia, PVC – premature ventricular complexes, RVOT – right ventricular outflow tract, VT ventricular tachycardia

**Table 2-3 Assessment of bias**

A) Non-randomised studies[1]

| Study | Pre-intervention | | At intervention | | Post intervention | | | Overall |
|---|---|---|---|---|---|---|---|---|
| | Confounding | Selection | Intervention classification | Deviation from intervention | Missing data | Measurement of outcome | Selection of reported result | Low, moderate, serious, critical |
| Bogun (2007) | Serious | Low | Moderate | Moderate | Low | Low | Low | Serious |
| Stec (2012) | Moderate | Low | Moderate | Serious | Low | Low | Low | Serious |
| Fang (2013) | Moderate | Low | Moderate | Serious | Moderate | Low | Low | Serious |
| Zhong (2014) | Serious | Low | Moderate | Serious | Moderate | Low | Low | Serious |

B) Randomised studies[2]

| Study | Random sequence generation | Allocation concealment | Blinding of participants and personnel | Blinding of outcome assessment | Incomplete outcome data | Selective reporting | Other bias |
|---|---|---|---|---|---|---|---|
| Ling (2014) | Low | Low | Low | Low | Low | Low | Low |

1. Using Risk of Bias in Non-randomized Studies - of Interventions (ROBINS-I) tool
2. Using Risk of Bias 2 (RoB 2) tool

## Table 2-4 Outcomes CA vs AADs for PVCs

| Study | PVC recurrence | PVC frequency | PVC burden | LVEF | Complications and Adverse Effects | Quality of Life and/or Symptoms | Cost |
|---|---|---|---|---|---|---|---|
| Bogun (2007) | Not reported | Not reported | Not reported | Patients who received AAD patients had stable EF (28 % to 29%) (NS). CA patients with reduced LVEF had an increase in LVEF from 34% to 53% (*P*<0.0001). | CA – 3.3% complication rate; 1 complete heart block requiring pacemaker, 1 allergic reaction to fentanyl requiring intubation. | Not reported | Not reported |
| Stec (2012) | Not reported | Not reported | >90% reduction in burden was achieved in 37% of patients treated with AADs (with acceptable drug tolerability) and 88% of patients with CA | Not reported | AADs – Pro-arrhythmia in 3.6%. Withdrawal of treatment due to intolerability in 21% of patients treated with metoprolol, 17% treated with propafenone and 15% treated with verapamil.<br>CA – No complications | AADs - 28/34 (82%) symptom free at long-term follow up vs 44/50 (88%) who received CA | Not reported |
| Fang (2013) | Not reported | Not reported | AAD - Mean 18.9% ± 5.2% to 6.7 % ± 5.1% p<0.05.<br>CA – Mean 19.2% ± 7.4% to 0.1% ± 0.1% p<0.001 | AAD - Mean 64.0%±5.5% to 66.1%±6.8% (NS)<br>CA – Mean 63.7%±4.9% to 66.2%±6.2% (NS) | Not reported | Not reported | Not reported |
| Ling (2014) | Recurrence of >300 RVOT PVCs in 24-hours at 1-year follow up:<br>AAD - 88.6% (CI 82.5-92.8)<br>CA - 19.4% (CI 13.9-26.5)<br>(*P*<0.001) | Not reported | AAD - Median 14% (IQR 12-21) to 7% (IQR 6-9)<br>CA – Median 14% (IQR 12-21) to 0.1% (IQR 0.05-0.20)<br>*P*<0.001 | AAD – Mean 64.5%±4.9% to 66.8%±6.1% (*P*<0.001)<br>CA – Mean 64.1%±5.2% to 66.4%±5.1% (*P*<0.001) | AAD – drug related adverse SEs 10.3% of patients - 7 sinus bradycardia, 3 symptomatic hypotension, 2 mild fatigue, 2 cold extremity, 3 recurrent headache<br>CA – 3 complications (2.4%) - 1 patient required cardioversion for VF during ablation, 1 AV fistula, 2 haematomas | Not reported | Not reported |

| | | | | | | | |
|---|---|---|---|---|---|---|---|
| Zhong (2014) | Not reported | AAD – Mean 17259±14512 => 8883±11734 (*P*<0.001)<br>CA – Mean 23554±18448 => 1755±3375 (*P*<0.001) | AAD – Mean 12.1%±12.8% => 7.2%±10.1% (*P*<0.001)<br>CA – Mean 18.4%±15.2% => 2.8%±5.3% (*P*<0.001) | AAD – Mean 52.1%±8.5% => 52.3%±6.4% (NS)<br>CA – Mean 53.0%±11.9% => 55.9%±11.2% (*P*<0.001) | AAD - 9.5% discontinued drugs<br>CA - 5.6% procedure complications. 7 arterial access complications - femoral or abdominal aortic artery pseudoaneurysm, bleeding, retro-peritoneal hematoma, or type B descending aortic dissection. 5 cardiac tamponades<br>requiring pericardiocentesis. | Not reported | Not reported |

Abbreviations: AAD – anti-arrhythmic drugs, CA – catheter ablation, CCB – calcium channel blocker, IQR – interquartile range, LVEF – left ventricular ejection fraction, LVOT – left ventricular outflow tract, NS – not significant, PVC – premature ventricular complexes, RVOT – right ventricular outflow tract

## Table 2-5 Upcoming clinical trials

| Study | Location | Year registered | Description | Estimated enrolment | Inclusion | Exclusion | Outcomes measured | Follow-up | Estimated Completion Date[1] | Status |
|---|---|---|---|---|---|---|---|---|---|---|
| ECTOPIA (Haanschoten et al.) | Isala hospital, Zwolle, Netherlands | 2019 | Randomized trial comparing CA with two different AADs (sotalol vs flecainide+verapamil) in a 1:1:1 ratio with a crossover design in the AAD arm. | 180 | PVC/NSVT burden ≥5% on 24-hr Holter monitor with no structural or coronary heart disease | Age >75, previous ablation, LVEF <55%, | Primary outcome<br>>80% reduction of PVC/VT burden after 3 months<br>Secondary outcomes<br>- PVC/VT burden<br>- Change in PVC/VT burden<br>- QoL (University of Toronto AF severity scale) | 12 months | May 2022 | Recruiting |
| PAPS pilot study (Huizar et al.) | McGuire VA Medical Center, Virginia, USA | 2017 | Randomised, open-label, prospective trial comparing CA vs AAD (amiodarone preferred) | 140 (39 to be collected in pilot) | PVCs (≥10% burden) and cardiomyopathy (LVEF ≤45%) | Current AAD use, severe symptoms unable to complete 3-month observation period, severe valvular disease, previous CA | Primary outcomes<br>- LVEF<br>- No. with LVEF increase ≥10%<br>Secondary outcomes<br>- >80% reduction of PVC burden<br>- Adverse events<br>- Composite arrhythmia burden (PVC recurrence, VT, arrhythmic sudden cardiac death | 12 months | August 2021 | Active, not recruiting |
| CAT-PVC (Hindricks et al.) | Heart Center Leipzig, Leipzig, Germany | 2017 | Randomised open label parallel assignment trial comparing CA and amiodarone | 80 | Structural heart disease with or without reduced LVEF PLUS PVC frequency >10,000 / 24-hr or symptoms or BiV pacing <92% | Previous ablation or amiodarone use | Primary outcome<br>- Change in PVC burden at 6-weeks<br>Secondary outcomes<br>- Change in QoL scores (EQ5D questionnaire)<br>- LVEF<br>- 6MWT<br>- NYHA class<br>- NT pro-BNP<br>- hospitalisations | 12 months | Actual completion Date – 4/3/2021 | Completed |

| | | | | | | | | | | |
|---|---|---|---|---|---|---|---|---|---|---|
| | | | | | | | - adverse effects at 12 months | | | |
| AVATAR (Bolognese et al.) | Ospedale S.Donato, Arezzo, Italy | 2013 | Randomised, parallel, open label study comparing CA and AAD (Flecainide or Propafenone or Sotalol) | N/A | Outflow tract PVC with frequency >2000 / 24-hr or symptomatic VT or reduced LVEF | Structural heart disease | Primary outcome QoL with SF-36 score | 6 months | 2014 | Unknown |

1. Date patient completes final visit

Abbreviations: 6MWT – six minute walk test, AAD – anti-arrhythmic drugs, CA – catheter ablation, CCB – calcium channel blocker, EQ5D – EuroQol- 5 Dimension, ICE – intracardiac echocardiography, LVEF – left ventricular ejection fraction, LVOT – left ventricular outflow tract, NSVT – non sustained ventricular tachycardia, NYHA – New York Heart Association, NT pro-BNP – N-terminal pro-brain natriuretic peptide, PVC – premature ventricular complexes, QoL – quality of life, RVOT – right ventricular outflow tract, SF-36 – Short Form 36 Health Survey Questionnaire, VT – ventricular tachycardia

# Chapter 3

# 3 WHOLE-HEART HISTOLOGICAL AND ELECTROANATOMIC ASSESSMENT OF POST-INFARCTION CARDIAC MAGNETIC RESONANCE IMAGING SCAR AND CONDUCTING CHANNELS

Author attribution statement

| **Title of published work** | **Whole-heart histological and electroanatomic assessment of post-infarction cardiac magnetic resonance imaging scar and conducting channels** |
|---|---|
| **Nature of the candidate's contribution** | Design of study, data collection and analysis including processing and annotation of electrograms, post-processing of histopathology and CMR, co-registration of data, statistical analyses, manuscript writing and submission to journal |
| **Co-Authors** | **Nature of contribution** |
| Timothy Campbell | Lead source animal experiments and histopathology staining and sectioning (prior to PhD candidate's thesis commencement). Discussion on methodology and manuscript. |
| Richard Bennett | Contributed towards animal experiments and comments on manuscript |
| Robert D. Anderson | Contributed towards animal experiments and comments on manuscript |
| Chris Davey | Software design for image integration of tissue histopathology to electroanatomic map |

| | |
|---|---|
| Alexandra K. O'Donohue | Contributed to histology experiments and comments on manuscript |
| Aaron Schindeler | Contributed to histology experiments and comments on manuscript |
| Samual Turnbull | Contributed to animal experiments and comments on manuscript |
| Dinesh Selvakumar | Contributed to animal experiments and comments on manuscript |
| Ashwin Bhaskaran | Comments on manuscript |
| Yasuhito Kotake | Comments on manuscript |
| Chi Jen Hsu | Advice on imaging experiments and comments on manuscript |
| James H. Chong | Comments on manuscript |
| Eddy Kizana | Comments on manuscript |
| Saurabh Kumar | Overall supervision. Animal experiments and experimental design. Comments on manuscript. |
| Signature of candidate<br>Kasun De Silva | |
| Signature of supervisor (signed on behalf of all co-authors)<br>Saurabh Kumar | |

## 3.1 Introduction

Accurate delineation of ventricular tachycardia (VT) substrate improves success of VT ablation. VT circuitry may be difficult to delineate by traditional activation and/or entrainment on electroanatomic mapping (EAM), due to haemodynamic instability, non-sustained arrhythmia, non-inducibility or conversion to another VT [423]. As an alternative strategy, VT isthmii may be delineated in sinus or paced rhythm by using substrate mapping [424]. Voltage mapping is a commonly used technique to identify myocardial scar, however it can be affected by electrode spacing, depolarization wavefront and intramural scar location[425,426]. More recent functional mapping strategies include identification of deceleration zones (DZ) through isochronal late activation mapping with DZs co-localizing to successful sites of VT termination with catheter ablation in 95% of cases [427].

Image integration of myocardial scar using commercially available software is a rapidly adopted complimentary strategy for VT ablation. This allows visualization of VT substrate prior to the procedure as well as registration with live EAM data [339,428]. ADAS-3D (Galgos Medical, Barcelona, Spain) is one such commercially available software which can aid identification of arrhythmogenic substrate using late gadolinium enhancement (LGE) cardiac magnetic resonance imaging (CMR), post-processed using signal intensity thresholds or by wall thinning as identified by multi-detector perfusion computed tomography. Image integration using ADAS-3D has been increasingly utilised worldwide to enhance catheter ablation for VT. Non-randomized studies have found that CA targeting CMR conducting channels (CMR-CCs) may be superior in reducing VT recurrence compared to a standard approach without targeting CMR-CCs.[340] Recent data has provided a mechanistic link between anatomic conduction channels and pathophysiologic

conduction characteristics with the finding that CMR-CCs are highly co-localised to DZs (94% of DZs co-localize to CMR-CCs). [429]

To our knowledge, there has been no systematic gold-standard histological validation of ADAS-3D defined scar nor CMR-CCs, according to varying signal intensity scar thresholding. No prior study has characterised the histology of DZs. In this study, we investigated ADAS-3D defined scar and CMR-CCs in an ovine infarction model and validated them by co-registered whole-heart histology as well as EAM. Further, we aimed to identify histological characteristics of CMR-CCs that co-localised with DZs.

## 3.2 Methods

This study was performed on castrated male merino sheep (weighing 53±7kg). This study was approved by the Animal Ethics Committee of Westmead Hospital. The study conformed with National Health and Medical Research Council of Australia animal research guidelines. The data that support the findings of this study are available from the corresponding author upon reasonable request. Animals underwent an infarction procedure and a subsequent CMR (116 ± 20 days, range 86-134 days after infarction) and EAM (129 ± 12 days, range 109-140 days after infarction). They were euthanized immediately after EAM. During all procedures (infarction, CMR and EAM) sheep were anesthetised with xylazine (0.5mg/kg intramuscular) and induction of anaesthesia with propofol (4mg/kg intravenously) before intubation. General anaesthesia was maintained with 1–4% isoflurane in 100% oxygen. 0.9% normal saline (100mL/h intravenously) was administered throughout the procedures.

### *3.2.1 Animal infarct model*

As previously described [430], animals were infarcted by inflation of a 2.75–3.5mm angioplasty balloon distal to the second diagonal branch bifurcation for 3 hours, causing an

anteroseptal myocardial infarction (MI). Oral sotalol was given pre- and post-infarction to prevent ventricular arrhythmias (VAs) and discontinued 7-days after the infarction procedure.

### *3.2.2 Cardiac magnetic resonance imaging and post-processing*

LGE CMR was performed with a 3T Prisma system (Siemens, Munich, Germany) with 4 lead ECG cardiac gating. All sequences were performed with breath-holding in end-expiration. Delayed enhancement images were acquired for tissue characterization using a segmented inversion recovery fast gradient echo sequence in short axis stack, left ventricle (LV), left atrial and 4- chamber planes. TI (time of inversion) scout was performed at 9 minutes post contrast to select appropriate inversion time (usually around 300ms) for delayed enhancement acquisitions which began at 11 minutes post-injection. The short axis stack was run with 30 contiguous slices of 4-5mm thickness, covering the entire heart with in plane resolution of 1.5mm x 1.5mm. Other delayed enhancement parameters were TR (repetition time): R-R interval of individual animal, TE (echo time): 1.65ms, flip angle: 20 degrees.

CMR post-processing was performed using commercially available ADAS-3D segmentation software. Manual tracing of the endocardial and epicardial borders were performed with subsequent semi-automatic generation of the LV shell, as previously described in the literature [431]. Based on quantitative analysis of pixel signal intensity (PSI), ADAS-3D created a total of 9 maps, each compromising 10% of myocardium from endocardium to epicardium (i.e. 10% layer, 20% layer, 30% layer etc) whereby LGE PSI is projected onto each map and coded according to a trilinear interpolation algorithm using 40% and 60% of the maximum intensity as scar thresholds ("6040" threshold). ≥60% PSI was tagged as dense scar (red) and ≤40% as healthy (blue) with intermediate (40-60% PSI) labelled border-zone (BZ, intermediate colour range). Furthermore, transmural maps were created in similar fashion of the 0-50% layers (henceforth

called endocardial) and 50-100% layers (henceforth called epicardial). Finally, to investigate the impact of thresholding on scar and CMR-CC identification, 3 alternative threshold categories (5545, 6535 and 7030) were also used in addition to the standard 6040 threshold [432].

CMR-CCs were defined automatically by the system as corridors within BZ that connected areas of normal myocardium and were surrounded by dense scar or mitral annulus.[338] CMR-CCs seen in two consecutive layers in the same myocardial segment and with similar orientation were considered as a single channel spanning multiple layers.

### *3.2.3 Electroanatomic mapping procedure and map analysis*

Following general anaesthesia and intubation, arterial and venous access was obtained. A quadripolar catheter was placed at the right ventricular apex for right ventricle pacing (RVp) or into the right atrium for atrial pacing and a decapolar catheter was inserted into the coronary sinus for left ventricular pacing (LVp). Catheter stability and contact were confirmed via catheter image deformation on EAM software, CARTO3™ (Biosense Webster, Irwindale, California, USA), or with intracardiac echocardiography (ICE). EAM was performed with a 20-pole Pentaray™ (Biosense Webster) 2-6-2 millimetre (mm) electrode spacing. Acquisition settings were tissue proximity indication, local activation time difference 3ms, the electrode position change of 3mm, point density of 1mm and QRS pattern >90%. Sequential endocardial voltage maps were obtained of the LV using three wavefronts: sinus rhythm (4/5 animals) or atrial pacing (1/5 animals), RVp (5/5 animals) and LVp (5/5 animals).

Mean bipolar and unipolar voltages, bipolar scar (<1.5mV) and dense bipolar scar (<0.5mV), unipolar scar (<8.3mV) and dense unipolar scar (<3mV), split potentials (>20ms isoelectric period between EGMs) and local abnormal ventricular activities (LAVA) were identified. Abnormal EGMs were classified using LAVA definitions[433]. Isochronal late activation

mapping was performed offline [427]. Local activation time was defined as the latest deflection of the electrocardiogram (EGM) through manual annotation and the whole activation of the chamber was then divided into 8 equally distributed activation time isochrones with red being the earliest and purple being latest. DZs were defined as regions with isochronal crowding with ≥3 isochrones within a 1-cm radius co-localising with LAVA or split potentials[272].

### *3.2.4 Histopathology analysis and 3D reconstruction*

A cotton filler was inserted into the LV cavity of explanted hearts, conserving natural chamber volume before being placed in 10% neutral buffered formalin for 7-days. After fixation, hearts were placed into a ballistic gelatine mould and sectioned into 5mm short-axis slices. Photography of slices from a fixed distance of 15cm was performed before being stored in 70% ethanol. Endocardial and epicardial LV borders were manually traced on the images (Figure 1A). Traced images were used to create scaled 3D meshes in MATLAB (Mathworks, R2019b). Wall thickness at each endocardial mesh vertex was calculated as the distance between the vertex and the endocardial wall along the vertex's normal vector.

Sections were embedded in paraffin blocks, and 5µm-thick slices were cut from the basal surface (RM2155, Leica Biosystems, Wetzlar, Germany). Picrosirius red staining was performed with a Weigert's haematoxylin counterstain to identify collagenous tissue. Image capture was performed using an Aperio ScanScope CS2 (Leica Biosystems, Wetzlar, Germany) or Olympus VS120 (Olympus Corporation, Tokyo, Japan) with brightfield illumination at 20x magnification. Histology images guided scar delineation on previously photographed slice images.

Biopsies with a width of 3mm (and gap of 3mm between biopsies) were systematically marked around the endocardial surface with a 3mm spacing. They were analysed on ImageJ (National Institutes for Health, Bethesda, Maryland, USA). For each endocardial (0-50%) and

epicardial (50-100%) segments of the biopsies, presence of scar was identified qualitatively. Furthermore, quantitative percentage of fibrosis and adiposity as defined by picrosirius red staining was determined as described using ImageJ (see Figure 1F). The remaining myocardium was deemed "viable" myocardium (VM).

### *3.2.5 Image integration and analysis*

Histology and CMR maps were co-registered with the EAM created during right ventricular pacing (Figure 1). Registration landmarks included the mitral and aortic annulus, LV apex and papillary muscles with cross-validation using intracardiac echocardiography shell (CARTOSOUND module, CARTO3$^{TM}$).

For scar analysis, each 3mm histological biopsy was compared to the co-registered transmurality ADAS-3D maps (of varying thresholds) and determined to correspond to CMR scar, BZ or healthy tissue [Figure 1]. Accuracy and agreement for scar in the endocardial and epicardial layers were compared (i.e. histological scar corresponding to CMR BZ or dense scar).

For CMR-CC analysis, each unique CMR-CC was compared to available transecting histological biopsies as shown in Figure 2. If the CMR-CC was replicated in different thresholds, then only the threshold with the shortest (overlapping) segment of the channel was retained with the other similar channels marked as "duplicate". Biopsies were then interrogated for a corresponding channel of viable myocardium surrounded by fibrosis or adiposity within the same endocardial-epicardial layer +/- 1 layer as defined by CMR (i.e. for a CMR-CC identified in the 70-80% layer, histological correlation was deemed correct if viable myocardium was found in the 60-90% layers of the histological biopsy surrounded by fibrosis) running in the same orientation as the CMR-CC (longitudinal or transverse). For each identified "histology confirmed-conducting channel" (HC-CC), the channel of viable myocardium (excluding surrounding compact fibrosis or

adiposity and excluding any visually identified blood vessels) was traced using ImageJ and then fibrosis, adiposity and VM percentages for these "within channel" segments were quantified. Each HC-CC was also assessed for presence of DZ in the corresponding EAM and DZ was localised to an entrance/exit or mid channel [Figure 2]. Histological analyses were performed blinded to absence or presence of DZs.

### *3.2.6 Statistical analysis*

Analysis performed with Statistical Package for the Social Sciences for Windows (Version 27). Continuous variables were expressed as median and interquartile range (IQR). Independent data were compared by the Mann-Whitney U test (non-parametric) or Kruskal-Wallis 1-way ANOVA (multiple groups). Independent categorical variables were compared by the Chi-square test. Volumes created by CMR, EAM and histopathology were compared by repeated measures ANOVA. Kappa values were generated to determine agreement. Two-tailed *P*-values were considered statistically significant when 0.05 or less. Authors KD and SK had full access to all data in the study and takes responsibility for its integrity and the data analysis.

## 3.3 Results

Six animals had a successful anteroseptal MI created, of which five animals underwent a CMR scan and subsequent EAM mapping. CMR could not be performed on the remaining animal due to ferrous material in its rumen and was excluded from analysis. LV ejection fraction was 41% (39-43%). LV end diastolic volume was 118mls (87–155mls). There were significant differences in the volumes generated by CMR post-processing (126.7mls (108.6-142.3mls)), EAM (97.1mls (83.5-102.5mls)) and whole-heart histopathology reconstructions (55.1mls (43.6-57.3mls)), $p<0.001$). Surface registration error (comparison of the vertices of each mesh) of the histopathology to the EAM was 4.9mm (3.8-6.3mm) and CMR to EAM was 4.7mm (4.2-5.1mm).

### *3.3.1 Gross scar topography and impact of thresholding*

As shown in Figure 3A, using the standard 6040 threshold, CMR had 83.8% accuracy for identifying histological scar in the endocardium and 61.4% in the epicardium. There were similar values but slightly poorer accuracy for the other thresholds. For the 6040 threshold there was substantial agreement between CMR and histological scar in the endocardium (Kappa 0.666) but only fair agreement (Kappa 0.276) in the epicardium (Figure 3B). The 6040 threshold performed best in the endocardium, but the 6535 threshold was best for the epicardium.

As shown in Supplementary Table 1, ADAS-3D defined "normal" tissue using the 6040 threshold had minimal fibrosis (endocardial - 7.4% (4.9-15.2%), epicardial - 12.2% (6.0-38.6%)), some adiposity (endocardial - 19.3% (12.8-25.1%), epicardial - 18.6% (11.7-24.6%)) and majority "viable myocardium (endocardial - 70.5% (61.2-78.1%), epicardial - 64.6% (35.8-75.2%)). In comparison, 6040 CMR "BZ" and 6040 CMR "scar" had higher fibrosis (BZ endocardial - 44.7% (25.4-61.1%), BZ epicardial - 41.8% (19.5-54.3%), "scar" endocardial - 42.5% (32.1-53.8%), "scar" epicardial - 42.0% (25.9-52.8%)), similar adiposity (BZ endocardial - 16.8% (10.9-23.8%)), BZ epicardial - 22.1% (15.3-31.6%), "scar" endocardial - 22.8% (14.9-32.8%), "scar" epicardial - 20.6% (14.7-26.1%)) and less "viable" myocardium (BZ endocardial - 27.6% (20.9-43.3%), BZ epicardial - 30.4% (23.4-53.5%), "scar" endocardial - 27.6% (20.9-43.3%), "scar" epicardial - 34.6% (21.2-51.1%)). This was similarly seen in the epicardium and across varying ADAS-3D thresholds as shown in Supplementary Table 1.

### *3.3.2 Identification of CMR-CCs*

A total of 37 CMR-CCs were identified by varying MRI thresholding. Of these, 23 (62%) were unique channels and 14 (38%) were duplicate channels (i.e. the same channel seen on multiple ADAS-3D threshold settings). Of these 23 unique CMR-CCs (described in Table 1), 6

(26%) were from threshold 5545, 8 (35%) from 6040, 4 (17%) from 6535 and 5 (22%) were from the 7030 threshold application.

Median channel length was 19mm (14-34mm). Threshold 5545 CMR-CCs tended to be shorter (12mm, 7-15mm) compared to 6040 (24mm, 17-42mm), 6535 (30mm, 20-33mm) and 7030 (21mm, 19-37mm) with a trend towards statistical difference between groups (P=0.053).

10/23 (44%) CMR-CCs were in the endocardial layers and 12/23 (52%) in the epicardial layers with 1 (4%) CMR-CC crossing from endocardium to epicardium. Most CMR-CCs were confined to a single 10% myocardial layer (15/23, 65%) and this did not differ between threshold groups (5545: 5/6 [83%], 6040: 5/8 [63%], 6535: 3/4 [75%] and 7030: 2/5 [40%], *P*=0.482). 18/23 (78%) CMR-CCs had a single entrance and exit whilst 5 (22%) had multiple entrances and/or exits.

### *3.3.3 Co-localization of DZs with CMR-CCs*

DZs co-localised to 19/23 (83%) of CMR-CCs (Table 1). There were no significant differences in identification of DZs co-localising with CMR-CCs when comparing by wavefront (18/19 were identified by all three wavefronts, 1/19 was identified by sinus rhythm and RVp but not LVp), see Figure 4. The presence of DZ was not different amongst varying threshold groups (P=0.320, 5545: 5/6 [83%], 6040: 7/8 [88%], 6535: 3/4 [75%], 7030: 4/5 [80%]). DZs co-localised to either the mid channel (9/19, 47%) or entrance/exit (10/19, 53%).

### *3.3.4 Histological validation of CMR-CCs*

Of the 23 unique CMR-CCs, 20 (87%) were histologically confirmed (HC-CCs). Representative examples are shown in Figures 2 and 5. Of the three histologically discordant CMR-CCs i.e. CMR channels which were not validated by histology, one was identified with 5545 thresholding (10% layer) and was 16mm in length whilst two were identified with 7030 thresholding and were 19mm (10% layer) and 14mm (70-80% layers) in length, respectively. For

one of these channels, histological biopsies were not available as the channel was significantly basal and remote from scar and biopsy segments.

For the 20 HC-CCs, there were 62 biopsies transecting these channels available for analysis (3 segments per channel, IQR 1-4). There were 33 entrance/exit segments and 29 mid channel segments. 25/62 (40.3%) were in regions with DZs identified by at least 1 wavefront. 22/62 (35.5%) were in regions with DZ identified by RVp, 18/62 (29.0%) by LVp and 19/62 (30.6%) by sinus rhythm or atrial pacing. Intramyocardial blood vessels (Figure 2 and 4) were found within or immediately adjacent to 46/62 (74%) of HC-CC segments with a median of 1 (1-2) blood vessels per segment.

Within channel fibrosis did not differ between pooled entrance/exit versus mid segments (26.7% (19.0-41.2%) vs 25.3% (13.1-34.7%), P=0.799). Similarly, there were no significant differences for within channel adiposity (11.6% (4.6-22.5%) vs 17.3% (9.1-25.6%) P=0.075) or "viable" myocardium (54.9% (41.3-65.8%) vs 51.9% (39.1-65.3%), P=0.203) between pooled entrance/exit versus mid segments.

As shown in Figure 6, within channel fibrosis did not differ at sites of DZs (identified by at least 1 wavefront) compared to those without DZs (25.0% (16.3-34.1%) vs 28.7% (19.0-41.2%), P=0.242). In contrast, there was significantly higher within channel adiposity for segments co-localizing to DZs compared to those without (24.1% (15.6-34.9%) vs 8.3% (4.6-17.2%), P<0.001). There was a trend towards lower remaining "viable" myocardium with presence of DZs (46.8% (37.4-59.3%) vs 58.9% (45-66.5%), P=0.054). These findings were largely consistent regardless of which wavefront was analysed (Supplementary table 2).

## 3.4 Discussion

In this study we examined the histologic and electroanatomic characteristics of CMR defined scar, CMR-CCs and DZ in an established ovine model of chronic myocardial infarction. We have made several important findings which include:

1. CMR-LGE defined scar has high correlation with the gold standard histological assessment of scar with substantial agreement to gold standard histology in the endocardium and fair agreement in the epicardium.
2. CMR-CCs correlate well with co-registered whole heart histopathology in identifying surviving myocyte bundles within dense scar or adiposity. Furthermore, histology confirms the three-dimensionality and intra-mural involvement of chronic ischaemic scar and resultant channels.
3. CMR-CCs correlate well with DZs, and this correlation appears to be robust when systematically assessed by varying activation wavefront.
4. Varying CMR thresholding beyond the current clinically used 6040 threshold for ADAS-3D software may have benefit in uncovering important arrhythmogenic substrate (these channels are validated by histology and by DZs).
5. Histologically validated within channel *adiposity* rather than *fibrosis* was associated with DZs, further supporting the concept of conduction slowing due to lipomatous metaplasia in ischaemic scar.
6. Small intramyocardial blood vessels co-localise closely with surviving CMR tagged CCs, possible supporting surviving myocyte bundles within infarcted myocardium.

### *3.4.1 Validation of CMR-LGE defined scar with gold standard histology*

Despite improvements in cardiac imaging and increasing use of post-processed CMR for catheter ablation of arrhythmia, few studies have correlated *in-vivo* CMR defined scar with whole-heart histology in either animals or humans. In a similar study, Pop et al. (2013) compared *ex-vivo* LGE and diffusion weighted imaging CMR in an infarct swine model (n=5) with picrosirius red stain identified collagenous fibrosis. Using n=9 short axis slices, they found that a ternary classification of LGE into scar, BZ and normal tissue demonstrated good correlation between imaging defined scar and BZ area with histology.[335] Other studies have also correlated gross histological post-infarct scar area with total CMR-LGE defined scar area [331,434]. Our study adds to this literature by using a current commercially available and clinically accessible method of CMR post-processing of *in-vivo* imaging to create a ternary definition of scar and describing its performance to as best as possible co-registered histology. Furthermore, in this study, the left ventricle was segmented to describe performance in the endocardium and epicardium. Interestingly, we have showed that performance of the CMR may be poorer in the epicardium than the endocardium. This could be because of signal contamination in the epicardial area from the nearby tissue, such as pericardial tissues or epicardial fat. Although the performance of alternate, less well accepted thresholds (of 6535 and 7030) was incrementally better for delineation of scar in the epicardium than the current clinically used 6040 threshold, these differences were small and the clinical difference of using differing settings purely for endocardial vs epicardial scar delineation is unlikely to be significant.

### *3.4.2 Chronic infarction model of anatomical CMR-CCs*

We have validated a large animal chronic infarction model with anatomical CMR-CCs co-registered to whole-heart histopathology. CMR had reasonable utility in identifying surviving myocyte bundles with varying amounts of fibrosis, adiposity and viable myocardium surrounded

by dense scar or dense adiposity. 87% of CMR-CCs were validated by histology. Furthermore, EAM suggested that, similar to previous data, DZs co-localised to the mid-channel in 47% and entrance/exit in 53% (45% and 52% respectively in work by Vasquez-Calvo et al.[429]).

HC- CCs in this ovine model appear quite similar to histological specimens at sites of human VT as described by de Bakker et al. which also showed fractionation and slowed conduction during intra-operative and ex-vivo mapping.[255] Whole-heart histology co-registered with EAM has been used to describe relationships between EAM myocardial voltage and fibrosis architecture in human and animal cardiomyopathy [70,425,426]. Furthermore, a ternary (dense scar, BZ and healthy tissue) classification of scar topography by CMR LGE has been validated in 5 swine with ex-vivo CMR (of explanted hearts) using the same Picrosirius red stain used in this study [335].

To our knowledge however, this study offers the first application of co-registered whole-heart histology to identify CMR-CCs. Such a model offers significant promise to investigate putative strategies to treat VT. CMR-CCs have been shown to predict arrhythmogenicity and ICD therapies in patients undergoing ICDs for primary prevention.[435] A randomized trial of upfront ablation of CMR-CCs in patients with chronic infarcts without VT to prevent sudden cardiac death is planned [436]. This ovine model offers opportunities to explore ablative strategies for scar-dechanneling as well as unveil possible mechanisms of how modern heart failure drugs such as SGLT2 inhibitors may have anti-arrhythmic therapies [437].

### *3.4.3 Varying CMR signal intensity thresholding to identify new channels*

Anatomical conducting channels were first defined using EAM, with manual raking of bipolar voltage to identify pathways of contiguous electrogram recordings within scar with a higher voltage than surrounding areas as determined by voltage map colour differences, with these channels subsequently validated by entrainment and activation [438]. CMR-CCs were similarly first

validated by comparison with EAM voltage maps in 10 patients and a total of 16 CMR-CCs.[338] Until our study, histological validation has been lacking and the CMR fibrosis threshold of 60% and 40% has been used (primarily as it identified 13/16 EAM channels compared to 50% and 70% dense scar thresholding). Importantly, of the 23 unique CMR-CCs we identified, 15/23 (65%) were from alternative thresholds. The presence of DZs did not differ between threshold groups. 13/15 (87%) of these non 6040 channels were validated by histology. These data suggest that varying CMR thresholding may help to uncover further arrhythmogenic substrate.

### *3.4.4 Co-localisation of DZs with CMR-CCs are robust despite varying activation wavefront*

To our knowledge, this is the second time that DZs have been assessed with differing activation wavefronts. We found that DZs co-localized with CMR-CCs irrespective of activation wavefront (18 of 19 co-localized DZs observed in 3 different wavefronts). In the seminal work by Aziz et al (2019) 13 cases were assessed with two distinct wavefronts of which 86% of cases were conserved.[427] In contrast to our series, this original series included variable scar patterns and aetiology (ischaemic and non-ischaemic) vs our fixed anteroseptal infarcts, and this heterogeneity may explain the slightly differing findings. Interestingly, for the 1 channel in our series where the LVp ILAM map did not identify the DZ seen in both SR and RVp, the activation wavefront appeared parallel to the CMR-CC (Figure 4). Aziz et al. (2019) present two multi-wavefront ILAM maps. In their first, the DZ is conserved across wavefronts despite pacing parallel to the line of block (see Figure 4, pp 1390, Aziz et al (2019)). In their second example however, like our findings, an activation wavefront parallel to the original DZ fails to uncover it (see Supplemental Figure 3, p8, Aziz et al (2019)). An important limitation of our work is that differential pacing was not performed to interrogate the observed DZs to demonstrate overt lines of block and/or delineate

the lateral isthmus boundaries of the channel and this would be important to assess in future work.[272]

### *3.4.5 Adiposity and not fibrosis is associated with the presence of DZs at sites of CMR-CCs*

This study attempted to identify the histological characteristics of DZs with regards to quantification of fibrosis, adiposity and VM. Interestingly, we found that within channels, segments co-localising with DZs had higher adiposity but similar fibrosis compared to segments without DZs. Differences in VM (remaining myocardium once adipose tissue and fibrosis were excluded) was likely driven by the marked difference in adiposity. Using co-registered CT, CMR and EAM, Sung et al. (2022) demonstrated that DZs were found primarily in regions with infiltrating fat plus scar or infiltrating fat without scar and less so scar without infiltrating fat [439]. Regions with higher amounts of infiltrating fat associated with more ablated tissue and sites of DZs. No such relationship was demonstrated in regions with higher fibrosis. Xu et al. (2022) found that 99% of corridors critical for VT either traverse or are adjacent to CT defined lipomatous metaplasia. In a similar animal model to our study, Pouliopoulos et al. (2013) demonstrated that intramyocardial adiposity correlated with reduced conduction velocity, possibly due to lateralization of Connexin-43 [430]. Longitudinal CMR studies have demonstrated that infarct size as defined by CMR progressively decreases over time however up to 24% of patients develop lipomatous metaplasia after 9 years [440]. In our study, we have shown that within channel regions of DZs (which may be considered surrogates for VT corridors) not only traverse near lipomatous metaplasia (as suggested by Xu et al. (2022)) but are in-fact composed of more adipose tissue than those without DZs. Together, these data suggest against previous hypotheses that post-infarction VTs are caused by heterogenous fibrosis and electrical changes over time. Instead, within channel

adiposity may be a key contributor to conduction slowing (and possibly arrhythmogenicity) of post-infarction substrate.

### *3.4.6 Co-localization of intramyocardial blood vessels with surviving CMR-CCs.*

In this study we have demonstrated co-localization of intramyocardial blood vessels with surviving CMR-CCs, most of which harbour DZs. In a 6 week swine model of MI, Dhanjal et al. (2017) demonstrated vascular enrichment at border zone sites harbouring VT critical isthmii (1.7 times vessels compared to border zone without VT critical isthmii as defined by pace-mapping).[441] These blood vessels could support the channels of surviving myocardium responsible for VT, and in particular, intramyocardial arrhythmogenic substrate. Interruption of vascular supply to these territories, abolishing surviving myocardium might be therapeutic. Transcoronary ethanol ablation has been shown to associated with a reduced burden of VT in traditional radiofrequency ablation refractory cases. [442]

### *3.4.7 Study Limitations*

This study was designed to validate EAM and CMR scar and CMR-CCs with ground truth histology. It involves a small number of animals studied at a single chronic time point. Furthermore, VT inducibility was not performed which affects interpretation of the results and is a missed opportunity for this dataset. Although DZs were used as a surrogate marker of arrhythmogenicity of CMR-CC anatomical channels and many prior studies have demonstrated that CMR-CCs and DZs co-localise with critical sites of VT, [339,429,443] this relationship is not always 1:1. Thus, although hypotheses can be made regarding the arrhythmogenicity of the histological within-channel lipomatous metaplasia observed within CMR-CCs and DZs, absence of VT inducibility means that this conclusion cannot be made definitively. Furthermore, although this study assessed ovine scar at 4 months post infarction, in humans, development of lipomatous

metaplasia is more chronic[440]. Importantly however, our work suggests that a fair degree of adiposity within ischaemic scar can be modelled using sheep in an attainable timeframe, offering an attractive large-animal model to further explore mechanisms and treatment for this phenomenon.

Secondly, there were significant differences in volume between the CMR, EAM and histopathological reconstructions. Whole-heart histological reconstructions are associated with significant tissue shrinkage. In a smaller animal model, Burton et al. (2014) demonstrated 37.2% anatomical shrinkage from *ex-vivo* CMR of Lagendorff perfused rabbit hearts to fixed histology sectioned at 10 μm intervals (1853 slices per heart).[444] In comparison, on our large animal model, there was 56.5% shrinkage compared to an *in-vivo* CMR with 5mm tissue sectioning. To our knowledge, despite multiple important large animal and human whole-heart histopathology vs electroanatomic studies, [70,426,445,446] ours is the first to describe and compare volumes between modalities. In our study, the average surface registration error of the histopathology mesh to the EAM mesh was 4.9mm (3.8-6.3mm), which performed similar to pioneering work by Glashan et al. (2019) who had a registration accuracy of 5.4 ± 3.7 mm in 9 swine[426] suggesting similar levels of shrinkage in either model. In our study CMR and pathology-identified fiducial landmarks were used for registrations to EAM landmarks identified with ICE for all cases. Arguably, validation of 20/23 CMR-CC channels by histology and good histological-CMR scar agreement despite this described shrinkage and co-registration error suggests that at worst, the accuracy of CMR is *under* rather than *over* called.

Thirdly, this study focused purely on CMR delayed enhancement to recognize fibrosis. Other CMR mapping techniques for fibrosis such as T1 mapping for diffuse fibrosis was not

performed in a short axis stack and hence could not be reconstructed into a 3D model to be co-registered with the histology in this study.

Fourthly, the version of ADAS-3D employed used in this study employed a full-width half maximum method to define scar. As has been demonstrated by Glashan et al. (2018), other methods of CMR delayed enhancement post-processing such as using standard deviation or maximal signal intensity can perform differentially in identifying scar and hence may offer better agreement to ground truth histology.[70] Furthermore, as this study was done in an infarct model, it is not clear whether agreement would be as effective in non-ischaemic cardiomyopathy. Finally, alternative commercially available post-processing software such as InHeart (IHU Lyric, Pessac, France) may perform differentially and this could be assessed in future work.

## 3.5 Conclusions

In this ovine chronic infarction model, LGE CMR derived scar and channels were validated by histology and EAM, offering an attractive model to trial future strategies to treat ventricular tachycardia. CMR post-processing and integration with EAM offers accurate delineation of histological scar (with better agreement in the endocardium than epicardium). Varying CMR pixel intensity thresholds beyond the current clinically used 6040 ADAS-3D threshold unveiled new histologically and EAM validated channels. Regions of CMR-CCs at sites of DZs had higher within channel adiposity but not higher fibrosis than regions without DZs suggesting a role for lipomatous metaplasia contributing to conduction slowing in post-infarction scar.

## 3.6 Figures

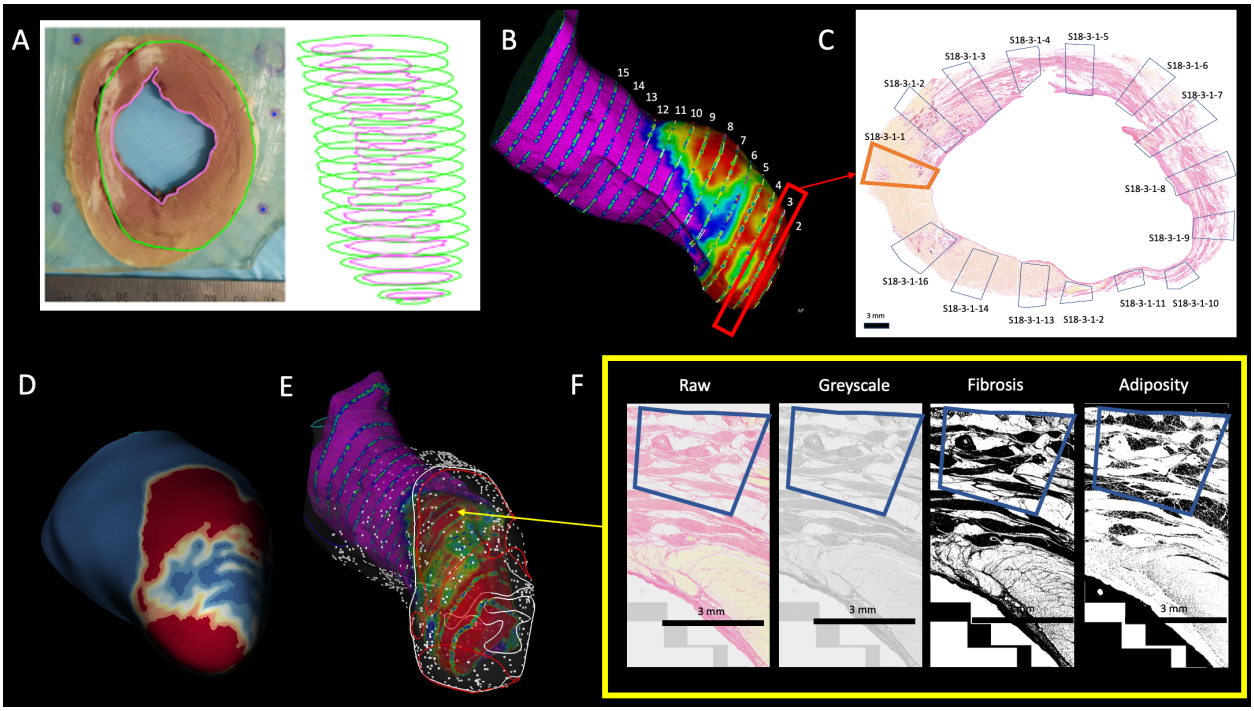


**Figure 3-1 Methodology of cardiac magnetic resonance imaging scar analysis and histological reconstruction**

Methodology of cardiac magnetic resonance imaging (CMR) scar analysis and histological reconstruction. **A.** After fixation, explanted hearts were sectioned into 5mm short-axis slices and photographed. Endocardial and epicardial borders were manually traced and imported into MATLAB to make scaled 3D meshes which could then be imported into Carto mapping software. **B.** A representative histological 3D mesh. Numbers 2-15 demonstrate cross-sectional slices with 5mm spacing. **C.** A scaled photograph of cross-section 3 taken at 20x magnification after staining with Picrosirius red to identify collagenous tissue. Biopsies were systematically conducted around the endocardial border of the short-axis sections – 3mm width with 3mm spacing between biopsies. Endocardial (0-50% of wall thickness of the biopsy) and endocardial (50-100% of wall thickness

of the biopsy) sections were interrogated. **D.** ADAS-3D map of the epicardial layers (50-100%) at the standard 60-40 threshold whereby blue represents normal tissue (regions with < 40% pixel signal intensity), red the dense fibrosis (>60%) and white/yellow the border zone regions (40-60%). **E.** Merged 3D histological reconstruction with overlying electroanatomic map (white dots represent individual electrograms from the mapping Pentaray catheter). Traced onto the electroanatomic map is the ADAS-3D CMR from D, whereby red outlines dense scar (>60% pixel signal intensity) and white border zone (40-60%). This allows direct co-registered comparison between histological biopsies in C with CMR. **F.** shows ImageJ analysis of a co-registered biopsy. It is taken from a CMR region of dense scar. As seen in the co-registered image, the epicardial histological layer has compact fibrosis (dense pink staining) with interspersed adiposity (white) and minimal "viable" myocardium (yellow). This was converted to a greyscale image before subsequent analysis for fibrosis (image panel 3) where the upper threshold limit was decreased to 180-220 to visually match fibrosis in raw image whereby fibrosis appears black and then adiposity (increased lower threshold limit to 245-250) whereby adipose tissue appears black.

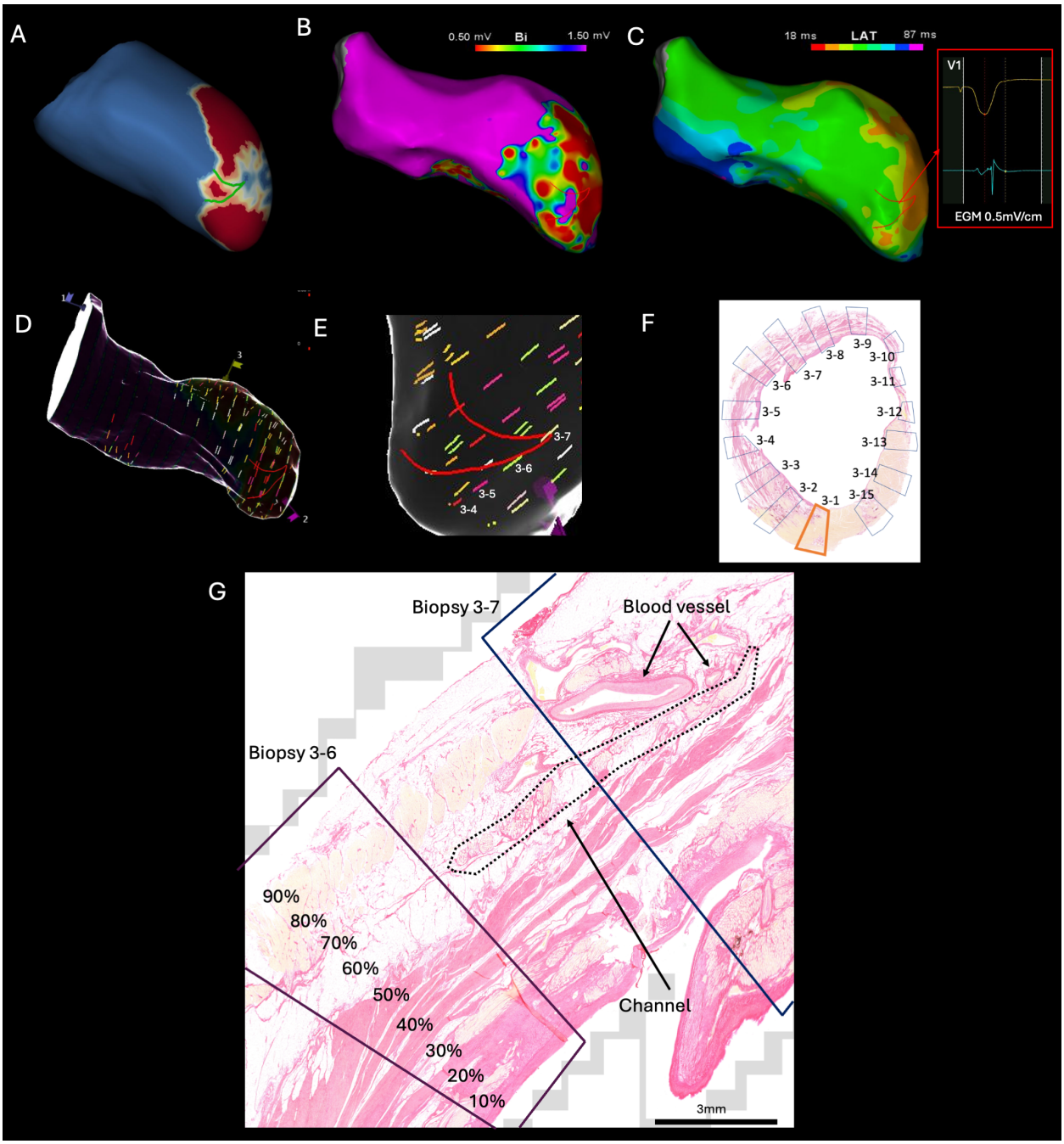


**Figure 3-2 Methodology of CMR channel analysis**

Methodology of cardiac magnetic resonance imaging (CMR) channel analysis. **A.** Using varying pixel signal intensity thresholds, ADAS-3D was used to identify scar topography in the endocardium (0-50% layers) and epicardium (50-100% layers) and identify channels (green). **B.**

Channel (seen in red) was traced onto electroanatomic map (EAM) after co-registration using standard fiducial markers i.e. aortic anulus, mitral anulus, apex papillary muscles with cross validation from intracardiac echocardiography. Bipolar map (dense scar <0.5mV, border zone <1.5mV). **C.** Isochronal late activation map with manual annotation of each electrogram to offset of bipolar electrogram. Deceleration zone (DZ) (crowding of ≥3 isochrones ) at mid channel. Bipolar electrogram at site of DZ demonstrates fractionation and splitting **D.** Co-registered shell of histological fibrosis with 3mm transmural biopsy lines spaced every 3mm. **E.** Zoom of co-registered shell of histological fibrosis with transmural biopsy lines transecting channel. F. 2D photograph of axial slice through which channel passes. Transmural biopsies 3-6 and 3-7 co-localise to channel at 60% layer as defined by CMR. G. Zoom of histology demonstrating a channel of surviving myocytes (pale yellow) at the 60% layer and at the 3-7 transmural biopsy surrounded by dense scar (pink) and adiposity (white). Blood vessels in close vicinity.

Abbreviations: Bi – bipolar, EGM – electrogram, LAT – local activation time.

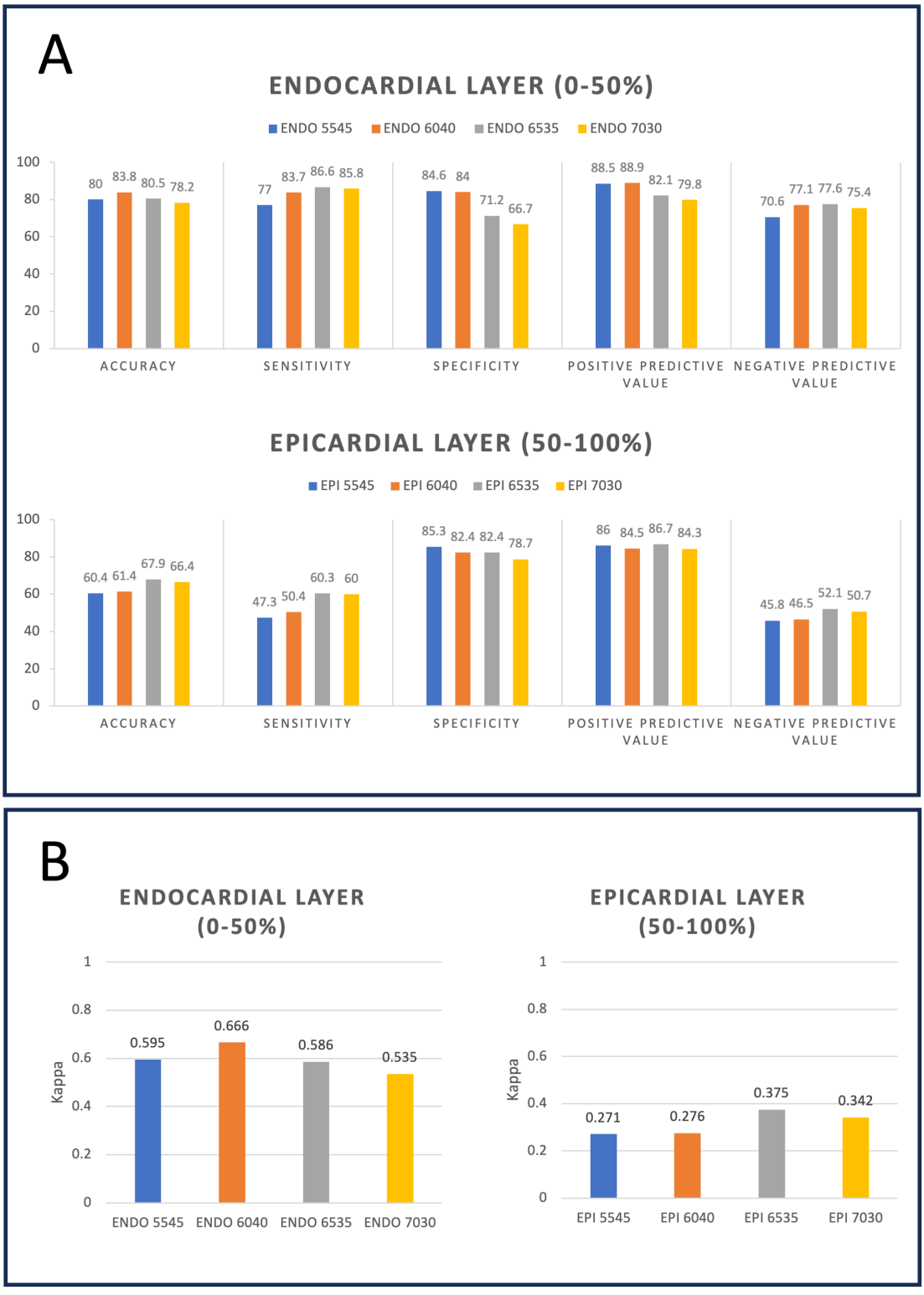


**Figure 3-3 Performance of CMR stratified by layer (endocardial and epicardial)**

Accuracy **(A)** and Agreement **(B)** of late gadolinium enhanced (LGE) derived cardiac magnetic resonance imaging (CMR) fibrosis (by varying thresholds) compared to histological scar. Abbreviations: Endo – endocardial 0-50% layers, Epi – epicardial 50-100% layers.

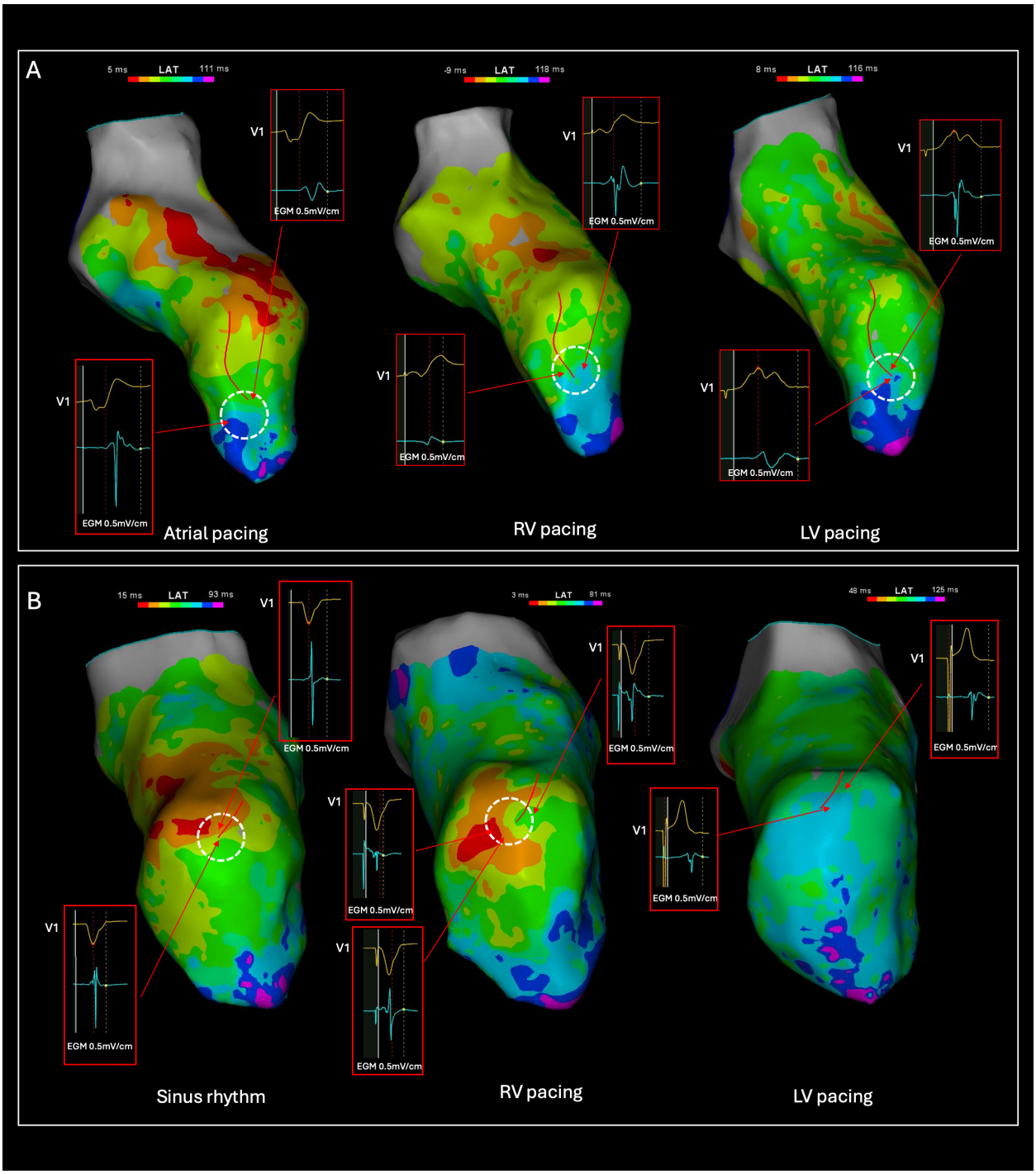


**Figure 3-4 Representative example of colocalization of CMR-CCs with DZs across wavefronts**

Eighteen of 23 CMR-CCs had agreement across wave fronts (sinus rhythm/atrial pacing, right ventricular pacing [RVp], and left ventricular pacing [LVp]). One of 23 CMR-CCs had agreement between sinus rhythm and RVp, but this DZ was not seen in LVp. **A**, CMR-CC is identified by 7030 pixel signal intensity (50% layer) and validated by histology (red line). It colocalizes with DZs at the entrance/exit of the channel in all 3 wave fronts (white dashed circles); atrial pacing: dark green, pale green and pale blue isochrones, RVp yellow, dark green, pale green and pale blue isochrones, LVp pale green, and pale blue and dark blue isochrones. **B**, CMR-CC is identified by 6040 threshold (50% layer) and validated by histology (red line). It colocalizes with DZ at the entrance/exit of the channel in sinus rhythm (red, orange, yellow, and dark green) and RVp (red, orange, yellow, and dark green) but not with LVp (pale green, pale blue). LAT indicates local activation time.

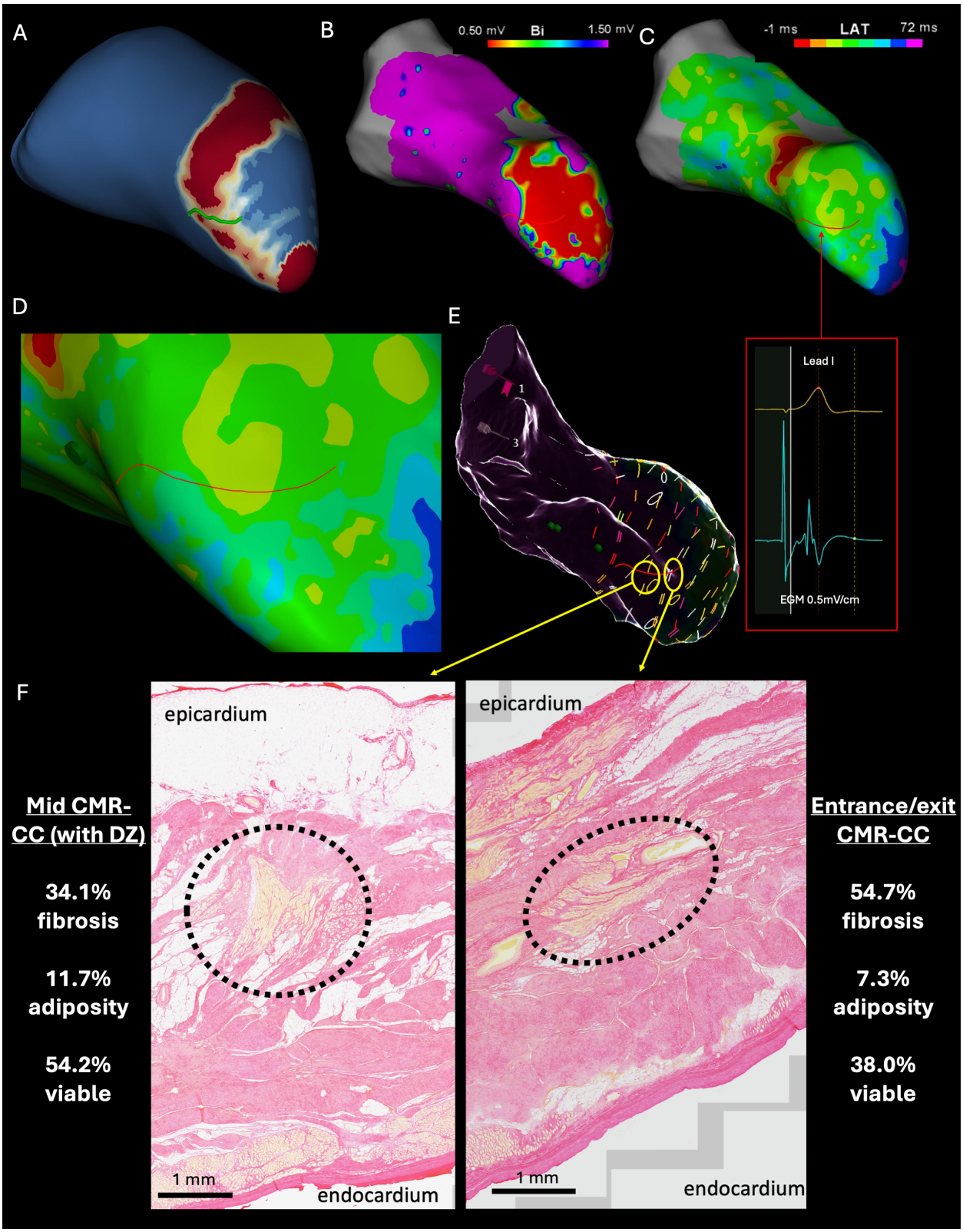


**Figure 3-5 CMR channel identified by 6040 signal intensity threshold and validated by histology**

**A**, ADAS-3D identification of channel topography (found in 60% layer). **B**, Coregistered bipolar voltage map (red denotes dense scar <0.5 mV, purple denotes healthy tissue >1.5 mV, and green denotes intermediate border zone 0.5–1.5 mV). The CMR channel is traced in red after coregistration. **C**, Deceleration zone (DZ) at mid-isthmus on isochronal late activation map (crowding of yellow, dark green, and pale green isochrones) during right ventricular pacing. Representative EGM shows fractionation at mid-isthmus. **D**, Zoom view of DZ. **E**, Coregistered histological fibrosis shell with ADAS-3D channel drawn and 3 mm transmural biopsies spaced every 3 mm. **F**, Histological biopsies are shown. **Left**, the mid-isthmus of the channel is identified on histology with surrounding dense scar and adiposity. Intrachannel fibrosis, myocardium, and viable tissue were quantified. **Right**, the entrance/exit segment of the channel is identified on histology with surrounding dense scar and adiposity. Surrounding blood vessels are visualized. There is higher adiposity in the mid-channel (where the DZ is located). CMR-CC in cardiac magnetic resonance imaging conduction channels; and LAT, local activation time.

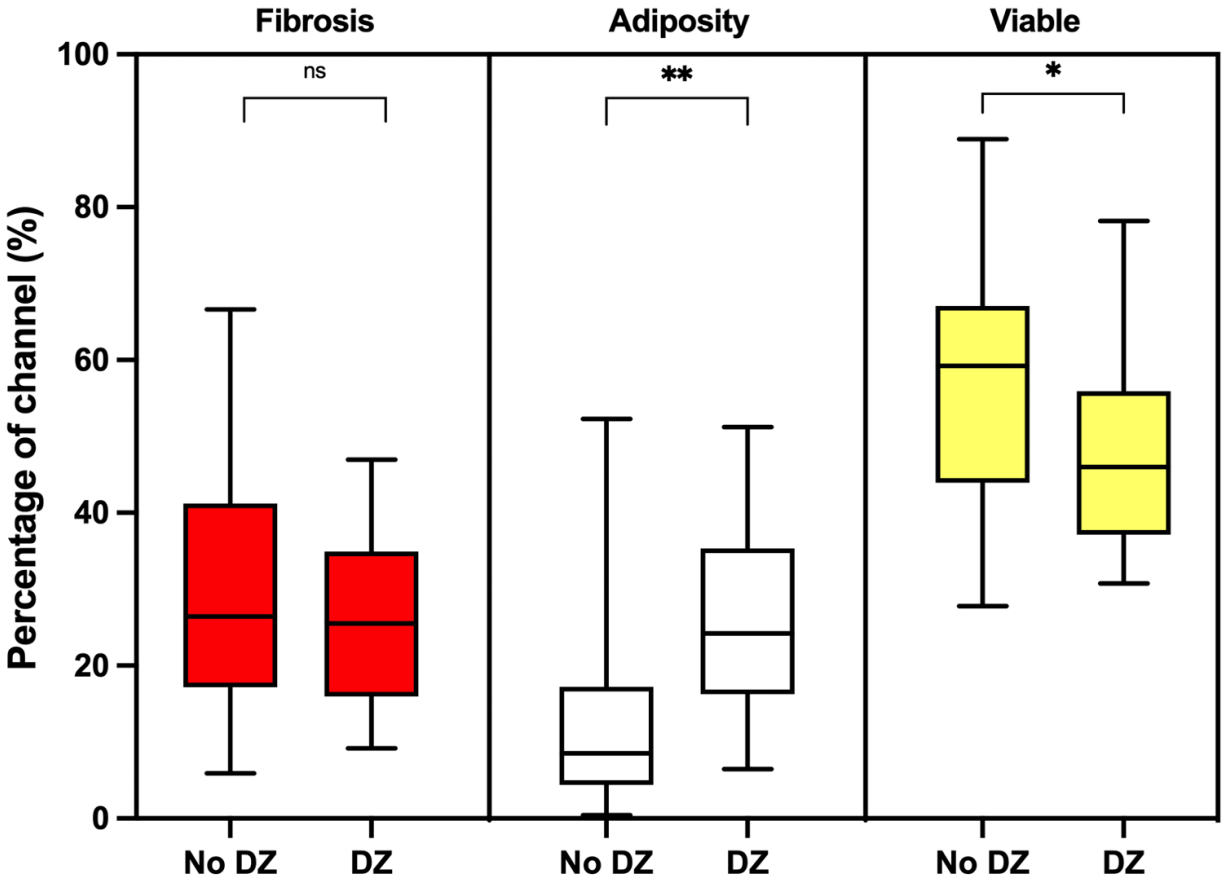


**Figure 3-6 Intra channel composition stratified by presence or absence of DZ identified by at least 1 wavefront**

Percentage of channel (traced with surrounding adiposity and fibrosis excluded) that has intrachannel fibrosis, adiposity, and viable tissue quantified stratified by presence or absence of deceleration zone (DZ) identified by at least 1 wave front. Statistical analysis with the Mann-Whitney *U* test, *P* values <0.05 are considered significant.

## 3.7 Tables

**Table 3-1 Description of CMR-CCs identified by various signal intensity thresholding**

| Channel | ADAS-3D threshold | Layers | Channel length (mm) | Histological confirmation | SR / Atrial paced DZ | RVp DZ | LVp DZ |
|---|---|---|---|---|---|---|---|
| 1 | 7030 | 60 | 21 | Yes | Entrance/Exit | Entrance/Exit | Entrance/Exit |
| 2 | 6040 | 60,70,80 | 27 | Yes | Mid | Mid | Mid |
| 3 | 6040 | 10,20,30,40 | 41 | Yes | Mid | Mid | Mid |
| 4 | 7030 | 20 | 37 | Yes | Mid | Mid | Mid |
| 5 | 5545 | 10 | 9 | Yes | Entrance/Exit | Entrance/Exit | Entrance/Exit |
| 6 | 5545 | 20 | 7 | Yes | Not present | Not present | Not present |
| 7 | 5545 | 20 | 6 | Yes | Entrance/Exit | Entrance/Exit | Entrance/Exit |
| 8 | 6040 | 90 | 15 | Yes | Not present | Not present | Not present |
| 9 | 6535 | 80 | 28 | Yes | Entrance/Exit | Entrance/Exit | Entrance/Exit |
| 10 | 6535 | 90 | 12 | Yes | Not present | Not present | Not present |
| 11 | 7030 | 10 | 19 | No | Not present | Not present | Not present |
| 12 | 5545 | 10 | 16 | No | Entrance/Exit | Entrance/Exit | Entrance/Exit |
| 13 | 6040 | 30,40 | 82 | Yes | Mid | Mid | Mid |
| 14 | 6040 | 50 | 10 | Yes | Entrance/Exit | Entrance/Exit | Not present |
| 15 | 6040 | 60 | 21 | Yes | Entrance/Exit | Entrance/Exit | Entrance/Exit |
| 16 | 5545 | 40,50 | 15 | Yes | Mid | Mid | Exit |
| 17 | 6040 | 50,60,70,90 | 42 | Yes | Mid | Mid | Mid |
| 18 | 6040 | 40 | 19 | Yes | Entrance/Exit | Entrance/Exit | Entrance/Exit |
| 19 | 6535 | 40,50 | 34 | Yes | Mid | Mid | Mid |
| 20 | 6535 | 90 | 32 | Yes | Mid | Mid | Mid |
| 21 | 7030 | 20,30,40,60 | 126 | Yes | Mid | Mid | Mid |
| 22 | 7030 | 70,80 | 14 | No | Entrance/Exit | Entrance/Exit | Entrance/Exit |
| 23 | 5545 | 90 | 15 | Yes | Entrance/Exit | Entrance/Exit | Entrance/Exit |

**Abbreviations:** DZ – deceleration zones, LVp – Left ventricular pacing, RVp – Right ventricular pacing, SR – sinus rhythm

## 3.8 Supplemental Material

### *3.8.1 Supplementary Tables*

**Supplemental Table 3-1 Fibrosis, adiposity and viable myocardium in ADAS 3D defined tissue stratified by threshold**

| Threshold | Location | ADAS 3D definition | Histological fibrosis (%) | Histological adiposity (%) | Histological remaining "viable" myocardium (%) |
|---|---|---|---|---|---|
| 5545 | Endocardium | Normal | 8.2 (5.1-19.0) | 19.4 (13.3-24.8) | 68.7 (59.4-77.7) |
| | | Borderzone | 44.6 (15.2-66.9) | 14.3 (9.7-22.8) | 35.2 (22.7-60.6) |
| | | Scar | 43.2 (32.3-53.8) | 22.3 (14.7-32.3) | 29.3 (21.3-42.2) |
| | Epicardium | Normal | 12.6 (5.9-38.7) | 19.0 (12.0-25.4) | 63.4 (34.3-74.2) |
| | | Borderzone | 41.6 (22.0-53.7) | 20.7 (14.3-27.4) | 30.4 (21.8-59.7) |
| | | Scar | 42.9 (26.5-53.7) | 20.0 (14.5-26.1) | 33.8 (21.0-51.1) |
| 6040 | Endocardium | *Normal* | 7.4 (4.9-15.2) | 19.3 (12.8-25.1) | 70.5 (61.2-78.1) |
| | | *Borderzone* | 44.7 (25.4-61.1) | 16.8 (10.9-23.8) | 32.4 (23.9-57.5) |
| | | *Scar* | 42.5 (32.1-53.8) | 22.8 (14.9-32.8) | 27.6 (20.9-43.3) |
| | Epicardium | *Normal* | 12.2 (6.0-38.6) | 18.6 (11.7-24.6) | 64.6 (35.8-75.2) |
| | | *Borderzone* | 41.8 (19.5-54.3) | 22.1 (15.3-31.6) | 30.4 (23.4-53.5) |
| | | *Scar* | 42.0 (25.9-52.8) | 20.6 (14.7-26.1) | 34.6 (21.2-51.1) |
| 6535 | Endocardium | Normal | 7.4 (5.0-13.8) | 19.6 (13.3 – 24.7) | 71.1 (62.3-78.1) |
| | | Borderzone | 38.7 (11.6-59.4) | 17.8 (10.9-24.6) | 37.4 (24.5-61.1) |
| | | Scar | 42.5 (32.0-53.7) | 22.6 (14.7-32.3) | 29.1 (21.3-45.1) |
| | Epicardium | Normal | 10.7 (5.3-29.9) | 18.9 (12.0-24.7) | 66.8 (45.4-76.3) |
| | | Borderzone | 41.6 (21.5-55.9) | 20.9 (14.0-30.7) | 29.3 (22.5-53.5) |
| | | Scar | 43.9 (28.5-53.7) | 19.4 (12.2-25.2) | 34.6 (21.2-51.1) |
| 7030 | Endocardium | Normal | 7.6 (5.0-15.2) | 19.3 (12.3-24.2) | 71.1 (61.3-78.1) |
| | | Borderzone | 38.4 (11.1-56.1) | 18.3 (11.2-24.7) | 37.8 (24.5-62.3) |
| | | Scar | 42.5 (31.8-53.2) | 24.1 (16.2-34.0) | 27.1 (20.3-42.6) |
| | Epicardium | Normal | 11.4 (5.6-32.1) | 18.4 (11.6-24.6) | 65.8 (43.1-76.1) |

| | | | | | |
|---|---|---|---|---|---|
| | | Borderzone | 41.4 (19.1-53.9) | 20.5 (14.0-28.9) | 31.0 (23.0-58.1) |
| | | Scar | 44.4 (28.2-53.7) | 21.3 (14.9-27.4) | 30.9 (20.4-49.4) |

All data presented are medians with interquartile range.

**Supplemental Table 3-2 Channel composition stratified by presence or absence of DZ and activation wavefront**

| Wavefront | Within channel composition | No DZ | DZ | P value |
|---|---|---|---|---|
| Any wavefront[1] | Fibrosis (%) | 28.7 (19.0-41.2) | 25.0 (16.3-34.1) | 0.242 |
| | Adiposity (%) | 8.3 (4.6-17.2) | 24.1 (15.6-34.9) | <0.001 |
| | Viable myocardium (%) | 58.9 (45.0-66.5) | 46.8 (37.4-59.3) | 0.054 |
| Sinus rhythm / atrial pacing | Fibrosis (%) | 25.6 (17.2-41.2) | 27.9 (16.3-35.6) | 0.840 |
| | Adiposity (%) | 8.8 (4.8-20.3) | 24.1 (15.6-34.9) | <0.001 |
| | Viable myocardium (%) | 58.0 (43.6-66.5) | 45.2 (37.4-54.2) | 0.024 |
| Right ventricular pacing | Fibrosis (%) | 26.5 (17.2-41.2) | 25.5 (16.3-34.7) | 0.566 |
| | Adiposity (%) | 8.5 (4.5-17.2) | 24.2 (16.5-34.9) | <0.001 |
| | Viable myocardium (%) | 59.2 (44.3-67.0) | 46.0 (37.4-54.8) | 0.021 |
| Left ventricular pacing | Fibrosis (%) | 26.5 (16.6-42.3) | 25.5 (17.2-34.1) | 0.545 |
| | Adiposity (%) | 9.0 (4.9-19.0) | 24.2 (15.6-36.8) | <0.001 |
| | Viable myocardium (%) | 58.0 (44.3-66.7) | 43.6 (36.3-54.2) | 0.021 |
| Wavefront agreement[2] | Fibrosis (%) | 24.6 (16.6-41.2) | 26.8 (17.3-35.2) | 0.913 |
| | Adiposity (%) | 8.4 (4.5-17.5) | 24.4 (17.5-38.3) | <0.001 |
| | Viable myocardium (%) | 60.7 (45.4-68.2) | 40.5 (35.1-51.5) | <0.001 |

1. Presence of deceleration zone (DZ) was scored if a DZ was co-localised to channel biopsy in at least 1 wavefront
2. Presence of DZ was scored if a DZ was co-localised to a channel biopsy in a majority of tested wavefronts (i.e. present in at least 2 of the 3 wavefronts)

All data presented are medians with interquartile range. Statistical analysis with Mann-Whitney U test, p value less than 0.05 considered significant.

# Chapter 4

# 4 UTILITY OF IMAGE INTEGRATION TO IDENTIFY HISTOLOGICAL AND ELECTROANATOMIC VENTRICULAR SCAR: AN INTER-VENDOR CLINICOPATHOLOGICAL STUDY

Author attribution statement

| **Title of submitted work** | **Utility of image integration to identify histological and electroanatomic ventricular scar: an inter-vendor clinicopathological study** |
|---|---|
| **Nature of the candidate's contribution** | Design of study, assisting in human catheter ablation, data collection and analysis including processing and annotation of electrograms, post-processing of histopathology and CMR, co-registration of data, statistical analyses, manuscript writing and submission to journal |
| **Co-Authors** | **Nature of contribution** |
| Timothy Campbell | Lead source animal experiments and histopathology staining and sectioning (prior to PhD candidate's thesis commencement). Comments on methodology and manuscript. |
| Richard Bennett | Contributed towards animal experiments and comments on manuscript |
| Robert D. Anderson | Contributed towards animal experiments and comments on manuscript |

| | |
|---|---|
| Chris Davey | Software design for image integration of tissue histopathology to electroanatomic map |
| Alexandra K. O'Donohue | Contributed to histology experiments and comments on manuscript |
| Aaron Schindeler | Contributed to histology experiments and comments on manuscript |
| Samual Turnbull | Contributed to animal experiments and comments on manuscript |
| Dinesh Selvakumar | Contributed to animal experiments and comments on manuscript |
| Ashwin Bhaskaran | Comments on manuscript |
| Yasuhito Kotake | Comments on manuscript |
| Chi Jen Hsu | Advice on imaging experiments and comments on manuscript |
| James H. Chong | Comments on manuscript |
| Eddy Kizana | Comments on manuscript |
| Saurabh Kumar | Overall supervision. Animal experiments and experimental design. Comments on manuscript. |
| Signature of candidate<br>Kasun De Silva | |
| Signature of supervisor (signed on behalf of all co-authors)<br>Saurabh Kumar | |

## 4.1 Introduction

The success of catheter ablation (CA) for ventricular tachycardia (VT) is predicated on the precise identification of the arrhythmogenic substrate and scar. Invasive electroanatomic mapping identifies myocardial scar by collecting an "electrical biopsy" of ventricular tissue at the site of the recording catheter electrodes, however, such electrograms are influenced by the direction of activation wavefront, interelectrode size and spacing, filtering settings and tissue contact.[27] Image integration of late gadolinium enhancement (LGE) cardiac magnetic resonance imaging (CMR) is an alternative and non-invasive way to identify the scar location and topography.[447] At present there are two commonly used commercial solutions to integrate CMR scar into VT CA - ADAS-3D (Barcelona, Spain) and inHEART (Bordeaux, France). Observational studies have shown an improvement in CA outcomes using these technologies.[339,340,448] It remains unclear, however, if there are differences in the performance of inter-vendor technologies to identify histological scars and also how such technologies could differentiate endocardial from intramural and epicardial scar. Furthermore, there are no direct comparisons of these vendors in humans for the identification of scar, critical VT circuit sites or functional substrate with CMR LGE.

We recently described a method for panoramic assessment of electrophysiologic substrate for VT in an ovine chronic infarct model whereby high-density electroanatomic data can be merged with CMR and explanted whole heart histology using in-house custom-designed software.[449] We demonstrated that CMR LGE border-zone "channels" correlate with deceleration zones (DZs) and histological channels of viable myocytes with associated lipomatous metaplasia at these sites of conduction slowing. Using this model, we now describe a clinicopathologic study whereby we sought to validate two commonly used vendor systems (ADAS-3D and inHEART) to integrate

CMR LGE to electroanatomic mapping (EAM) in CA of VT, firstly in an *in vivo* post-infarction ovine model and subsequently, in a series of human patients with VT undergoing catheter ablation.

## 4.2 Methods

This study was performed on castrated merino sheep and human patients undergoing VT CA. All animal experiments were approved by the Animal Ethics Committee of Westmead Hospital and the study conformed with the animal research guidelines of the National Health and Medical Research Council of Australia. Human data for this study was collected as a part of the VA-West registry, with ethics approved by the Western Sydney Local Health District Human Research Ethics Committee. Data from this study is available for sharing on reasonable request for the purposes of replicating the results.

### *4.2.1* ***Ovine infarct experiment***

The animal experiment from which the data for this study originated has been described in our previous publications.[254,449] In brief from this experiment, of the 10 sheep available (6 infarcted distal to the second diagonal branch for 3 hours, 4 controls without infarction), 5 sheep (weighing 53±7kg) went on to have a CMR and EAM and were included in this study.

#### ***4.2.1.1 CMR acquisition***

For the animals, LGE CMR was performed with a 3T Prisma system (Siemens, Munich, Germany) with 4-lead ECG cardiac gating and all sequences were performed with breath-holding in end-expiration. Delayed enhancement images were acquired using a segmented inversion recovery fast gradient echo sequence in short-axis stack (4-5mm slice thickness with in-plane resolution of 1.5x1.5mm). The time of inversion scout was performed at 9 minutes post

contrast to select appropriate inversion time (usually around 300 milliseconds) for delayed enhancement acquisitions, which began at 11 minutes post injection.

#### *4.2.1.2 CMR post processing*

CMR post-processing was performed using two commercially available software. For ADAS-3D, manual tracing of the endocardial and epicardial borders was performed by the study team with subsequent semiautomatic generation of the left ventricle (LV) shell. So that direct comparison could be made with inHEART, ADAS-3D was used to create a total of three maps (endocardial - inner third, intramural - middle third and epicardial - outer third) whereby LGE pixel signal intensity is projected onto each map and coded according to a trilinear interpolation algorithm using 40% and 60% of the maximum intensity for border-zone and dense scar respectively. For inHEART, the CMR was shared on a cloud-based platform for segmentation by the commercial product team. Previous inHEART publications have reported a similar trilinear algorithm to ADAS-3D, (35% and 55% of maximum intensity for border-zone and dense scar respectively).[341] Endocardial, intramural and epicardial scar maps were exported. For the purposes of this analysis, CMR scar was defined to encompass both borderzone/gray zone and dense scar. Segmented models were merged into the EAM (CARTO 3, version 7, Biosense Webster) using the CARTOMERGE module. They were co-registered using >3 fiducial points (e.g. coronary arteries, aortic root, mitral annulus and LV apex) identified by 3-dimensional intracardiac echocardiography (ICE) using the CARTOSOUND module.

#### *4.2.1.3 Electroanatomic mapping*

For the EAM, multiple-wavefront mapping was performed (4/5 sinus rhythm, 1/5 right atrial pacing, 5/5 right ventricular (RV) pacing, 5/5 LV pacing). Standard bandpass filtering was performed at 16-500 Hertz for bipolar electrograms and 2-240 Hertz for unipolar electrograms.

Mapping was performed with the multielectrode Pentaray catheter (Biosense Webster). Bipolar scar (<1.5 mV), unipolar scar (<8.3 mV), split potentials (>20 milliseconds isoelectric period between EGMs), and other local abnormal ventricular activities (LAVA) classified using previously published LAVA definitions, were identified.[20]

Whole-heart histological reconstruction and co-registration was performed as shown in Figure 1. Hearts were filled with cotton filler to maintain shape and fixed in 10% neutral buffered formalin (7 days) prior to being placed in a ballistic gelatine mould and sectioned at 5mm intervals along the short axis. Photographs of these sections were underwent endocardial and epicardial borders tracing to create three-dimensional meshes in MATLAB (Mathworks, R20196b) using a custom algorithm which were also imported into the EAM (CARTOMERGE). Furthermore, the 5mm slices were embedded in paraffin blocks and then 5µm-thick slices were cut from the basal surface (RM2155, Leica Biosystems, Wetzlar, Germany). Collagenous tissue was identified with Picrosirius red staining performed with a Weigert's haematoxylin counterstain. Stained sections were imaged with brightfield illumination at 20x magnification. Biopsies with a width of 3mm were systematically marked around the endocardial surface with a 3mm spacing. For each endocardial (inner third of myocardium), intramural (middle third of myocardium) and epicardial (outer third of myocardium) segments of the biopsies, scar was identified by the presence of collagenous tissue (pink with picrosirius red staining). The ADAS-3D and inHEART CMR scar was matched to whole heart histology as shown in Figure 1. Further, biopsies were analysed on ImageJ (National Institutes for Health, Bethesda, Maryland, USA) to identify fibrosis, adiposity and remaining "viable myocardium" as previously described.[449]

### *4.2.2 Clinical experiments*

Human patients with structural heart disease who underwent CMR with LGE, LV (endocardial ± epicardial) mapping and had both ADAS-3D and inHEART CMR scar maps available for analysis were recruited retrospectively. These studies were selected due to availability of both inHEART and ADAS-3D post processing from the VA-West Registry as well as the presence of complete LV ± RV ± epicardial substrate mapping.

#### *4.2.2.1 CMR acquisition and processing*

CMR studies for human patients were not obtained specifically for image integration and hence no standardised protocol was observed. Slice thickness of the delayed enhancement short axis stack ranged from 4-8mm and studies were performed on both 1.5 and 3 Tesla machines. Wide-band sequence was not available for any of these selected studies. For 1 of the 5 patients, both ADAS 3D and inHEART maps were available during CA, 2 of the 5 were guided by inHEART and the remaining 2 by ADAS 3D. For the latter 4, post-processing with the alternative vendor was performed off-line and these maps were retrospectively co-registered.

#### *4.2.2.2 Electroanatomic mapping*

Our approach to VT CA has been described previously.[450] In brief, non-invasive programmed stimulation was performed under light conscious sedation prior to general anaesthesia. Epicardial access was obtained (at operator discretion), guided by those who had previously had unsuccessful endocardial ablation and/or cardiac magnetic resonance imaging that suggested epicardial delayed enhancement. If VT was not induced with non-invasive programmed stimulation, VT induction was performed with a quadripolar catheter advanced into the RV apex, with an 8 beat 400ms drive train and up to 4 extra stimuli, with each introduced at 300ms and decrementing by 10ms down to ventricular refractoriness. If VT was not inducible with programmed electrical stimulation, burst RV pacing and repeat programmed electrical stimulation

with/without isoprenaline challenge up to 40 microg/min was performed. The LV was accessed via transeptal approach with ICE guidance after systemic anticoagulation with intravenous heparin. ICE was also used to define anatomical landmarks and ventricular scar and to facilitate CMR integration.

High density substrate mapping in all cases was performed with CARTO 3 using a multi-electrode catheter (DecaNav, Biosense Webster) with sinus rhythm, atrial pacing or RV pacing depending on haemodynamic tolerability. Bipolar (<1.5mV) and unipolar (<8.3mV) scar as well as late potentials and LAVA were identified. DZs were identified by isochronal late activation mapping (3 or more isochrones with associated LAVA or split potentials).[271] Critical sites (VT isthmus, entrance or exit) were identified primarily by pace-mapping (PM) using a deflectable, 3.5 mm, open irrigated-tip contact force sensing ablation catheter (ThermoCool SmartTouch SF, Biosense Webster). PM (usually at a cycle length of 600ms) was performed from the tip of the ablation catheter using strict criteria: (1) contact force greater than 10 grams and (2) 10 milliAmps and 2 ms output (or 10 mA and 9 ms if no capture with former).[235] The correlation score using the CARTO 3 proprietary algorithm (PASO, Biosense Webster) was displayed on a colour coded map. The PM colouring was displayed as a 30% range using the best PM score as the upper limit to identify two patterns; abrupt change - PM correlation difference of at least 30% across two PM points within 10 mm; or centrifugal attenuation - a gradual attenuation of paced QRS correlations seen as a centrifugal correlation reduction outward from the best pace map point.[235] At sites of best pace-match, the isthmus was confirmed by entrainment or activation but haemodynamic intolerance limited this approach.

Critical sites determined by PM were identified by PM score >90%. A critical site isthmus was defined as PM score >90% with stim-QRS >40ms[451] and with abrupt change pattern.

If no abrupt change was seen, or best PM was <90%, the VT was deemed to be three-dimensional (from the intramural or contralateral surface of the LV).[452] In this case, the exit of the VT was determined at the site with PM score >90% with centrifugal attenuation pattern. If no PM score >90% was found, the VT was determined to be from an intramural circuit with passive breakout into the PM-mapped endocardial and/or epicardial surface.

Radiofrequency ablation was delivered using the same ablation catheter as used for PM. Radiofrequency energy was delivered at a power of 30-50 Watts, aiming for an impedance drop between 10-20 ohms. ICE was used for real-time visualization of the catheter tip to monitor contact and lesion formation. CA targeted VT critical sites, DZs, and LAVA/late potentials. The procedural endpoint was the non-inducibility of VT with programmed stimulation (4 extra-stimuli).

Scar areas were measured (total CMR and voltage scar, i.e. including dense scar and borderzone) as well as relationship of critical VT sites and DZ to imaging scar were measured retrospectively.

### *4.2.3* ***Statistical analysis***

Analyses were performed using Statistical Package for the Social Sciences for Windows (Version 27) and Graphpad Prism (Version 9). Continuous variables were expressed as median and interquartile range (IQR). Independent continuous data were compared by non-parametric Mann-Whitney U test. For multiple groups either Kruskal-Wallis 1-way ANOVA or Friedmans test (for matched/repeated measures) was performed with subsequent Dunn's multiple comparison test if the former was significant. Independent categorical variables were compared by the Chi-square test. For the CMR - histological comparisons, accuracy, AUC, sensitivity, specificity and agreement (Cohens Kappa, κ) were calculated. Scar sizes were correlated with linear regression

and then agreement was determined using Bland-Altman plots to describe mean difference (MD), limits of agreement (LOA) and any proportional bias. Two-tailed P-values were considered statistically significant when 0.05 or less.

## 4.3 **Results**

### *4.3.1* ***Ovine post infarction model***

Five sheep (weighing 53±7kg) had CMR (at a median 116 days IQR 86-134) and EAM (at median 129 days IQR 109-140). As previously reported, for the infarcted animals, LV ejection fraction and LV end-diastolic volumes were 41% (39-43%) and 118mls (87–155mls) respectively.[449] A total of 399 biopsies were sampled with layer-specific information available for the endocardium, intramural and epicardium (totalling 1197 biopsy segments).

Histology in all infarcted animals demonstrated complex three-dimensional scar that was not only sub-endocardial at region of infarction but often transmural, demonstrating intramural and epicardial involvement, and also sparing at the endocardium at scar border. Of the 399 biopsies, 223 (56%) contained endocardial scar, 247 (62%) intramural scar and 251 (63%) epicardial scar. Importantly, scar composition differed between the three layers. In the endocardium, 170/223 (76%) scar segments had compact scar and 53/223 (24%) had non-compact (patchy, interstitial or diffuse scar). In the intramural space, 212/247 (86%) had compact vs 35/247 (14%) non-compact scar. In the epicardium, 174/251 (69%) scar segments were compact and 77/251 (31%) were non-compact.

### *4.3.2* ***Human subjects***

Five patients were recruited (5/5 male, median age 44 (IQR 50-54). Their characteristics are described in Table 1. One had post-infarction cardiomyopathy and four had non-ischaemic

cardiomyopathy (NICM). Of these, one was gene elusive arrhythmogenic cardiomyopathy, one was recurrent myocarditis and two were undifferentiated NICM. CMR was performed median 140 days (IQR 13-265) prior to CA. Two of the five patients had a device in situ at time of the scan (ICD n=1, dual chamber pacemaker n=1).

### *4.3.3 Validation of ADAS-3D and inHEART with whole-heart histology*

As shown in Figure 2A, ADAS-3D and inHeart had comparably similar performance to identify histological scar (all scar types). Both ADAS-3D and inHeart had high accuracy to identify endocardial (75.6% and 76.5% respectively) and intramural scar (76.9% and 73.3%). There was poorer accuracy in the epicardial layer (68.1% and 59.7%) respectively. Poor performance of both vendors to identify epicardial scar was driven by low sensitivity (59.8% for ADAS-3D and 49% for inHEART). Agreement between CMR and histology for ADAS-3D and inHeart was moderate for the endocardial layers (κ 0.502 and 0.523 respectively), moderate for the intramural layers (κ 0.543 and 0.565 respectively) and fair for the epicardium (κ 0.381 and 0.238 respectively).

When stratified by compact versus non-compact scar (patchy, interstitial or diffuse scar; Figure 2B and 2C), ADAS-3D and inHEART were seen to have high sensitivity, specificity and accuracy for compact scar but poorer performance for non-compact scar with appreciable low sensitivity for non-compact scar in all three layers and with both modalities. Agreement between CMR and compact scar for ADAS-3D and inHEART was moderate for the endocardial layers (κ 0.573 and 0.585 respectively), moderate for the intramural layers (κ 0.581 and 0.486 respectively) and fair-moderate for the epicardium (κ 0.462 and 0.382 respectively). In contrast, agreement between CMR and non-compact scar for ADAS-3D and inHeart was only fair in the endocardium (κ 0.235 and 0.296 respectively) and intramural layers (κ 0.351 and 0.280 respectively. Agreement

between CMR and non-compact scar was fair in the epicardium for ADAS-3D (κ 0.317) but there was no agreement for inHEART (κ 0.002).

The histological composition of CMR scar and non-scar segments is shown in Table 2. ADAS-3D and inHEART had comparable histological percentage fibrosis, adiposity and viable myocardium in both scar and non-scar segments in all three layers. Percentage fibrosis was higher and percentage viable myocardium lower in scar vs non-scar segments in all three layers for both ADAS-3D and inHEART (Table 2).

### *4.3.4 **ADAS-3D vs inHeart scar size and agreement***

The ADAS-3D and inHEART scar sizes (pooled for animal and human subjects) are compared in Figure 3. They were significantly correlative for the endocardial ($R^2 = 0.949$, $P < 0.001$), intramural ($R^2 = 0.932$, $P < 0.001$) and epicardial layers ($R^2 = 0.776$, $P < 0.001$). Bland-Altman analyses demonstrated that there was no systematic bias between ADAS-3D and inHEART for the endocardial (MD -0.39 cm2, P=0.842, LOA -12.27-11.48 $cm^2$) and epicardial (MD -1.17 cm2, P=0.663, LOA -17.33-14.98 $cm^2$). In the intramural layer however, inHEART measurements were systemically lower than ADAS-3D (MD -6.92 cm2, P=0.01, LOA -20.12-6.28 $cm^2$). Figure 3 also demonstrates that in the intramural layer there was significant proportional bias (β=-0.261, P=0.02) being that as scar size increased, there were larger differences between ADAS-3D and inHEART for the intramural layer.

### *4.3.5 **Relationship between critical sites and CMR scar in humans***

In total, 24 VTs were induced with a median of 5 VTs (IQR 3-7) per patient. All VTs had LV endocardial pace-mapping and 17/24 (71%) had mapping of the contralateral ventricular surface (i.e. RV septum or LV epicardium) so that their three-dimensional circuitry could be determined. As shown in Table 3, a critical site (either isthmus or exit) was determined for 18/24

(75%) by pace-mapping. The remaining 6/24 (25%) were determined to be intramural circuits without endocardial and/or epicardial exit (1/6 had 76% best pace-match in LV endocardium with paucity of points and without mapping of the contralateral epicardium, 5/6 had < 90% pace-match on either endocardium or contralateral RV septum/LV epicardium). One critical site was excluded as it arose from the right ventricular outflow tract (not encompassed by ADAS-3D or inHEART CMR segmentation) leaving a total of 17 critical sites. These consisted of endocardial isthmii (4/17, 24%), epicardial isthmus (1/17, 6%), endocardial exits (5/17, 29%) and epicardial exits (7/17, 41%).

For both ADAS-3D and inHEART, 15/17 (88%) of critical sites were within at least one layer of scar. Scar was 10mm adjacent to but not encompassing 1/17 (6%) and 2/17 (12%) of critical sites using ADAS-3D and inHEART respectively. A representative example of VT critical sites and ADAS-3D and inHEART scar is shown in Figure 4.

For ADAS-3D, there was scar on the ipsilateral surface of the critical site in 13/17 (76%), intramural to the critical site in 14/17 (82%) and on the contralateral surface of the critical site in 12/17 (71%). For isthmus critical sites, 5/5 (100%) had ipsilateral surface scar, 5/5 (100%) intramural scar and 3/5 (60%) contralateral surface scar. For exit critical sites, 7/12 (58%) had ipsilateral surface scar, 9/12 (75%) intramural scar and 9/12 (75%) contralateral surface scar.

For inHEART, there was scar on the ipsilateral surface of the critical site in 13/17 (76%), intramural to the critical site in 15/17 (88%) and on the contralateral surface of the critical site in 12/17 (71%). For isthmus critical sites, 5/5 (100%) had ipsilateral surface scar, 5/5 (100%) intramural scar and 3/5 (60%) contralateral surface scar. For exit critical sites, 8/12 (67%) had ipsilateral surface scar, 10/12 (83%) intramural scar and 9/12 (75%) contralateral surface scar.

Of all critical sites, 14/17 (82%) had ADAS-3D scar in more than one layer and 15/17 (88%) had inHEART scar in more than one layer.

### *4.3.6 Relationship between functional substrate and CMR scar*

Isochronal late activation mapping was performed on the 5 human subjects (5 LV endocardial EAMs, 2 epicardial EAMs, median 1241 points (IQR 927-2321 points). A total of 7 DZs were identified (Table 4). 6/7 DZs co-localised with critical VT sites (1/7 co-localised with the best endocardial PM of an intramural circuit, PM 84%). 4/7 (57%) of DZs were in bipolar low voltage scar (<1.5mV in endocardium or <1.0mV in epicardium) and 7/7 in unipolar car (7/7). All DZs (7/7) were encompassed in ADAS-3D and inHEART scar.

## 4.4 Discussion

Here we have described the results of a multi-vendor clinic-pathological validation of CMR LGE image integration to guide substrate delineation for CA of VT. We have made several important findings:

1. ADAS-3D and inHEART have comparably high accuracy with moderate agreement to identify endocardial and intramural scar compared to gold-standard whole-heart histology but poorer performance (modest accuracy and fair agreement) in the epicardial layers.
2. Performance of both vendors was excellent for compact scar but poor for detection of non-compact scar subtypes.
3. ADAS-3D and inHEART scar sizes are comparable in the endocardial and epicardial layers. There is a significant mean difference in intramural scar size with proportional bias.
4. Critical sites of VT co-localise reliably with ADAS-3D and inHEART scar (88% falling within one scar layer). Importantly more than 80% of VT critical sites demonstrated CMR LGE scar in more than 1 layer (reinforcing the three-dimensional nature of VT circuits).
5. Functional substrate (DZs) in humans undergoing EAM co-localize comparably with ADAS-3D and inHEART scar.

### *4.4.1 Multi-vendor validation of CMR by gold-standard histology*

Few studies have validated the performance of CMR image integration software against gold-standard histopathology with most available studies comparing CMR-LGE scar areas to that of gross macropathological post-infarction scar area.[331,434] One such study to do so was by Pop et al. (2013) found that imaging defined scar (from ex-vivo CMR LGE and diffusion weighted CMR) and borderzone area correlated well with histology.[335] In contrast, in our study we report results of more clinically reproducible in-vivo CMR (performed as would be done for scar assessment in human subjects). Furthermore layer-specific performance is not available which is of interest to the VT ablationist. We have previously reported that when the ventricular wall is divided into two layers (an endocardial 0-50% vs epicardial 50-100%) there is similarly high accuracy for endocardial ADAS-3D scar and only modest accuracy for the epicardium.[449] A limitation of that work was that the intramural space was not separately considered (important as more than 61% of VTs are estimated to have three dimensional circuits)[15] and it is unclear if the inaccuracy of CMR-image integration was purely in the epicardium or also in the intramural space. This study extends the previous findings by using multi-vendor commercially available and clinically accessible methods of CMR post-processing with segmentation of the left ventricle to describe performance in the endocardium, intramural space and epicardium as well as by evaluating CMR LGE with consideration of scar sub-type. The poorer performance of both ADAS-3D and inHEART in the epicardium may be due to signal contamination from nearby tissue in the epicardium or may be a reflection of scar pattern, with more non-compact vs. compact scar in the epicardium of this post-infarct model.

Although non-compact scar formed a minority of sampled segments (14-31% of all histological scar segments in this analysis), the relatively poorer performance of both ADAS-3D and inHEART to identify this scar pattern was a novel observation. Glashan et al. (2018) have

performed the first definitive whole-heart histological analysis of NICM patients with sustained monomorphic VT and found that fibrosis architecture in such patients are often patchy or diffuse with compact scar only seen rarely (55% and 34% vs 3% of examined transmural biopsies).[70] In their study they present a single NICM patient with co-registered CMR and histology, demonstrating a transmural histological biopsy with greater than 50% diffuse (non-compact) fibrosis that was not detected by CMR LGE. Our findings of poorer performance in the epicardium (which had more non-compact scar vs the endocardium/intramural layers) and poorer performance for non-compact scar is consistent with data from Glashan *et al*'s study and may suggest a limit to performance of LGE CMR. Whether different thresholding methods such as those based on standard deviation applied to the CMR to identify such scar may be more beneficial is unclear. Notably however, Glashan et al. found that this scar segment was missed irrespective of the segmentation method for the CMR.

### *4.4.2 **Agreement between ADAS-3D and inHEART scar size***

Differences in scar size between the two modalities are not unexpected given differing signal intensity scar thresholding of the CMR LGE by vendor. ADAS-3D allows the operator discretion to alter the thresholds for dense scar (standard 60%) and borderzone (standard 40%) whereas inHEART currently provides processed and segmented CMR to the end-user. Previous publications suggest that inHEART has similar thresholding (dense scar 50% and borderzone 35%).[341] The difference in scar size of the intramural layer (with proportional bias, suggesting that inHEART intramural scar tends to increase in size compared to ADAS-3D as overall scar size increases) may be an artefact of the small sample size (n=10) of this study or may be due to different processing techniques of the CMR. Nevertheless, despite scar size differences, there was no discernible difference in either modality to identify histological scar or critical sites.

### *4.4.3 **ADAS-3D and inHEART to identify critical sites and functional substrate***

One of the first studies to investigate the relationship between CMR LGE and critical sites of VT found that 31/31 (100%) of critical VT re-entry sites (predominantly identified by PM) co-localised with CMR LGE segmented by standard deviation (SD) approach (borderzone 2SDs above mean signal intensity, dense scar 3SDs above mean signal intensity).[453] Using a 17 segment model, Andreu et al. (2014) demonstrated that CMR LGE by visual assessment co-localised to sites of successful VT CA in 96.3% of cases in an 80 patient cohort.[454] CMR LGE maps have also been used to identify "channels" of borderzone or heterogenous tissue which co-localise with electroanatomic conducting channels and sites of the VT critical isthmus, the first such validation of which was done in 2011.[29] Since this, in early validation studies of ADAS-3D, critical sites for VT as identified by PM or entrainment were seen to localise with CMR channels in 74-79% of cases.[338,455] In an early validation of inHEART, Yamashita et al. found that 89% of VT termination sites co-localised to imaging defined scar.[342] Our results in a small human cohort are the first to compare the two technologies and have found that similarly, 15/17 (88%) of critical sites co-localised to ADAS-3D and inHEART scar (at any layer). Of the two remaining identified critical sites, the first had ADAS-3D scar within 10mm and the second had inHEART scar within 10mm of best PM. In this small series, with either technology between 94% and 100% of VT critical sites can be found within or near CMR scar.

The primary method of localizing critical sites of VT in this study was PM which is well-validated in both post-infarction and NICM CA.[452] We used a strict criteria of >90% PM to identify sites of interest and, as we have previously reported, inferred the presence of an isthmus vs. exit site by the spatial pattern of high-density PM (abrupt change to suggest isthmus vs centrifugal attenuation to suggest exit from a deeper isthmus site).[235] Our results, finding scar on

the ipsilateral surface of PM sites with abrupt change vs. centrifugal attenuation (5/5 (100%) for both vendors vs. 7/12 (58%) for ADAS 3D and 8/12 for inHEART (75%) respectively) support the use of spatial patterns of high-density PM to surmise the three-dimensional structure of the VT isthmus.[452] The majority of critical sites (>80%) had multi-layer scar suggesting once more the complex three-dimensional architecture of the VT circuit.

Finally, functional substrate (DZs by isochronal late activation mapping) have been shown to colocalise with ADAS-3D CMR channels,[284] though to our knowledge there has been no similar validation in inHEART CMR scar. Our results are in keeping with these studies and we have shown that functional substrate identified by isochronal late activation mapping comparably correlates with both ADAS-3D and inHEART scar.

### *4.4.4* ***Limitations***

This study has several limitations worth considering. First, although it systematically evaluated CMR by precisely co-registered histology in animal subjects prior to further validation in humans, the recruited numbers of both were small. Furthermore, in the clinical series, EAM was guided by one or the other technology which could have biased results (though we note this was balanced in the included dataset). Given the small numbers and clinical question, we do not report outcome data in this cohort. The majority of human patients in this dataset had NICM expanding the role of these technologies beyond the animal infarction model. Even with this small dataset several novel findings have been elicited including a quantitative description of scar pattern type on performance of multi-vendor CMR LGE segmentation to identify histological scar. Secondly, we have predominantly used a PM approach to identify critical sites of VT as, in our experience, the majority of VTs induced were not hemodynamically tolerated to permit activation or entrainment mapping. Thirdly, this study focused purely on CMR LGE. Other CMR mapping

techniques such as T1 mapping for diffuse fibrosis were not performed in a short axis stack and hence could not be reconstructed into a 3D model to be co-registered with the histology in this study. Finally, as this was a comparative study between ADAS-3D and inHEART and as the identification of CMR channels is not currently available in the latter, we have not reported data on CMR channels and histology or critical sites. We and others have explored this in our previous work.[284,339,449]

## 4.5 **Conclusion**

In this multi-vendor clinico-pathologic study of CMR LGE image integration we have found that two available technologies, ADAS-3D and inHEART perform comparably to identify endocardial and intramural scar with comparatively poorer performance in the epicardium and for non-compact scar types. Despite this, critical sites of VT and functional substrate co-localise with CMR LGE scar, suggesting that these technologies can be useful to guide VT CA. Randomised data are required to establish the role of image integration in VT CA and this study establishes that perhaps both multiple vendors should be incorporated in such a study to maintain generalisability.

## 4.6 Figures

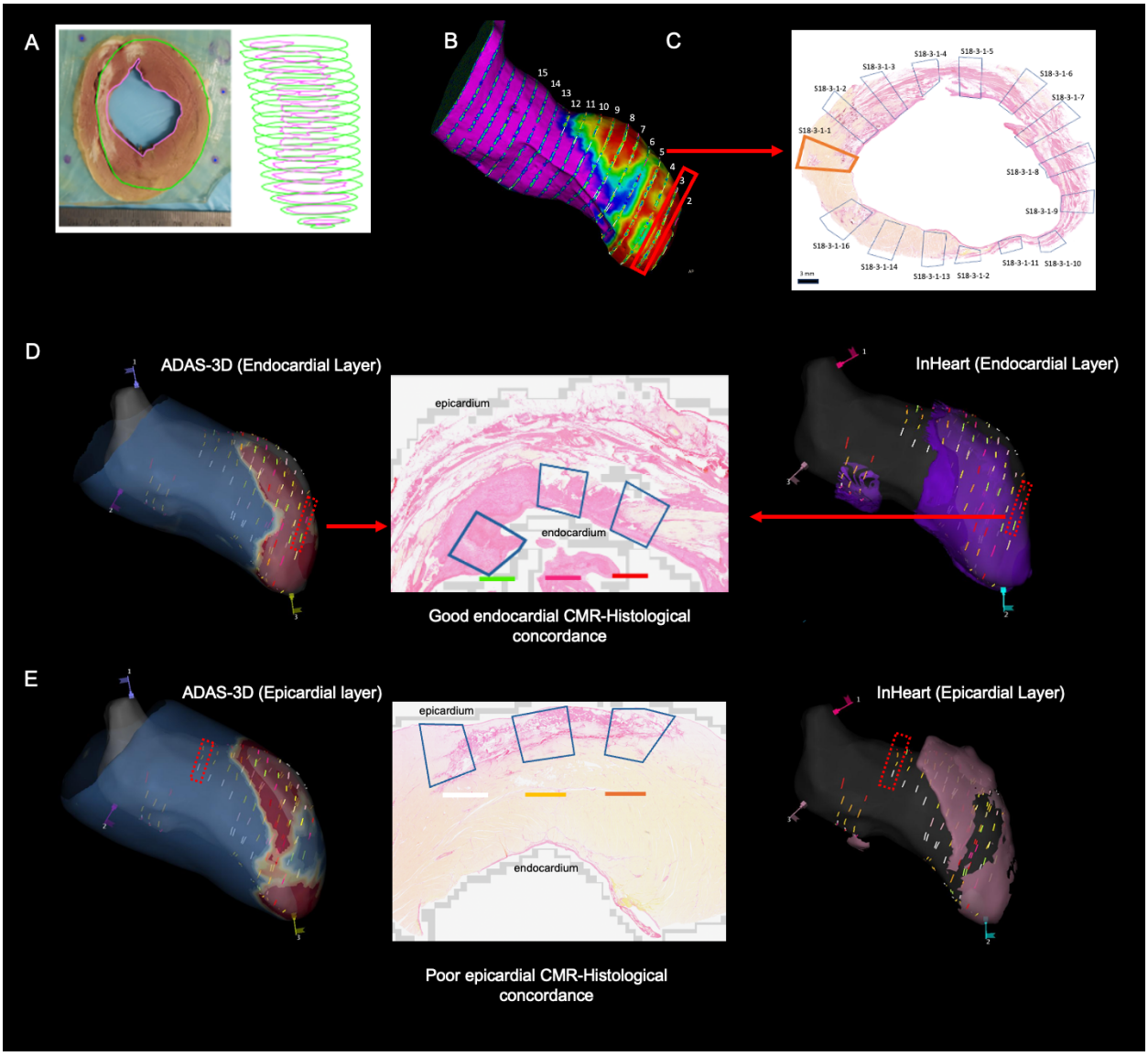


**Figure 4-1 Study workflow to identify agreement between ADAS-3D and inHEART cardiac magnetic resonance imaging (CMR) scar segmentation and whole heart histological scar.**

**A.** Explanted hearts were filled, fixed and then sectioned into 5mm short-axis slices. Endocardial and epicardial contours were traced and imported into Matlab to create a custom three-dimensional histopathological shell. **B.** Representative example of a histopathological shell that was imported into mapping software. Numbers 2-15 denote 5mm cross-sectional slices and coloured lines represent 3mm biopsy tracings. **C.** A scaled photograph of cross-section 3 from Figure 1B, taken at 20x magnification after staining with Picrosirius red to identify collagenous tissue. Biopsies

were systematically conducted around the endocardial border of the short-axis sections – 3mm width with 3mm spacing between biopsies. **D.** ADAS-3D and inHEART were segmented into endocardial (inner third), intramural (middle third) and epicardial (outer third) layers and co-registered with whole-heart histology. A representative example of good agreement between ADAS-3D and inHEART and whole heart histology in the endocardial layer is shown here. In the histology, pink represents fibrosis, yellow healthy (viable) myocardium and white intramyocardial adiposity. Three virtual biopsies (yellow, pink and red lines) are matched in the histology to the CMR showing CMR and histological scar. **E.** A representative example of poor agreement between ADAS-3D and inHEART in the epicardial layer. Three biopsies (white, yellow, orange lines) show epicardial non-compact scar. Co-registered ADAS-3D and inHEART demonstrate no CMR scar at corresponding biopsy sites.

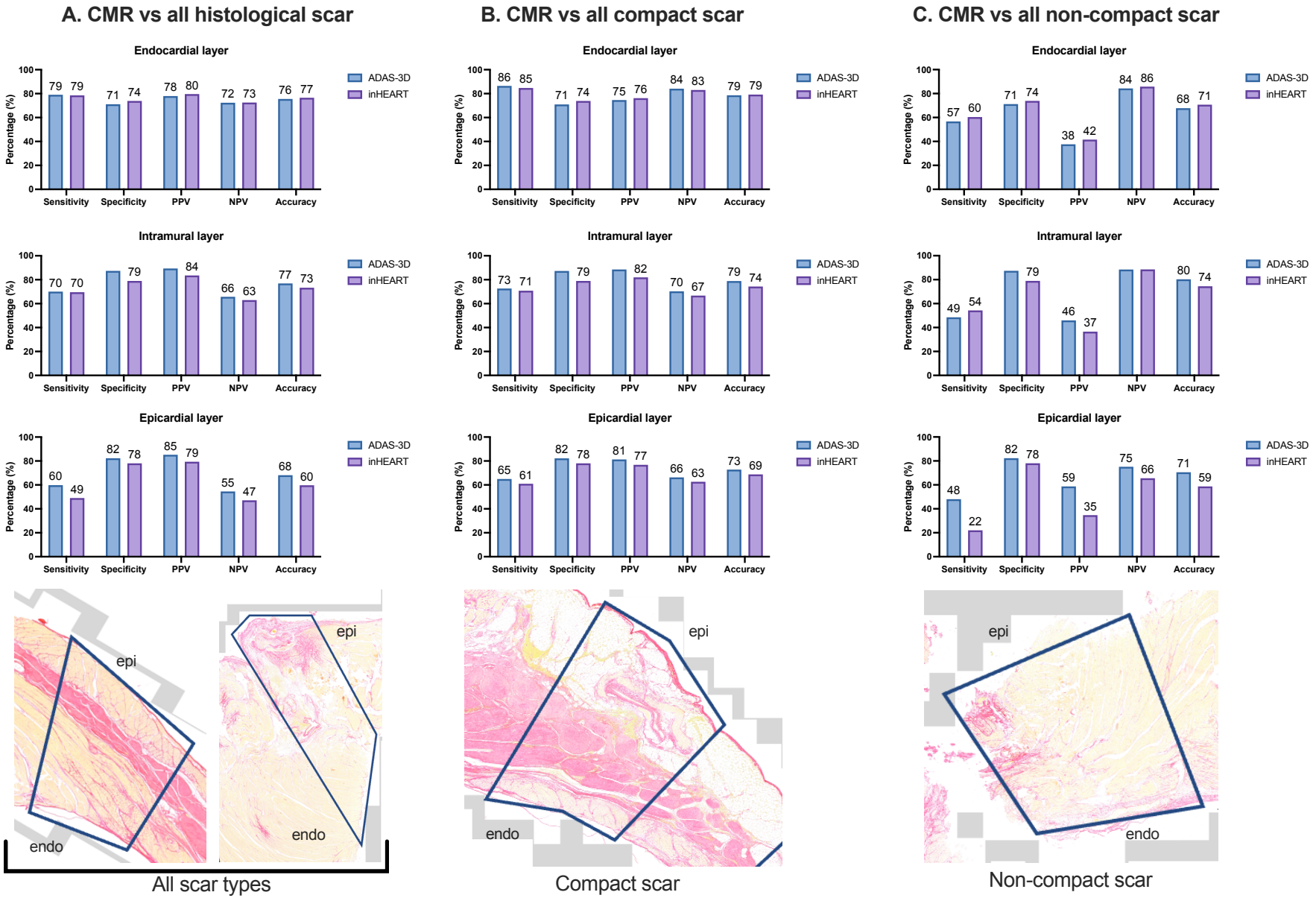
A. CMR vs all histological scar
B. CMR vs all compact scar
C. CMR vs all non-compact scar
Endocardial layer
Intramural layer
Epicardial layer
Percentage (%)
Sensitivity
Specificity
PPV
NPV
Accuracy
ADAS-3D
inHEART
79 79 71 74 78 80 72 73 76 77
70 70 79 84 66 63 77 73
60 49 82 78 85 79 55 47 68 60
86 85 71 74 75 76 84 83 79 79
73 71 79 82 70 67 79 74
65 61 82 78 81 77 66 63 73 69
57 60 71 74 38 42 84 86 68 71
49 54 79 46 37 80 74
48 22 82 78 59 35 75 66 71 59
epi
endo
All scar types
Compact scar
Non-compact scar

**Figure 4-2 Performance of ADAS-3D and inHEART CMR segmentation to identify whole-heart co-registered histological scar stratified by scar subtype**

In panel **A** the sensitivity, specificity, positive predictive value (PPV), negative predictive value (NPV) and accuracy of ADAS-3D and inHEART to identify all histological scar patterns is shown. Panel **B** and **C** demonstrate the performance of both technologies to identify compact **(B)** and non-compact (**C)** scar. Representative examples of each scar type are shown in the histological biopsies (stained with picrosirius red such that healthy myocardium is pale yellow, fibrosis is pink and fat is white).

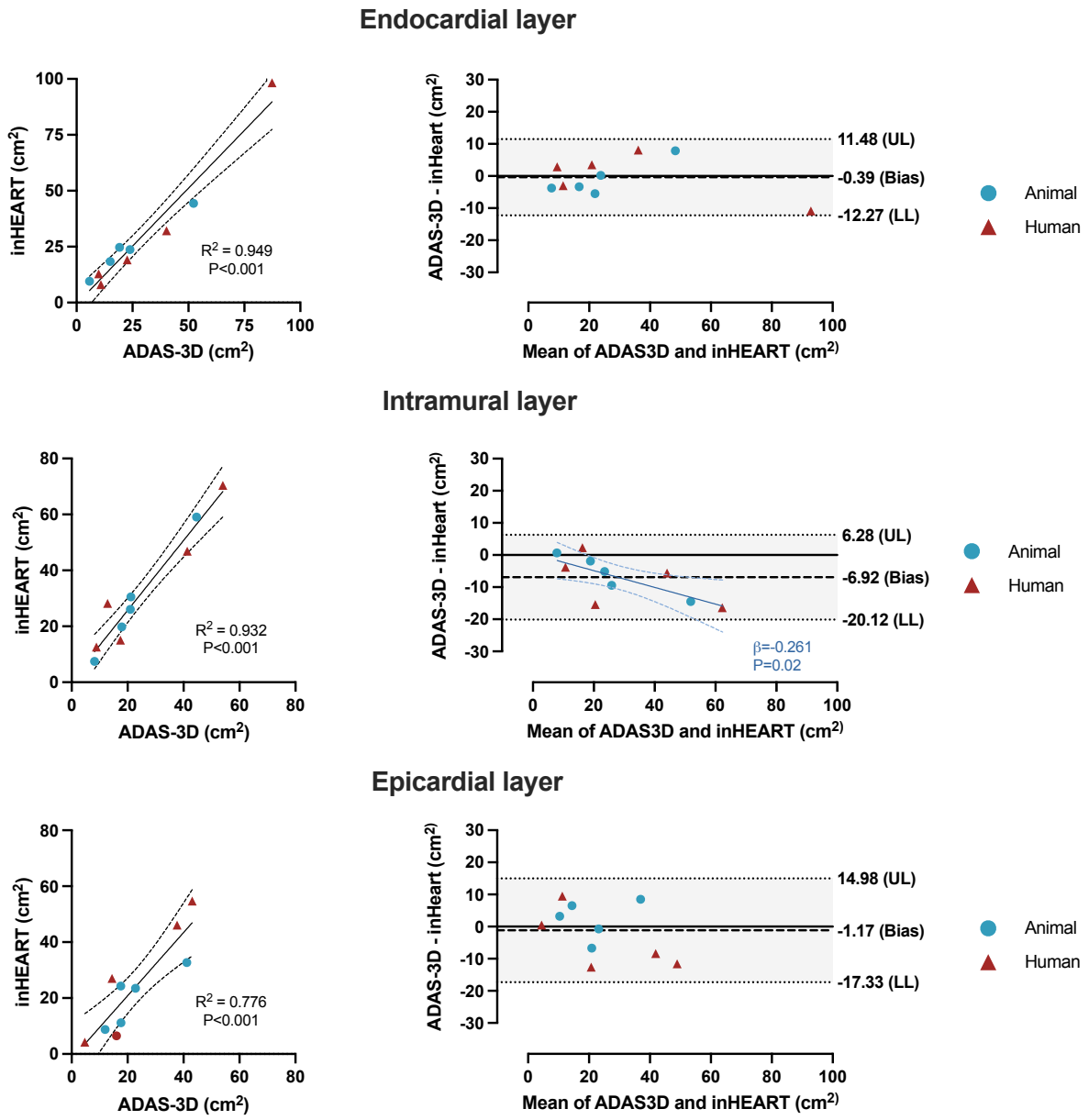


**Figure 4-3 Scar size comparison between ADAS-3D and inHEART stratified by layer**

The left panels demonstrate correlation (linear regression) between scar types and the right panel demonstrates Bland-Altman plots. ADAS-3D and inHEART scar were correlated (P<0.001 in all comparisons). There was no significant bias between ADAS-3D and inHEART for the endocardial and epicardial layers but a significant bias was seen in the intramural layer (beta = -0.261, p-0.02). UL (upper limit) and LL (lower limit) demonstrate the limits of agreement.

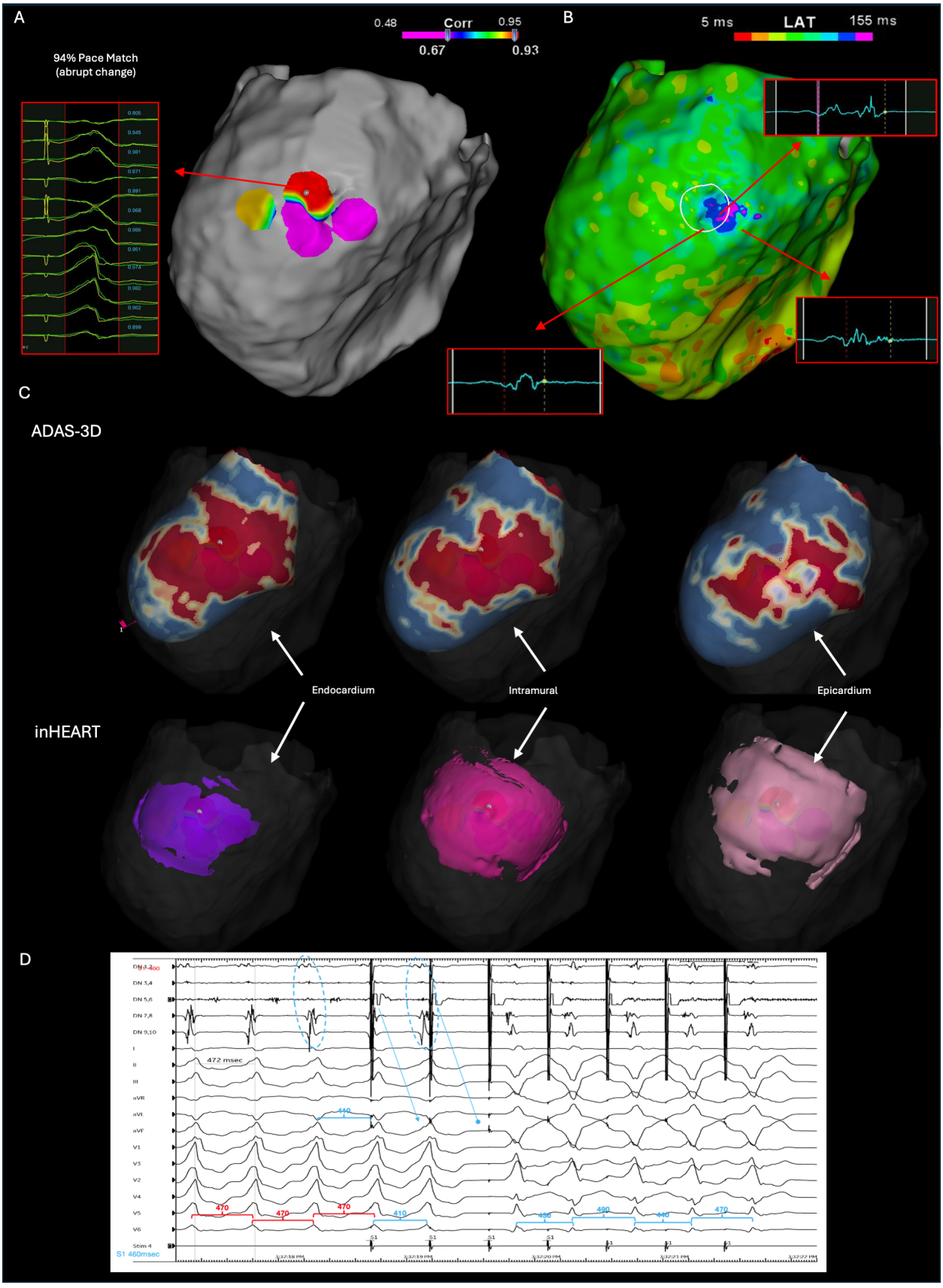
A
0.48
Corr
0.95
0.67
0.93
94% Pace Match
(abrupt change)
B
5 ms
LAT
155 ms
C
ADAS-3D
Endocardium
Intramural
Epicardium
inHEART
D
472 msec
S1 460msec

**Figure 4-4 Representative example of correlation between critical site of VT with ADAS-3D and inHEART Scar.**

**A** demonstrates pace mapping identification of an epicardial VT isthmus with 94% pace match and abrupt change spatial pattern. This site correlates well with the primary epicardial deceleration zone identified by isochronal late activation mapping (**B).** In panel **C**, the ADAS-3D and inHEART scar is presented overlying this critical site demonstrating transmural scar at this site with both technologies. In panel **D** we confirm that the site of best pace-match is an epicardial isthmus. Here we show pacing from DN 5,6 which likely overlies critical isthmus (mid-diastolic signals during VT). The first paced beat accelerates the following QRS (VT CL 470, pacing CL 460ms, first CL after first paced beat is ~410msec). Mid-diastolic signals on DN 5,6 are advanced and subsequent pacing stimulus falls on last component of the local EGM suggesting downstream entrainment (where activation has been advanced without changing the actual sequence. Note that first QRS complex after first paced beat is similar to VT – likely orthodromic conduction down isthmus and through the same exit. However, second stimulus results in termination (less likely to be loss of capture since there is still a small signal after pacing artefact on DN3,4). This is likely due to termination of the VT due to antidromic conduction through the isthmus and wavefront collision with the incoming activation wavefront of the previous beat through the circuit entrance. This is then followed by consistent local capture and different VT morphology (notably negative vector in inferior leads and positive I) with long S-QRS, suggesting exit through the circuit entrance.

## 4.7 Tables

**Table 4-1 Baseline patient characteristics**

| Patient | Age | Sex | Cardiomyopathy | LVEF | Device at time of CMR | Days from CMR to ablation |
|---|---|---|---|---|---|---|
| 1 | 64 | Male | Post-infarction | 44 | ICD | 13 |
| 2 | 43 | Male | Gene elusive arrhythmogenic cardiomyopathy | 40 | Nil* | 140 |
| 3 | 42 | Male | Recurrent myocarditis | 30 | Dual chamber Pacemaker* | 265 |
| 4 | 72 | Male | NICM | 59 | Nil* | 1 |
| 5 | 74 | Male | NICM | 54 | Nil* | 333 |

Abbreviations: CMR – cardiac magnetic resonance imaging, LVEF – left ventricular ejection fraction, NICM – non-ischaemic cardiomyopathy

**Table 4-2 Composition of ADAS-3D and inHEART scar by layer**

| | | Fibrosis (%) | | Adiposity (%) | | Viable myocardium (%) | |
|---|---|---|---|---|---|---|---|
| | | Scar | No scar | Scar | No Scar | Scar | No scar |
| Endocardial | ADAS-3D | 40.66 (16.53-56.02) | 8.00 (4.61-17.06) | 19.28 (11.99-27.46) | 20.67 (13.85-26.89) | 33.7 (24.23-57.46) | 68.22 (58.67-77.84) |
| | inHEART | 38.55 (16.51-55.10) | 8.36 (4.86-19.46) | 20.22 (12.33-28.35) | 19.75 (12.94-26.32) | 33.95 (24.23-59.19) | 67.42 (55.64-77.24) |
| Intramural | ADAS-3D | 47.54 (27.60-65.19) | 10.77 (4.96-24.28) | 18.46 (9.11-29.08) | 19.11 (11.81-26.68) | 23.84 (14.22-43.82) | 68.68 (52.54-78.05) |
| | inHEART | 44.36 (22.30-61.55) | 11.37 (5.42-25.42) | 20.03 (10.18-30.16) | 17.66 (11.13-25.79) | 26.4 (15.38-52.18) | 67.67 (43.45-76.99) |
| Epicardial | ADAS-3D | 28.31 (16.07-40.26) | 9.52 (4.78-23.22) | 32.50 (15.48-45.24) | 19.66 (8.72-35.92) | 32.25 (21.79-48.66) | 65.77 (33.69-81.63) |
| | inHEART | 28.65 (16.31-40.37) | 11.92 (5.61-24.21) | 30.23 (14.99-45.15) | 21.17 (9.31-38.54) | 32.95 (21.42-49.47) | 59.74 (29.97-79.91) |

**Table 4-3 Characterisation of critical sites of VT by pace-mapping and their relationship to CMR LGE scar (ADAS-3D and inHEART)**

| VT | Patient | VT description | Best PM LV endocardium | Best PM Epicardium/RV septum | Critical site | ADAS-3D scar at best PM site | inHEART scar at best PM site |
|---|---|---|---|---|---|---|---|
| 1 | 1 | LB trs V3 LI axis, CL380ms | 97% (abrupt) stim-QRS 51ms | - | Endocardial isthmus | Endocardial-Intramural | Endocardial-Intramural |
| 2 | 1 | RB trs V2 RS axis, CL 290ms | 95% (abrupt) stim-QRS 57ms | - | Endocardial isthmus | Transmural | Transmural |
| 3 | 1 | RB trs V6 RI axis, CL 333ms | 94% (insufficient), stim-QRS | - | Endocardial exit | Transmural | Transmural |
| 4 | 1 | LB trs V5, LS axis, CL 397ms | 90% (abrupt), stim-QRS 61ms | - | Endocardial isthmus | Transmural | Transmural |
| 5 | 1 | RB trs V6, RS axis, CL 411ms | 73% (insufficient), stim-QRS 32ms | - | Nil (paucity of pace-mapping) | NA | NA |
| 6 | 2 | RB trs V5 LS axis, CL 309ms | 91% (centrifugal), stim-QRS 70ms | 86% (centrifugal), stim-QRS 47ms | Endocardial exit | Transmural | Intramural-Epicardial |
| 7 | 2 | RB trs V5, RS axis, CL283ms | 84% (centrifugal), stim-QRS 24ms | 73% (centrifugal), stim-QRS 48ms | Nil (intramural circuit) | Intramural-Epicardial | Intramural-Epicardial |
| 8 | 2 | RB trs V5 RS axis, CL337ms | 80% (centrifugal), stim-QRS 59ms | 87% (centrifugal), stim-QRS 45ms | Nil (intramural circuit) | Transmural | Intramural |
| 9 | 2 | LB trs V2 LS axis, CL 228ms | 76% (centrifugal), stim-QRS 63% | 93% (centrifugal), stim-QRS 41ms | Epicardial exit | Transmural | Transmural |
| 10 | 2 | RB trs V5 horizontal axis, CL 552ms | 94% (centrifugal), stim-QRS 45ms | 76% (insufficient), stim-QRS 76ms | Endocardial exit | Epicardial | Intramural-Epicardial |

| | | | | | | | |
|---|---|---|---|---|---|---|---|
| 11 | 2 | RB trs V5 horizontal axis, CL 237ms | 79% (centrifugal), stim-QRS 33%) | 61 (insufficient), stim-QRS 60ms | Nil (intramural circuit) | Epicardial | Intramural-Epicardial |
| 12 | 2 | RB trs V4 LS axis CL 708ms | 85% (centrifugal), stim-QRS 33ms | 96% (centrifugal), stim-QRS 44ms | Epicardial exit | No scar* | No scar* |
| 13 | 3 | RB -ve concordance RH axis CL 277ms | 45% (insufficient), stim-QRS 49ms | 43% (insufficient), stim-QRS 30ms | Nil (intramural circuit) | NA | NA |
| 14 | 3 | RB +ve concordance RI axis, CL 475ms | 95 (centrifugal), stim-QRS 28ms | 95% (abrupt), stim-QRS 86ms | Epicardial isthmus | Transmural | Transmural |
| 15 | 3 | LB trs V2 LS axis, CL 281ms | 40% (insufficient), stim-QRS 45ms | 91% (insufficient), stim-QRS 74ms | Epicardial Exit | Transmural | Transmural |
| 16 | 4 | RB +ve concordance, LS axis CL 330ms | 84% (centrifugal), stim-QRS 47ms | 67% (centrifugal), stim-QRS 33ms | Nil (intramural circuit) | Transmural | Transmural |
| 17 | 4 | LB trs V4 LI axis, CL 275ms | 50% (centrifugal), stim-QRS 27ms | 90% (centrifugal), stim-QRS 43ms | Epicardial exit | Transmural | Transmural |
| 18 | 4 | LB trs V5 LI axis, CL 253ms | 49% (centrifugal), stim-QRS 30ms | 96% (centrifugal), stim-QRS 57ms | Epicardial exit | Transmural | Transmural |
| 19 | 4 | LB trs V5 LI axis, CL 275ms | 61% (centrifugal), stim-QRS 23 | 95% (centrifugal). stim-QRS 54ms | Epicardial exit | Endocardial-Intramural | Transmural |
| 20 | 4 | LB trs V4, RI axis, CL 257ms | 58% (centrifugal), stim-QRS 28 | 93% (centrifugal), stim-QRS 61ms | RVOT | No scar | No scar |
| 21 | 4 | RB pattern | 93% (insufficient), stim-QRS 32 | 66% (centrifugal), stim-QRS 55ms | Endocardial exit | No scar | No scar[1] |

| | | | | | | | |
|---|---|---|---|---|---|---|---|
| | | break V2, RI axis, CL 237ms | | | | | |
| 22 | 4 | RB +ve concordance LS axis, CL 358ms | 80% (centrifugal), stim-QRS 60ms | 91% (centrifugal), stim-QRS 48ms | Epicardial exit | Transmural | Transmural |
| 23 | 5 | LB trs V2 LI axis CL382ms | 97% (abrupt) stim-QRS 53ms | - | Endocardial Isthmus | Endocardial-Intramural | Endo-Intra |
| 24 | 5 | LB trs V3 LI axis, CL 346ms | 91% (centrifugal), stim-QRS 46ms | | Endocardial Exit | Endocardial-Intramural | Endo-Intra |

1. Scar seen within 10mm of critical site

Abbreviations: +ve concordance – positive concordance, LB – left bundle branch block morphology, LI – left inferior, LS – left superior, ms – milliseconds, RB – right bundle branch block morphology, RI – right inferior, RS – right superior, trs – transition, RVOT – right ventricular outflow tract

**Table 4-4 Association of Deceleration zones with LGE CMR scar**

| DZ | Patient | Map | ADAS-3D scar | inHEART scar | Bipolar voltage scar (<1.5mV for endocardium, <1mV for epicardium) | Unipolar voltage scar <8.3mV | Critical site co-localising with DZ |
|---|---|---|---|---|---|---|---|
| 1 | 1 | LV endocardium | Transmural | Transmural | Yes | Yes | Yes |
| 2 | 2 | LV endocardium | Transmural | Transmural | No | Yes | Yes |
| 3 | 2 | LV endocardium | Intramural-Epicardial | Intramural-Epicardial | No | Yes | Yes |
| 4 | 2 | LV epicardium | Transmural | Transmural | Yes | Yes | Yes |
| 5 | 2 | LV epicardium | Epicardial | Intramural-Epicardial | No | Yes | Yes |
| 6 | 3 | LV epicardium | Transmural | Transmural | Yes | Yes | Yes |
| 7 | 4 | LV endocardium | Transmural | Endocardial-Intramural | Yes | Yes | No[1] |

1. Co-localised with the best endocardial PM of an intramural circuit, PM 84%

**Abbreviations:** DZ – deceleration zone, LV – left ventricle, mV millivolt

# Chapter 5

# 5 FEASIBILITY OF MACHINE LEARNED INTRACARDIAC ELECTROGRAMS TO PREDICT POST-INFARCTION VENTRICULAR SCAR TOPOGRAPHY

Author attribution statement

| **Title of published work** | **Feasibility of machine learned intracardiac electrograms to predict post-infarction ventricular scar topography** |
|---|---|
| **Nature of the candidate's contribution** | Design of study, source of grant funding for bioinformatic collaboration, data collection and analysis including processing and annotation of electrograms, post-processing of histopathology and CMR, co-registration of data, leading inter-disciplinary collaboration with computer scientists, statistical analyses, manuscript writing and submission to journal |
| **Co-Authors** | **Nature of contribution** |
| Timothy Campbell | Lead source animal experiments and histopathology staining and sectioning (prior to PhD candidate's thesis commencement). Comments on manuscript. |
| Richard Bennett | Contributed towards animal experiments and comments on manuscript |
| Samual Turnbull | Contributed to animal experiments, advised on study methodology and comments on manuscript |

| | |
|---|---|
| Ashwin Bhaskaran | Advised on study methodology and comments on manuscript |
| Robert D. Anderson | Contributed towards animal experiments and comments on manuscript |
| Chris Davey | Software design for image integration of tissue histopathology to electroanatomic map |
| Alexandra K. O'Donohue | Contributed to histology experiments and comments on manuscript |
| Aaron Schindeler | Contributed to histology experiments and comments on manuscript |
| Dinesh Selvakumar | Contributed to animal experiments and comments on manuscript |
| Yasuhito Kotake | Comments on manuscript |
| Chi Jen Hsu | Advice on imaging experiments and comments on manuscript |
| James H. Chong | Comments on manuscript |
| Eddy Kizana | Comments on manuscript |
| Saurabh Kumar | Overall supervision. Animal experiments and experimental design. Comments on manuscript. |
| Signature of candidate<br>Kasun De Silva | |
| Signature of supervisor (signed on behalf of all co-authors)<br>Saurabh Kumar | |

## 5.1 Introduction

Accurate delineation of arrhythmic ventricular substrate and scar is important for successful catheter ablation (CA) of ventricular tachycardia (VT). VT circuits are often three-dimensional[15,272] and ventricular scar can be similarly complex.[235] Improved demarcation of ventricular scar topography (including its depth and location), prior to epicardial mapping, would be advantageous.

Traditionally, bipolar and unipolar electrogram amplitude have been used to localize scar using foundational thresholds established by Marchlinski and colleagues.[19,245,247] However, electrogram characteristics can differ based on wall thickness, inter-electrode spacing, contact quality, electrode orientation and wavefront direction.[27] High density mapping with a multi-electrode catheter demonstrates only modest sensitivity and specificity of voltage scar to ex-vivo cardiac magnetic resonance imaging (CMR) scar.[252] Therefore, efforts have been made to assess electrogram features beyond voltage. Within the time domain, electrogram characteristics including duration and fractionation relate to transmural and mid-wall scar identified by CMR in post-infarction VT.[456] Recent data suggest that frequency domain analysis of unipolar electrograms can identify mid-myocardial fibrosis.[324]

Signal processing into multiple frequency and time domains, combined with supervised machine learning therefore offers the potential to improve the discriminative capacity of individual electrograms. Further, deep learning, using convolutional neural networks (CNNs), has shown promise in analysing body surface electrocardiograms but has yet to be systematically applied to ventricular intracardiac electrograms. We have recently published our experience with an ovine model of infarction with high density multi-electrode mapping and co-registered histopathology.[449] Using this model, we hypothesized that scar pattern can be delineated from

modern multielectrode catheters using both time and frequency domain features. Here we explore the relationship between intracardiac electrograms and scar topography, modulated by signal processing and deep-learning, and assess whether such novel features are superior to traditional voltage criteria to identify scar.

## 5.2 Methods

This study was performed on castrated merino sheep. All animal experiments were approved by the Animal Ethics Committee of Westmead Hospital and the study conformed with the animal research guidelines of the National Health and Medical Research Council of Australia. Code used for generating these analyses will be made publicly available on publication in an online Github repository (https://github.com/Sydney-Informatics-Hub/PIPE-4779-Intracardiac-Electrograms). The data used is also available for sharing on reasonable request for the purposes of replicating the results.

### *5.2.1 Infarction*

The infarcted sheep used in this study (n=5, weighing 53±7kg) have been described in our previous publication.[449] In brief, animals were infarcted by inflation of a 2.75–3.5mm angioplasty balloon distal to the second diagonal branch bifurcation for 3 hours. They were pretreated with oral sotalol (continued for 7 days post infarction). Sheep underwent a CMR (116 days post infarction, IQR 86-134) and EAM (129 days post infarction, IQR 109-140). In addition, a single control sheep was also included.

### *5.2.2 Electroanatomic mapping*

Following general anaesthesia and intubation, multiple-wavefront mapping was facilitated using a quadripolar catheter at the right ventricular apex for right ventricle pacing (RVp) or right

atrium for atrial pacing. A decapolar catheter in the coronary sinus allowed left ventricular pacing (LVp). Electroanatomic mapping (EAM) was performed using a 20-pole Pentaray$^{TM}$ (Biosense Webster) 2-6-2-millimetre (mm) electrode spacing using standard electrode configuration. Acquisition settings were tissue proximity indication, local activation time difference 3ms, the electrode position change of 3mm, point density of 1mm and QRS pattern >90%. Standard bandpass filtering was performed at 16-500 Hertz for bipolar electrograms and 2-240 Hertz for unipolar electrograms. Catheter stability and contact were confirmed via catheter deformation on EAM software, CARTO3$^{TM}$ (Version 6, Biosense Webster, Irwindale, California, USA), or with intracardiac echocardiography (ICE). EAM was performed sequentially across three wavefronts: sinus rhythm (4/6 animals) or atrial pacing (1/6 animals), RVp (6/6 animals) and LVp (6/6 animals) such that 18 EAMs (three wavefronts per animal) were obtained). Intracardiac electrograms were individually assessed, and electrograms from catheter-induced or spontaneous ectopic beats occurring within the complete 2.5-second electrogram acquisition period were excluded. For each animal and wavefront, a window of interest (WOI) around the ECG reference was manually determined to exclude pacing artefact and include late potentials. Mean bipolar and unipolar voltages, bipolar scar (<1.5mV) and dense bipolar scar (<0.5mV), unipolar scar (<8.3mV), split potentials (>20ms isoelectric period between electrograms). Abnormal electrograms were classified using traditional local abnormal ventricular activities (LAVA) definitions[20] by two authors (KD and TC, if there was disagreement this was adjudicated by a third investigator, [SK]). Neither programmed stimulation nor extrastimuli were used to clarify LAVA sites.

### *5.2.3 Whole-heart histological reconstruction and co-registration*

Hearts were packed with cotton filler to maintain shape and fixed in 10% neutral buffered formalin (7 days) prior to being placed in a ballistic gelatine mould and sectioned at 5mm intervals

along the short axis. Slices were photographed from a fixed distance, with endocardial and epicardial borders traced to create three-dimensional meshes in MATLAB (Mathworks, R20196b) using a custom algorithm. The 5mm slices were embedded in paraffin blocks and then 5µm-thick slices were cut from the basal surface (RM2155, Leica Biosystems, Wetzlar, Germany). Collagenous tissue was identified with Picrosirius red staining performed with a Weigert's haematoxylin counterstain. Image capture was performed using an Aperio ScanScope CS2 (Leica Biosystems, Wetzlar, Germany) or Olympus VS120 (Olympus Corporation, Tokyo, Japan) with brightfield illumination at 20x magnification.

Histology images guided scar delineation on previously photographed slice images. Biopsies with a width of 3mm were systematically marked around the endocardial surface with a 3mm spacing. They were analysed on ImageJ (National Institutes for Health, Bethesda, Maryland, USA) as previously described to identify fibrosis, adiposity and remaining "viable myocardium."[449]

For each endocardial (inner third of myocardium), intramural (middle third of myocardium) and epicardial (outer third of myocardium) segments of the biopsies, scar was identified by the presence of collagenous tissue (pink with picrosirius red staining). In this way, scar pattern for each 3mm biopsy could be categorised as having "*no scar*" (no scar in any of endocardial, intramural or epicardial layers), "*scar*" (scar in any of the endocardial, intramural ± epicardial layers), "*at least endocardial scar*" (scar in endocardial layers ± scar in intramural ± epicardial layers), "*at least intramural scar*" (no scar in endocardium, scar in intramural layer ± scar in epicardium) and "*epicardial only*" (no scar in endocardial or intramural layer with scar in epicardial layers only). Representative examples are shown in Figure 1E.

Whole-heart histological and CMR reconstructions were co-registered with the EAM. Registration landmarks included the mitral and aortic annulus, LV apex and papillary muscles with cross-validation using intracardiac echocardiography anatomy (CARTOSOUND module, CARTO3$^{TM}$). All electrograms corresponding to the co-registered histological biopsy (or within 1.5mm of the edge of the biopsies) were assigned to their respective biopsy as shown in Figure 1D to enable the determination of histological characteristics specific to each electrogram.

### *5.2.4 Electrogram Analysis and Signal processing*

Whole data exports were performed on the CARTO3$^{TM}$ mapping system. A continuous 2.5 second period was acquired at each electrogram location of the electroanatomic map, sampling electrograms at 1000 Hertz (Hz). Using a custom Python (v3.13.0) script, the positional co-ordinates, bipolar and unipolar voltages, local activation time (LAT), WOI and the bipolar and unipolar time series (2.5 second output) were extracted. Both bipolar and unipolar electrograms (restricted to the WOI, hereafter referred to as "windowed") were reconstructed as a time series (Figure 1). Similarly, the complete 2.5 second acquisitions were also reconstructed as time series. These will be hereafter referred to as "complete" bipolar and unipolar time series. These extracted time series were matched to underlying histological scar categories.

As shown in Figure 2, first, automatically calculated voltages from the EAM (bipolar, unipolar or combined bipolar and unipolar voltages) were used to train a Gradient Boost machine-learning algorithm (using gradient boost, sci-kit learn (Python) package, 100 trees, learning rate 0.100, depth limit of individual trees 3) against the four scar patterns. Class imbalance was addressed with synthetic minority oversampling technique.[457] Data was divided into 80% train, 20% test sets. Receiver operating characteristics (area under the curve (AUC)), accuracy, Matthews Correlation Coefficient (MCC) were calculated. These were compared to performance

of traditional scar voltage cut-offs (bipolar scar <1.5mV, bipolar dense <0.5mV, unipolar scar <8.3mV) using logistic regression (with balanced classes).

Secondly, signal processing of the extracted windowed bipolar electrograms was performed using the automated tsfresh (Time Series FeatuRe Extraction on basis of Scalable Hypothesis, version 0.20.3) Python package to extract 794 time series features.[458] Features were imported into Orange Data Mining (version 3.37.0). The top 20 and top 100 features were selected using a fast correlation-based filter.[459] The top 100 and top 20 features were in turn interrogated with the same Gradient Boost machine-learning algorithm described above. Permutation feature importance was used to evaluate performance of the model and rank features.

Finally, a CNN was trained using windowed bipolar electrograms, as well as complete bipolar and unipolar time series data. This training was conducted using tsai (timeseriesAI), an open-source deep learning platform built on PyTorch. The tsai package employs InceptionTime, an ensemble of five deep learning models specifically designed for time series classification.[460] Each model within the ensemble utilizes inception modules, which apply filters of varying lengths simultaneously to extract relevant features from the time series data. The architecture of this CNN is depicted in Figure 2. The dataset was divided into training and testing subsets, with 80% allocated for training and 20% for testing. The training process spanned 100 epochs, with class weighting applied to balance the distributions of the classes. The CNN was trained separately for the three wavefront classes: 'LVp', 'RVp', and 'sinus rhythm'. Model performance was evaluated using AUC, accuracy, and MCC on the test data.

### *5.2.5 Statistical analysis*

In addition to the machine learning algorithms described above, further analyses were performed using Statistical Package for the Social Sciences for Windows (Version 27) and

Graphpad Prism (Version 9). Continuous variables were expressed as median and interquartile range (IQR). Independent continuous data were compared by non-parametric Mann-Whitney U test. For multiple groups either Kruskal-Wallis 1-way ANOVA or Friedmans test (for matched/repeated measures) was performed with subsequent Dunn's multiple comparison test if the former was significant. Independent categorical variables were compared by the Chi-square test. Two-tailed P-values were considered statistically significant when 0.05 or less. Authors KD and SK had full access to all data in the study and takes responsibility for its integrity and the data analysis.

## 5.3 Results

For the infarcted animals, LV ejection fraction and LV end-diastolic volumes were 41% (39-43%) and 118mls (87–155mls) respectively. Surface registration error (comparison of the vertices of each mesh) of the histopathology to the EAM was 4.9mm (3.8-6.3mm), and CMR to EAM was 4.7mm (4.2-5.1mm).

A total of 20,091 electrograms were collected across three wavefronts (after excluding electrograms collected during ectopy), with a median of 1108 (IQR 986-1259) per map. Median bipolar electrogram voltages were 2.22mV (IQR 2.16-2.64mV) for infarcted animals and 2.96mV (IQR 2.89-3.02mV) for the non-infarcted control animal. Median unipolar electrogram voltages were 6.25mV (IQR 5.90-7.32mV) for infarcted animals and 8.75mV (IQR 8.45-8.93mV) for the control animal. There was a median of 238 LAVAs (IQR 175-326.5) and 36 split potentials (IQR 23-103) per infarcted animal map versus 94 LAVAs (IQR 88.5-101) and 3 split potentials (2-3) per control animal map. Scar areas are described in Supplementary Table S1.

Of the total electrograms, 11,551 were matched to 421 transmural biopsies divided into thirds for endocardial, intramural and epicardial regions. Each biopsy was matched to 24 (IQR

16-35) electrograms. For each biopsy 8 (IQR 5-15) matched electrograms were sinus or atrial paced, 7 (IQR 4-11) RVp and 7 (IQR 3-11) LVp. There was less viable myocardium by layer in regions containing scar (Figure 3). Median transmural biopsy wall thickness was 8.8mm (IQR 5.45-11.75mm) for infarcts and 12.15mm (10.78-14.78mm) for control.

### *5.3.1 **Discriminative performance of bipolar and unipolar voltage to identify scar***

Median bipolar voltage was lower for electrograms colocalizing with at least endocardial (1.11mV IQR 0.50-1.98mV), at least intramural (1.58mV IQR 0.93-2.48mV) and epicardial only scar (1.62mV IQR 0.70-2.55mV) compared to no scar (1.89mV IQR 0.98-3.12mV, ANOVA $P<0.0001$ for all between group comparisons to no scar, Figure 4A). Median unipolar voltage was lower for electrograms colocalising with at least endocardial (5.04mV IQR 3.67-7.35mV) compared to no scar (6.45mV IQR 4.79-8.37mV, ANOVA $P<0.0001$, between groups $P<0.0001$) but not significantly different for at least intramural (6.50mV IQR 4.65mV-9.44mV, $P=0.456$) or epicardial only (5.96mV IQR 4.49-7.72mV, $P=0.183$, Figure 4B).

The AUC, accuracy, MCC, sensitivity and specificity for a gradient boost model using bipolar voltage alone, unipolar voltage alone or combined bipolar and unipolar voltages together is reported in in Supplementary Table S2. The model incorporating both bipolar and unipolar voltage together performed best, with respective AUCs and accuracy of 0.703 and 0.640 for no scar, 0.706 and 0.632 for at least endocardial scar, 0.593 and 0.860 for at least intramural scar and 0.586 and 0.710 for epicardial only scar (Figure 4C and 4D). Sensitivity and specificity were better for no scar (45.9%, 78.0% respectively) and at least endocardial scar (41.8%, 81.6% respectively). In contrast sensitivity was very poor for at least intramural or epicardial only scar (19.8% and 31.6% respectively). Nevertheless, this model performed better than a multinomial logistic regression model incorporating traditional dichotomous voltage cutoffs (dense bipolar scar

<0.5mV, bipolar scar <1.5mV or unipolar scar <8.3mV) which had AUCs ranging from 0.574-0.656 and accuracies 0.586-0.800) (see Supplementary Table S3).

### *5.3.2 Signal processing and feature selection of windowed bipolar electrograms*

A total of 794 signal processing features were extracted from the windowed bipolar electrograms. Using gradient boost machine learning, these features were used to classify intracardiac electrograms by scar type. The top 100 features (sorted by group) are shown in Figure 5A and summarized in Supplementary Table S4. Of the top 100 features, 39 (39%) involve transformation into the frequency domain (predominantly Fourier transformation), with the remaining 61 (61%) being time domain features. 9 (9%) can be readily identifiable by visually inspecting the electrogram (Figure 5B). These features resemble traditionally used markers of fractionation such as the number of peaks with a duration of more than 50ms (rank 2) or times crossing a specific voltage (-1mV (rank 36) and 1mv (rank 58)), electrogram length (rank 29) and voltage characteristics (length of electrogram with voltage higher than mean (rank 4), number of points above mean voltage (rank 33), range i.e. bipolar voltage (rank 49), minimum voltage (59) and maximum voltage (97).

Of the 20 highest ranked features (Table 1, Figure 5C), 14 (70%) involve transformation of the electrograms into the frequency domain. Fourier transformation encompassed high (>100 Hertz), mid (50-100 Hertz) and low (less than 50 Hertz) frequencies. 1 (5%) of the top 20 features can be readily identified by visual inspection (number of peaks greater than 50ms in duration).

Using the top 20 features to classify the electrograms (gradient boost), higher AUCs, accuracy and MCCs were achieved compared with voltage criteria alone (Figure 5C). Performance was stronger for no scar (AUC 0.815, accuracy 0.728, MCC 0.455, sensitivity 73.4%, specificity 72.4%) or at least endocardial scar (AUC 0.810, accuracy 0.680, MCC 0.381,

sensitivity 38.1%, specificity 93.1%) with relatively worse performance for at least intramural (AUC 0.704, accuracy 0.832, MCC 0.172, sensitivity 43.6%, specificity 85.3%) or epicardial only scar (AUC 0.681, accuracy 0.835, MCC 0.128, sensitivity 34.5%, specificity 86.2%). The performance of this model using the top 20 features was similar to a model including all 794 extracted features (Supplementary Table S5).

This Gradient boost model was interrogated using the permutation feature importance technique to determine post-hoc the contribution of the top 20 features to performance (see Supplementary Figure 1). The most significant feature was energy in the first segment of 10 versus the entire series followed by the number of peaks greater than 50ms in duration, longest consecutive sequence higher than the mean and the time point of 10% of cumulative mass. Further frequency domain features: the angle values of the Fourier coefficients at 621Hz and 484Hz and skewness of the absolute values of the Fourier Transform were also important contributors to the model.

### *5.3.3 CNN approach to classify bipolar and unipolar electrogram by scar type*

To improve classification further, a CNN was engineered to classify the windowed and complete bipolar and unipolar time series. This was performed with TimeSeries AI (TSAI) using the InceptionTime CNN module trained for each input wavefront (sinus rhythm/atrial pacing, RVp or LVp).

Results are shown in Table 2. Compared with windowed bipolar electrograms, both the complete bipolar and unipolar time series improved performance. The complete unipolar time series performed best. Model performance (averaged across wavefront) was: no scar - AUC 0.977, accuracy 0.929, sensitivity 91.7%, specificity 93.4%; at least endocardial scar - AUC 0.970, accuracy 0.919, sensitivity 91.3%, specificity 92.0%; at least intramural scar - AUC 0.909,

accuracy 0.959, sensitivity 42.9%, specificity 98.8%; epicardial only car - AUC 0.926, accuracy 0.961, sensitivity 52.4%, specificity 98.4%. Performance of the CNN across wavefronts (when averaging the scar patterns) appeared similar ( Supplementary Figure 2).

### *5.3.4 Creation of a three-dimensional scar pattern prediction map*

From the above data, the complete unipolar time series was selected as the input for a prediction model of scar pattern using the InceptionTime algorithm. With custom code, a three-dimensional anatomic reconstruction readily importable into the EAM system was created using input electrograms from an entire left ventricular electroanatomic map to predict scar location and pattern. In Figure 6 we show a sample scar prediction map of a single infarcted sheep. Predominantly anterior, anteroseptal and apical infarction involving the endocardium was identified with the intramural and epicardial substrate at the border of the scar.

## 5.4 Discussion

This study created an atlas of ventricular electrogram characteristics that matched the co-registered histological scar pattern. To this, a suite of signal processing features, as well as a CNN, was applied systematically to demonstrate that these intracardiac electrograms, derived from a multi-electrode catheter, can accurately determine scar pattern. We have made several significant findings:

1. The bipolar and unipolar voltages of individual electrograms performed modestly to determine scar pattern even when optimised with a supervised machine learning model without attention to traditional voltage cutoffs.
2. Time and frequency domain features extracted through signal processing of the windowed bipolar electrogram offered improved performance to voltage alone.

3. Many bipolar electrogram features that contributed to determining scar pattern are unappreciable with only visual inspection.
4. Assessment of the complete 2.5s unipolar electrogram acquisition using the InceptionTime CNN offered the best-performing delineation of scar pattern.
5. Using the results from this CNN, a scar pattern prediction map could be generated for EAM reintegration.

### *5.4.1 Electrogram voltage and scar pattern*

Abnormal bipolar and unipolar voltage thresholds, derived initially with a 95% cut-off from mapping human hearts without structural heart disease using a 4 mm tipped ablation catheter[19,245,247], have been shown to correlate to gross scar area in swine models[57] and to epicardial bipolar low voltage areas.[245] In contrast, Tung et al. (2016) suggested modest sensitivity and specificity of voltage amplitudes to CMR-defined scar (57% sensitivity, 79% specificity for endocardial bipolar voltage < 1.5mV (2mm electrode spacing) and 81% sensitivity, 58% specificity for unipolar voltage <8.3mV) to account for scar in endocardial, mid-myocardial and/or epicardial layers. Elegant co-registered whole-heart histological experiments in infarcted swine hearts[446], remodelled and non-remodelled post-infarct human myocardium[253] and non-ischaemic cardiomyopathy[70] by Zeppenfeld and colleagues demonstrate the complex interaction of wall thickness, electrode size and spacing, ventricular remodelling, transmural viable myocardium percentage and related voltages, suggesting that single voltage cutoffs may not be appropriate to classify scar. Interestingly, in one experiment, by considering multiple voltages of a novel catheter (utilising bipolar, unipolar and microelectrode bipolar) rather than a single cut-off value, the sensitivity of voltage mapping to identify transmural fibrosis was improved to 93%.[446]

Ours is one of the first study to compare such voltages to various scar patterns of differing "depth" of scar (i.e. scar in the immediate endocardial layer adjacent to the recording electrode vs scar remote from the recording electrode with healthy tissue in between (at least intramural and epicardial only scar). We showed similar modest sensitivity and specificity when using traditional scar voltage cutoffs, with particularly poor performance in the outer layers. Due to these findings, we then attempted to use gradient boost to classify scar pattern based on bipolar, unipolar or both electrograms without pre-specifying a voltage cut-off. This approach still only achieved low to modest AUCs and accuracy in predicting scar pattern beyond the mid-myocardium. As suggested by Tung et al. (2016) this is could be due to 3-D spatial averaging where the catheter tip fails to identify scar at greater depth vs width.[252] Whilst voltage thresholds continue to be a standard of clinical practice, our results confirm that the complexity of underlying scar tissue is underappreciated by reducing electrograms to purely an amplitude dimension.

### *5.4.2 Feature analysis of electrograms to identify scar pattern*

If voltage criteria alone are inadequate, then how do alternative visual and hidden electrogram features perform to identify areas of interest in the ventricular myocardium? We found that using the top 20 (of 794) ranked signal processing features improved the discriminative classification ability of electrograms for scar pattern substantially compared to voltage alone. Visually appreciable and commonly reported electrogram features such as fractionation, electrogram duration and voltage performed poorly compared to more complex features in the frequency and time domains.

Notably, two-thirds of the top 20 features involved transformation of the bipolar electrogram into the frequency domain. Previous frequency analysis of unipolar electrograms support the importance of such analyses. Wavelet and Fast Fourier transformation of epicardial

unipolar electrograms derived from multielectrode plunge needles in a similar ovine model suggest that higher frequency spectra are associated with myocardial tissue heterogeneity and increased propensity to ventricular tachycardia.[323] Frequency analyses of unipolar electrograms derived from an ablation catheter had an average within patient AUC of 0.841 for mid-myocardial fibrosis in non-ischaemic cardiomyopathy (0.591 for unipolar voltage alone).[324] Importantly, as our data suggests, analyses of a single (or few) electrogram features from the frequency domain alone are likely insufficient to identify ventricular sites of interest. Campos et al. (2015) found that using a ratio of high to low bipolar electrogram frequency (derived from Fast Fourier Transformation), only 60% of VT circuits could be identified.[461] This is compared with 100% of VT circuits identified when incorporating electrogram fractionation (a time domain feature). We found that novel time domain features with limited application to electrograms to date, such as autocorrelation, absolute energy and linear trend of the electrogram time series, were also important for scar pattern classification and may warrant future study.

Recent clinical studies have highlighted the importance of frequency analyses in identifying VT regions of interest using the Ensite X Omnipolar technology's near-field algorithm, which employs wavelet transform to identify peak frequency. Using this algorithm, low voltage area peak frequency >220Hz has been shown to have 91% sensitivity and 85% specificity for detecting late potentials and LAVA, could predict deceleration zones in 9 out of 10 patients.[301] However, low voltage area peak frequency >200Hz showed lower performance in identifying the VT isthmus (sensitivity 69%; specificity 64%).[302] Peak frequency analyses of VT activation maps indicated that sites with peak frequency >405Hz during VT predicted VT termination within 5 seconds during ablation (AUC 0.811), likely due to higher peak frequencies identifying near-field VT circuitry.[303] Nonetheless, a study by Tonko et al. (2024) found that peak frequency analyses

alone did not differentiate the dominant VT site from low-voltage bystander sites.[304] Perhaps incorporating other novel time and frequency domain analyses, as explored in this manuscript, could enhance the identification of the VT isthmus from the substrate map.

### *5.4.3 Deep learning CNN to classify electrograms into scar pattern*

To our knowledge, this is the first study to apply deep learning using a CNN trained on raw biologically obtained electrogram time series. Such a classifier substantially improved electrogram performance to identify scar pattern suggesting further hidden features within the electrogram beyond even signal processing techniques. Importantly, compared to all previous approaches, with a CNN, there were much better sensitivity and specificity to identify at least intramural (42.9%, 98.8%) and epicardial only scar (52.4%, 98.4%).

Intriguingly, the CNN performed better when trained on complete bipolar or unipolar electrograms (2.5s recording) compared to the manually windowed bipolar electrograms that is used clinically. One possible reason for this may be because time series classification is more effective if all data is of the same length[462] (compared to the windowed bipolar electrograms where each animal and wavefront had a specific WOI). Alternatively, it could also be that repetition of the electrogram features on multiple heartbeats preceding the last captured beat allowed an assessment of catheter contact (i.e. poor contact would suggest variable electrogram morphology in preceding beats) and artefact. Furthermore characteristics of activation and repolarization[463] may also be more appreciable with multi-beat recordings. The better performance of the unipolar electrograms compared to bipolar could be due to improved field of view, providing more information of the far field which may have been of use to the CNN. Wavefront dependence of the bipolar electrograms could be another reason for this finding.

The only other study to assess individual intracardiac electrograms using deep learning was performed by Ntagiantas et al. (2024).[325] They applied a feed forward CNN with an Encoder-Decoder architecture to assess the performance of computer-simulated atrial electrograms to identify tissue conductivity and fibrosis. Their results showed that an array of concurrent simulated unipolar electrograms can identify underlying atrial scar, supporting, like our data, the plausibility that deep learning networks can infer the structural properties of tissues (albeit in an in-silico model). These analyses did not incorporate bipolar electrograms, and most importantly, did not utilise biologically obtained electrograms with ground-truth histology. Our work extends that of Ntagiantas et al. (2024) by systematically comparing simpler machine learning feature selection (on tsfresh extracted features) to more complex-deep learning methods (InceptionTime CNN). It shows the capability of deep learning to utilise data from a single electrogram acquisition to reliably predict scar pattern.

### *5.4.4 Clinical Implications*

Based on the above findings, we have written code to automatically read an entire EAM export, extract unipolar electrogram time series and then use the trained CNN to predict scar pattern and topography. These predictions are then automatically projected onto a coloured importable three-dimensional mesh. This will allow future work to validate these electrogram definitions in human patients. Although an alternative to this approach is image integration of CMR or MDCT, we have recently shown that the co-registered CMR can miss epicardial substrate using this same model.[464] Furthermore, not all patients with VT needing CA can access good quality CMR due to the emergent need for ablation, cost, implantable cardioverter-defibrillator contraindications, and artefact.

It should be noted that functional substrate mapping may offer improved sensitivity and specificity to identify VT circuits compared to fixed scars, as identified by our algorithm. Some currently used approaches rely on the annotation of the bipolar electrograms in the time domain to latest deflection (for isochronal late activation mapping)[271] or latest sharp component after extrastimulus for decrement evoked potential mapping.[26] Whether further computational time or frequency domain features can identify conduction slowing or functional block with higher specificity is unknown, nor do we know whether such areas can be automatically determined by deep learning of electrograms obtained in sinus or stable pacing rhythm. Our model serves as an important proof of concept that systematic computational analyses of electrograms using signal processing and deep learning may be important to identify electroanatomical areas of interest in the heart.

### *5.4.5 Limitations*

This study has several limitations worth considering. Firstly, it used a small number of animals for a model of post-infarction ventricular scar with a single healthy control. Electrograms were hence imbalanced and enriched for scar. To address this, we also report MCC, which is less sensitive to the distribution of classes and a more rigorous test for imbalanced datasets. MCC metrics support the substantial classification improvement of the deep learning CNN, particularly for at least intramural and epicardial only scar. Secondly the at least endocardial scar pattern encompassed scar from the endocardium to mid-myocardium to complete transmural scar. There could be differences in electrograms between endocardial scar with healthy mid-myocardium/epicardium vs transmural scar. Thirdly, it is unclear if our results would apply to human post-infarction hearts or in non-ischaemic cardiomyopathy (where scar is often patchy). Due to limited access to human electrograms with co-registered histology, our model is yet to be

validated by an external dataset. This is a common issue with current electrogram machine learning studies due to paucity of well labelled data. [324,325] To address this, we have chosen to share the code to generate our three-dimensional prediction maps upon publication for further independent verification. Fourthly, our model does not incorporate wall thickness nor the location of the intracardiac electrogram within the left ventricle native Purkinje signals may confound frequency domain analyses. We chose not to consider electrogram location nor information from neighbouring electrograms as it has not seemed to confound previous frequency unipolar machine learning analyses[324] and because our intention was to create a simple workflow to interrogate whole electroanatomic map exports and then project classified individual electrograms onto clinically usable three-dimensional maps. Such Purkinje signals may have been obscured by pacing. If these signals significantly impacted the model's performance, we would have expected differences in AUC or MCC across wavefronts using the CNN, which we did not observe. Fifth, it is well recognized that filter configurations can dramatically alter both bipolar[465] and unipolar[466] electrograms. Although our used filter settings are relatively standard, variability in lab-to-lab settings might affect performance of the model. Finally, it is unclear if these results can be extrapolated to alternative multielectrode mapping catheters with variable electrode positioning.

## 5.5 Conclusion

In this proof-of-concept study, we have shown that unipolar electrograms generated with a multi-electrode catheter with fine inter-electrode spacing can identify post-infarction mid-myocardial and epicardial scar with excellent AUC and accuracy through use of deep learning. This has been leveraged to create custom code of a readily importable scar topography map that can be used to automatically interrogate whole LV electroanatomic mapping data and classify electrograms into scar pattern labels. Although further studies are needed to validate this prediction

model, taken together, these data suggest the importance of novel computational analyses of intracardiac electrogram shape to identify areas of interest for ablation.

## 5.6 Figures

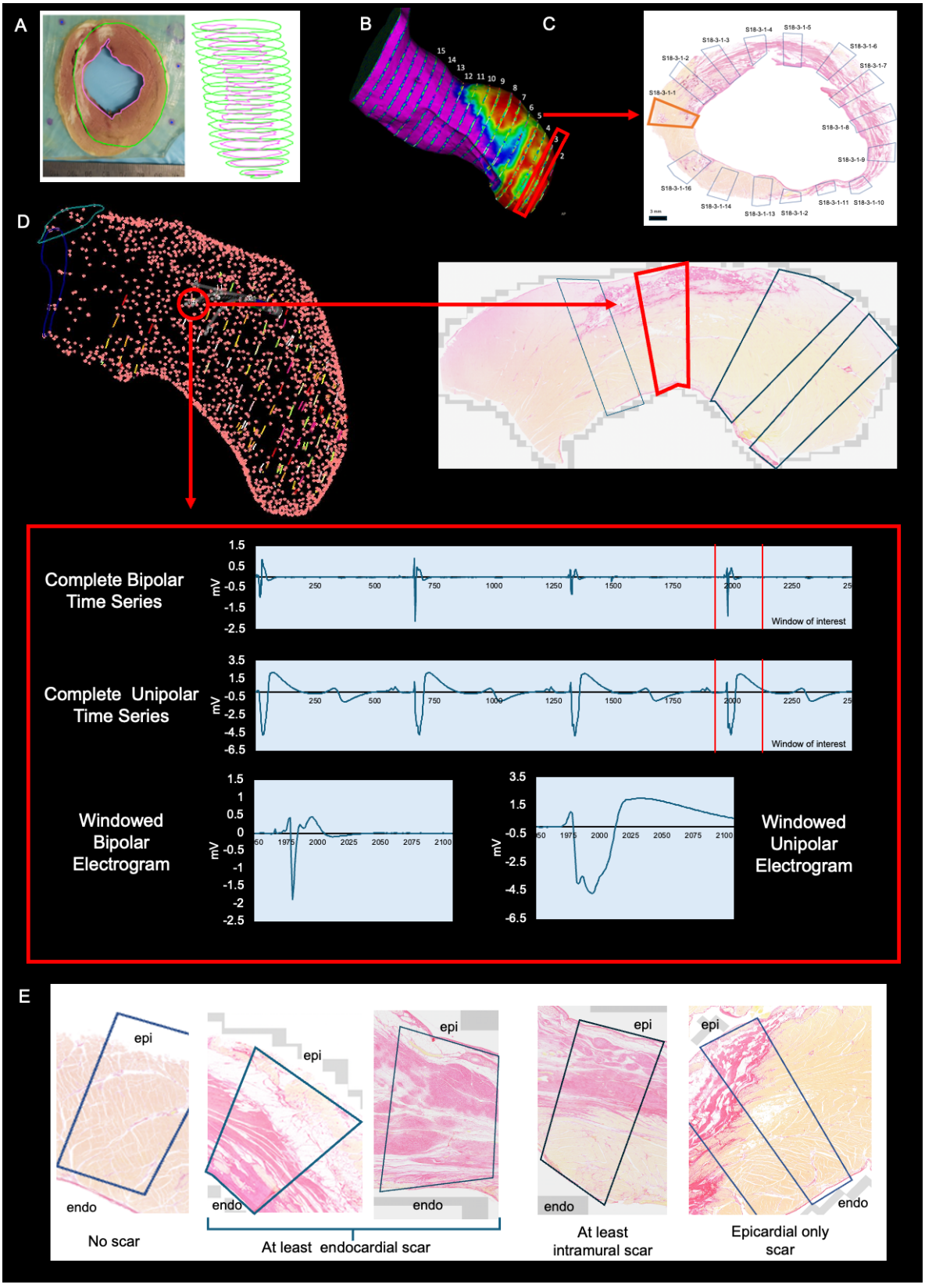
A
B
C
D
Complete Bipolar Time Series
Complete Unipolar Time Series
Windowed Bipolar Electrogram
Windowed Unipolar Electrogram
Window of interest
mV
E
epi
endo
No scar
At least endocardial scar
At least intramural scar
Epicardial only scar

**Figure 5-1 Methodology of electrogram extraction and whole-heart histological co-registration.**

Methodology of electrogram extraction and whole-heart histological co-registration. **A.** Explanted hearts were filled, fixed and then sectioned into 5mm short-axis slices. Contours were traced of the endocardium and epicardium and imported into Matlab to create a custom three-dimensional histopathological shell. **B.** Representative example of a histopathological shell that was imported into mapping software. Numbers 2-15 denote 5mm cross-sectional slices and coloured lines represent 3mm biopsy tracings. **C.** A scaled photograph of cross-section 3 from Figure 1B, taken at 20x magnification after staining with Picrosirius red to identify collagenous tissue. Biopsies were systematically conducted around the endocardial border of the short-axis sections – 3mm width with 3mm spacing between biopsies. **D.** Co-registered electroanatomic map with histological shell (made transparent). The colourful lines represent the 3mm biopsies. The red circle encompasses all electrograms (within 1.5mm radius of the biopsy) that co-localise with one such biopsy. The biopsy on the histological image demonstrates Epicardial only scar (pink compact fibrosis affecting only the epicardium and sparing the endocardial and intramural layers). A representative corresponding family of electrograms is shown with both the windowed bipolar and unipolar electrograms, and the complete 2.5-second acquisitions. The windowed electrograms are restricted to the manually determined window of interest (chosen to eliminate pacing artefact and maximise capture of late potentials). These electrograms were extracted from whole study exports on the CARTO system using custom Python code, and each was matched to a corresponding histopathological scar with labelled scar pattern (one of four options, i.e. no scar, at least endocardial scar, at least intramural scar or epicardial only scar). **E.** Representative

transmural biopsies of the four scar pattern labels; no scar, at least endocardial scar (scar in endocardial layer +/- scar in intramural/epicardial layers), at least intramural scar (scar in intramural layer +/- epicardial layer sparing endocardium) and epicardial only scar (sparing endocardial and intramural layers). Note the at least endocardial scar pattern encompasses all scar with at least an endocardial component i.e. includes endocardial + intramural scar and transmural scar. Yellow represents healthy myocardium, pink fibrosis and white adiposity. Panel A-C from De Silva et al. (2024).[464]

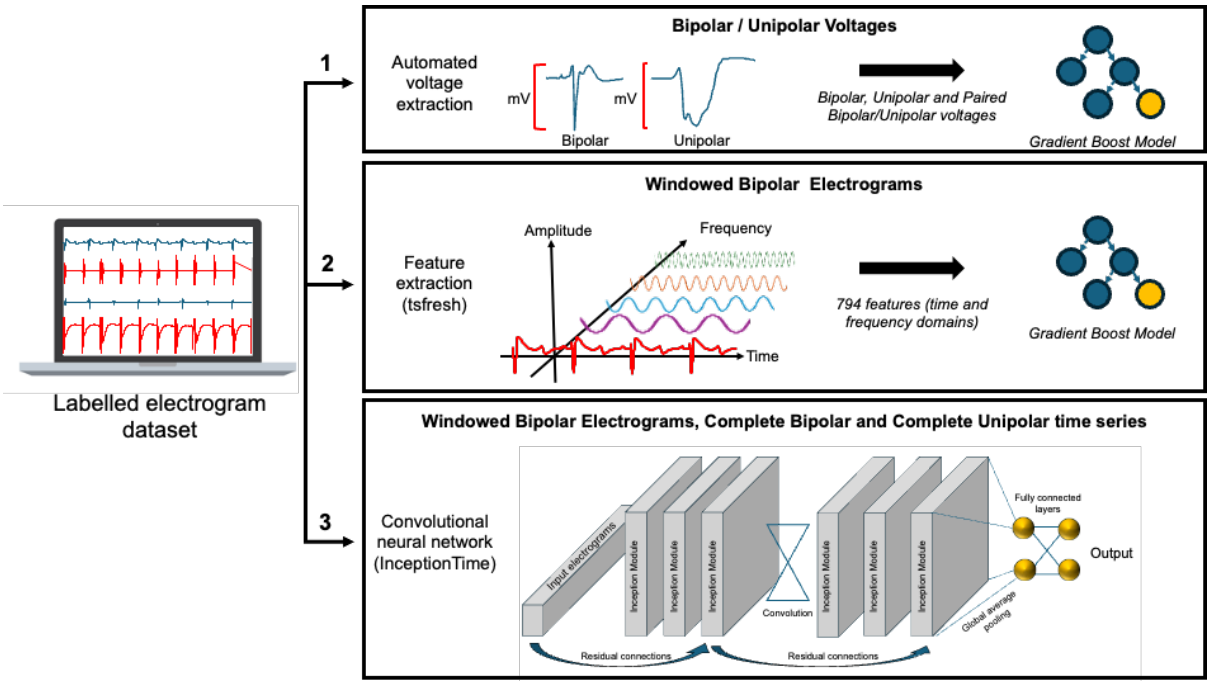


**Figure 5-2 Pipeline for electrogram analyses.**

Labelled electrograms were analysed with three workflows. First automatically calculated bipolar and/or unipolar voltages were used to train a supervised gradient boost machine learning algorithm. Second, feature extraction of the windowed bipolar electrograms was performed using the tsfresh (Time Series FeatuRe Extraction on basis of Scalable Hypothesis, version 0.20.3) python package into 794 time and domain features. After feature ranking (using a fast correlation based filter), features were used to train a supervised gradient boost machine learning algorithm. Finally, a convolutional neural network (CNN) called InceptionTime (an ensemble of five deep learning models designed for time series classification where each model utilises inception modules to interrogate the time series with filters of different lengths simultaneously to extract relevant features) was trained using the windowed bipolar electrograms as well as the complete bipolar and complete unipolar electrograms.

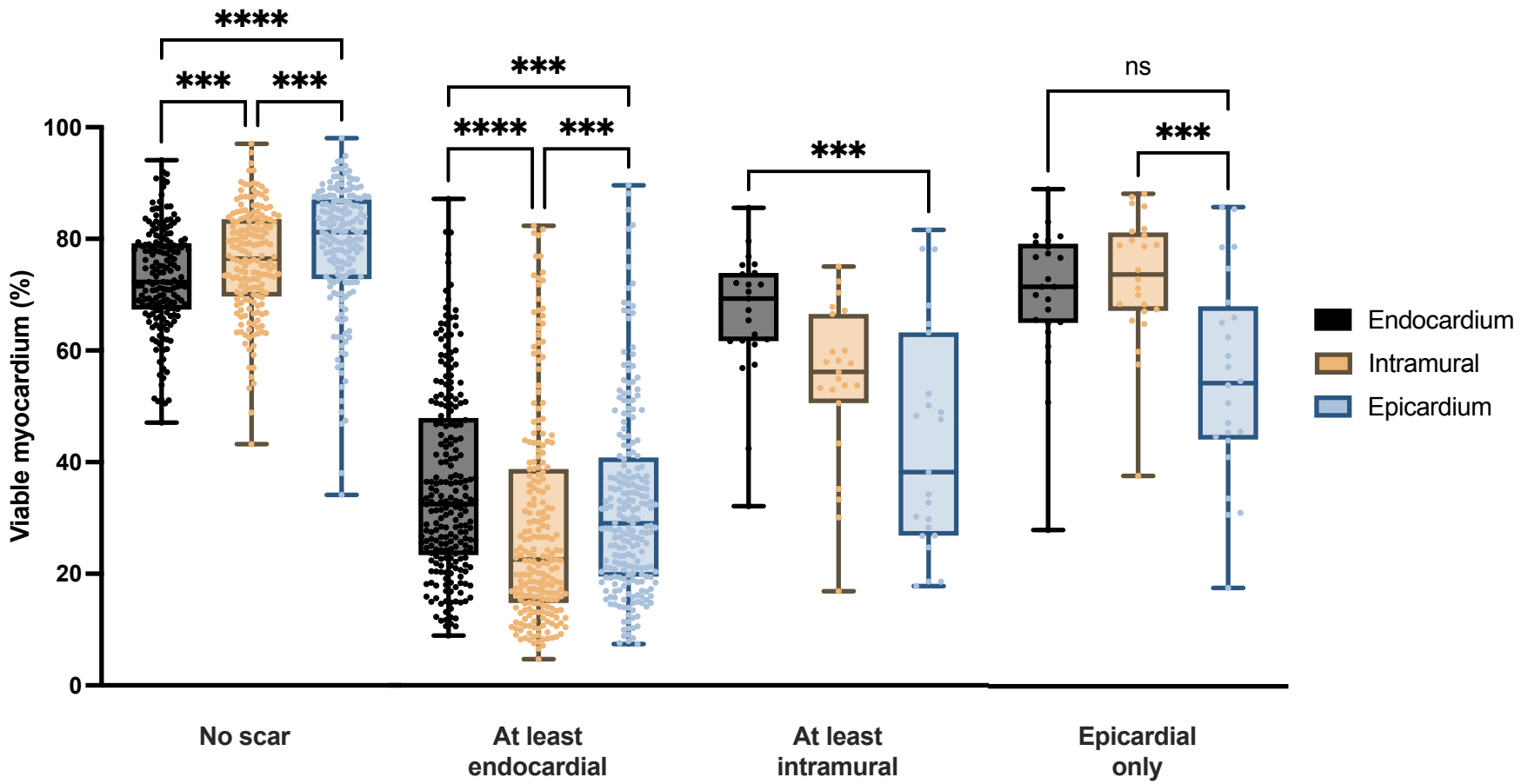


**Figure 5-3 Distribution of viable myocardium by scar pattern**

Distribution of viable myocardium within the endocardial, intramural and epicardial layers for each scar pattern category. Viable myocardium was determined using ImageJ (total area minus area with fibrosis and adiposity). The scar pattern labels were no scar (no visual scar in all three layers), at least endocardial scar (scar in endocardial layer +/- intramural +/- epicardial layers), at least intramural

(no scar in the endocardium, scar in the intramural +/- epicardial layers) and epicardial only (no scar in the endocardial or intramural layers but scar in the epicardium). Analyses performed using Friedmans test (non-parametric test for multiple groups with repeated measures), $P<0.0005$ for each scar label and subsequent Dunn's multiple comparison test (*** = $P<0.0005$, **** = $P<0.0001$, ns = non-significant).

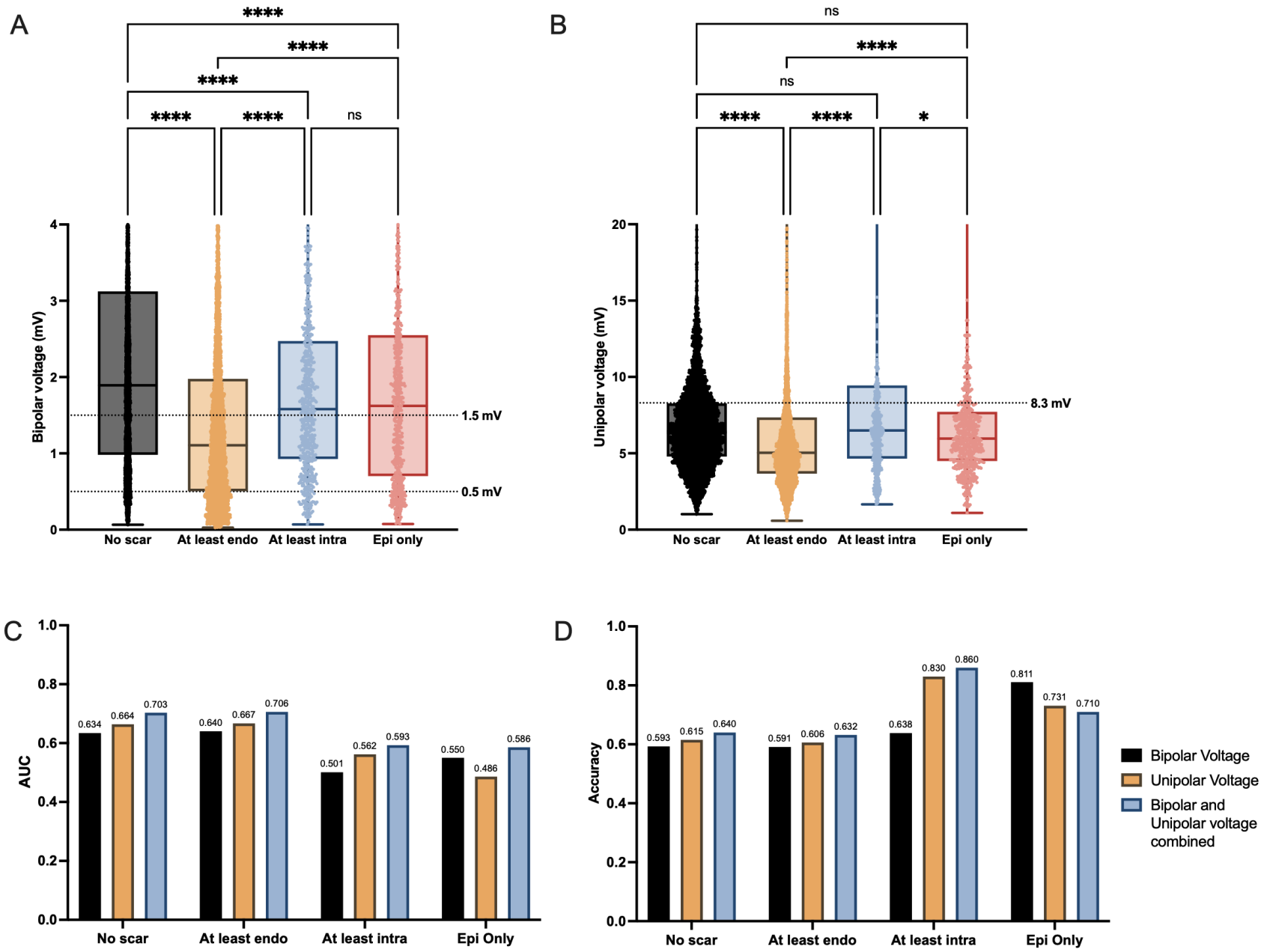
A
****
****
****
****
****
ns
Bipolar voltage (mV)
1.5 mV
0.5 mV
No scar
At least endo
At least intra
Epi only
B
ns
****
ns
****
****
*
Unipolar voltage (mV)
8.3 mV
No scar
At least endo
At least intra
Epi only
C
AUC
0.634
0.664
0.703
0.640
0.667
0.706
0.501
0.562
0.593
0.550
0.486
0.586
No scar
At least endo
At least intra
Epi Only
D
Accuracy
0.593
0.615
0.640
0.591
0.606
0.632
0.638
0.830
0.860
0.811
0.731
0.710
No scar
At least endo
At least intra
Epi Only
Bipolar Voltage
Unipolar Voltage
Bipolar and Unipolar voltage combined

**Figure 5-4 Relationship between automated bipolar and unipolar electrogram voltage and scar pattern label**

**A.** and **B.** represent spread of bipolar and unipolar voltage across scar pattern labels. Y axes for bipolar and unipolar voltage have been restricted to 4mV and 20mV respectively (clinically meaningful values). For bipolar voltage, standard voltage thresholds of 1.5mV (scar) and 0.5mV (dense scar) have been labelled. Similarly for unipolar voltage standard voltage threshold of 8.3mV (scar) has been labelled. Analyses performed using Kruskall Wallis non-parametric tests ($P<0.0001$ for both bipolar and unipolar voltage) and Dunn's multiple comparison test (**** $P<0.0001$, * $P<0.05$, ns = non-significant). **C.** AUCs for bipolar voltage, unipolar voltage and combined bipolar and unipolar voltage to identify scar pattern as determined by gradient boost. **D.** Accuracy for bipolar voltage, unipolar voltage and combined bipolar and unipolar voltage to identify scar pattern as determined by gradient boost.

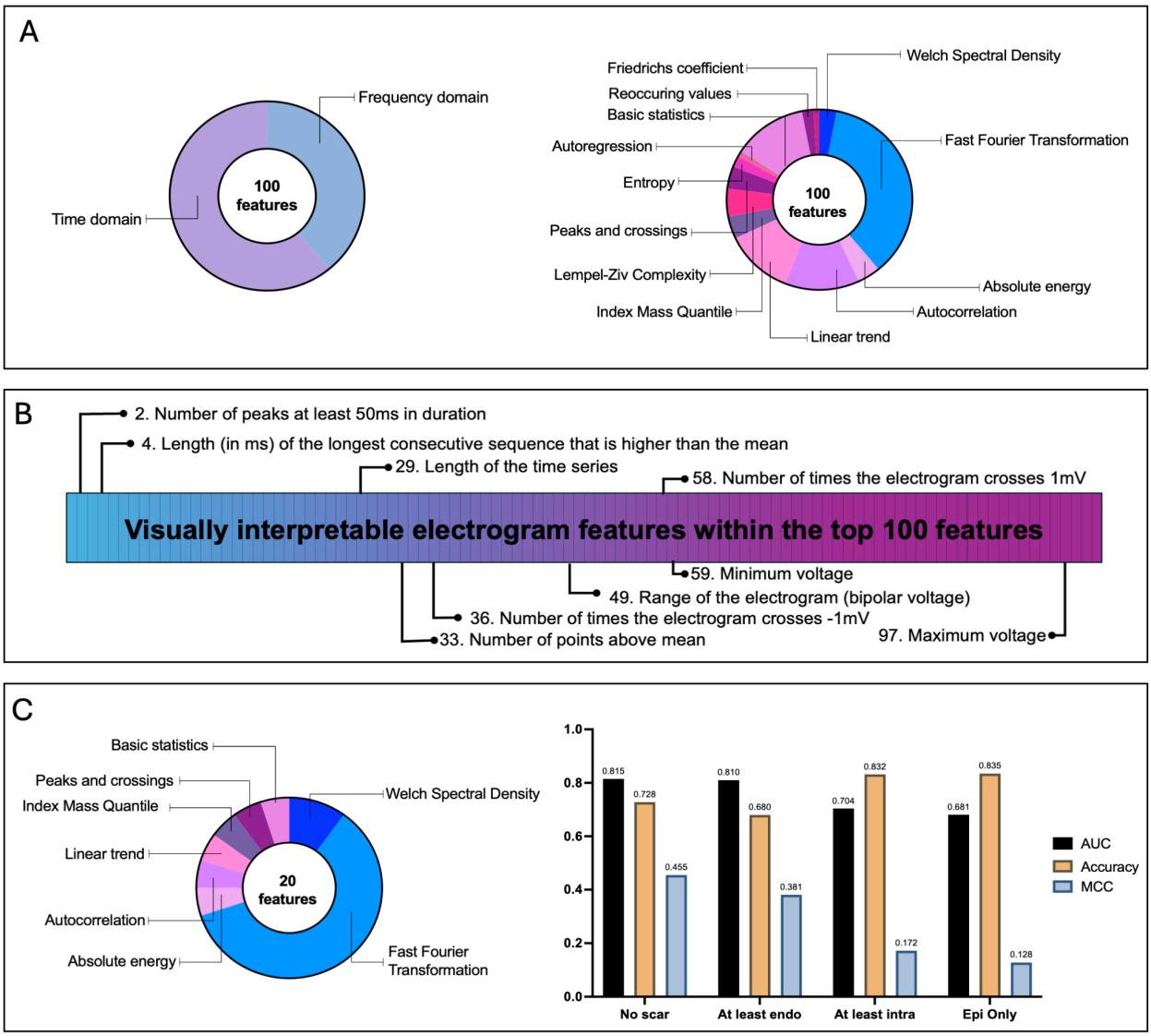


**Figure 5-5 Signal processed features of the windowed bipolar electrogram**

**A.** Chart of the top 100 bipolar electrogram features (extracted from tsfresh, python) useful to identify ventricular scar pattern classified by feature type. See Supplementary Table S4 for individual breakdown of sub-categories. **B.** 9 visually interpretable bipolar electrogram features ranked within the top 100. **C.** Top 20 bipolar electrogram features classified by feature type. Gradient boost model AUC, Accuracy and MCC for these top 20 signal processed features to identify various scar patterns.

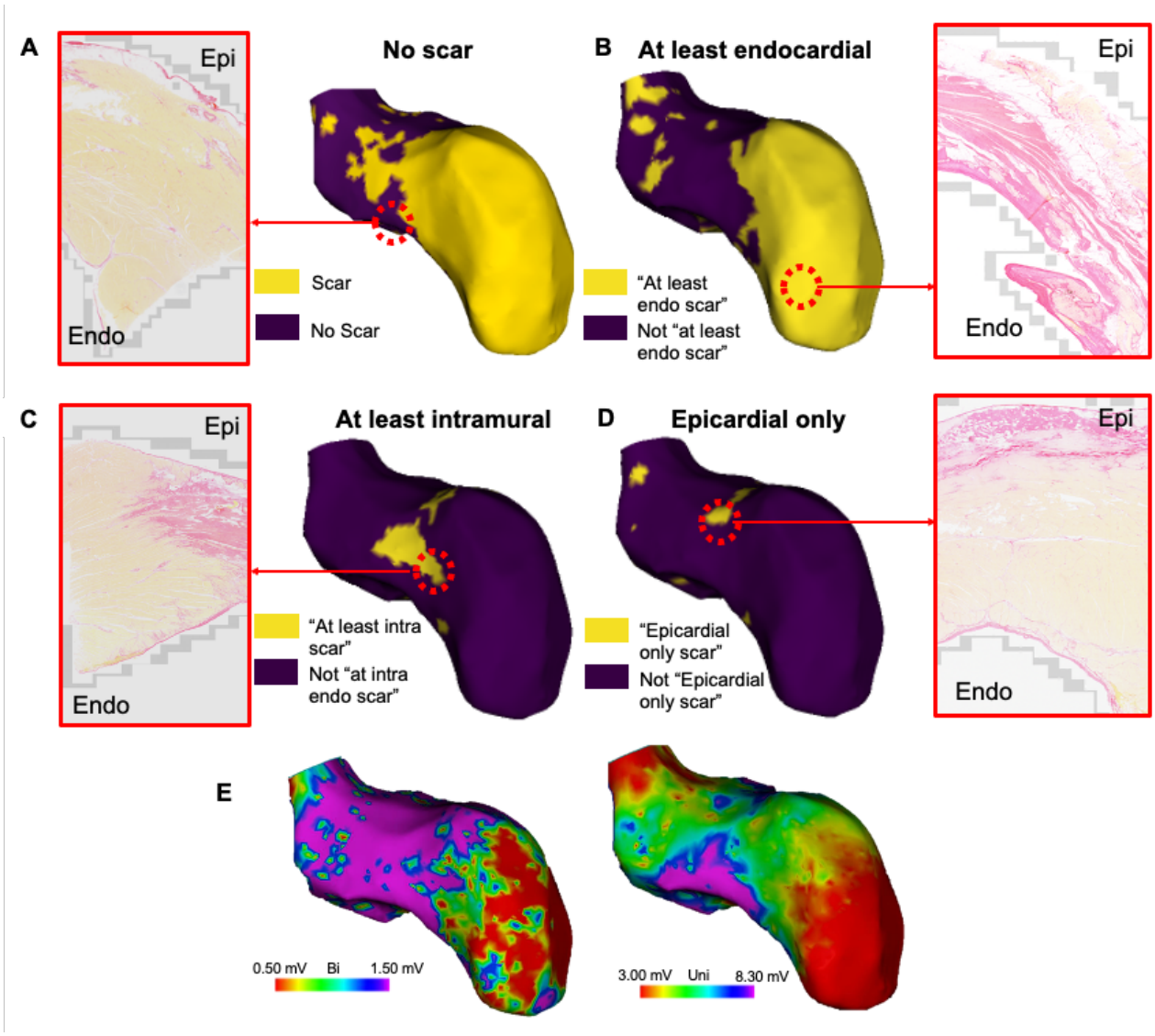


**Figure 5-6 A sample three-dimensional scar pattern prediction map**

A sample three-dimensional scar pattern prediction map, ready for import into the electroanatomic mapping software. Here the final convolutional neural network model was applied to the right ventricular paced (RVp) electroanatomic map of one of the infarcted sheep. Panels **A-D** show individual scar pattern maps to describe regions of no scar, at least endocardial scar, at least intramural scar and epicardial only scar (see Figure Legends for each individual map). A sample histological biopsy is shown for each scar map to qualitatively demonstrate histological agreement

with the scar prediction model. In Panel **E**. standard Bipolar and Unipolar maps during RVp using standard thresholds (Bipolar - 0.50mV dense scar, 1.5mV border zone and Unipolar 8.3mV scar) are also shown for reference.

## 5.7 Tables

**Table 5-1 Top 20 ranked windowed bipolar electrogram features for scar pattern classification.**

| Rank | Feature | Description | Category |
|---|---|---|---|
| **1** | x__spkt_welch_density__coeff_5 | Cross power spectral density at 5 frequencies | Frequency |
| **2** | x__number_peaks__n_50 | Count of peaks that are greater than 50ms | Time |
| **3** | x__fft_aggregated__aggtype_"skew" | Skewness of the absolute values of the Fourier Transform (asymmetry in distribution of the frequency components) | Frequency |
| **4** | x__longest_strike_above_mean | The length of the longest consecutive sequence that is bigger than the mean | Time |
| **5** | x__fft_coefficient__attr_"angle"__coeff_89 | Angle value of the Fourier coefficient at 582Hz | Frequency (High) |
| **6** | x__fft_coefficient__attr_"angle"__coeff_74 | Angle value of the Fourier coefficient at 484Hz | Frequency (High) |
| **7** | x__fft_coefficient__attr_"angle"__coeff_95 | Angle value of the Fourier coefficient at 621Hz | Frequency (High) |
| **8** | x__fft_coefficient__attr_"abs"__coeff_5 | Absolute value of the Fourier coefficient at 33Hz | Frequency (Low) |
| **9** | x__fft_coefficient__attr_"abs"__coeff_6 | Absolute value of the Fourier coefficient at 39Hz | Frequency (Low) |
| **10** | x__fft_coefficient__attr_"abs"__coeff_4 | Absolute value of the Fourier coefficient at 26Hz | Frequency (Low) |
| **11** | x__fft_coefficient__attr_"abs"__coeff_7 | Absolute value of the Fourier coefficient at 46Hz | Frequency (Low) |
| **12** | x__spkt_welch_density__coeff_8 | Cross power spectral density at 8 frequencies | Frequency |
| **13** | x__fft_coefficient__attr_"abs"__coeff_8 | Absolute value of the Fourier coefficient at 52Hz | Frequency (Mid) |
| **14** | x__partial_autocorrelation__lag_2 | Partial autocorrelation at 2ms | Time |
| **15** | x__fft_coefficient__attr_"abs"__coeff_9 | Absolute value of the Fourier coefficient at 59Hz | Frequency (Mid) |
| **16** | x__index_mass_quantile__q_0.1 | Time point of 10% of cumulative mass | Time |
| **17** | x__fft_coefficient__attr_"abs"__coeff_10 | Absolute value of the Fourier coefficient at 65Hz | Frequency (Mid) |
| **18** | x__energy_ratio_by_chunks__num_segments_10__segment_focus_0 | Energy in first segment of 10 vs. entire series | Time |
| **19** | x__fft_coefficient__attr_"abs"__coeff_3 | Absolute value of the Fourier coefficient at 20Hz | Frequency (Low) |
| **20** | x__agg_linear_trend__attr_"stderr"__chunk_len_50__f_agg_"var" | Standard error of the linear trend across the variance of all 50ms chunks | Time |

Legend: Windowed bipolar electrograms were extracted and transformed using the tsfresh (Time Series FeatuRe Extraction on basis of Scalable Hypothesis, version 0.20.3) Python package. Top 20 features for scar pattern were determined using a fast correlation based filter.

**Table 5-2 Performance of the convolutional neural network to classify bipolar and unipolar electrograms by scar pattern.**

| Input | Scar pattern label | Wavefront | AUC | Accuracy | MCC | Sensitivity (%) | Specificity (%) |
|---|---|---|---|---|---|---|---|
| Windowed Bipolar | No Scar | SR | 0.899 | 0.839 | 0.630 | 73.8 | 88.7 |
| | | LVp | 0.901 | 0.834 | 0.668 | 81.6 | 85.4 |
| | | RVp | 0.915 | 0.829 | 0.655 | 75.8 | 88.8 |
| | At least endocardial scar | SR | 0.893 | 0.810 | 0.611 | 85.9 | 74.6 |
| | | LVp | 0.917 | 0.861 | 0.699 | 82.9 | 87.8 |
| | | RVp | 0.914 | 0.845 | 0.688 | 85.2 | 83.9 |
| | At least intramural scar | SR | 0.825 | 0.948 | 0.463 | 38.3 | 98.5 |
| | | LVp | 0.847 | 0.950 | 0.422 | 34.1 | 98.6 |
| | | RVp | 0.839 | 0.960 | 0.377 | 33.5 | 98.5 |
| | Epicardial only scar | SR | 0.862 | 0.959 | 0.483 | 44.4 | 98.4 |
| | | LVp | 0.730 | 0.932 | 0.310 | 30.2 | 97.1 |
| | | RVp | 0.842 | 0.950 | 0.550 | 48.9 | 98.3 |
| Complete Bipolar | No scar | SR | 0.920 | 0.871 | 0.701 | 75.8 | 92.5 |
| | | LVp | 0.951 | 0.894 | 0.787 | 89.3 | 89.5 |
| | | RVp | 0.940 | 0.869 | 0.735 | 84.3 | 89.1 |
| | At least endocardial scar | SR | 0.923 | 0.849 | 0.694 | 85 | 84.8 |
| | | LVp | 0.933 | 0.877 | 0.734 | 84.5 | 89.5 |
| | | RVp | 0.947 | 0.896 | 0.789 | 87.4 | 91.3 |
| | At least intramural scar | SR | 0.802 | 0.952 | 0.470 | 31.9 | 99.3 |
| | | LVp | 0.917 | 0.958 | 0.531 | 43.9 | 98.8 |
| | | RVp | 0.842 | 0.964 | 0.474 | 44.4 | 98.5 |
| | Epicardial only scar | SR | 0.881 | 0.965 | 0.550 | 47.2 | 98.9 |
| | | LVp | 0.848 | 0.945 | 0.426 | 37.2 | 98.1 |
| | | RVp | 0.850 | 0.946 | 0.506 | 44.7 | 98.2 |
| Complete Unipolar | No scar | SR | 0.984 | 0.942 | 0.867 | 90.1 | 96.2 |
| | | LVp | 0.974 | 0.917 | 0.834 | 90.8 | 92.7 |
| | | RVp | 0.972 | 0.927 | 0.855 | 94.3 | 91.4 |
| | At least endocardial scar | SR | 0.968 | 0.917 | 0.831 | 93.4 | 89.6 |
| | | LVp | 0.967 | 0.902 | 0.789 | 89.5 | 90.5 |
| | | RVp | 0.976 | 0.937 | 0.873 | 91 | 95.9 |
| | At least intramural scar | SR | 0.919 | 0.956 | 0.592 | 57.4 | 98.1 |
| | | LVp | 0.916 | 0.952 | 0.411 | 26.8 | 99.3 |
| | | RVp | 0.893 | 0.970 | 0.530 | 44.4 | 99.1 |

| | | | | | | | |
|---|---|---|---|---|---|---|---|
| | Epicardial only scar | SR | 0.936 | 0.965 | 0.570 | 52.8 | 98.6 |
| | | LVp | 0.931 | 0.954 | 0.543 | 51.2 | 98.1 |
| | | RVp | 0.912 | 0.954 | 0.593 | 53.2 | 98.5 |

Performance of the InceptionTime (timeseries AI, python) neural network to classify windowed bipolar electrograms and complete bipolar and unipolar electrogram time series for scar pattern stratified by mapping wavefront.

## 5.8 Supplemental Material

### *5.8.1 Supplemental Figures*

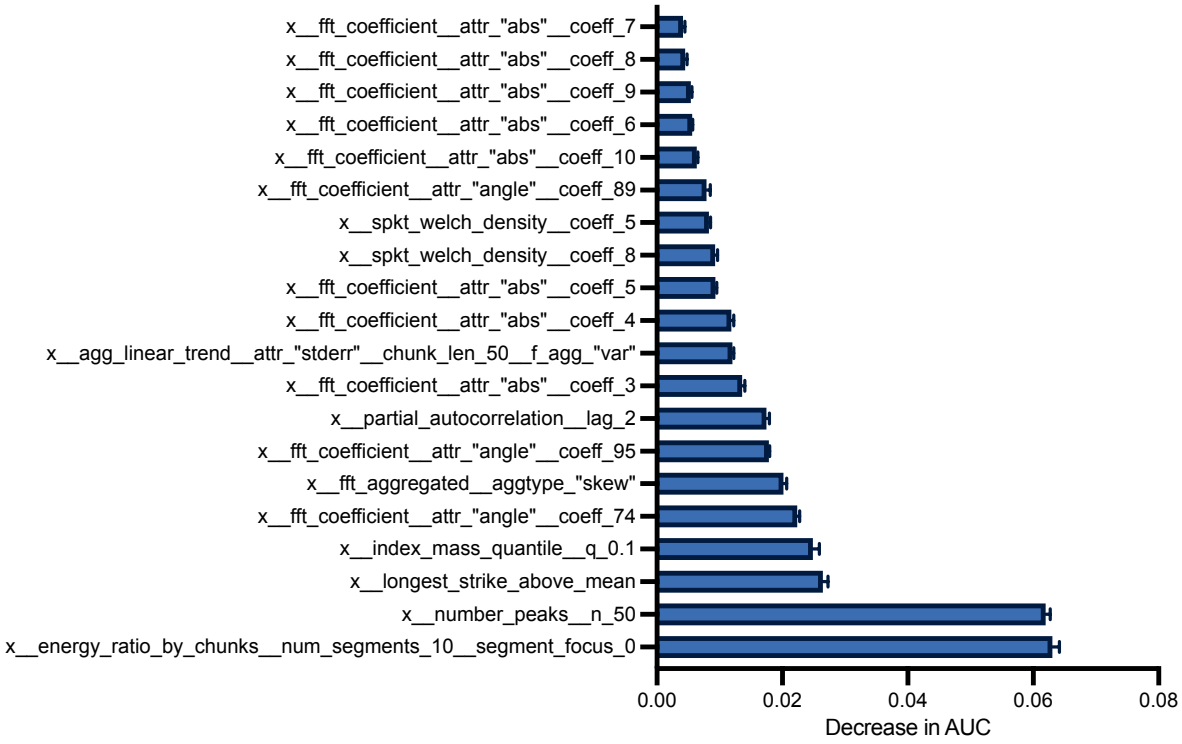


**Supplemental Figure 5-1 Ranking of features contributing to gradient boost model performance (area under the curve) based on permutation feature importance**

Permutation feature importance was used to rank the features contributing to performance of the Top20 tsfresh feature Gradient Boost model.

Abbreviations: AUC – Area under the curve

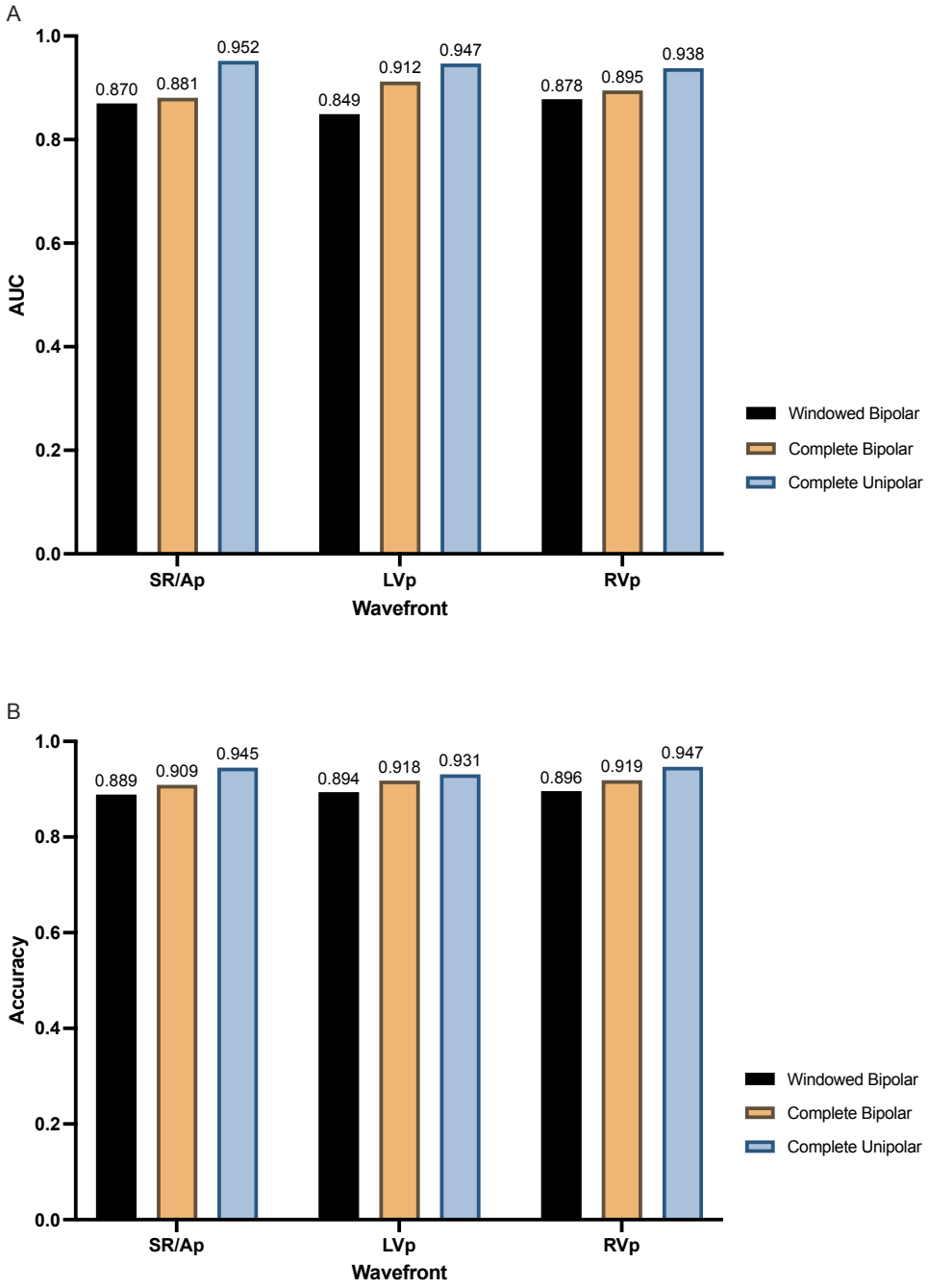


**Supplemental Figure 5-2 Performance of the convolutional neural network to classify bipolar and unipolar electrograms by wavefront (averaged across scar patterns)**

Performance of the convolutional neural network (InceptionTime) applied to windowed bipolar electrograms, complete bipolar time series acquisition and complete unipolar time series

acquisition. A. Area under curve and B. Accuracy. Values provided are an average of the performance of InceptionTime model across all four scar patterns (no scar, at least endocardial scar, at least intramural scar and at least epicardial scar).

### *5.8.2 Supplemental Tables*

**Supplemental Table 5-1 Baseline characteristics of each animal**

| Animal | | 1 (infarct) | | | 2 (infarct) | | | 3 (infarct) | | | 4 (infarct) | | | 5 (infarct) | | | 6 (control) | | |
|---|---|---|---|---|---|---|---|---|---|---|---|---|---|---|---|---|---|---|---|
| Wavefront | | SR | RVp | LVp | SR | RVp | LVp | SR | RVp | LVp | SR | RVp | LVp | SR | RVp | LVp | SR | RVp | LVp |
| Number of points | | 899 | 1185 | 1010 | 1283 | 1177 | 497 | 1625 | 980 | 1154 | 957 | 1160 | 1043 | 1456 | 1004 | 1308 | 874 | 1062 | 1417 |
| Mean bipolar voltage (mV) | | 2.033 | 2.184 | 2.216 | 2.8 | 2.776 | 3.014 | 2.182 | 2.503 | 2.415 | 2.389 | 2.828 | 2.185 | 1.621 | 2.145 | 1.843 | 2.963 | 3.084 | 2.82 |
| Mean unipolar voltage (mV) | | 5.575 | 6.16 | 5.885 | 7.387 | 8.556 | 7.57 | 5.802 | 6.101 | 7.247 | 5.92 | 7.161 | 6.25 | 5.507 | 6.318 | 20.102 | 8.751 | 9.1 | 8.157 |
| Bipolar Scar area <1.5mV | Area (cm2) | 25.5 | 26.2 | 28.3 | 18 | 12.4 | 11.9 | 24.4 | 13.7 | 15.9 | 28 | 21.9 | 37.4 | 57.9 | 42.8 | 47.3 | 4.3 | 4.4 | 6.6 |
| | % of total LV area | 26.18% | 25.99% | 30.36% | 14.74% | 15.40% | 15.47% | 20.23% | 12.74% | 15.88% | 25.34% | 21.43% | 36.81% | 43.86% | 34.24% | 39.55% | 5.83% | 6.16% | 8.44% |
| Bipolar Dense Scar area <0.5mV | Area (cm2) | 5.2 | 2.5 | 2.4 | 5.3 | 5.2 | 3.2 | 3.9 | 1.7 | 3.4 | 1.6 | 1.8 | 5.5 | 19.6 | 12.1 | 5.5 | 0 | 0.3 | 0.2 |
| | % of total LV area | 5.34% | 2.48% | 2.58% | 4.34% | 6.46% | 4.16% | 3.23% | 1.58% | 3.40% | 1.45% | 1.76% | 5.41% | 14.85% | 9.68% | 4.60% | 0.00% | 0.42% | 0.26% |
| Unipolar Scar area <8.3mV | Area (cm2) | 65.6 | 77.5 | 64.7 | 66.9 | 38.2 | 47.1 | 91.6 | 85 | 57.8 | 88.2 | 69 | 76 | 106.1 | 97.3 | 0 | 24.5 | 35 | 41 |
| | % of total LV area | 67.35% | 76.88% | 69.42% | 54.79% | 47.45% | 61.25% | 75.95% | 79.07% | 57.74% | 79.82% | 67.51% | 74.80% | 80.38% | 77.84% | 0.00% | 33.24% | 49.02% | 52.43% |
| Split potentials | N | 36 | 42 | 31 | 19 | 31 | 10 | 100 | 85 | 118 | 26 | 11 | 17 | 127 | 133 | 105 | 3 | 3 | 1 |
| | % of total points | 4.00% | 3.54% | 3.07% | 1.48% | 2.63% | 2.01% | 6.15% | 8.67% | 10.23% | 2.72% | 0.95% | 1.63% | 8.72% | 13.25% | 8.03% | 0.34% | 0.28% | 0.07% |
| LAVA | N | 166 | 214 | 150 | 207 | 121 | 35 | 348 | 238 | 305 | 184 | 280 | 243 | 640 | 394 | 489 | 108 | 83 | 94 |
| | % of total points | 18.46% | 18.06% | 14.85% | 16.13% | 10.28% | 7.04% | 21.42% | 24.29% | 26.43% | 19.23% | 24.14% | 23.30% | 43.96% | 39.24% | 37.39% | 12.36% | 7.82% | 6.63% |

**Abbreviations:** LAVA – local abnormal ventricular activities, mV – millivolts

**Supplemental Table 5-2 Performance of bipolar and unipolar voltage in a Gradient Boost model to identify scar patterns**

| | | AUC | Accuracy | MCC | Sensitivity (%) | Specificity (%) |
|---|---|---|---|---|---|---|
| Bipolar voltage alone | No scar | 0.634 | 0.593 | 0.138 | 27.1 | 84.2 |
| | At least endo | 0.640 | 0.591 | 0.168 | 37.5 | 77.8 |
| | At least intra | 0.501 | 0.638 | -0.014 | 31.5 | 65.4 |
| | Epicardial only | 0.550 | 0.811 | -0.010 | 17.1 | 84.5 |
| Unipolar voltage alone | No scar | 0.664 | 0.615 | 0.196 | 39.5 | 78.5 |
| | At least endo | 0.667 | 0.606 | 0.201 | 61.0 | 76.6 |
| | At least intra | 0.562 | 0.830 | 0.052 | 22.5 | 86.0 |
| | Epicardial only | 0.486 | 0.731 | -0.014 | 21.4 | 75.8 |
| Bipolar and Unipolar voltage | No scar | 0.703 | 0.640 | 0.253 | 45.9 | 78.0 |
| | At least endo | 0.706 | 0.632 | 0.258 | 41.8 | 81.6 |
| | At least intra | 0.593 | 0.860 | 0.062 | 19.8 | 89.3 |
| | Epicardial only | 0.586 | 0.710 | 0.023 | 31.6 | 73.1 |

Gradient boost model with an 80% train, 20% test dataset using three input variables (bipolar voltage alone, unipolar voltage alone and bipolar and unipolar voltage together.

**Supplemental Table 5-3 Performance of traditional voltage cut-offs to identify scar patterns**

| | | AUC | Accuracy | MCC | Sensitivity (%) | Specificity (%) |
|---|---|---|---|---|---|---|
| Dense bipolar scar <0.5mV | No scar | 0.611 | 0.63 | 0.233 | 46.4 | 75.9 |
| | At least endo | 0.423 | 0.535 | 0 | 0 | 100 |
| | At least intra | 0.616 | 0.375 | 0.105 | 88.3 | 35.0 |
| | Epicardial only | 0.561 | 0.949 | 0 | 0.0 | 100.0 |
| Bipolar scar <1.5mV | No scar | 0.511 | 0.563 | 0 | 0 | 100 |
| | At least endo | 0.522 | 0.514 | 0.045 | 63.0 | 41.4 |
| | At least intra | 0.572 | 0..610 | 0.063 | 53.2 | 61.3 |
| | Epicardial only | 0.603 | 0.949 | 0 | 0.0 | 100.0 |
| Unipolar scar <8.3mV | No scar | 0.545 | 0.504 | 0.116 | 87.0 | 22.0 |
| | At least endo | 0.469 | 0.535 | 0 | 0 | 100 |
| | At least intra | 0.523 | 0.793 | 0.026 | 22.5 | 82.2 |
| | Epicardial only | 0.451 | 0.949 | 0 | 0.0 | 100.0 |
| Combination dense bipolar (<0.5mV), bipolar (<1.5mV) and unipolar (<8.3mv) scar | No scar | 0.656 | 0.630 | 0.233 | 46.4 | 75.9 |
| | At least endo | 0.574 | 0.586 | 0.159 | 29.4 | 83.9 |
| | At least intra | 0.612 | 0.800 | 0.030 | 22.5 | 82.9 |
| | Epicardial only | 0.586 | 0.717 | 0.031 | 32.5 | 73.8 |

Multinomial logistic regression model with an 80% train, 20% test dataset using traditional dichotomous voltage criteria for scar (dense bipolar scar <0.5mV, bipolar scar <1.5mV, unipolar scar <8.3mV or combination of all three variables).

**Supplemental Table 5-4 Top 100 windowed bipolar electrogram tsfresh features ranked by fast correlation based filter**

| Rank | Feature | Category | Subcategory |
|---|---|---|---|
| **1** | x__spkt_welch_density__coeff_5 | Frequency Domain Features | Welch Density |
| **2** | x__number_peaks__n_50 | Time Domain Features | Peaks and Crossings |
| **3** | x__fft_aggregated__aggtype_“skew” | Frequency Domain Features | Fast Fourier Transformation |
| **4** | x__longest_strike_above_mean | Time Domain Features | Basic Statistics |
| **5** | x__fft_coefficient__attr_“angle”__coeff_89 | Frequency Domain Features | Fast Fourier Transformation |
| **6** | x__fft_coefficient__attr_“angle”__coeff_74 | Frequency Domain Features | Fast Fourier Transformation |
| **7** | x__fft_coefficient__attr_“angle”__coeff_95 | Frequency Domain Features | Fast Fourier Transformation |
| **8** | x__fft_coefficient__attr_“abs”__coeff_5 | Frequency Domain Features | Fast Fourier Transformation |
| **9** | x__fft_coefficient__attr_“abs”__coeff_6 | Frequency Domain Features | Fast Fourier Transformation |
| **10** | x__fft_coefficient__attr_“abs”__coeff_4 | Frequency Domain Features | Fast Fourier Transformation |
| **11** | x__fft_coefficient__attr_“abs”__coeff_7 | Frequency Domain Features | Fast Fourier Transformation |
| **12** | x__spkt_welch_density__coeff_8 | Frequency Domain Features | Welch Density |
| **13** | x__fft_coefficient__attr_“abs”__coeff_8 | Frequency Domain Features | Fast Fourier Transformation |
| **14** | x__partial_autocorrelation__lag_2 | Time Domain Features | Autocorrelation |
| **15** | x__fft_coefficient__attr_“abs”__coeff_9 | Frequency Domain Features | Fast Fourier Transformation |
| **16** | x__index_mass_quantile__q_0.1 | Time Domain Features | Mass |
| **17** | x__fft_coefficient__attr_“abs”__coeff_10 | Frequency Domain Features | Fast Fourier Transformation |
| **18** | x__energy_ratio_by_chunks__num_segments_10__segment_focus_0 | Time Domain Features | Energy |
| **19** | x__fft_coefficient__attr_“abs”__coeff_3 | Frequency Domain Features | Fast Fourier Transformation |
| **20** | x__agg_linear_trend__attr_“stderr”_chunk_len_50__f_agg"var" | Time Domain Features | Linear Trend |
| **21** | x__ar_coefficient__coeff_1__k_10 | Time Domain Features | Autoregression |
| **22** | x__fft_coefficient__attr_“abs”__coeff_11 | Frequency Domain Features | Fast Fourier Transformation |
| **23** | x__abs_energy | Time Domain Features | Energy |
| **24** | x__agg_linear_trend__attr_“rvalue”_chunk_len_10__f_agg"var" | Time Domain Features | Linear Trend |
| **25** | x__index_mass_quantile__q_0.2 | Time Domain Features | Mass |
| **26** | x__fft_coefficient__attr_“abs”__coeff_12 | Frequency Domain Features | Fast Fourier Transformation |

| | | | |
|---|---|---|---|
| **27** | x__range_count__max_0__min_-1000000000000.0 | Time Domain Features | Basic Statistics |
| **28** | x__fft_coefficient__attr_“real”__coeff_6 | Frequency Domain Features | Fast Fourier Transformation |
| **29** | x__length | Time Domain Features | Basic Statistics |
| **30** | x__agg_linear_trend__attr_“rvalue”_chunk_len_50__f_agg"min" | Time Domain Features | Linear Trend |
| **31** | x__mean_n_absolute_max__number_of_maxima_7 | Time Domain Features | Basic Statistics |
| **32** | x__partial_autocorrelation__lag_8 | Time Domain Features | Autocorrelation |
| **33** | x__count_above_mean | Time Domain Features | Basic Statistics |
| **34** | x__agg_linear_trend__attr_“rvalue”_chunk_len_5__f_agg"var" | Time Domain Features | Linear Trend |
| **35** | x__partial_autocorrelation__lag_9 | Time Domain Features | Autocorrelation |
| **36** | x__number_crossing_m__m_-1 | Time Domain Features | Peaks and Crossings |
| **37** | x__agg_linear_trend__attr_“rvalue”_chunk_len_50__f_agg"var" | Time Domain Features | Linear Trend |
| **38** | x__fft_coefficient__attr_“abs”__coeff_13 | Frequency Domain Features | Fast Fourier Transformation |
| **39** | x__fft_coefficient__attr_“real”__coeff_7 | Frequency Domain Features | Fast Fourier Transformation |
| **40** | x__partial_autocorrelation__lag_6 | Time Domain Features | Autocorrelation |
| **41** | x__partial_autocorrelation__lag_7 | Time Domain Features | Autocorrelation |
| **42** | x__fft_coefficient__attr_“real”__coeff_5 | Frequency Domain Features | Fast Fourier Transformation |
| **43** | x__lempel_ziv_complexity__bins_2 | Time Domain Features | Complexity |
| **44** | x__index_mass_quantile__q_0.3 | Time Domain Features | Mass |
| **45** | x__fft_coefficient__attr_“real”__coeff_4 | Frequency Domain Features | Fast Fourier Transformation |
| **46** | x__agg_linear_trend__attr_“rvalue”_chunk_len_10__f_agg"min" | Time Domain Features | Linear Trend |
| **47** | x__fft_coefficient__attr_“abs”__coeff_14 | Frequency Domain Features | Fast Fourier Transformation |
| **48** | x__absolute_sum_of_changes | Time Domain Features | Basic Statistics |
| **49** | x__range_count__max_1000000000000.0__min_0 | Time Domain Features | Basic Statistics |
| **50** | x__spkt_welch_density__coeff_2 | Frequency Domain Features | Welch Density |
| **51** | x__partial_autocorrelation__lag_5 | Time Domain Features | Autocorrelation |
| **52** | x__lempel_ziv_complexity__bins_5 | Time Domain Features | Complexity |
| **53** | x__lempel_ziv_complexity__bins_10 | Time Domain Features | Complexity |
| **54** | x__fft_coefficient__attr_“real”__coeff_8 | Frequency Domain Features | Fast Fourier Transformation |
| **55** | x__fft_coefficient__attr_“real”__coeff_9 | Frequency Domain Features | Fast Fourier Transformation |
| **56** | x__fft_coefficient__attr_“abs”__coeff_15 | Frequency Domain Features | Fast Fourier Transformation |
| **57** | x__partial_autocorrelation__lag_4 | Time Domain Features | Autocorrelation |
| **58** | x__number_crossing_m__m_1 | Time Domain Features | Peaks and Crossings |

| | | | |
|---|---|---|---|
| **59** | x__minimum | Time Domain Features | Basic Statistics |
| **60** | x__fft_coefficient__attr_“imag”__coeff_6 | Frequency Domain Features | Fast Fourier Transformation |
| **61** | x__lempel_ziv_complexity__bins_3 | Time Domain Features | Complexity |
| **62** | x__sum_of_reoccurring_values | Time Domain Features | Reoccurring Values |
| **63** | x__range_count__max_1__min_-1 | Time Domain Features | Basic Statistics |
| **64** | x__fft_coefficient__attr_“imag”__coeff_7 | Frequency Domain Features | Fast Fourier Transformation |
| **65** | x__partial_autocorrelation__lag_3 | Time Domain Features | Autocorrelation |
| **66** | x__variance | Time Domain Features | Basic Statistics |
| **67** | x__standard_deviation | Time Domain Features | Basic Statistics |
| **68** | x__root_mean_square | Time Domain Features | Basic Statistics |
| **69** | x__c3__lag_1 | Time Domain Features | Autocorrelation |
| **70** | x__fft_coefficient__attr_“abs”__coeff_16 | Frequency Domain Features | Fast Fourier Transformation |
| **71** | x__c3__lag_2 | Time Domain Features | Autocorrelation |
| **72** | x__number_cwt_peaks__n_1 | Time Domain Features | Peaks and Crossings |
| **73** | x__fft_aggregated__aggtype_“kurtosis” | Frequency Domain Features | Fast Fourier Transformation |
| **74** | x__agg_linear_trend__attr_“rvalue”_chunk_len_10__f_agg"max" | Time Domain Features | Linear Trend |
| **75** | x__agg_linear_trend__attr_“rvalue”_chunk_len_50__f_agg"max" | Time Domain Features | Linear Trend |
| **76** | x__fft_coefficient__attr_“real”__coeff_10 | Frequency Domain Features | Fast Fourier Transformation |
| **77** | x__fft_coefficient__attr_“imag”__coeff_74 | Frequency Domain Features | Fast Fourier Transformation |
| **78** | x__fft_coefficient__attr_“imag”__coeff_5 | Frequency Domain Features | Fast Fourier Transformation |
| **79** | x__fft_coefficient__attr_“imag”__coeff_8 | Frequency Domain Features | Fast Fourier Transformation |
| **80** | x__sample_entropy | Time Domain Features | Entropy |
| **81** | x__energy_ratio_by_chunks__num_segments_10__segment_focus_1 | Time Domain Features | Energy |
| **82** | x__agg_linear_trend__attr_“intercept”_chunk_len_50__f_agg"var" | Time Domain Features | Linear Trend |
| **83** | x__sum_of_reoccurring_data_points | Time Domain Features | Reoccurring Values |
| **84** | x__lempel_ziv_complexity__bins_100 | Time Domain Features | Complexity |
| **85** | x__agg_linear_trend__attr_“rvalue”_chunk_len_5__f_agg"max" | Time Domain Features | Linear Trend |
| **86** | x__agg_linear_trend__attr_“rvalue”_chunk_len_5__f_agg"min" | Time Domain Features | Linear Trend |
| **87** | x__agg_linear_trend__attr_“stderr”_chunk_len_50__f_agg"min" | Time Domain Features | Linear Trend |
| **88** | x__fft_coefficient__attr_“abs”__coeff_17 | Frequency Domain Features | Fast Fourier Transformation |
| **89** | x__partial_autocorrelation__lag_1 | Time Domain Features | Autocorrelation |
| **90** | x__autocorrelation__lag_1 | Time Domain Features | Autocorrelation |

| | | | |
|---|---|---|---|
| **91** | x__fft_coefficient__attr_“imag”__coeff_10 | Frequency Domain Features | Fast Fourier Transformation |
| **92** | x__fft_coefficient__attr_“imag”__coeff_69 | Frequency Domain Features | Fast Fourier Transformation |
| **93** | x__c3__lag_3 | Time Domain Features | Autocorrelation |
| **94** | x__approximate_entropy__m_2__r_0.3 | Time Domain Features | Entropy |
| **95** | x__index_mass_quantile__q_0.4 | Time Domain Features | Mass |
| **96** | x__fft_coefficient__attr_"imag"__coeff_9 | Frequency Domain Features | Fast Fourier Transformation |
| **97** | x__absolute_maximum | Time Domain Features | Basic Statistics |
| **98** | x__energy_ratio_by_chunks__num_segments_10__segment_focus_2 | Time Domain Features | Energy |
| **99** | x__friedrich_coefficients__coeff_2__m_3__r_30 | Time Domain Features | Friedrich Coefficient |
| **100** | x__fft_coefficient__attr_“abs”__coeff_18 | Frequency Domain Features | Fast Fourier Transformation |

**Supplemental Table 5-5 Comparison of performance of Gradient Boost Model using top 20 or all 794 tsfresh features.**

| | | AUC | Accuracy | MCC | Sensitivity (%) | Specificity (%) |
|---|---|---|---|---|---|---|
| Top 20 Features | *No scar* | 0.815 | 0.728 | 0.455 | 73.4 | 72.4 |
| | *At least endo* | 0.810 | 0.680 | 0.381 | 38.1 | 93.1 |
| | *At least intra* | 0.704 | 0.832 | 0.172 | 43.6 | 85.3 |
| | *At least epi* | 0.681 | 0.835 | 0.128 | 34.5 | 86.2 |
| All features | *No scar* | 0.887 | 0.810 | 0.615 | 78.6 | 83.0 |
| | *At least endo* | 0.871 | 0.781 | 0.558 | 75.4 | 80.4 |
| | *At least intra* | 0.780 | 0.941 | 0.353 | 20.5 | 98.0 |
| | *At least epi* | 0.703 | 0.894 | 0.130 | 22.7 | 93.0 |

# Chapter 6

# 6 PULSED FIELD ABLATION OF VENTRICULAR ARRHYTHMIAS ARISING FROM INTRACAVITARY STRUCTURES: INSIGHTS FROM A CLINICAL CASE SERIES

| **Title of published work** | **Pulsed field ablation of ventricular arrhythmias arising from intracavitary structures: insights from a clinical case series** |
|---|---|
| **Nature of the candidate's contribution** | Data collection and analysis including processing and annotation of electrograms and intracardiac echocardiography, statistical analyses, manuscript writing and submission to journal |
| **Co-Authors** | **Nature of contribution** |
| Tai Chung So | Co-first author. Contributed to patient recruitment, assistance during clinical cases and comments on manuscript. |
| Samual Turnbull | Contributed to animal experiments, advised on study methodology and comments on manuscript |
| Max Bickley | Data collection (Holter and ICD interrogation), comments on manuscript |
| Kenji Hashimoto | Comments on manuscript |
| Ashwin Bhaskaran | Comments on manuscript |
| Saurabh Kumar | Overall supervision. Clinical ablation. Comments on manuscript. |

| | |
|---|---|
| Signature of candidate<br>Kasun De Silva | |
| Signature of supervisor (signed on behalf of all co-authors)<br>Saurabh Kumar | |

## 6.1 Introduction

Premature ventricular complexes (PVCs) can arise from complex intracavitary mobile structures including left and right ventricular papillary muscles and the right ventricular moderator band. PVCs from these sites, though forming only 2-5% of all ablation cases[187,467], can be extremely challenging to treat. Long term arrhythmia free survival rates can be as low as 60%[187,468] for papillary muscle PVCs and 80% for PVCs arising from the moderator band[469], often with the requirement for multiple procedures and prolonged procedural times.[467,470] Challenges include anatomical variations, including differences in the size and position of these structures[3], radiofrequency (RF)-induced automaticity[4], deep intramural arrhythmia origins in some cases, and, most importantly, the shape and mobile nature of these structures, which can result in poor catheter contact and stability during lesion delivery. [468] To address the latter, technologies beyond traditional RF ablation have been shown to have promise, including focal and ballon cryoablation. [467,471-473] Although these technologies have improved procedural success, ablation is still challenging with procedural duration in a recent series exceeding 4 hours.[467]

Pulsed field ablation (PFA) is an emerging technology designed to cause irreversible electroporation of cell membranes, leading to cell death and lesion formation in both healthy and diseased myocardium.[369,370] Whilst the depth of lesion formation is still dependant on catheter contact in PFA,[370] a recent pre-clinical study using a large footprint lattice-tip catheter showed good lesion formation in papillary muscles and the moderator band in a swine model with preservation of valvular function.[372] Whilst designed to target cardiomyocytes, PFA has also been shown to affect the electrical conduction system and eliminate Purkinje fibre potentials, which can reduce vulnerability to ventricular fibrillation (VF).[371] Given the dense Purkinje fibre network and propensity for PVC mediated VF from these structures, we hypothesised that PFA would be a

useful strategy to target PVCs from these intracavitary structures. Furthermore, it is conceivable that such a large footprint system may overcome limits of contact and stability and RF induced automaticity which could improve outcomes in these cases.

Here we present a proof-of-concept case series of ventricular arrhythmia ablation of the intracavity structures- namely, the moderator band and right and left ventricular papillary muscle- using PFA.

## 6.2 Methods

Between 2023 and 2024, three patients underwent PFA for treatment of intracavitary PVCs at a single tertiary referral centre (Westmead Hospital) and were included in this case series. All patients provided informed consent to the off-label use of PFA for targeting their arrhythmia prior to their procedure. Data for this study was collected as a part of the VA-West registry, approved by the Western Sydney Local Health District Human Research Ethics Committee.

Transthoracic echocardiography ± cardiac multi-detector computed tomography (CT) ± cardiac magnetic resonance imaging was obtained on patients during pre-procedural workup to assess for structural heart disease and evaluate ventricular function. Holter monitoring for a minimum of 24 hours was conducted to evaluate the pre-procedural PVC burden.

### *6.2.1 **Electroanatomic mapping***

Our approach to mapping PVCs has been described previously.[238] Antiarrhythmic drugs (AADs) were ceased at least 5 half-lives prior to the procedure, except in the case of an emergent indication. General anaesthesia was administered after recording the 12-lead electrocardiogram pattern of the clinical PVC.

Vascular access was obtained under ultrasound guidance. A series of venous sheathes were inserted: (1) an SL3 sheath (Abbott Medical, IL) to perform coronary sinus venography and insert

a decapolar catheter into the coronary sinus; (2) a short sheath for the insertion of a quadripolar catheter into the right ventricular apex: (3) a short sheath for an ICE catheter (CARTO; Biosense Webster, CA) and finally, (4) For the LV; an SL0 sheath (Abbott Medical, IL) for transeptal puncture under ICE guidance, exchanged for a large curved Agilis catheter (Abbott Medical, IL) for mapping, or, for RV; a small curved Agilis catheter for mapping and ablation of the right ventricle. These were subsequently exchanged for the Faradrive steerable sheath (Boston Scientific, MA) for PFA.

ICE was used with CartoSound (Biosense Webster, CA) to create endocardial shells of the chamber of interest, with particular attention given to demarcating intracavitary structures. It was also utilised to monitor catheter contact of the activation mapping (DecaNav, Biosense Webster, CA), RF ablation and PFA catheter.

If PVCs were too scarce to permit activation mapping, several provocation manoeuvres were employed. Burst RV pacing down to ventricular refractoriness was performed from the RV apex. This was then repeated on the highest tolerated dose of isoprenaline (up to 40 μG/min). Programmed electrical stimulation was also performed using a 400 ms drive train with 4 extrastimuli beginning at 300 ms, decrementing by 10 ms down to ventricular refractoriness. Sustained VT was defined as monomorphic VA with duration >10 seconds. Activation mapping was performed to find site of earliest origin (and position on intracavitary structures was confirmed by ICE.

If there were paucity of PVCs to permit activation mapping even with provocation, bipolar pacing from the ablation catheter at a fixed rate of 600 ms (or 10 ms below baseline rate) with an output of 10 mA and 2 ms pulse width was performed. Tissue contact was monitored aiming for

contact force (CF) of ≥10g. If there was no pace capture, the pacing output was increased to 10 mA and 9 ms as required. Captured beats were analyzed using the PASO (Carto) algorithm.

### *6.2.2 Radiofrequency and pulsed field ablation*

For PFA, a 31mm multielectrode pentaspline Farapulse (Boston Scientific, MA) PFA catheter was advanced into RV or LV via a deflectable Faradrive steerable sheath. It was advanced into the ventricle over the wire in basket configuration. The catheter was visualised at all times by ICE entering into the ventricle to monitor for entanglement with valvular chordae. The manipulation of the PFA catheter was guided by ICE. The catheter was predominantly used in ’basket’ configuration ; however, the 'flower' configuration was attempted if contact was poor. It was visualised as a virtual catheter in CARTO 3D mapping system (connection of 3$^{rd}$ electrode of every spline to the CARTO system). The contact and stability of catheter with tissue was visualized under ICE. Repetitive applications of PFA using standard settings: (2.0-kV output, 5 biphasic and bipolar pulses 200 milliseconds (ms) in duration each with 300 ms pause (2.5 seconds per application), aiming for suppression of PVCs. Importantly, prior to lesion delivery with PFA, the position and contact of the PFA catheter in either “basket” or “flower” configuration was confirmed in precise detail with ICE. This safety measure confirmed that PFA splines were not inadvertently in contact with and inadvertently ablating surrounding structures.

Where required, adjuvant RF ablation was performed using a 3.5-mm-tip open-irrigation catheter ThermoCool SmartTouch (Biosense Webster, CA). Ablation was delivered aiming for a contact force of ≥10 grams. RF energy of up to 50 watts was delivered, aiming for an impedance drop of between 10 and 20 ohms. As with PFA, catheter position and stability were determined with ICE.

### *6.2.3 Follow up*

All patients underwent a 24-hour period of cardiac monitoring immediately following the procedure. After discharge, patients were followed up through a combination of outpatient clinical reviews, up to 5-day Holter monitoring and/or device checks to monitor ventricular arrhythmia and PVC counter. Hospital medical records and outpatient clinic assessments were used to complete clinical follow-up. Follow-up was defined as the time from final ablation procedure to the last documented clinical review.

## 6.3 Results

The baseline characteristics of the three patients are summarised in Table 1. The procedural characteristics are summarised in Table 2.

### *6.3.1 Case 1*

A 55-year-old man, with history of PVC mediated VF arrest presented with recurrent implantable cardioverter defibrillator (ICD) shocks. His first episode of VF was at age 29 and at that stage an ICD was implanted. An RV biopsy after initial presentation suggested possible right ventricular dysplasia (fatty infiltration and fibrosis in RV myocardium), and 12-lead ECGs showed frequent left bundle branch block morphology PVCs. However, gene testing revealed two variants of unknown significance that were non-phenotypical of arrhythmogenic right ventricular cardiomyopathy (ARVC). An endocardial/epicardial substrate map was within normal limits. He underwent four endocardial RF catheter ablations followed by one endocardial/epicardial RF catheter ablation, but PVC-mediated VF and shocks persisted. During his most recent procedure, the PVC was mapped to the moderator band, and RF energy was applied without success.

In view of failure and/or intolerance of multiple anti-arrhythmic drugs, including amiodarone, a high PVC burden on Holter (10.13%), and PVC-triggered VF, repeat catheter ablation was offered. Three PVC morphologies were identified (summarised in Table 2) however,

they were too infrequent for activation mapping, even with provocation. Pace mapping with ICE guidance showed good matches at anterior RV free wall at an accessory insertion site of moderator band into the RV wall (Figure 1A). RF ablation at the best pace map area failed to eliminate the PVCs. In view of prior failed ablations, adjuvant PFA was employed.

The PFA catheter was advanced into RV, and its manipulation was guided by ICE. The catheter was in basket configuration and was visualised as a virtual lasso shaped catheter on the electroanatomic mapping system. The contact and stability of catheter with tissue was visualised under ICE (Figure 1B). A total of 28 applications were performed in the previously ablated area and over the moderator band. There was loss of capture in PFA ablated area at high output pacing (20-mA/9-ms) (Figure 1C). The patient developed right bundle branch block (RBBB) after PFA which persisted after the case. The ICD lead parameters remained stable after the procedure. There was no significant haemoglobin reduction post procedure. The PVC counter on his device decreased from 83,700 over a 36-day period prior to ablation to 196 (Figure 1D), with no further episodes of ventricular fibrillation observed during a follow-up period of 293 days after ablation."

### *6.3.2 Case 2*

A 74-year-old woman presented with symptomatic high-burden PVCs (35% on Holter) despite taking slow-release Verapamil 180mg. Cardiac MRI showed a mildly dilated RV with reduced systolic function (RVEF 41%). However, she did not otherwise meet ARVC criteria. A genetic panel for cardiomyopathy demonstrated no medically significant variants. She underwent RF ablation for a moderator band PVC, during which the septal insertion of RV moderator band was ablated. Despite this, she had persistent symptoms and a high PVC burden (27%).

Repeat catheter ablation was offered. The PVC was left bundle branch block morphology, negative concordance and left superior axis. Activation map with ICE guidance showed earliest

activation at apical lateral RV at the base of a complex RV anterior papillary muscle -32ms pre-QRS and with 98% pace match (Figure 2). Due to prior failed ablation and the complexity of the RV moderator band-papillary muscle complex, PFA was employed. The PFA catheter was guided by fluoroscopy and ICE. A total of 8 applications of PFA were performed at the site of best activation/pace map. However, the PFA catheter was not able to advance further apically to contact the apical side of the target area, which was still captured electrically when paced at high output (10-mA/ 9-ms). Therefore, adjuvant RF ablation was performed to the apical area where the PFA catheter could not reach. No PVCs were observed after the ablation, despite high-dose isoproterenol infusion (10mcg/min). There was no significant reduction in haemoglobin or other complications. At 50 days follow-up, the PVC burden on a five-day Holter monitor was reduced to 1.5%

### *6.3.3 Case 3*

A 69-year-old man with history of post-infarction cardiomyopathy (LVEF 41%, moderate mitral regurgitation) presented with an ICD shock due to PVC-triggered VF 4 years ago. He was started on amiodarone but subsequently developed amiodarone-induced thyroiditis Following the cessation of amiodarone and the commencement of sotalol, he continued to experience symptoms. Cardiac MRI demonstrated subendocardial scarring in the mid-distal anterior and anteroseptal wall and basal-mid inferior wall. Late gadolinium enhancement was also noted on the base and body of the posteromedial papillary muscle.

Catheter ablation was offered due to failed medical treatment. Substrate mapping demonstrated a low voltage area over basal to middle inferior wall and apical region. The PVC was right bundle branch block morphology with transition in V4 and left superior axis. Activation mapping of the PVC showed a focal centrifugal activation pattern with earliest activation time -

26ms pre QRS at the base of the posteromedial papillary muscle (Figure 3). The local electrograms at this site were fractionated. Due to the known scarring in the posteromedial papillary muscle, anticipated poor RF contact and deep substrate, upfront PFA was performed. PFA was applied at the earliest activation site, the posteromedial papillary muscle, and further substrate modification of inferior wall and apex was done performed with PFA. A total of 30 applications were required as manipulation of the PFA catheter via the steerable sheath was difficult. There were no PVCs seen immediately after the final ablation. There was no significant reduction in haemoglobin. The ICD lead parameters remained stable post procedure and there were no complications. Cardiac echocardiogram the day after PFA showed an LVEF of 48% with unchanged moderate mitral regurgitation (MR).

## 6.4 Discussion

This preliminary report highlights the feasibility of PFA in the ablation of intracavitary structures. In all three cases, PVCs originating from intracavity structures (the RV moderator band, RV papillary muscle complex, and LV posteromedial papillary muscle) were successfully ablated. We have made several important findings

1. PFA delivery to mobile intracavitary structures is feasible with excellent acute success, despite failed prior RF ablations in 2/3 cases.
2. Difficult manoeuvrability of the pentaspline catheter necessitated adjuvant RF ablation in 1/3 cases.
3. PFA delivery to mobile intracavitary structures is safe. The only complication noted was a persistent RBBB with PFA delivery to the moderator band in Case 1. There was no significant reduction in haemoglobin, vasospasm, stroke or deterioration in valvular function.

There are now three published reports describing outcomes of PFA for PVCs (n=21[474], n=20[475] and n=11[476]). These series, however, included a majority of outflow tract PVCs and all employed focal monopolar ablation using the Centauri system (Cardiofocus Inc, MA). Peichl et al. (2024) described three patients with papillary muscle arrhythmia (one scar related) and though success rates are not available for this group specifically, at least 1 is described to have late recurrence at 3 months.[474] In their case series, Della Roca et al. (2024) described five patients (25%) with intracavitary PVCs (two moderator band, two posteromedial papillary muscle, one RV papillary muscle) of which 4/5 had long term success (recurrence from RV papillary muscle).[475] Four out of 5 of these cases had irritative ventricular firing, a phenomenon which we did not observe (possibly due to our alternative bipolar PFA system or possibly by chance). Indeed, the lack of ventricular ectopy during or after lesion delivery in our series is a counterpoint to ectopy induced during radiofrequency ablation which itself can limit lesion duration. Similar to our Case 1, both patients in this series developed RBBB after ablation of the moderator band (1 transient).[475] Finally in the most recent series by Ruwald et al. (2025), the only moderator band case and 1 of 2 papillary muscle cases had long term recurrence.[476] PFA for one of the papillary muscle cases resulted in a minor stroke with remission of symptoms.

It is difficult to compare the success in our series with a pentaspline bipolar ablation catheter against these few cases due to low numbers and different substrate (2/3 patients in our series had PVC induced VF, 1/3 significant ventricular scar). However, it is conceivable that the catheter shape and large footprint aided catheter contact and lesion delivery and informed differing success rates. We note two recent case reports demonstrating success with pentaspline PFA delivery to the papillary muscles, [477,478] further supporting our strategy in these difficult to ablate structures.

Important pre-clinical studies have established the ability for PFA to delivery good quality lesions in the ventricle. No significant differences were seen in lesion depth between the focal and basket Farapulse catheters during bipolar PFA in both healthy and infarcted myocardium, though the larger footprint catheter invariably led to increased lesion width.[369] More recently, Nies et al. (2024) delivered lesions to intracavitary structures including the papillary muscles and moderator band with ICE guidance using a large footprint monopolar lattice tipped catheter, crucially with ICE, fluoroscopy and electroanatomic mapping guidance.[372] Papillary muscle lesions with good catheter contact had greater lesion dimensions (18.3mm x 15.3mm x 5.8mm deep) whilst lesions with intermittent contact had similar length and width but significantly less depth (3.9mm, p=0.014).

It is important to note that, as with other studies, the manipulation of such a large, non-deflectable over the wire catheter in ventricle was difficult.[479] This difficulty may be worse within non-dilated ventricles, particularly in the presence of valvular chordae. Furthermore, this limited manoeuvrability can make contact with the ventricular surface difficult. We noted limited manoeuvrability, as reflected in Case 2 and also in Case 3. To address this, our cases were guided by multimodality imaging including 3D mapping, ICE and fluoroscopy, which may help to overcome such difficulty. Despite poor manoeuvrability, we successfully eliminated PVCs from the moderator band in Case 2, possibly due to transmural lesion formed by PFA. Alternatively, the adjuvant effect of RFA may have helped. Further, as shown in Figures 1-3, careful delineation of the target structure with ICE was integral to lesion delivery and could in a large way explain the success of these procedures.[468] Others have reported on the manoeuvrability of this system in the ventricle. Importantly Lozana-Granero et al. were able to target ventricular arrhythmia from a basal LV aneurysm, mid inferolateral LV and basal inferolateral RV[479] whilst others have been similarly

able to target LV papillary muscle structures.[477,478] This confirms that this system can afford enough contact for sufficient ablation of arrhythmia sites though certainly a deflectable catheter itself (such as a focal monopolar PFA catheter) would offer promise in addressing this challenge. Another solution that may offer more reach and manoeuvrability for the FaraWave catheter in the ventricle, which was not trialled in this cohort, is the use of an alternative 13 French steerable sheath such as an Agilis NxT Steerable Dual-Reach sheath (Abbott, Illinois, United States) where a large curl might facilitate more contact of the PFA catheter with the ventricular endocardium.

Our study did not find significant safety concerns with delivery of PFA to intracavitary structures in the ventricle. Firstly, despite repeated applications with at times poor catheter contact, we report no significant reduction in haemoglobin or significant microbubble emboli. Secondly, although ventricular arrhythmias induced during pre-clinical studies could be attributed to the arrhythmogenicity of the swine model,[369] irritative ventricular firing[475] and even initiation of ventricular tachycardia[480] has been noted in human reports. We did not encounter any VF or ectopy during PFA in ventricle and the incidence remained to be studied and determined. Thirdly, in our series, a range of 8-30 PFA applications (with repetitive applications in the same site) were delivered considering the possibility of intermittent contact and swine studies showing repetition improves lesion dimensions.[481] A safety concern could be myocardial stunning by PFA, which may theoretically lead to transient depression of LVEF and even heart failure compensation or hemodynamic instability. This was not observed in our cases; in fact, for our patient in Case 3, echocardiography the day after ablation (and delivery of 30 PFA lesions) saw improvement in EF post ablation (LVEF 41% to 48%). Fourth, ICD lead parameters were not affected by PFA despite proximity of lead to apical ablation site as showed in cases 1 and 3. We note that the effect of PFA in ventricular ablation on ICD leads is still unclear and potential interactions with ICD leads should

not be neglected. Finally, we did note a single incidence of RBBB following ablation of the moderator band which has been described in other studies.[475] Longer term follow up is required to understand the effects on the RV of transmural lesion creation in the moderator band.

### *6.4.1 Limitations*

This study has limitations worth noting. This is a small case series and therefore it is not possible to make treatment comparisons to RF, cryoenergy and alternative PFA delivery systems. We note the relative paucity of cases involving these structures in most ablation cohorts (2-5%). However, these observational results may be of value as a proof-of-concept report describing a strategy to ablate such arrhythmias using PFA guided by ICE such as to inspire further research in this field. Importantly, cryoablation offers promise in treating these structures and this was not offered to any patients in this series. As our cases are limited to acute success and short-term outcomes, further studies are needed to assess long term outcomes and further delineate the role of PFA in ventricular ablation of intracavitary structures. We did not measure markers of haemolysis such as lactate dehydrogenase, free plasma haemoglobin and haptoglobin and hence subclinical haemolysis may have occurred in these cases which were not detected. Further though we describe our experience with a large footprint bipolar PFA catheter with biphasic lesion delivery, variation in voltage delivery, waveform, packet duration, packet number, delivery, catheter configuration and monopolar vs bipolar lesion delivery can all affect procedural success and complications.[482] Determining optimal configurations for lesion formation in these structures requires more pre-clinical and clinical validation.

## 6.5 Conclusion

In conclusion, this case series, though small, provides a proof of concept and novel strategy to ablate difficult to target arrhythmias from intracavitary structures. Further pre-clinical and clinical validation studies are required to establish the role of PFA to treat ventricular arrhythmias.

## 6.6 Figures

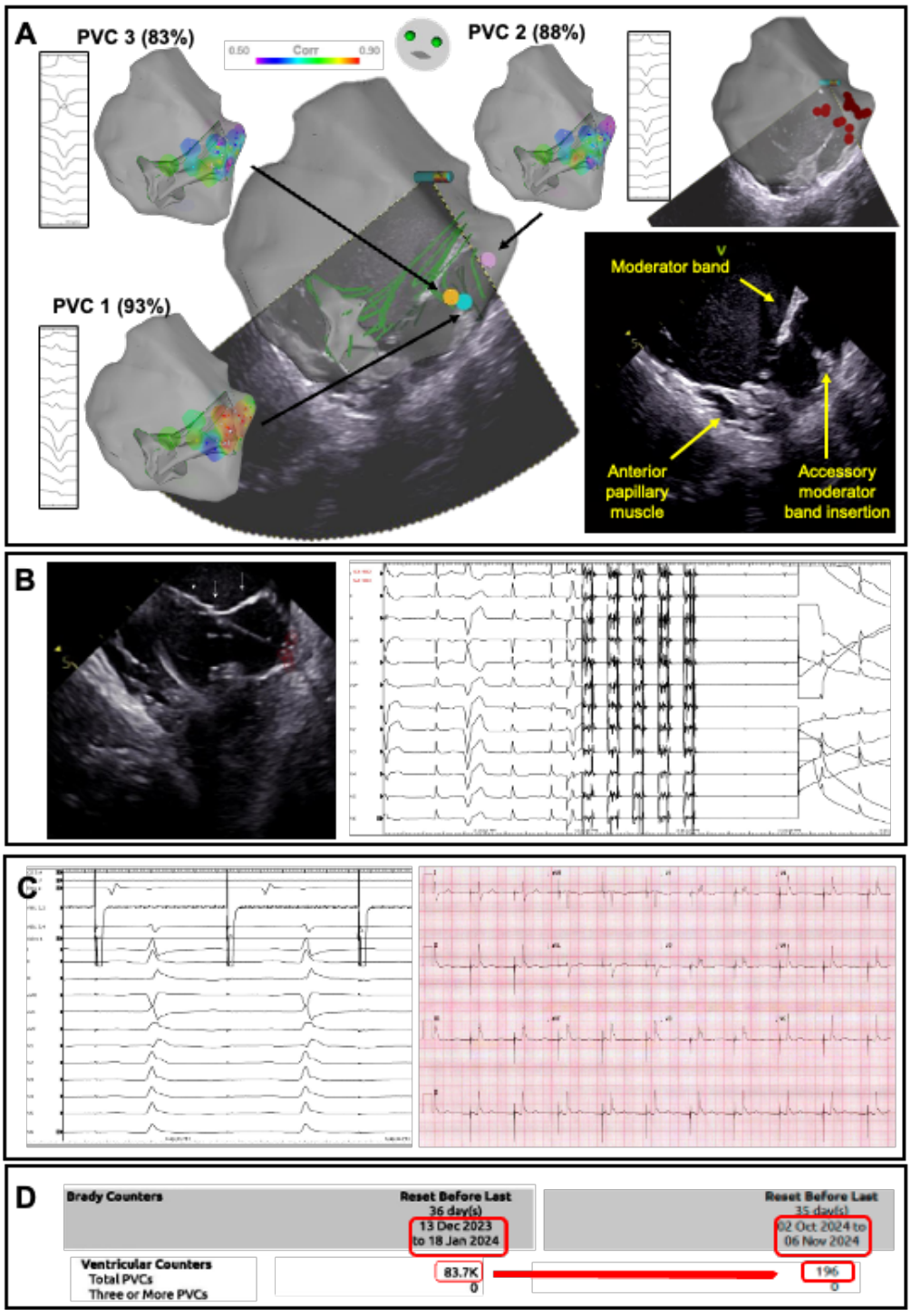


**Figure 6-1 Case 1**

A. The morphology of the right ventricular moderator band, it's insertion into the right ventricular wall and insertion into the right ventricular anterior papillary muscle is appreciable on intracardiac

echocardiography (ICE). 3 PVC morphologies were encountered during the case. Pace map scores superimposed upon the moderator band – right ventricular papillary muscle complex are shown. Best pace map score for PVC1 was 93% localised to an accessory insertion from the right ventricular moderator band to the right ventricular apex (blue dot). Best pace map score for PVC 2 was 88% to the moderator band body. Best pace map for PVC 1 was 83% to a similar region to PVC1. On the right most electroanatomic map, the location of radiofrequency lesions to target these sites are displayed. B. ICE demonstrates good catheter contact of the Farapulse catheter in "basket" formation to the region of interest. A single application of PFA (2kv, 5 pulses, 200ms duration for each packet with 300ms gap) is demonstrated. C. Post ablation testing for ventricular capture with the ablation catheter demonstrates electrical inexcitability with newly noted right bundle branch block (also seen on post procedural ECG). D. Post PFA procedure, dramatic reduction in PVC counter on ICD follow up (293 days post ablation).

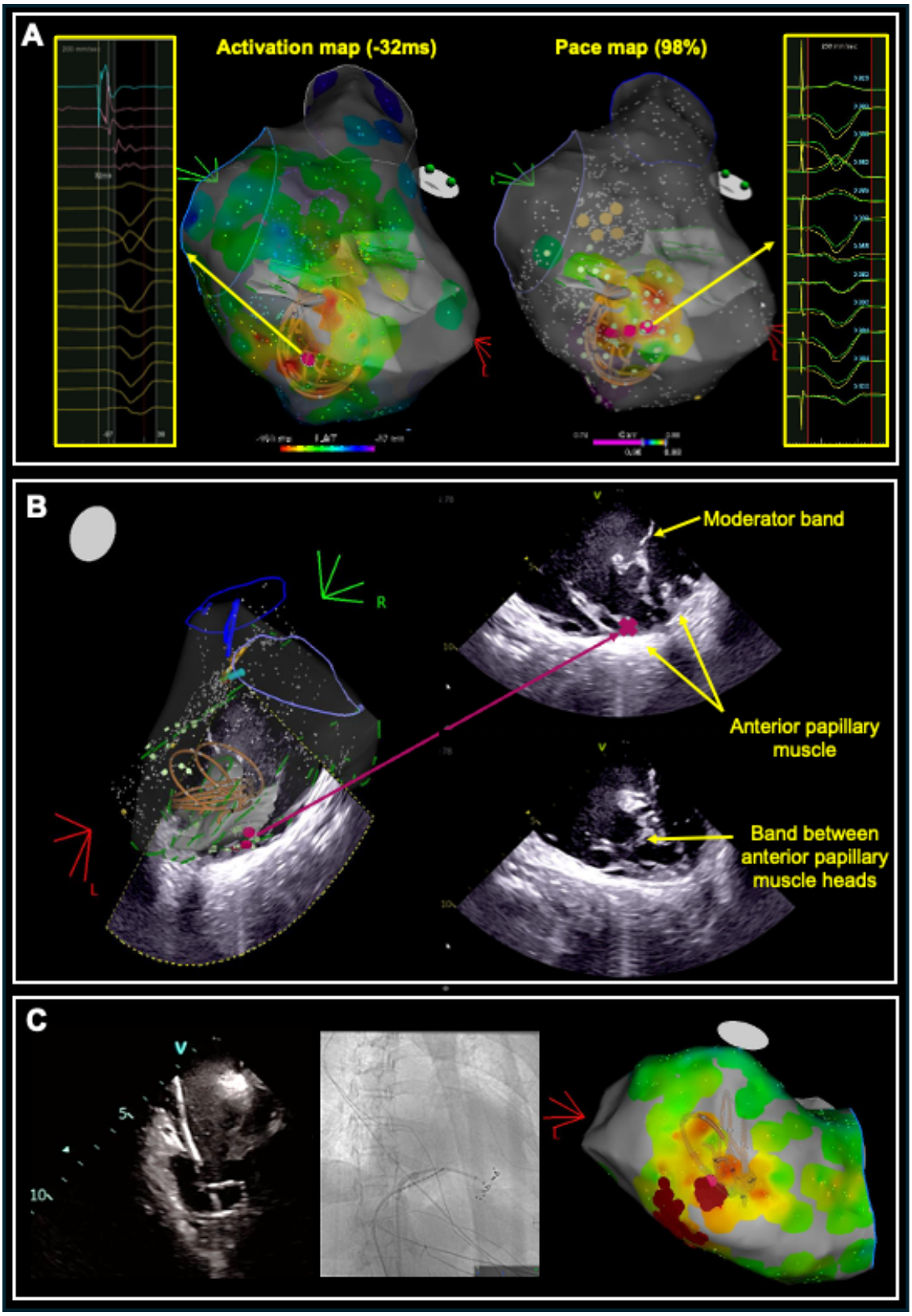


**Figure 6-2 Case 2**

A. Activation and Pace map demonstrates localisation of the PVC to the right ventricular papillary muscle (pink dot is best site). Map has been made transparent to demonstrate location of PFA catheter (shown on this electroanatomic map as a lasso shaped virtual catheter). B. Intracardiac echocardiography (ICE) demonstrates a complex right ventricular papillary muscle (band noted between two heads), localising the region to the base of the muscle. C. ICE demonstrates manoeuvring of PFA catheter in "basket" formation into the RV apex. Fluoroscopy (right anterior oblique 30) demonstrates difficulty to advance catheter further to apex. Electroanatomic map demonstrates adjuvant lesion delivery with radiofrequency ablation.

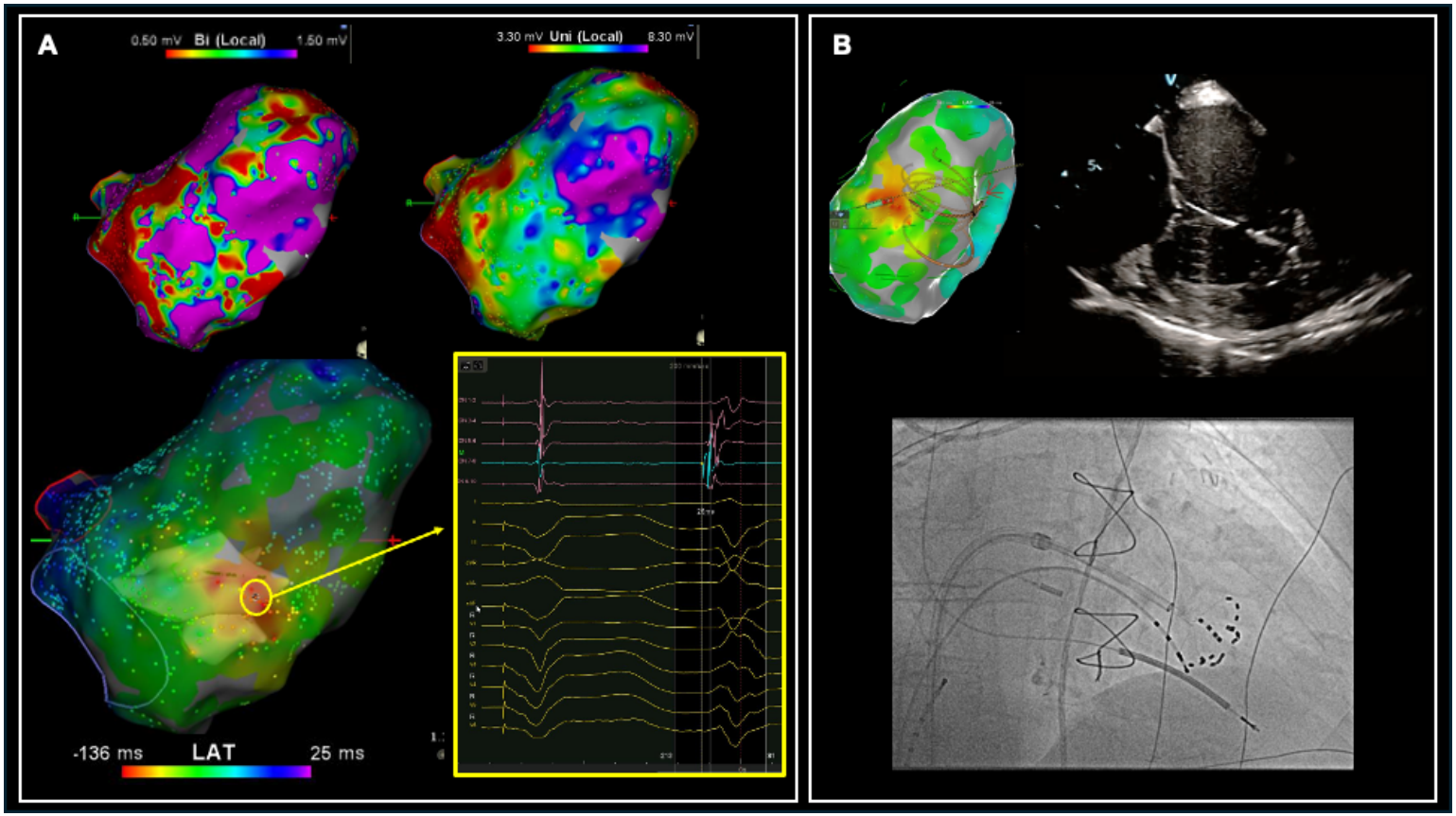


**Figure 6-3 Case 3**

A. Bipolar and unipolar voltage maps demonstrate post-infarction scarring of the left ventricle. The activation map (made transparent to show the papillary muscles delineated by intracardiac echocardiography) shows earliest site of activation at the base of the posteromedial papillary muscle. The site of earlies activation -26ms pre QRS shows a multicomponent fractionated electrogram without clear isolated Purkinje potential

at the base of the posteromedial papillary muscle. B. Electroanatomic map shows the location of the PFA catheter during lesion delivery, also shown on intracardiac echocardiography where the catheter can be seen with good contact with the papillary muscles. The fluoroscopy image shows flexion of the catheter to aid contact with the posteromedial papillary muscle.

## 6.7 Tables

### Table 6-1 Patient Characteristics

| Case number | Age | Sex | LVEF (%) | Cardiomyopathy | IHD | VA | AADs | Previous ablations |
|---|---|---|---|---|---|---|---|---|
| 1 | 55 | Male | 67 | Possible right ventricular dysplasia on RV biopsy (fat infiltration and fibrosis) but negative gene panel and normal endocardial/epicardial voltage mapping. | No | PVC induced VF | Pre-ablation: Metoprolol XL<br><br>Failed/Not tolerated: Amiodarone, flecainide, carvedilol, verapamil, mexiletine<br>Phenytoin | 5 |
| 2 | 74 | Female | 56 | Mild RV systolic dysfunction on CMR not meeting ARVC criteria. Negative gene panel. | No | PVC | Pre-ablation: Bisoprolol<br><br>Failed/Not tolerated: verapamil | 1 |
| 3 | 69 | Male | 41 | Post-infarction cardiomyopathy. CMR demonstrated subendocardial scar involving mid-distal anterior/anteroseptum and basal-mid inferior wall including base/body of posteromedial papillary muscle | Yes | PVC induced VF | Pre-ablation: Sotalol<br><br>Failed/Not tolerated: Amiodarone | 0 |

**Abbreviations** : AADs – antiarrhythmic drugs, ARVC – arrhythmogenic right ventricular cardiomyopathy, CMR – cardiac magnetic resonance imaging, IHD – ischaemic heart disease, LVEF – left ventricular ejection fraction, PVC – premature ventricular complex, RV – right ventricle, VF – ventricular fibrillation

**Table 6-2 Procedural characteristics**

| Case number | PVC site | PVC description | Earliest activation (ms) | Best pace map score (%) | PFA applications | RFA touch up | RFA touch up applications | Procedural time (mins) | Fluoroscopy time (mins) |
|---|---|---|---|---|---|---|---|---|---|
| 1 | RV Moderator band | PVC1: LB transition V6, LS axis<br>PVC2: LB -ve concordance, Left axis (II/III discordance)<br>PVC3: LB -ve concordance, LS axis | - | PVC1:93<br>PVC2: 88<br>PVC3: 83 | 28 (in basket formation) | No | - | 197 | 12.22 |
| 2 | RV anterior papillary muscle/moderator band complex | LB -ve concordance, RS axis | -32 | 98 | 8 (in basket formation) | Yes | 16 | 122 | 7.41 |
| 3 | LV Posteromedial papillary muscle | RB, transition V4, LS axis | -26 | - | 30 (basket and flower) | No | - | 142 | 23.5 |

# Chapter 7

# 7 RADIOTHERAPY FOR VENTRICULAR TACHYCARDIA IN ADVANCED STRUCTURAL HEART DISEASE: PROTOCOL FOR A RANDOMISED CONTROLLED TRIAL (RADIOABLATE-VT)

## 7.1 Aim

To examine in a randomised trial in patients with advanced structural heart disease and ventricular tachycardia if stereotactic body radiation therapy (SBRT) in addition to medical therapy is superior to current clinical management comprising of medical therapy plus/minus catheter ablation (CA) in reducing the burden of VT with acceptable safety.

## 7.2 Hypothesis

We hypothesise that in an open label randomised controlled trial of patients with advanced structural heart disease and VT that SBRT with medical therapy (guided by state-of-the-art multimodality imaging, EAM and ECG analysis) will be superior in reducing VT burden compared to standard care comprising of medical therapy +/- CA with acceptable safety and adverse events.

## 7.3 Background

Sudden cardiac death (SCD) claims 15,000 Australian lives annually [1]. Ventricular tachycardia (VT) is the most common cause. Treatment for VT to prevent SCD include defibrillators (ICD), however ICDs can cause inappropriate shocks and are fallible; one third patients with ICDs suffer SCD [483]. Other treatments include anti-arrhythmic drugs (AADs) (though they have side-effects) and catheter ablation (CA). Despite CA, long term VT recurrence in

patients with structural heart disease ranges from 26-52%. [484] CA fails due to epicardial or intramural substrate which may be beyond the reach of lesion depth achievable by conventional ablation techniques, or the presence of VT substrate in close proximity to critical structures, or if the region of VT substrate cannot be accessed safely (e.g. prior cardiac surgery with epicardial substrate). [485]

Recently, stereotactic body radiation therapy (SBRT), widely used in oncology to treat tumours, has been innovatively used as a therapeutic modality for VT refractory to CA. After first in-human use in 2015,[374] a small case series (n=5) demonstrated 99.9% reduction in VT burden after 6-week blanking.[375] Localised inflammatory lung changes were noted, resolving at 12 months. One patient experienced a fatal stroke (although is unclear if SBRT caused the same). Subsequently, a Phase 1/II clinical trial (n=19 patients) has demonstrated a reduction in VT burden of 94% at 6 months.[376] Longer term, 2-year overall survival was 58%.[377] A retrospective case series (n=10) in Ostrava, Czech Republic demonstrated a VT burden reduction by 87.5% at 12 months.[378] Multiple further case series but no randomised studies have been published.[379-381] The first SBRT in Australia was performed in February of 2022 at Royal Melbourne Hospital. SBRT is now also supported and available for use by the Radiation Oncology Department at Westmead Hospital.

Treatment planning for requires accurate characterization of substrate to generate a 3D target for radiation. Scar can be assessed with multi-modality imaging e.g. multi-detector computed tomography (MDCT) or cardiac magnetic resonance imaging (cMRI) using third party software (i.e. ADAS, Galgo Medical S.L., Barcelona, Spain and InHeart, IHU LIRYC, Bordeaux, France). These reconstructions can be co-registered with three-dimensional electroanatomic maps and 12 lead ECG of induced VT to determine VT exit and substrate requiring ablative therapy.

Australian and New Zealand, US and EU clinical trials registries describe 8 active registered trials investigating SBRT in VT of which three are RCTs. The first, (from Ostrava Czech Republic, NCT04612140) seeks to randomise 100 patients reporting 3-month safety and efficacy outcomes as well as VT burden and survival at 2 years. The second, (from Texas USA, NCT05084391) will have phase 1 safety trial of 15 patients followed by randomisation of patients n=25 to SBRT or current standard of care. It will report survival at 6 and 12 months as well as cost effectiveness, quality of life, VT burden, LVEF and long-term toxicity. This single-centre trial will exclude patients with LVEF <15% and with > 5 morphologies of VTs. These patients are more likely to have high risk or fail repeated CA. Recruitment has not commenced. The third, (from Ottawa Heart, NCT NCT05047198) seeks to recruit 244 patients with cardiomyopathy and recurrent VT despite CA or at high risk of CA and randomise to catheter ablation or SBRT guided by non-invasive pre-procedural planning using ECGi. There are no clinical trials registered in Australia. Further studies are needed to ascertain the safety and efficacy of SBRT.

#### *7.3.1.1 Summary of rationale*

SBRT offers a potential paradigm shift in the treatment of VT, offering outpatient therapy lasting approximately 15 minutes with potentially large cost savings to health as well as significant improvement in patient morbidity. In comparison, the average procedure time for VT ablation in advanced structural heart disease from our cohort at Westmead Hospital over the past 4 years was 210 minutes. Multiple centres are establishing SBRT programs worldwide, but the ideal patient population is uncertain and urgent randomised controlled trials (such as RADIOABLATE-VT) are needed. We anticipate that if the safety and efficacy of SBRT is established in this cohort, conceivably, SBRT could be expanded to a larger, lower risk population of patients experiencing VT, potentially as a first line alternative to current standard of care.

### *7.3.2 Trial/Study Design*

#### *7.3.2.1 Study Design:*

This is an open label randomised controlled trial of SBRT (guided by state-of-the-art multimodality imaging, EAM and ECG analysis) versus standard of care for patients with advanced structural heart disease. Patients will be randomised in a 1:1 manner to receive either SBRT or standard of care and followed for a minimum of 12 months. Measurement of and verification of outcomes will be blinded.

#### *7.3.2.2 Assignment of interventions and randomisation*

Randomisation of intervention and control will be in the ratio 1:1. Randomisation will occur in variable block sizes from 2-6 and will be performed using a secure, password-protected web portal (REDCap).

### *7.3.3 Methods: Participants, interventions, and outcomes*

#### *7.3.3.1 Study Setting and recruitment*

Recruitment will be at Westmead Hospital, Sydney, New South Wales from inpatient care, outpatient clinic, and remote monitoring clinics with plan to add additional sites when there is in interest. Given the pressing clinical need for new ablative strategies for this life-threatening condition, we anticipate this trial will be completed within 12-18 months.

We will contact cardiologists referring to the department of cardiology to assist in identifying potentially eligible patients. The research coordinator will work with cardiologists and electrophysiologists to identify potentially eligible patients, screen them and then invite them to face to face meetings to provide informed consent. We will only randomise patients that meet eligibility criteria and provide informed consent.

## 7.4 Eligibility Criteria

### *7.4.1 Inclusion Criteria*

1. Structural heart disease (including ischaemic cardiomyopathy[1], non-ischaemic cardiomyopathy or congenital heart disease and defined as any one of
2. 
    a. segmental or global decreased ventricular wall motion as defined by TTE, CT or cMRI
    b. myocardial hypertrophy
    c. myocardial scar (evidenced by late gadolinium enhancement on cMRI, wall thinning on cardiac CT, low voltage on electrophysiological study or abnormal intracardiac echocardiography)
3. Recurrent monomorphic VT which can include
    a. at least one episode of VT treated by ICD and/or
    b. sustained VT (lasting >30s) and/or
    c. inducible sustained VT on invasive electrophysiological study (EPS) or non-invasive programmed stimulation (NIPS)

[1] Ischaemic cardiomyopathy will be defined as previous or current coronary occlusion > 70% in a coronary artery with resultant evidence of scar (defined by regional wall motion abnormality on transthoracic echocardiogram or wall thinning on CT perfusion study or late gadolinium enhancement on cardiac MRI in this same territory). Non-ischaemic cardiomyopathy will be defined as scar (as defined by echocardiogram, CT perfusion or cardiac MRI as above) in a territory without associated coronary disease (previous or current coronary occlusion > 70%) in corresponding vessel. Co-incident coronary artery disease may be present in patients with non-ischaemic cardiomyopathy. Diagnosis of ischaemic or non-ischaemic cardiomyopathy as above will be left to the treating cardiologist with adjudication by trial PI (Saurabh Kumar) if there is any disagreement

4. PAINESD[2] score of ≥9 points and/or at least moderate risk of VT recurrence or death as defined by the I-VT[3] score. Both are validated tools used clinically to identify patient at high risk of VT recurrence and/or mortality after CA.

### *7.4.2 Exclusion criteria*

Patients will be excluded if they are:

1. Age < 18 years
2. Life expectancy < 3 months
3. Catheter ablation deemed futile or with prohibitive risk by cardiac electrophysiologist.
4. Unwilling or unable to provide consent
5. Known cardiac channelopathies (e.g. Catecholaminergic polymorphic ventricular tachycardia (CPVT), long- or short QT syndrome, Brugada syndrome)
6. Contraindications to radiotherapy as deemed by referring physician and/or radiation oncologist
7. Pregnancy or breast feeding

## 7.5 Interventions

### *7.5.1 Study treatment*

[2] PAINESD Score is a score composed of pulmonary disease, age, ischaemic cardiomyopathy, NYHA class, ejection fraction, presence of VT storm and diabetes. PAINESD score > 9 suggests > intermediate risk of acute haemodynamic deterioration post catheter ablation. Muser, Daniele, et al. "Identifying risk and management of acute haemodynamic decompensation during catheter ablation of ventricular tachycardia." *Arrhythmia & Electrophysiology Review* 7.4 (2018): 282.

[3] I-VT score is a predictive score for identifying survival and recurrence risk profile of patients undergoing catheter ablation. Vergara, Pasquale, et al. "Predictive score for identifying survival and recurrence risk profiles in patients undergoing ventricular tachycardia ablation: the I-VT score." Circulation: Arrhythmia and Electrophysiology 11.12 (2018): e006730.

All included patients will be managed with appropriate, clinically indicated medical therapy by their usual medical practitioners.

Standard medical therapy will be applied to both groups on discretion of the treating cardiologist which may include:

1. Optimisation of heart failure status to achieve an euvolemic state with initiation or escalation of diuretics;
2. Standard medical therapy known to improve outcomes in cardiomyopathy including initiation titration of ß-blockers, angiotensin converting enzyme inhibitors (ACE-I), aldosterone antagonists, angiotensin receptor – neprilysin inhibitors (ARNI) and Sodium-Glucose Cotransporter-2 Inhibitors (SGLT2i)

   For all patients, ICD settings will be programmed according to standard HRS guidelines.[486]

### *7.5.2 Control arm*

Patients randomised to the control arm will be managed as per current clinical care in consultation with a cardiac electrophysiologist and will include optimisation and/or uptitration of anti-arrhythmic therapy plus consideration of CA where appropriate as per current guidelines. The objective of the control arm is to replicate what would constitute standard of care for patients with VT and advanced structural heart disease for which SBRT is currently unavailable. Multiple drugs and ablation procedures to control VT are permitted during follow up, upon discretion of the treating cardiologist.

Anti-arrhythmic drug optimisation will be as per current guidelines. At the discretion of the treating cardiologist acute management of VT can include intravenous or oral administration of amiodarone and/or esmolol and/or mexiletine. Long term drug management will be with oral amiodarone and/or mexiletine and/or sotalol / propranolol / long acting metoprolol.

CA procedure(s) will be offered to patients where the risk/benefit profile is felt to be beneficial to the patient at the discretion of the treating cardiologist and cardiac electrophysiologist and as per wishes of the patient.

CA procedures will be performed in the standard fashion, as accepted by international guidelines.[487] Procedures will be performed under conscious sedation or general anaesthesia, as per the operator preference. This will include venous and/or arterial femoral vascular access, advancement of electrode catheters to the coronary sinus, right ventricle and induction of VT with programmed ventricular stimulation. Epicardial access will be taken at operator discretion (either via percutaneous approach or via surgical epicardial window). Advanced CA using extracorporeal membrane oxygenation, surgical cryoablation or ethanol ablation will also be permitted. Pre-procedural imaging will be encouraged and if available will be analysed using either ADAS 3D or InHeart software to be integrated real-time into the procedure.

Programmed ventricular simulation will be performed from the right ventricular apex, using a well validated stimulation protocol., extensively described previously.[488] A drive train of 400 ms will be used with each extra-stimulus introduced at 300 ms and decremented by 10ms until ventricular refractoriness. An additional extra-stimulus will then be added until all 4 extra-stimuli are refractory. The endpoint for stimulation will be sustained monomorphic VT lasting >10s or polymorphic VT of VF lasting $\geq$10s.[488]

Ablation will be guided by a combination of mapping techniques, as per standard practice, and described in the guidelines for catheter ablation for VT.[402] An endocardial and/or epicardial approach will be used, based on the operator's discretion, based on 12 lead ECG at baseline, 12 lead ECG of the clinical or induced VT, scar location seen on advanced imaging techniques such as cardiac CT or cardiac MRI. A three-dimensional substrate map will be used to identify the scar

using bipolar and unipolar voltage criteria. Low voltage scar will be defined as voltage <1.5mV [489] on bipolar and <8.3mV (for LV)[245] and <5.5mV (for RV) [246] for unipolar mapping. If VT is hemodynamically tolerated, activation and entrainment mapping may be used to guide ablation to terminate VT. If it is not hemodynamically tolerated, ablation targets will be identified using pace mapping, as well mapping of late, isolated or fractionated potentials, delineation of conduction channels and/or late abnormal ventricular activities (LAVA), as described previously.[490] Irrigated radiofrequency (RF) ablation will be performed at standard power settings 30-50 Watts (W) for 30-90 seconds, aiming for an impedance fall of 10-20 ohms. The endpoint will be non-inducibility of any VT using 4 extra-stimuli or isoprenaline.

Intravenous heparin will be given at the beginning (bolus) and during the procedure, especially if endocardial left ventricular access is planned to prevent risk of systemic and/or venous thromboembolism, as per published guidelines.[490] Further heparin boluses are given to maintain an ACT >300s, as per published guidelines. The procedure may be performed on uninterrupted warfarin and/or dabigatran, or bridging therapy with intravenous heparin or subcutaneous enoxaparin, as per the operator discretion. Post procedural anticoagulation is recommended but not mandated if extensive ablation (RF time ≥10 minutes) is performed.

Pre- and post-CA, AAD management will not be prescriptive, and is left upon the discretion of the treating cardiologist, however typically in this population control of VT involves treatment with oral amiodarone + a ß-blocker, with addition of mexiletine if VT is not controlled or a ß-blocker alone (if intolerant to amiodarone), with addition of mexiletine if VT is not controlled. Post CA AAD use will be as per discretion of the cardiologist. Peri-procedural oral anticoagulation will be instituted with a transient switch to anticoagulant with reversibility (e.g.

IV heparin, dabigatran) in the 48 hours prior to the procedure and switched back to the original to be continued for 6 weeks, or continued indefinitely for other clinical indications.

### *7.5.3 Intervention arm*

Patients randomised to the intervention arm will be expected to have the SBRT procedure within 6 weeks post randomisation. AADs can be used before and after SBRT, as is standard of care.

Pre-procedural planning will involve arranging a 12-lead ECG of spontaneous or induced VT, accessing any 3D electroanatomic mapping (EAM) performed within the last 6 months, cardiac gated contrast multi-detector computed tomography and cardiac MRI (where available). CT/cMRI data will be co-registered with EAM and then imported into the radiation treatment planning software (Eclipse, Varian, Palo Alto, CA). A multi-disciplinary team of at least two electrophysiologists and one radiation oncologist will create a target internal volume.

The patient will attend a simulation session (lasting 1 hour) to collect CT images and necessary information for treatment planning. Subsequently the patient will attend a follow up session (approximately 2 weeks later) for treatment delivery. The patient will receive 25Gy dose in a single fraction to the defined target. X-ray image guidance will be utilised to ensure accurate delivery of treatment dose. Patients will subsequently be monitored in hospital until satisfaction of the treating team (in general for outpatients this means same day discharge). Anticoagulation (NOAC/warfarin) will be prescribed for 6 weeks post SBRT.

If there is recurrence of VT in the SBRT arm requiring medical intervention, further management of VT will be at the discretion of the treating cardiologist in conjunction with a cardiac electrophysiologist. VT will be managed medically with hospitalisation, treatment with IV AADs, or crossover to CA. CA has been performed following SBRT – in a series of 5 patients, 3

patients at 12 months follow-up had repeat RFCA for clinically significant VT [491]. Further, there is preliminary data suggesting the utility of repeat SBRT – in a case series of 3 patients receiving repeat SBRT, no acute toxicity was described and for two patients, no side effects were observed at 22 months follow-up. [492]

For patients treated with SBRT, research blood tests will be collected. The bloods from patients pre and post treatment will be collected and stored at -80 degrees until processing for future research involving metabolomics/transcriptomics at the end of study (until samples are collected from all the patients). Briefly 3x1ml samples of blood will be drawn and stored in -80 degrees freezer at Westmead Institute of Medical Research until processing. Metabolomics/transcriptomics data which will help identify therapeutic markers (metabolites or genes in patients which affect the response to SBRT) to improve treatment outcomes. Samples will be stored and secured at Westmead Institute of Medical Research and de-identified before leaving WSLHD premises. They will be stored for up to 7 years.

## 7.6 Control of bias

Blinding of patients is not possible as many of the interventions are invasive and based on current data, a sham procedure would be considered unethical. We will institute the following to minimise the potential for bias:

a. Ensure adequate management of heart failure with maintenance of euvolemic state;
b. Optimisation and maintenance of electrolytes;
c. Devices will be programmed as per ACC international society guidelines
d. Study personnel measuring outcomes (e.g. LV function, scar size) as well as analysing data will be blinded to intervention allocation.
e. A pre-specified statistical analysis plan will be published

These measures will reduce the possibility of contamination and co-intervention effects. In addition, a clinical event committee blinded to treatment allocation will be used to objectively adjudicate the events associated with the primary and secondary endpoints.

## 7.7 Study Risks and Deviation from Usual Care

SBRT is an emerging medical technology, and this will be one of the first published randomised trials of SBRT world-wide. It is not an experimental procedure but instead has been used in patients with advanced structural heart disease in multiple registries. It has not been compared to standard care in a randomised fashion as has been described in this protocol.

The study team at both sites will meet fortnightly to monitor the clinical status of patients. SAE are reportable to DSMC as soon as they are identified.

Investigations commonly used in clinical practice for the evaluation of structural heart disease aetiology and its severity may include one or more of echocardiography, coronary angiography, cardiac magnetic resonance imaging (MRI), cardiac CT scanning, biopsy, cardiac positron emission tomography (PET) scan, genetic testing for familial dilated cardiomyopathies, and blood work to evaluate renal, thyroid and hepatic function. Routine clinical follow up at 6-monthly intervals is considered clinical standard of care and so is echocardiography at ~6-monthly intervals in the first year to detect subsequent changes in ventricular function and to screen for valvular heart disease. Whilst on AADs, it is routine to screen bloodwork for abnormalities in full blood count parameters, renal and thyroid function due to the known toxicities of AADs. In addition to this, research blood work will be collected for patients who receive SBRT (before therapy, day of therapy and at 6 months and 12 months).

## 7.8 Study Outcomes

The study will have a 42 day "blanking period" after SBRT or standard care until assessment of study outcomes, except for safety which will be included in this period. This is because the anti-arrhythmic effect of SBRT is thought to occur after the first 6 weeks after radiation is delivered to the heart. The 6 week treatment period also allows for optimisation of anti-arrhythmic therapy and/or CA procedure(s) if the treating physician felt that the VT source was not sufficiently targeted on the index procedure and required mapping on epicardial surface or was located intramurally and further ablation is needed on both sides of the ventricular wall (e.g. LV, then RV septum; or endocardial, then epicardial ablation).

### *7.8.1 Primary Outcome*

Proportion of patients with a ≥75% reduction in VT burden at 6 months (number of VT episodes in 6 months post treatment compared to the number of VT episodes in the 6 months prior to randomisation excluding a 6-week blanking period after treatment initiation)

### *7.8.2 Secondary Outcomes*

These will be assessed at 6,12,24 and 36 months (except for mortality and safety endpoints which will be assessed from randomisation, all others will be assessed after a 42-day blanking period after treatment initiation):

#### *7.8.2.1 Secondary efficacy endpoints*

1. Recurrent sustained VT ascertained by implanted cardioverter defibrillator (ICD) (VT identified and treated by the ICD with anti-tachycardia pacing (ATP) and/or internal ICD delivered shock or ≥30 seconds of VT if untreated by ICD);

2. VT storm (three or more documented episodes of VT within 24 hours or incessant VT);
3. Absolute % reduction in VT burden compared to pre-ablation;
4. ICD shocks
5. Cardiovascular hospitalisation
    a. All cause cardiovascular hospitalisation
    b. Heart Failure
    c. Hospitalisation for arrhythmia
6. Mortality
    a. All-cause mortality
    b. Cardiac death
7. Composite outcome of VT recurrence/hospitalisation/death/ cardiac transplantation
8. Effect of intervention on ventricular function as assessed by transthoracic echocardiography from baseline
9. Number of AADs
10. Change in quality of life at 6 and 12 months (compared to pre-intervention) as measured by SF-36 / MASQ (Modified Arrhythmia Specific Questionnaire) / ICDC (Cardioverter Defibrillator Patient Concerns Questionnaire)
11. Feasibility data for SBRT
    a. How many patients were excluded because SBRT could not be delivered safely
    b. Dose of radiation to key healthy tissues and cardiac structures – coronaries, atrial, non-targeted myocardium
12. Scar-size as measured by cardiac MRI compared to preceding cMRI (where available)
13. Changes in signal averaged ECG metrics

14. Cost effectiveness of treatment at 12 months

15. Cross-over rate and need for repeated ablations

#### *7.8.2.2 **Secondary safety endpoints***

Serious Adverse Events (SAE) and Adverse Events of Special Interest (AESI) will be recorded throughout the trial from immediately post randomisation up to 36 months follow-up

a. AESI related to effects of SBRT
b. AESI related to standard care e.g. medical anti-arrhythmic drug therapy or catheter ablation or heart transplantation

These pre-specified secondary endpoints will help to understand the findings if the trial does not demonstrate a difference between treatment allocations as well as to help plan future clinical trials.

### *7.8.3 Cost effectiveness analysis*

A comprehensive economic evaluation from the health system perspective will be conducted to assess the relative cost-effectiveness of the intervention relative to usual care. We will collect data on the costs associated with delivering the intervention including costs of inpatient hospital treatment, outpatient clinic and emergency department visits, disposal equipment used (including catheters), and total costs of CA or SBRT (equipment and personnel). Participants will be asked to report primary care use for the preceding period through questionnaires at each point of follow-up. The key outcomes will be incremental cost-effectiveness rations measuring the cost per primary outcome averted/gained and Quality adjusted life years (QALYs) gained over the duration of the trial and follow-up period. QALYs will be calculated using health related quality of life outcome estimates collected in the trial. Bootstrapping will be used to estimate a distribution around costs and health outcomes, and to calculate the confidence intervals around the incremental cost effectiveness ratio. Sensitivity analyses will be conducted around key variables to test the

robustness of results to variations in key inputs. This analysis will provide important information to policymakers and administrators responsible for investment decisions in the field and will inform the development and implementation of clinical guidelines for treatment of these patients.

## 7.9 Methods for follow up

Patients will be followed until the end of the trial (36 months) or death with preliminary analysis at 6 months. Patients will be evaluated at baseline, then at 1, 3 and 6-monthly thereafter until study end date (last patient has been followed for a minimum of 1 year). All events will be adjudicated by the event committee blinded to the treatment allocation. Effects of ablation on ventricular function will be assessed by routine echocardiography reported by a core group of blinded experts in imaging at Westmead Hospital, using standard techniques at 6,12 and 36 months post intervention commencing. They will be blinded to group allocation.

### *7.9.1 Participant Timeline*

All eligible participants will be randomised and followed up for a minimum period of 12 months. Randomised participants who deviate from the protocol will still be followed up as their data will be analysed on the ‘intention to treat’ principle. Figure 1 illustrates the trial schema and

Table 1 shows the nature and timing of the data collection required during the study period.

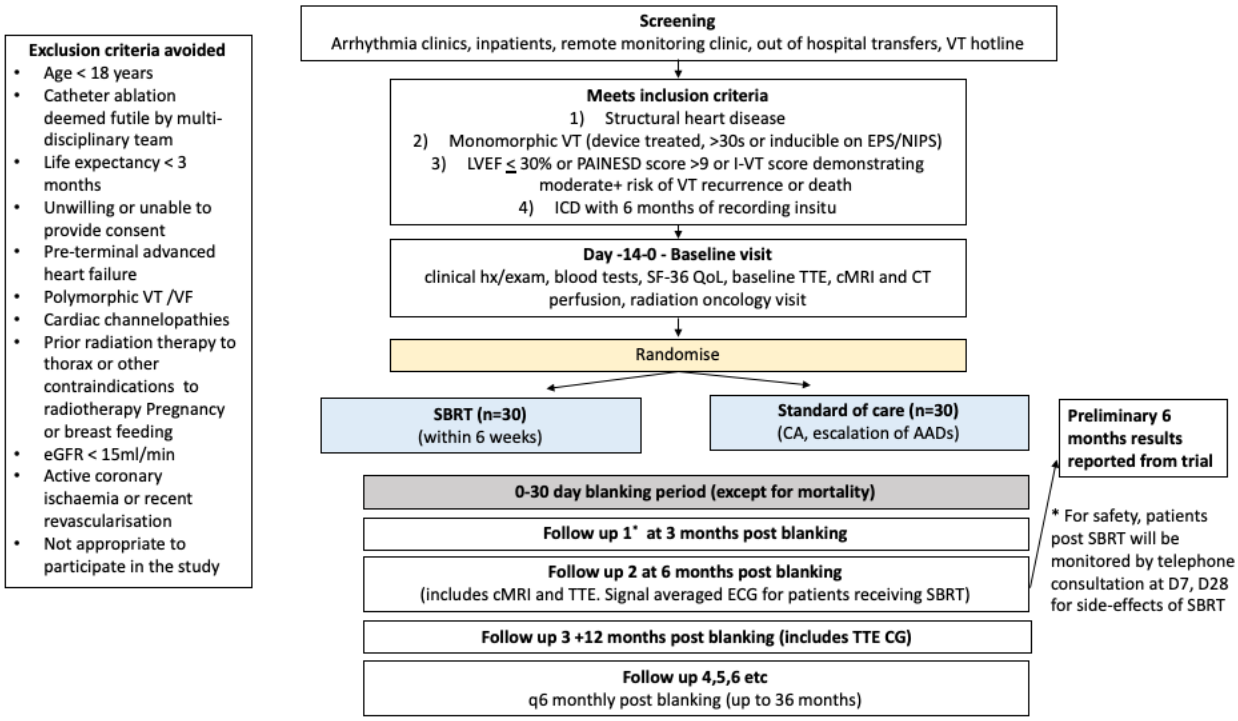


**Figure 7-1Trial Schema**

**Table 7-1 Table of trial visits**

| Study Periods | Baseline | Randomisation | Time after Treatment | | | | | | | | | |
|---|---|---|---|---|---|---|---|---|---|---|---|---|
| Study Week | -14 to 0 days | 0 days | 0 days (if receiving SBRT only) | 7 days (if receiving SBRT only) | 28 days (if receiving SBRT only) | 3 months | 6 months | 12 months | 18 months | 24 months | 30 months | 36 months |
| Study visit window from randomisation | ± 14 days | N/A | | ± 3 days | ± 14 days | ± 14 days | ± 14 days | ± 14 days | ± 14 days | ± 14 days | ± 14 days | ± 14 days |
| Evaluation | | | | | | | | | | | | |
| Informed Consent | x | | | | | | | | | | | |
| Inclusion/exclusion criteria | x | | | | | | | | | | | |
| Randomisation | | x | | | | | | | | | | |
| Clinical History | x | | | | | | | | | | | |
| Physical examination | x | | | | | | | | | | | |
| ICD check* | x | | | | | | x | x | x | x | x | x |
| Ensure ICD programmed to trial settings | x | | | | | | | | | | | |
| Research blood tests | x | | x | | | | x | x | | | | |
| TTE (including strain) | x | | | | | | x | x | | x** | | x |
| Signal averaged ECG | x | | | | | | x | | | | | |
| CT perfusion study | x | | | | | | | | | | | |
| cMRI (including LGE) | x | | | | | | x** | | | | | |
| QoL surveys (mailed or emailed) | x | | | | | | x | x | | | | x |
| Telephone follow up of outcomes | | | | x | x | x | x | x | x | x | x | x |
| Adverse events | | | | x | x | x | x | x | x | x | x | x |

Nb for safety, telephone reviews will be made with patient post SBRT at D7,28

*Only if a patient does not have remote monitoring will they have 6, 12, 18, 24, 30, 36 months ICD checks.

**Strongly recommended but not mandated by study.

### 7.10 Screening Process

All participants screened will be recorded by the study team and entered in the case report form (CRF). This initial contact may be via telephone or face to face. Initial screening activities will include a brief verbal assessment of the potential participant's medical history, their willingness to participate, and current medications. If the member of the study team determine that the potential participant may be suitable for the study an invitation package including a copy of

the Participant Information sheet will be provided to the potential participant. If the patient is not eligible the main reason as to why a participant is excluded will be recorded on a screening log form.

### *7.10.1 Baseline visit*

For baseline assessment, the information listed in Table 1 will be collected from each participant. This will include details of medical history, physical exam, concomitant medications, and if clinically available, results of blood tests and baseline imaging. 6 monthly VT burden will be obtained (from device interrogation and review of patients' previous device interrogation reports. All baseline and subsequent follow up will be recorded in pre-formed REDCap database.

All screened patients deemed eligible for the trial will be offered a consultation with a radiation oncologist to discuss SBRT risks and benefits and expected prior to randomisation.

### *7.10.2 Randomisation*

Randomisation will be 1:1 to intervention and control. Randomisation will be by a computerised system that will allow for variable block sizing (2-6). Randomisation will be performed by using a secure, password-protected web portal (REDCap). Each participant will be assigned with a randomisation number. Randomisation data will be collected as in Appendix 1.

### *7.10.3 Subsequent visits*

Information shown in Table 1 will be collected on subsequent visits. For safety, additional follow-ups will be performed at D7, D28 after SBRT to monitor for treatment adverse events. Research blood tests will be offered to SBRT patients prior to therapy, at day 1 post therapy and at 6 months and 12 months.

## 7.11 Informed Consent

Written informed consent will be obtained from all participants before conducting any study-specific procedures including screening assessments. The informed consent form will be stored in the participant's study records and a copy given to the participant to keep. All completed consent forms will be signed and dated. Prospective participants will be informed as part of the consent discussion that the screening phase will determine eligibility for the trial and that signing the consent form does not guarantee enrolment into the trial.

Premature withdrawal and early study termination

If a participant wishes to withdraw or the study team / responsible physician decides it is in the best interest of the participant to withdraw from the study, every effort should be made to conduct all assessments until the date of the last follow up.

### *7.11.1 Retention*

The study team will retain all study records and by the applicable regulatory bodies in a secure and safe facility for a minimum period of 5 years.

## 7.12 Statistical Considerations

### *7.12.1 Sample size*

There is no prior randomised trial comparing standard care versus SBRT, making an accurate sample size estimation difficult. This trial will also provide the first data set to plan for future randomised trials in this space. The rationale for a target sample size of 60 patients is as follows. The largest series of SBRT (n=19) in a high risk population who had either failed CA or had contraindications to it, with advanced SHD (left ventricular ejection fraction mean 25%, and 75% with New York Heart Association Classification class III or IV heart failure) reported that

89% of patients have a VT burden reduction of ≥75% after SBRT at 6 months, compared to 6 months pre-ablation. It is anticipated that we will recruit patients at much lower risk (those who have not failed prior CA, nor have advanced heart failure), which conceivable will improve the success rate to ~95% (clinical consensus by investigators).

The closest comparable population to the aforementioned SBRT group could be derived from CIA Kumar's published experience of ~100 patients undergoing CA. When CA procedures are unable to eliminate the targeted VT, only 56% of patients had a ≥75% reduction in VT burden in 6 months after CA, compared to 6 months prior. To obtain a conservative absolute risk reduction of ~33% with SBRT (from 89% vs. 56%), with power 80%, 1-sided significance of $P<0.05$, ~10% dropout, we estimate that ~60 patients (30 in each arm) will be required. This study number is feasible, as described earlier.

### *7.12.2 Statistical analysis*

All data analysis will be performed by a statistician independent of the study investigators. A detailed statistical analysis plan will be developed prior to analysis. The primary analysis approach will be by intention to treat. The Chi-square test will be used to compare the primary endpoints. The corresponding statistical analyses for each of the secondary endpoints will be as follows: time to VT recurrence, cardiovascular hospitalisation, transplant, all-cause mortality and composite endpoint of VT recurrence/transplant/mortality (Kaplan-Meir analysis, nonparametric log rank test procedure for comparing the survival curves), AE and AESI (Chi squared test), absolute % reduction in VT burden at 6, 12, 24, 36 months post treatment compared to pre-treatment, change in ventricular function at 6, 12, 24, 36 months compared to pre-treatment, QOL scores (linear regression models, adjusting for baseline clinical variables). The primary analysis

will be done at 6 months. The follow-up analysis will be done at 36 months and takes into account repeated measures in the model.

### 7.13 Data management

All paper forms including consents and follow up information will be locked in secure filing cabinets in locked areas of the Cardiology Department, Westmead hospital. Electronic data will be stored in an electronic database (stored on the WSLHD Microsoft Sharepoint sever) that will be accessible only to designated individuals and password locked. A random sample of 10% of key data entered will be examined against source documents. We will run statistical quality checks, e.g. to check for out-of-range values.

### 7.14 Steering Committee

The steering committee will form the principal leadership structure of the study. Members of the steering committee will be the listed PIs on this application. The steering committee will be responsible for the overall conduct of the trial, its conception and termination, and interpretation and publication of the results.

### 7.15 Other committees

A data monitoring committee (DMC) will be appointed. The DMC will have full access to trial documents.

The DMC will review the safety, ethics and outcomes of the study. Major responsibilities of this committee will include: (i) monitor response variables and safety outcomes for early dramatic benefits or potential harmful effects and provide reports to the Study Steering Committee on recommendations to continue or temporarily halt recruitment to the study. The DMC will be governed by a charter that will outline their responsibilities, procedures and confidentiality. The

DMC will also review unblinded data from the study at regular intervals during follow-up, and will monitor outcomes, drop-out and event rates. The first meeting will be held after the first 10 patients have been recruited and completed 6 months follow up. Formal interim reviews will be done at 12-monthly intervals and will be planned to review data relating to outcome rates from a safety perspective, patient safety and quality of trial conduct. Prior to the analysis a detailed Statistics Analysis Plan (SAP) will be developed to:

I. Describe the details of the statistical analysis methodology.

II. Specify rules on data handling conventions used to perform the analyses.

III. Describe the procedure to be used to account for missing data.

An events committee (EC) will be appointed. This committee will be blinded to treatment allocation of enrolled patients and will review de-identified CRFs, and source documents including Holter monitors, TTEs and hospitalisation records, and will primarily adjudicate on endpoints. The EC will individually examine the validity of noted events using available records of events. Consensus will be sought to classify an event as accurate or not.

### 7.16 Adverse Events

Any adverse event occurring as a result of SBRT or catheter ablation will be recorded. An adverse event is defined as any untoward medical occurrence in a subject or clinical investigation subject administered a pharmaceutical product at any dose or a medical procedure that does not necessarily have to have a causal relationship with this treatment.

**Procedure-related adverse event** is any adverse event that, in the investigator's opinion, is a complication of the catheter ablation procedure and occurs within 48 hours of catheter insertion.

**Adverse Reaction** will be defined as a harmful and unintended response to an approved and marketed health product. This includes any undesirable patient effect suspected to be associated with health product use. Unintended effect, overdose, interaction (including drug-drug, and drug-food interactions) are all considered to be reportable adverse events in this study.

**Serious Adverse Event (SAE)** will be defined as any untoward medical occurrence that:

- results in death;
- is life threatening in the opinion of the attending clinician (i.e. the patient was at risk of death at the time of the event; it does not refer to an event that might hypothetically have caused death had it been more severe);
- requires inpatient hospitalisation or prolongation of existing hospitalisation (Any hospitalisation that was planned prior to randomisation will not meet SAE criteria. Any hospitalisation that is planned post randomisation will meet the SAE criteria);
- results in persistent or significant disability or incapacity;
- is an important medical event in the opinion of the attending clinician that is not immediately life-threatening and does not result in death or hospitalisation but which may jeopardise the patient or may require intervention to prevent one of the other outcomes listed above.

An adverse event that meets the above categories between when the informed consent form is signed, the end of study at 3 years will be reported as an SAE. All SAEs will be reported to DMC within 24-hours of the study team first becoming aware of the event. The SAE will also be required to be reported to the relevant HREC within the timeframe specified in the relevant committee guidelines. Adverse events which do not fall into these categories are defined as non-serious.

**Suspected Unexpected Serious Adverse Reaction (SUSAR).** An unexpected adverse reaction (UAR) is an adverse reaction, the nature or severity of which is not consistent with the applicable product information. A Suspected Unexpected Serious Adverse Reaction is any UAR that at any dose meets the definition of an SAE. Any event that meets the definition of a SUSAR between when the informed consent form is signed and the end of study at 3 years will be reported to the local HREC and the relevant regulatory authorities as per local requirements and ICH Clinical Safety Data Management: Definitions and Standards for Expedited Reporting.

## 7.17 Auditing

The study may be audited by the third parties and inspected by government regulatory authorities. CRFs, source documents and other study files must be accessible at all study sites at the time of auditing and inspection during the study and after the completion of the study.

## 7.18 Ethics and Dissemination

### *7.18.1 Regulatory and Ethical Compliance*

This study protocol was designed and shall be implemented and reported in accordance with the ICH Guidelines for Good Clinical Practice, NHMRC National Statement on Ethical Conduct in Human Research, applicable local regulations including European Directive, US Code of Federal Regulations Title 21, Therapeutics Goods Administration (TGA), and with the ethical principles laid down in the World Medical Associations (WMA) Declaration of Helsinki.

The protocol and the proposed informed consent form and any subsequent modifications will be reviewed and approved by the Human Research Ethics Committee before any participant is enrolled. Prior to study start, investigators are required to sign a protocol signature page confirming his/her agreement to conduct the study in accordance with these documents and all of

the instructions and procedures found in this protocol and to give access to all relevant data and records to CCC monitors, auditors, HRECs, and regulatory authorities as required. If an inspection of the clinical site is requested by a regulatory authority, the investigator must inform The University of Sydney immediately that this request has been made.

### *7.18.2 Informed Consent*

Potential participants may only be included in the study after providing written informed consent. The associate investigator will issue the information sheet and consent forms, and will obtain consent from participants. Before the start of the study, a member of the study team will have the participant information sheet and consent form that will be provided to the participants reviewed and approved by the HREC. This review and approval will be documented and stored with other study documents. The associate investigator must fully inform the participant of all relevant aspects of the trial. During the consultation with participants, the associate investigator will explain the details of the study, and provide an information sheet detailing the aims, methodology, and possible outcomes of the research proposal. Participants will be given information about their rights to refuse consent, right to confidentiality, right for their information to be secured in a locked facility if they choose to participate in the study. Participants will be given opportunity to communicate their choice of participating or not. During this time, support will be provided to answer any questions or comments arising from the consent process. A copy of the signed written informed consent will be given to the participant. The participant must be allowed ample time to ask about the details of the study and to decide as to whether to participate in the study. If the participant is unable to read and write, a witness must be present during the informed consent discussion and at the time of informed consent signature.

### *7.18.3 Confidentiality*

Every precaution will be taken to respect the privacy of participants in the conduct of the study. Only de-identified data will be entered in the central study database to maintain participant confidentiality. In the course of monitoring data quality and adherence to the study protocol, the monitor will refer to medical records at the participating study site. This information will be included in the PICF. All individual and site information will be de-identified in reporting data and results to protect the confidentiality of participants. For the purpose of tracking of clinical and adverse events however, a log will be kept separately from the study database containing information about the participant number and their corresponding clinical details in a re-identifiable format.

### *7.18.4 Trial Sponsorship*

This trial will be sponsored by the Western Sydney Local Health District.

### *7.18.5 Dissemination Policy*

Full editorial control will reside with a Writing Committee approved by the Steering Committee (SC). Authors of publications must meet the International Committee of Medical Journal Editors (ICMJE) guidelines.

### *7.18.6 Data sharing*

Throughout the study, un-identifiable imaging and radiotherapy data will be shared with University of Sydney researchers from the ImageX Institute (c/o Professor Paul Keall University of Sydney, Image X Institute, Ph. 02 8627 1159, Email: paul.keall@sydney.edu.au

Data to be shared is

- CT simulation images and any associated MRI or PET scans used for planning
- Treatment plan

- CBCT scans including projections and imaging details
- Intra-treatment imaging projections and imaging details
- Surface imaging
- ECG data during treatment
- ICD manufacturer and any information about the ICD leads and lead tips
- Treatment details including immobilisation and motion management strategies
- Couch used, couch positions and which coordinate system followed.
- Linac type and coordinate system

These data will be de-identified prior to sharing. Coded image files will be saved, securely transferred to the University of Sydney and stored on a departmental server with access limited to University of Sydney study personnel. Information about data sharing will be provided to study participants in the Patient Information Sheet.

### *7.18.7 Funding*

This study is supported by a National Heart Foundation Vanguard Grant (2 year grant) as well as an NHMRC Synergy Grant.

# Chapter 8

## 8 CONCLUSIONS AND FUTURE DIRECTIONS

At the outset of this thesis, we defined the problem of treating VA with ablation as requiring the cardiac electrophysiologist to solve two problems: (1) identifying the critical circuitry and arrhythmogenic substrate conducive to these arrhythmias, and (2) successfully abolishing this substrate to ensure acute procedural success and prevent long-term recurrence. Addressing these two challenges is crucial for advancing the success of VA treatments and improving patient outcomes. This need is urgent because VAs place a significant burden on the lives of Australians and indeed patients worldwide, with attendant risks of sudden death, heart failure, ICD shocks, and significant symptoms that exact a heavy toll on a patient's quality of life.

Our ability to treat VA has improved tremendously over the last 30 years, largely driven by the efforts of pioneers and giants in the field. With what were, at least compared with modern-day EAM, quite rudimentary mapping technologies, they unraveled the mysteries of ventricular arrhythmogenesis and charted a course towards cure for these deadly rhythms.

In comparison, the current proceduralist is equipped with a dizzying array of complex technologies to delineate and treat VA, and must decipher a multitude of available data, including results from multi-modality imaging, precision genotype and phenotype studies in non-ischaemic cardiomyopathies, and the many gigabytes of electrogram signals that make up a high-density modern-day electrophysiological procedure. They must then determine the best strategy to ablate or modify this substrate, moving beyond decisions limited to the use of solid-tipped non-irrigated ablation catheters to considerations regarding the choice of irrigant, ablation energy, and ablative strategy.

Unfortunately, despite the richness of data and the variety of available choices, meta-regression studies of published VT trials by publication date suggest that longer-term success rates for CA of VA in SHD have plateaued.[13] There is therefore a pressing need for mechanistic and translational studies to refine our understanding of arrhythmogenesis, to validate and improve current strategies for identifying arrhythmogenic substrate, and to innovate novel approaches that push the boundaries of EAM and ablation. Hand in hand with this is the need for good quality randomised data to establish the role of these strategies in achieving durable cure for our patients.

In the case of PVCs, before we seek to improve CA techniques, first we must establish whether CA at all is the optimal strategy for good quality, long term, patient-centered outcomes. Compared to multiple RCTs and systematic reviews that have investigated the role of CA in treatment of VT with SHD, there is a paucity of trial-level data for management of PVCs, with only a single RCT, and that too targeting PVCs from a single site.[194] In chapter 2, we completed the first published systematic review of CA vs AADs for treatment of PVCs and confirmed that there is limited evidence comparing AADs and CA for non-RVOT PVCs, with all such available observational studies having serious concerns of bias. Within this limitation, we demonstrated that CA appeared superior to AAD in reducing the burden or frequency of PVCs with the caveat that the head-to-head impact of either strategy on patient QoL, symptoms, or cost to the health care system is unclear. Further, we established that modern technologies including ICE and contact force-sensing catheters were not systematically studied in published data to date, reinforcing the need for new trials in this space.

Multi-modality imaging with CMR and MDCT offers the ability to dramatically alter our understanding of arrhythmogenic substrate and provocatively, may offer ablative targets that obviate the need EAM.[340] LGE CMR channels co-localise with both critical sites of VT[229] and

functional substrate[284,292] but our use of these technologies are predicated on fundamental assumptions regarding optimal signal thresholding, which were established in a small series of 10 human patients and against voltage scar rather than histopathology.[338] In Chapter 3, we utilised an ovine experiment with meticulously co-registered high density multi-wavefront mapping of chronic post-infarction scar, whole-heart tissue histopathology and delayed enhancement CMR at fine slice thickness to validate CMR-CCs identified using a commonly used third party image integration platform (ADAS-3D). This work established that CMR thresholding with 60% of maximal signal intensity for core scar and 40% for borderzone had substantial agreement and good accuracy to identify histopathological scar in the endocardium but poorer performance in the epicardium. 87% of CMR-CCs identified by varied signal intensity thresholding could be validated with histological channels of surviving myocytes surrounded by fibrosis, and this relationship was robust for multiple signal intensity thresholds. These same channels co-localised with functional substrate (DZs, validated with multiple activation wavefronts). Most critically, we were able to unravel the histopathological characteristics at sites of DZ co-localising with CMR-CCs which had three-fold higher intra-channel adiposity, but similar amounts of fibrosis compared to CMR-CC sites without DZs. This study therefore supported a prevailing hypothesis that lipomatous metaplasia and not only fibrosis drives conduction slowing and electrogram fractionation at arrhythmogenic sites. The ovine model we have studied offers promise for future studies targeting modulation of lipomatous metaplasia which may offer the capacity to modify the substrate conducive to VT in both ischaemic and non-ischaemic cardiomyopathies.

A limitation of the work we published in Chapter 3 was that the animal model did not have available data for VT inducibility and further, multi-vendor comparisons of CMR image integration were not studied. Therefore, in Chapter 4, we compared the performance of ADAS 3D

and inHEART which are the two presently used proprietary software for CMR image integration. Using the same animal experiment as in Chapter 3, we found that both vendors had comparable efficacy to identify endocardial and intramural substrate with poor performance in the epicardium. To address limitations of the animal data, we performed the first clinical comparison of these two technologies to identify both VT critical sites and functional substrate in patients with SHD and monomorphic VT. In a small clinical series of predominantly NICM, we demonstrated that critical VT sites co-localise reliably with both ADAS-3D and inHEART scar (88% falling within one scar layer). Importantly, more than 80% of VT critical sites demonstrated CMR LGE scar in more than 1 layer (reinforcing the three-dimensional nature of VT circuits). These results pave the way for future randomised clinical trials utilising both platforms to delineate VT arrhythmogenic substrate and improve longer term VT free survival.

Given in Chapter 3 and 4 there was an established limitation of CMR to identify epicardial scar substrate, we hypothesised that further improvements in mapping scar depth and patterns could be made by harnessing signal processing and machine learning of invasively collected intracardiac electrograms. In Chapter 5 we established that, like previous studies, [252] voltage amplitude from endocardial mapping alone is a poor discriminator of scar in deeper tissue. In an interdisciplinary study, we used the same ovine experiment to co-register 11,551 electrograms with scar depth. Signal processing demonstrated that a combination of time and frequency domain features could be used to train a gradient boost machine learning algorithm to delineate scar depth. Further, a time series convolutional neural network was applied to unprocessed electrograms, demonstrating that complete 2.5s unipolar acquisitions could determine intramural and epicardial fibrosis (with healthy endocardial myocardium) with remarkable 95% accuracy. These mechanistic findings have been leveraged into open-source code that can generate scar depth maps

readily importable into live EAM from whole chamber LV voltage maps. These findings will need future validation in human patients to identify if such scar depth maps can improve procedural planning (need for epicardial approach) and outcomes in clinical cases.

In Chapter 6, we then turned our attention to the second problem that the ablationist faces, adequate lesion formation. CA of intracavitary PVCs is challenging due to limitations in catheter contact with moving structures and ectopy during ablation. PFA is a novel energy source with limited validation in the ventricle. In a small pilot case series of 3 patients, we described our experience with this technology to tackle challenging intracavitary PVCs. Though we achieved good success, this proof-of-concept trial requires validation in larger case series and probably alternative PFA catheters due to the difficulty of maneuvering the Farawave catheter in the ventricle.

Finally, these novel approaches to CA of VA described in chapters 3-5 have direct relevance to the field of SBRT where multi-modality assessment of ventricular tachycardia scar substrate is the key to ablation outcomes. Despite multiple case series describing variable outcomes in prospective cohorts of patients with SHD and VA refractory to CA, there are no randomised data establishing the role of SBRT in VA treatment. In Chapter 7 we have designed an Australian first, pragmatic RCT which compares SBRT against the care such patients would receive without availability of this technology (which can include escalation of AADs or VA CA). Ethics approval, trial registration and establishment of rigorous data safety monitoring board protocols have occurred, and patient recruitment is underway. We expect results from this trial in eighteen to twenty-four months and these data are likely to meaningfully impact the way VT in advanced SHD is approached.

Taken together, the work of this thesis therefore offers incremental but important improvements to solve the problem of VA ablation with validation and development of new strategies for identification and abolishment of VA substrate. We hope this work continues to advance the field towards control and hopefully cure of these deadly arrhythmias.

# REFERENCES


1. Wong CX, Brown A, Lau DH, Chugh SS, Albert CM, Kalman JM, Sanders P. Epidemiology of sudden cardiac death: global and regional perspectives. *Heart, Lung and Circulation*. 2019;28:6-14.
2. Könemann H, Ellermann C, Zeppenfeld K, Eckardt L. Management of ventricular arrhythmias worldwide: comparison of the latest ESC, AHA/ACC/HRS, and CCS/CHRS guidelines. *JACC: Clinical Electrophysiology*. 2023;9:715-728.
3. Josephson M, Wellens HJ. Implantable defibrillators and sudden cardiac death. *Circulation*. 2004;109:2685-2691.
4. Lee DS, Krahn AD, Healey JS, Birnie D, Crystal E, Dorian P, Simpson CS, Khaykin Y, Cameron D, Janmohamed A. Evaluation of early complications related to de novo cardioverter defibrillator implantation: insights from the Ontario ICD database. *Journal of the American College of Cardiology*. 2010;55:774-782.
5. Desai H, Aronow WS, Ahn C, Gandhi K, Hussain S, Lai HM, Sharma M, Frishman WH, Cohen M, Sorbera C. Risk factors for appropriate cardioverter-defibrillator shocks, inappropriate cardioverter-defibrillator shocks, and time to mortality in 549 patients with heart failure. *The American journal of cardiology*. 2010;105:1336-1338.
6. Sherrid MV, Daubert JP. Risks and challenges of implantable cardioverter-defibrillators in young adults. *Progress in cardiovascular diseases*. 2008;51:237-263.

7. van Rees JB, Borleffs CJW, de Bie MK, Stijnen T, van Erven L, Bax JJ, Schalij MJ. Inappropriate implantable cardioverter-defibrillator shocks: incidence, predictors, and impact on mortality. *Journal of the American College of Cardiology*. 2011;57:556-562.

8. Daubert JP, Zareba W, Cannom DS, McNitt S, Rosero SZ, Wang P, Schuger C, Steinberg JS, Higgins SL, Wilber DJ. Inappropriate implantable cardioverter-defibrillator shocks in MADIT II: frequency, mechanisms, predictors, and survival impact. *Journal of the American College of Cardiology*. 2008;51:1357-1365.

9. Goldstein RE, McCarthy ML, Krone RJ, Haigney MC, Zareba W, MADIT-CRT Investigators. Sudden Unexpected Death in Patients With Implanted Cardiac Defibrillators: Results of Postmortem Interrogation in MADIT-CRT. *JACC: Clinical Electrophysiology*. 2025.

10. Camm AJ. Hopes and disappointments with antiarrhythmic drugs. *International Journal of Cardiology*. 2017;237:71-74.

11. Roden DM, Darbar D, Kannankeril PJ. Antiarrhythmic drugs. *Cardiovascular medicine*. 3rd Edition. 2007:2085-2102.

12. Ravi V, Poudyal A, Khanal S, Khalil C, Vij A, Sanders D, Larsen T, Trohman RG, Aksu T, Tung R. A systematic review and meta-analysis comparing radiofrequency catheter ablation with medical therapy for ventricular tachycardia in patients with ischemic and non-ischemic cardiomyopathies. *Journal of Interventional Cardiac Electrophysiology*. 2023;66:161-175.

13. Kanagaratnam A, Virk SA, Pham T, Anderson RD, Turnbull S, Campbell T, Bennett R, Thomas SP, Lee G, Kumar S. Catheter ablation for ventricular tachycardia in ischaemic

versus non-ischaemic cardiomyopathy: a systematic review and meta-analysis. *Heart, Lung and Circulation*. 2022;31:1064-1074.

14. Yokokawa M, Desjardins B, Crawford T, Good E, Morady F, Bogun F. Reasons for recurrent ventricular tachycardia after catheter ablation of post-infarction ventricular tachycardia. *Journal of the American College of Cardiology*. 2013;61:66-73.

15. Tung R, Raiman M, Liao H, Zhan X, Chung FP, Nagel R, Hu H, Jian J, Shatz DY, Besser SA. Simultaneous endocardial and epicardial delineation of 3D reentrant ventricular tachycardia. *Journal of the American College of Cardiology*. 2020;75:884-897.

16. Bhaskaran A, Nayyar S, Porta-Sánchez A, Jons C, Massé S, Magtibay K, Aukhojee P, Ha A, Bokhari M, Tung R. Direct and indirect mapping of intramural space in ventricular tachycardia. *Heart Rhythm*. 2020;17:439-446.

17. Neira V, Santangeli P, Futyma P, Sapp J, Valderrabano M, Garcia F, Enriquez A. Ablation strategies for intramural ventricular arrhythmias. *Heart Rhythm*. 2020;17:1176-1184.

18. Ciaccio EJ, Hsia HH, Saluja DS, Garan H, Coromilas J, Yarmohammadi H, Biviano AB, Peters NS. Ventricular tachycardia substrate mapping: What's been done and what needs to be done. *Heart Rhythm*. 2025;(in press).

19. Marchlinski FE, Callans DJ, Gottlieb CD, Zado E. Linear ablation lesions for control of unmappable ventricular tachycardia in patients with ischemic and nonischemic cardiomyopathy. *Circulation*. 2000;101:1288-1296.

20. Jaïs P, Maury P, Khairy P, Sacher F, Nault I, Komatsu Y, Hocini M, Forclaz A, Jadidi AS, Weerasooryia R. Elimination of local abnormal ventricular activities: a new end point for substrate modification in patients with scar-related ventricular tachycardia. *Circulation*. 2012;125:2184-2196.

21. Jamil-Copley S, Vergara P, Carbucicchio C, Linton N, Koa-Wing M, Luther V, Francis DP, Peters NS, Davies DW, Tondo C. Application of ripple mapping to visualize slow conduction channels within the infarct-related left ventricular scar. *Circulation: Arrhythmia and Electrophysiology*. 2015;8:76-86.

22. Harris L, Downar E, Mickleborough L, Shaikh N, Parson I. Activation sequence of ventricular tachycardia: endocardial and epicardial mapping studies in the human ventricle. *Journal of the American College of Cardiology*. 1987;10:1040-1047.

23. Brunckhorst CB, Delacretaz E, Soejima K, Maisel WH, Friedman PL, Stevenson WG. Identification of the ventricular tachycardia isthmus after infarction by pace mapping. *Circulation*. 2004;110:652-659.

24. Tung R, Mathuria N, Michowitz Y, Yu R, Buch E, Bradfield J, Mandapati R, Wiener I, Boyle N, Shivkumar K. Functional pace-mapping responses for identification of targets for catheter ablation of scar-mediated ventricular tachycardia. *Circulation: Arrhythmia and Electrophysiology*. 2012;5:264-272.

25. Stevenson WG, Friedman PL, Sager PT, Saxon LA, Kocovic D, Harada T, Wiener I, Khan H. Exploring postinfarction reentrant ventricular tachycardia with entrainment mapping. *Journal of the American College of Cardiology*. 1997;29:1180-1189.

26. Jackson N, Gizurarson S, Viswanathan K, King B, Massé S, Kusha M, Porta-Sanchez A, Jacob JR, Khan F, Das M. Decrement evoked potential mapping: basis of a mechanistic strategy for ventricular tachycardia ablation. *Circulation: Arrhythmia and Electrophysiology*. 2015;8:1433-1442.

27. Josephson ME, Anter E. Substrate mapping for ventricular tachycardia: assumptions and misconceptions. *JACC: Clinical Electrophysiology*. 2015;1:341-352.

28. Bunch TJ, Weiss JP, Crandall BG, Day JD, DiMarco JP, Ferguson JD, Mason PK, McDANIEL G, Osborn JS, Wiggins D. Image integration using intracardiac ultrasound and 3D reconstruction for scar mapping and ablation of ventricular tachycardia. *Journal of cardiovascular electrophysiology*. 2010;21:678-684.

29. Perez-David E, Arenal Á, Rubio-Guivernau JL, Del Castillo R, Atea L, Arbelo E, Caballero E, Celorrio V, Datino T, Gonzalez-Torrecilla E. Noninvasive identification of ventricular tachycardia-related conducting channels using contrast-enhanced magnetic resonance imaging in patients with chronic myocardial infarction: comparison of signal intensity scar mapping and endocardial voltage mapping. *Journal of the American College of Cardiology*. 2011;57:184-194.

30. Esposito A, Palmisano A, Antunes S, Maccabelli G, Colantoni C, Rancoita PMV, Baratto F, Di Serio C, Rizzo G, De Cobelli F. Cardiac CT with delayed enhancement in the characterization of ventricular tachycardia structural substrate: relationship between CT-segmented scar and electro-anatomic mapping. *JACC: Cardiovascular Imaging*. 2016;9:822-832.

31. Kautzner J, Peichl P. Pulsed Field Ablation in Ventricular Arrhythmias. *Cardiac Electrophysiology Clinics*. 2025.

32. Liulu X, Balaji P, Barber J, De Silva K, Murray T, Hickey A, Campbell T, Harris J, Gee H, Ahern V. Radiation therapy for ventricular arrhythmias. *Journal of Medical Imaging and Radiation Oncology*. 2024;68:893-913.

33. Anderson RD, Kumar S, Kalman JM, Sanders P, Sacher F, Hocini M, Jais P, Haïsaguerre M, Lee G. Catheter ablation of ventricular fibrillation. *Heart, Lung and Circulation*. 2019;28:110-122.

34. Pathak RK, Ariyarathna N, Garcia FC, Sanders P, Marchlinski FE. Catheter ablation of idiopathic ventricular arrhythmias. *Heart, Lung and Circulation*. 2019;28:102-109.

35. Sirichand S, Killu AM, Padmanabhan D, Hodge DO, Chamberlain AM, Brady PA, Kapa S, Noseworthy PA, Packer DL, Munger TM. Incidence of idiopathic ventricular arrhythmias: a population-based study. *Circulation: Arrhythmia and Electrophysiology*. 2017;10:e004662.

36. Nakagawa M, Takahashi N, Nobe S, Ichinose M, Ooie T, Yufu F, Shigematsu S, Hara M, Yonemochi H, Saikawa T. Gender differences in various types of idiopathic ventricular tachycardia. *Journal of cardiovascular electrophysiology*. 2002;13:633-638.

37. Pham TV, Sosunov EA, Gainullin RZ, Danilo Jr P, Rosen MR. Impact of sex and gonadal steroids on prolongation of ventricular repolarization and arrhythmias induced by I K-blocking drugs. *Circulation*. 2001;103:2207-2212.

38. Yamada T. Idiopathic ventricular arrhythmias: relevance to the anatomy, diagnosis and treatment. *Journal of Cardiology*. 2016;68:463-471.

39. Tzeis S, Asvestas D, Ho SY, Vardas P. Electrocardiographic landmarks of idiopathic ventricular arrhythmia origins. *Heart*. 2019;105:1109-1116.

40. Iwai S, Cantillon DJ, Kim RJ, Markowitz SM, Mittal S, Stein KM, Shah BK, Yarlagadda RK, Cheung JW, Tan VR. Right and left ventricular outflow tract tachycardias: evidence for a common electrophysiologic mechanism. *Journal of cardiovascular electrophysiology*. 2006;17:1052-1058.

41. Enriquez A, Supple GE, Marchlinski FE, Garcia FC. How to map and ablate papillary muscle ventricular arrhythmias. *Heart rhythm*. 2017;14:1721-1728.

42. Nava A, Thiene G, Canciani B, Martini B, Daliento L, Buja G, Fasoli G. Clinical profile of concealed form of arrhythmogenic right ventricular cardiomyopathy presenting with apparently idiopathic ventricular arrhythmias. *International journal of cardiology*. 1992;35:195-206.

43. Chimenti C, Calabrese F, Thiene G, Pieroni M, Maseri A, Frustaci A. Inflammatory left ventricular microaneurysms as a cause of apparently idiopathic ventricular tachyarrhythmias. *Circulation*. 2001;104:168-173.

44. Nucifora G, Muser D, Masci PG, Barison A, Rebellato L, Piccoli G, Daleffe E, Toniolo M, Zanuttini D, Facchin D. Prevalence and prognostic value of concealed structural abnormalities in patients with apparently idiopathic ventricular arrhythmias of left versus right ventricular origin: a magnetic resonance imaging study. *Circulation: Arrhythmia and Electrophysiology*. 2014;7:456-462.

45. Basile P, Soldato N, Pedio E, Siena P, Carella MC, Dentamaro I, Khan Y, Baggiano A, Mushtaq S, Forleo C. Cardiac magnetic resonance reveals concealed structural heart disease in patients with frequent premature ventricular contractions and normal echocardiography: A systematic review. *International Journal of Cardiology*. 2024:132306.

46. Rodriguez B, Trayanova N, Noble D. Modeling cardiac ischemia. *Annals of the New York academy of sciences*. 2006;1080:395-414.

47. Saffitz JE. The pathology of sudden cardiac death in patients with ischemic heart disease—arrhythmology for anatomic pathologists. *Cardiovascular Pathology*. 2005;14:195-203.

48. Akar JG, Akar FG. Regulation of ion channels and arrhythmias in the ischemic heart. *Journal of Electrocardiology*. 2007;40:S37-S41.

49. Rodriguez B, Tice BM, Eason JC, Aguel F, Ferrero Jr JM, Trayanova N. Effect of acute global ischemia on the upper limit of vulnerability: a simulation study. *American Journal of Physiology-Heart and Circulatory Physiology*. 2004;286:H2078-H2088.

50. Di Diego JM, Antzelevitch C. Ischemic ventricular arrhythmias: experimental models and their clinical relevance. *Heart rhythm*. 2011;8:1963-1968.

51. Heusch G. Myocardial ischemia/reperfusion: Translational pathophysiology of ischemic heart disease. *Med*. 2024;5:10-31.

52. Pandozi C, Mariani MV, Chimenti C, Maestrini V, Filomena D, Magnocavallo M, Straito M, Piro A, Russo M, Galeazzi M. The scar: the wind in the perfect storm—insights into the mysterious living tissue originating ventricular arrhythmias. *Journal of interventional cardiac electrophysiology*. 2023;66:27-38.

53. Mallory GK, White PD, Salcedo-Salgar J. The speed of healing of myocardial infarction: a study of the pathologic anatomy in seventy-two cases. *American Heart Journal*. 1939;18:647-671.

54. Reimer KA, Lowe JE, Rasmussen MM, Jennings RB. The wavefront phenomenon of ischemic cell death. 1. Myocardial infarct size vs duration of coronary occlusion in dogs. *Circulation*. 1977;56:786-794.

55. Baroldi G, Silver MD, De Maria R, Parodi O, Pellegrini A. Lipomatous metaplasia in left ventricular scar. *The Canadian journal of cardiology*. 1997;13:65-71.

56. Pouliopoulos J, Chik WW, Kanthan A, Sivagangabalan G, Barry MA, Fahmy PN, Midekin C, Lu J, Kizana E, Thomas SP. Intramyocardial adiposity after myocardial infarction: new implications of a substrate for ventricular tachycardia. *Circulation*. 2013;128:2296-2308.

57. Reddy VY, Wrobleski D, Houghtaling C, Josephson ME, Ruskin JN. Combined epicardial and endocardial electroanatomic mapping in a porcine model of healed myocardial infarction. *Circulation*. 2003;107:3236-3242.

58. Miyazaki S, Fujiwara H, Onodera T, Kihara Y, Matsuda M, Wu D, Nakamura Y, Kumada T, Sasayama S, Kawai C. Quantitative analysis of contraction band and coagulation necrosis after ischemia and reperfusion in the porcine heart. *Circulation*. 1987;75:1074-1082.

59. Glashan CA, Tofig BJ, Tao Q, Blom SA, Jongbloed MR, Nielsen JC, Lukac P, Kristiansen SB, Zeppenfeld K. Multisize electrodes for substrate identification in ischemic cardiomyopathy: validation by integration of whole heart histology. *JACC: Clinical Electrophysiology*. 2019;5:1130-1140.

60. Wijnmaalen AP, Schalij MJ, von der Thüsen JH, Klautz RJ, Zeppenfeld K. Early reperfusion during acute myocardial infarction affects ventricular tachycardia characteristics and the chronic electroanatomic and histological substrate. *Circulation*. 2010;121:1887-1895.

61. Piers SR, Wijnmaalen AP, Borleffs CJW, van Huls van Taxis CF, Thijssen J, van Rees JB, Cannegieter SC, Bax JJ, Schalij MJ, Zeppenfeld K. Early reperfusion therapy affects inducibility, cycle length, and occurrence of ventricular tachycardia late after myocardial infarction. *Circulation: Arrhythmia and Electrophysiology*. 2011;4:195-201.

62. Richardson P. Report of the 1995 World Health Organization/International Society and Federation of Cardiology Task Force on the definition and classification of cardiomyopathies. *Circulation*. 1996;93:841-842.

63. Maron BJ, Towbin JA, Thiene G, Antzelevitch C, Corrado D, Arnett D, Moss AJ, Seidman CE, Young JB. Contemporary definitions and classification of the cardiomyopathies: an American Heart Association scientific statement from the council on clinical cardiology, heart failure and transplantation committee; quality of care and outcomes research and functional genomics and translational biology interdisciplinary working groups; and council on epidemiology and prevention. *Circulation*. 2006;113:1807-1816.

64. Elliott P, Andersson B, Arbustini E, Bilinska Z, Cecchi F, Charron P, Dubourg O, Kühl U, Maisch B, McKenna WJ. Classification of the cardiomyopathies: a position statement from the European Society Of Cardiology Working Group on Myocardial and Pericardial Diseases. *European heart journal*. 2008;29:270-276.

65. Soejima K, Stevenson WG, Sapp JL, Selwyn AP, Couper G, Epstein LM. Endocardial and epicardial radiofrequency ablation of ventricular tachycardia associated with dilated cardiomyopathy: the importance of low-voltage scars. *Journal of the American College of Cardiology*. 2004;43:1834-1842.

66. Oloriz T, Silberbauer J, Maccabelli G, Mizuno H, Baratto F, Kirubakaran S, Vergara P, Bisceglia C, Santagostino G, Marzi A. Catheter ablation of ventricular arrhythmia in nonischemic cardiomyopathy: anteroseptal versus inferolateral scar sub-types. *Circulation: Arrhythmia and Electrophysiology*. 2014;7:414-423.

67. De Frutos F, Ochoa JP, Fernández AI, Gallego-Delgado M, Navarro-Peñalver M, Casas G, Basurte MT, Larrañaga-Moreira JM, Mogollón MV, Robles-Mezcua A. Late gadolinium enhancement distribution patterns in non-ischaemic dilated cardiomyopathy: genotype–phenotype correlation. *European Heart Journal-Cardiovascular Imaging*. 2024;25:75-85.

68. Liuba I, Frankel DS, Riley MP, Hutchinson MD, Lin D, Garcia FC, Callans DJ, Supple GE, Dixit S, Bala R. Scar progression in patients with nonischemic cardiomyopathy and ventricular arrhythmias. *Heart Rhythm*. 2014;11:755-762.

69. Bhaskaran A, Bhat A, Trivic I, Muthiah K, Barrett W, Liang S, Kanthan A, Kumar S. Biventricular, endocardial, and epicardial substrate characterization for ventricular tachycardia and correlation with whole-heart macropathology and histopathology in a patient with lamin A/C cardiomyopathy. *HeartRhythm Case Reports*. 2019;5:128-133.

70. Glashan CA, Androulakis AF, Tao Q, Glashan RN, Wisse LJ, Ebert M, de Ruiter MC, van Meer BJ, Brouwer C, Dekkers OM. Whole human heart histology to validate electroanatomical voltage mapping in patients with non-ischaemic cardiomyopathy and ventricular tachycardia. *European heart journal*. 2018;39:2867-2875.

71. Bennett RG, Garikapati K, Anderson RD, Silva KD, Campbell T, Kotake Y, Turnbull S, Tonchev I, Lee G, Kalman J. Clinical, electroanatomic and electrophysiologic characterization and outcomes of catheter ablation for ventricular tachycardia following valvular intervention. *Journal of Cardiovascular Electrophysiology*. 2022;33:589-604.

72. Isbister J, Semsarian C. Sudden cardiac death: an update. *Internal medicine journal*. 2019;49:826-833.

73. Kitamura T, Iwami T, Kawamura T, Nitta M, Nagao K, Nonogi H, Yonemoto N, Kimura T. Nationwide improvements in survival from out-of-hospital cardiac arrest in Japan. *Circulation*. 2012;126:2834-2843.

74. Jennings PA, Cameron P, Walker T, Bernard S, Smith K. Out-of-hospital cardiac arrest in Victoria: rural and urban outcomes. *Medical Journal of Australia*. 2006;185:135-139.

75. Butters A, Arnott C, Sweeting J, Winkel BG, Semsarian C, Ingles J. Sex disparities in sudden cardiac death. *Circulation: Arrhythmia and Electrophysiology*. 2021;14:e009834.

76. Fox CS, Evans JC, Larson MG, Kannel WB, Levy D. Temporal trends in coronary heart disease mortality and sudden cardiac death from 1950 to 1999: the Framingham Heart Study. *Circulation*. 2004;110:522-527.

77. Ghajar A, Sargeant MM, Catanzaro JN, Philips B, Assis FR, Nekkanti R, Sears SF, Shantha G. US National trends in mortality related to ventricular tachycardia/ventricular fibrillation. *Journal of Interventional Cardiac Electrophysiology*. 2025:1-3.

78. Holmberg M, Holmberg S, Herlitz J. The problem of out-of-hospital cardiac-arrest prevalence of sudden death in Europe today. *The American journal of cardiology*. 1999;83:88-90.

79. Beck B, Bray J, Cameron P, Smith K, Walker T, Grantham H, Hein C, Thorrowgood M, Smith A, Inoue M. Regional variation in the characteristics, incidence and outcomes of out-of-hospital cardiac arrest in Australia and New Zealand: results from the Aus-ROC Epistry. *Resuscitation*. 2018;126:49-57.

80. Gorenek B, Wijnmaalen AP, Goette A, Mert GO, Porter B, Gustafsson F, Dan GA, Ector J, Stuehlinger M, Spartalis M, Gosau N, Amir O, Chioncel O. Ventricular arrhythmias in acute heart failure: a clinical consensus statement of the Association for Acute CardioVascular Care, the European Heart Rhythm Association, and the Heart Failure Association of the European Society of Cardiology. *Europace*. 2024;26:euae235.

81. Ebinger MW, Krishnan S, Schuger CD. Mechanisms of ventricular arrhythmias in heart failure. *Current heart failure reports*. 2005;2:111-117.

82. Franz MR, Cima R, Wang D, Profitt D, Kurz R. Electrophysiological effects of myocardial stretch and mechanical determinants of stretch-activated arrhythmias. *Circulation*. 1992;86:968-978.

83. Chrispin J, Merchant FM, Lakdawala NK, Wu KC, Tomaselli GF, Navara R, Torbey E, Ambardekar AV, Kabra R, Arbustini E. Risk of arrhythmic death in patients with nonischemic cardiomyopathy: JACC review topic of the week. *Journal of the American College of Cardiology*. 2023;82:735-747.

84. Beuckelmann DJ, Näbauer M, Erdmann E. Alterations of K+ currents in isolated human ventricular myocytes from patients with terminal heart failure. *Circulation research*. 1993;73:379-385.

85. Santangeli P, Rame JE, Birati EY, Marchlinski FE. Management of ventricular arrhythmias in patients with advanced heart failure. *Journal of the American College of Cardiology*. 2017;69:1842-1860.

86. Sohns C, Fink T, Crijns HJ, Costard-Jaeckle A, Marrouche NF, Sossalla S, Schramm R, El Hamriti M, Moersdorf M, Didenko M. Preventive catheter ablation for ventricular arrhythmias in patients with end-stage heart failure referred for heart transplantation evaluation: Rationale for and design of the CASTLE-VT trial. *European journal of heart failure*. 2024.

87. World Health Organization. Constitution the World Health Organization. *Bulletin of the World Health Organization*. 1947;1:29-41.

88. Nichol G, Stiell IG, Hebert P, Wells GA, Vandemheen K, Laupacis A. What is the quality of life for survivors of cardiac arrest? A prospective study. *Academic Emergency Medicine*. 1999;6:95-102.

89. Wachelder EM, Moulaert V, van Heugten C, Verbunt JA, Bekkers SC, Wade DT. Life after survival: long-term daily functioning and quality of life after an out-of-hospital cardiac arrest. *Resuscitation*. 2009;80:517-522.

90. HUANG CX, LIANG JJ, Yang B, Jiang H, TANG QZ, LIU XJ, WAN WG, JIAN XL. Quality of life and cost for patients with premature ventricular contractions by radiofrequency catheter ablation. *Pacing and clinical electrophysiology*. 2006;29:343-350.

91. Januszkiewicz Ł, Barra S, Providencia R, Conte G, de Asmundis C, Chun JK, Farkowski MM, Guerra JM, Marijon E, Boveda S. Long-term quality of life and acceptance of implantable cardioverter-defibrillator therapy: results of the European Heart Rhythm Association survey. *EP Europace*. 2022;24:860-867.

92. Zormpas C, Kahl KG, Hohmann S, Oswald H, Stiel C, Veltmann C, Bauersachs J, Duncker D. Depressive symptoms and quality of life in patients with heart failure and an implantable cardioverter-defibrillator. *Frontiers in psychiatry*. 2022;13:827967.

93. Herbst JH, Goodman M, Feldstein S, Reilly JM. Health-related quality-of-life assessment of patients with life-threatening ventricular arrhythmias. *Pacing and Clinical Electrophysiology*. 1999;22:915-926. doi: 10.1111/j.1540-8159.1999.tb06816.x

94. Anderson RD, Lee G, Trivic I, Campbell T, Pham T, Nalliah C, Kizana E, Thomas SP, Trivedi SJ, Watts T. Focal ventricular tachycardias in structural heart disease: prevalence, characteristics, and clinical outcomes after catheter ablation. *JACC: Clinical Electrophysiology*. 2020;6:56-69.

95. Vetulli HM, Elizari MV, Naccarelli GV, Gonzalez MD. Cardiac automaticity: basic concepts and clinical observations. *Journal of Interventional Cardiac Electrophysiology*. 2018;52:263-270.

96. Enriquez A, Riley M, Marchlinski F. Noninvasive clues for diagnosing ventricular tachycardia mechanism. *Journal of Electrocardiology*. 2018;51:163-169.

97. Markowitz SM, Lerman BB. Mechanisms of focal ventricular tachycardia in humans. *Heart Rhythm*. 2009;6:S81-S85.

98. Nerbonne JM, Kass RS. Molecular physiology of cardiac repolarization. *Physiological reviews*. 2005;85:1205-1253.

99. Ciaccio EJ, Anter E, Coromilas J, Wan EY, Yarmohammadi H, Wit AL, Peters NS, Garan H. Structure and function of the ventricular tachycardia isthmus. *Heart Rhythm*. 2022;19:137-153.

100. Ciaccio EJ, Coromilas J, Wit AL, Peters NS, Garan H. Formation of functional conduction block during the onset of reentrant ventricular tachycardia. *Circulation: Arrhythmia and Electrophysiology*. 2016;9:e004462.

101. Martin R, Hocini M, Haïsaguerre M, Jaïs P, Sacher F. Ventricular tachycardia isthmus characteristics: insights from high-density mapping. *Arrhythmia & Electrophysiology Review*. 2019;8:54.

102. WELLENS HJ, Schuilenburg RM, Durrer D. Electrical stimulation of the heart in patients with ventricular tachycardia. *Circulation*. 1972;46:216-226.

103. De Bakker J, Van Capelle F, Janse MJ, Tasseron S, Vermeulen JT, de Jonge N, Lahpor JR. Slow conduction in the infarcted human heart. 'Zigzag'course of activation. *Circulation*. 1993;88:915-926.

104. Sugrue DD, Holmes Jr DR, Gersh BJ, Edwards WD, McLaran CJ, Wood DL, Osborn MJ, Hammill SC. Cardiac histologic findings in patients with life-threatening ventricular

arrhythmias of unknown origin. *Journal of the American College of Cardiology*. 1984;4:952-957.

105. Roberts DE, Hersh LT, Scher AM. Influence of cardiac fiber orientation on wavefront voltage, conduction velocity, and tissue resistivity in the dog. *Circulation research*. 1979;44:701-712.

106. Spach MS, Miller 3rd W, Geselowitz DB, Barr RC, Kootsey JM, Johnson EA. The discontinuous nature of propagation in normal canine cardiac muscle. Evidence for recurrent discontinuities of intracellular resistance that affect the membrane currents. *Circulation research*. 1981;48:39-54.

107. Gough WB, Mehra R, Restivo M, Zeiler RH, El-Sherif N. Reentrant ventricular arrhythmias in the late myocardial infarction period in the dog. 13. Correlation of activation and refractory maps. *Circulation Research*. 1985;57:432-442.

108. Pogwizd SM, Corr PB. Reentrant and nonreentrant mechanisms contribute to arrhythmogenesis during early myocardial ischemia: results using three-dimensional mapping. *Circulation research*. 1987;61:352-371.

109. El-Sherif N, Gough WB, Zeiler RH, Hariman R. Reentrant ventricular arrhythmias in the late myocardial infarction period. 12. Spontaneous versus induced reentry and intramural versus epicardial circuits. *Journal of the American College of Cardiology*. 1985;6:124-132.

110. Anter E, Tschabrunn CM, Buxton AE, Josephson ME. High-resolution mapping of postinfarction reentrant ventricular tachycardia: electrophysiological characterization of the circuit. *Circulation*. 2016;134:314-327.

111. Stevenson WG, Khan H, Sager P, Saxon L, Middlekauff H, Natterson P, Wiener I. Identification of reentry circuit sites during catheter mapping and radiofrequency ablation

of ventricular tachycardia late after myocardial infarction. *Circulation*. 1993;88:1647-1670.

112. Graham AJ, Orini M, Lambiase PD. Limitations and challenges in mapping ventricular tachycardia: new technologies and future directions. *Arrhythmia & electrophysiology review*. 2017;6:118.

113. Josephson ME, Harken AH, Horowitz LN. Endocardial excision: a new surgical technique for the treatment of recurrent ventricular tachycardia. *Circulation*. 1979;60:1430-1439.

114. Kaltenbrunner W, Cardinal R, Dubuc M, Shenasa M, Nadeau R, Tremblay G, Vermeulen M, Savard P, Page P. Epicardial and endocardial mapping of ventricular tachycardia in patients with myocardial infarction. Is the origin of the tachycardia always subendocardially localized? *Circulation*. 1991;84:1058-1071.

115. Fenoglio Jr J, Pham TD, Harken A, Horowitz L, Josephson M, Wit A. Recurrent sustained ventricular tachycardia: structure and ultrastructure of subendocardial regions in which tachycardia originates. *Circulation*. 1983;68:518-533.

116. Bolick DR, Hackel D, Reimer K, Ideker R. Quantitative analysis of myocardial infarct structure in patients with ventricular tachycardia. *Circulation*. 1986;74:1266-1279.

117. Kostin S, Rieger M, Dammer S, Hein S, Richter M, Klövekorn W-P, Bauer EP, Schaper J. Gap junction remodeling and altered connexin43 expression in the failing human heart. *Molecular and Cellular Biochemistry*. 2003:135-144.

118. Smith J, Green C, Peters N, Rothery S, Severs N. Altered patterns of gap junction distribution in ischemic heart disease. An immunohistochemical study of human myocardium using laser scanning confocal microscopy. *The American journal of pathology*. 1991;139:801.

119. Greener ID, Sasano T, Wan X, Igarashi T, Strom M, Rosenbaum DS, Donahue JK. Connexin43 gene transfer reduces ventricular tachycardia susceptibility after myocardial infarction. *Journal of the American College of Cardiology*. 2012;60:1103-1110.

120. Donahue JK, Chrispin J, Ajijola OA. Mechanism of ventricular tachycardia occurring in chronic myocardial infarction scar. *Circulation research*. 2024;134:328-342.

121. Bogun F, Krishnan S, Siddiqui M, Good E, Marine JE, Schuger C, Oral H, Chugh A, Pelosi F, Morady F. Electrogram characteristics in postinfarction ventricular tachycardia: effect of infarct age. *Journal of the American College of Cardiology*. 2005;46:667-674.

122. Crawford T, Cowger J, Desjardins B, Kim HM, Good E, Jongnarangsin K, Oral H, Chugh A, Pelosi F, Morady F. Determinants of postinfarction ventricular tachycardia. *Circulation: Arrhythmia and Electrophysiology*. 2010;3:624-631.

123. Su L, Siegel JE, Fishbein MC. Adipose tissue in myocardial infarction. *Cardiovascular Pathology*. 2004;13:98-102.

124. Mordi I, Radjenovic A, Stanton T, Gardner RS, McPhaden A, Carrick D, Berry C, Tzemos N. Prevalence and prognostic significance of lipomatous metaplasia in patients with prior myocardial infarction. *JACC: Cardiovascular Imaging*. 2015;8:1111-1112.

125. Ichikawa Y, Kitagawa K, Chino S, Ishida M, Matsuoka K, Tanigawa T, Nakamura T, Hirano T, Takeda K, Sakuma H. Adipose tissue detected by multislice computed tomography in patients after myocardial infarction. *JACC: Cardiovascular Imaging*. 2009;2:548-555.

126. Cokic I, Chan SF, Guan X, Nair AR, Yang H-J, Liu T, Chen Y, Hernando D, Sykes J, Tang R. Intramyocardial hemorrhage drives fatty degeneration of infarcted myocardium. *Nature Communications*. 2022;13:6394.

127. Samanta R, Kumar S, Chik W, Qian P, Barry MA, Al Raisi S, Bhaskaran A, Farraha M, Nadri F, Kizana E. Influence of intramyocardial adipose tissue on the accuracy of endocardial contact mapping of the chronic myocardial infarction substrate. *Circulation: Arrhythmia and Electrophysiology*. 2017;10:e004998.

128. Sasaki T, Calkins H, Miller CF, Zviman MM, Zipunnikov V, Arai T, Sawabe M, Terashima M, Marine JE, Berger RD. New insight into scar-related ventricular tachycardia circuits in ischemic cardiomyopathy: Fat deposition after myocardial infarction on computed tomography--A pilot study. *Heart rhythm*. 2015;12:1508-1518.

129. Sung E, Prakosa A, Aronis KN, Zhou S, Zimmerman SL, Tandri H, Nazarian S, Berger RD, Chrispin J, Trayanova NA. Personalized digital-heart technology for ventricular tachycardia ablation targeting in hearts with infiltrating adiposity. *Circulation: Arrhythmia and Electrophysiology*. 2020;13:e008912.

130. Xu L, Zahid S, Khoshknab M, Moss J, Berger RD, Chrispin J, Callans D, Marchlinski FE, Zimmerman SL, Han Y. Lipomatous metaplasia facilitates slow conduction in critical ventricular tachycardia corridors within postinfarct myocardium. *Clinical Electrophysiology*. 2023;9:1235-1245.

131. Xu L, Khoshknab M, Berger RD, Chrispin J, Dixit S, Santangeli P, Callans D, Marchlinski FE, Zimmerman SL, Han Y. Lipomatous metaplasia enables ventricular tachycardia by reducing current loss within the protected corridor. *Clinical Electrophysiology*. 2022;8:1274-1285.

132. Xu L, Zahid S, Khoshknab M, Moss J, Berger RD, Chrispin J, Callans D, Marchlinski FE, Zimmerman SL, Han Y. Lipomatous metaplasia prolongs repolarization and increases

repolarization dispersion within post-infarct ventricular tachycardia circuit cites. *Europace*. 2023;25:496-505.

133. Xu L, Khoshknab M, Moss J, Berger RD, Chrispin J, Callans D, Marchlinski FE, Zimmerman SL, Han Y, Trayanova N. Lipomatous metaplasia is associated with ventricular tachycardia recurrence following ablation in patients with nonischemic cardiomyopathy. *JACC: Clinical Electrophysiology*. 2024;10:1135-1146.

134. Xu L, Khoshknab M, Moss J, Yang LC, Berger RD, Chrispin J, Callans D, Marchlinski FE, Zimmerman SL, Han Y. Lipomatous Metaplasia Facilitates Ventricular Tachycardia in Patients With Nonischemic Cardiomyopathy. *JACC: Clinical Electrophysiology*. 2024;10:2325-2336.

135. Mirowski M, Mower MM, Gott VL, Brawley RK. Feasibility and effectiveness of low-energy catheter defibrillation in man. *Circulation*. 1973;47:79-85.

136. Mirowski M, Mower M, Langer A, Heilman M, Schreibman J. A chronically implanted system for automatic defibrillation in active conscious dogs. Experimental model for treatment of sudden death from ventricular fibrillation. *Circulation*. 1978;58:90-94.

137. Mirowski M, Reid PR, Mower MM, Watkins L, Gott VL, Schauble JF, Langer A, Heilman M, Kolenik SA, Fischell RE. Termination of malignant ventricular arrhythmias with an implanted automatic defibrillator in human beings. *New England Journal of Medicine*. 1980;303:322-324.

138. Lown B, Axelrod P. Implanted standby defibrillators. *Circulation*. 1972;46:637-639.

139. Echt DS, Armstrong K, Schmidt P, Oyer P, Stinson E, Winkle R. Clinical experience, complications, and survival in 70 patients with the automatic implantable cardioverter/defibrillator. *Circulation*. 1985;71:289-296.

140. Kelly PA, Cannom DS, Garan H, Mirabal GS, Harthorne JW, Hurvitz RJ, Vlahakes GJ, Jacobs ML, Ilvento JP, Buckley MJ. The automatic implantable cardioverter defibrillator: efficacy, complications and survival in patients with malignant ventricular arrhythmias. *Journal of the American College of Cardiology*. 1988;11:1278-1286.

141. Investigators AvID. A comparison of antiarrhythmic-drug therapy with implantable defibrillators in patients resuscitated from near-fatal ventricular arrhythmias. *New England Journal of Medicine*. 1997;337:1576-1584.

142. Connolly SJ, Gent M, Roberts RS, Dorian P, Roy D, Sheldon RS, Mitchell LB, Green MS, Klein GJ, O'Brien B. Canadian Implantable Defibrillator Study (CIDS) a randomized trial of the implantable cardioverter defibrillator against amiodarone. *Circulation*. 2000;101:1297-1302.

143. Kuck K-H, Cappato R, Siebels Jr, Rüppel R. Randomized comparison of antiarrhythmic drug therapy with implantable defibrillators in patients resuscitated from cardiac arrest: the Cardiac Arrest Study Hamburg (CASH). *Circulation*. 2000;102:748-754.

144. Connolly SJ, Hallstrom A, Cappato R, Schron EB, Kuck K-H, Zipes DP, Greene HL, Boczor S, Domanski M, Follmann D. Meta-analysis of the implantable cardioverter defibrillator secondary prevention trials. *European heart journal*. 2000;21:2071-2078.

145. Moss AJ, Hall WJ, Cannom DS, Daubert JP, Higgins SL, Klein H, Levine JH, Saksena S, Waldo AL, Wilber D. Improved survival with an implanted defibrillator in patients with coronary disease at high risk for ventricular arrhythmia. *New England Journal of Medicine*. 1996;335:1933-1940.

146. Moss AJ, Zareba W, Hall WJ, Klein H, Wilber DJ, Cannom DS, Daubert JP, Higgins SL, Brown MW, Andrews ML. Prophylactic implantation of a defibrillator in patients with

myocardial infarction and reduced ejection fraction. *New England Journal of Medicine*. 2002;346:877-883.

147. Goldenberg I, Gillespie J, Moss AJ, Hall WJ, Klein H, McNitt S, Brown MW, Cygankiewicz I, Zareba W, II ECotMADIT. Long-term benefit of primary prevention with an implantable cardioverter-defibrillator: an extended 8-year follow-up study of the Multicenter Automatic Defibrillator Implantation Trial II. *Circulation*. 2010;122:1265-1271.

148. Hohnloser SH, Kuck KH, Dorian P, Roberts RS, Hampton JR, Hatala R, Fain E, Gent M, Connolly SJ. Prophylactic use of an implantable cardioverter–defibrillator after acute myocardial infarction. *New England Journal of Medicine*. 2004;351:2481-2488.

149. Bardy GH, Lee KL, Mark DB, Poole JE, Packer DL, Boineau R, Domanski M, Troutman C, Anderson J, Johnson G. Amiodarone or an implantable cardioverter–defibrillator for congestive heart failure. *New England Journal of Medicine*. 2005;352:225-237.

150. Bänsch D, Antz M, Boczor S, Volkmer M, Tebbenjohanns Jr, Seidl K, Block M, Gietzen F, Berger Jr, Kuck KH. Primary prevention of sudden cardiac death in idiopathic dilated cardiomyopathy: the Cardiomyopathy Trial (CAT). *Circulation*. 2002;105:1453-1458.

151. Strickberger SA, Hummel JD, Bartlett TG, Frumin HI, Schuger CD, Beau SL, Bitar C, Morady F, Investigators A. Amiodarone versus implantable cardioverter-defibrillator: randomized trial in patients with nonischemicdilated cardiomyopathy and asymptomaticnonsustained ventricular tachycardia—AMIOVIRT. *Journal of the American College of Cardiology*. 2003;41:1707-1712.

152. Kadish A, Dyer A, Daubert JP, Quigg R, Estes NM, Anderson KP, Calkins H, Hoch D, Goldberger J, Shalaby A. Prophylactic defibrillator implantation in patients with

nonischemic dilated cardiomyopathy. *New England Journal of Medicine*. 2004;350:2151-2158.

153. Køber L, Thune JJ, Nielsen JC, Haarbo J, Videbæk L, Korup E, Jensen G, Hildebrandt P, Steffensen FH, Bruun NE. Defibrillator implantation in patients with nonischemic systolic heart failure. *New England Journal of Medicine*. 2016;375:1221-1230.

154. Leyva F, Nisam S, Auricchio A. 20 years of cardiac resynchronization therapy. *Journal of the American College of Cardiology*. 2014;64:1047-1058.

155. Bristow MR, Saxon LA, Boehmer J, Krueger S, Kass DA, De Marco T, Carson P, DiCarlo L, DeMets D, White BG. Cardiac-resynchronization therapy with or without an implantable defibrillator in advanced chronic heart failure. *New England Journal of Medicine*. 2004;350:2140-2150.

156. Moss AJ, Hall WJ, Cannom DS, Klein H, Brown MW, Daubert JP, Estes Iii NAM, Foster E, Greenberg H, Higgins SL. Cardiac-resynchronization therapy for the prevention of heart-failure events. *New England Journal of Medicine*. 2009;361:1329-1338.

157. Tang AS, Wells GA, Talajic M, Arnold MO, Sheldon R, Connolly S, Hohnloser SH, Nichol G, Birnie DH, Sapp JL. Cardiac-resynchronization therapy for mild-to-moderate heart failure. *New England Journal of Medicine*. 2010;363:2385-2395.

158. Sapp JL, Sivakumaran S, Redpath CJ, Khan H, Parkash R, Exner DV, Healey JS, Thibault B, Sterns LD, Lam NHN. Long-term outcomes of resynchronization–defibrillation for heart failure. *New England Journal of Medicine*. 2024;390:212-220.

159. Ruwald MH, Solomon SD, Foster E, Kutyifa V, Ruwald A-C, Sherazi S, McNitt S, Jons C, Moss AJ, Zareba W. Left ventricular ejection fraction normalization in cardiac resynchronization therapy and risk of ventricular arrhythmias and clinical outcomes:

results from the Multicenter Automatic Defibrillator Implantation Trial With Cardiac Resynchronization Therapy (MADIT–CRT) trial. *Circulation*. 2014;130:2278-2286.

160. Sapp JL, Parkash R, Wells GA, Yetisir E, Gardner MJ, Healey JS, Thibault B, Sterns LD, Birnie D, Nery PB. Cardiac resynchronization therapy reduces ventricular arrhythmias in primary but not secondary prophylactic implantable cardioverter defibrillator patients: Insight from the resynchronization in ambulatory heart failure trial. *Circulation: Arrhythmia and Electrophysiology*. 2017;10:e004875.

161. Vaughan Williams EM. Classification of antidysrhythmic drugs. *Pharmacology & Therapeutics. Part B: General and Systematic Pharmacology*. 1975;1:115-138.

162. Ho DS, Zecchin RP, Richards DA, Uther JB, Ross DL. Double-blind trial of lignocaine versus sotalol for acute termination of spontaneous sustained ventricular tachycardia. *The Lancet*. 1994;344:18-23.

163. Gorgels AP, van den Dool A, Hofs A, Mulleneers R, Smeets JL, Vos MA, Wellens HJ. Comparison of procainamide and lidocaine in terminating sustained monomorphic ventricular tachycardia. *The American journal of cardiology*. 1996;78:43-46.

164. Nasir Jr N, Taylor A, Doyle TK, Pacifico A. Evaluation of intravenous lidocaine for the termination of sustained monomorphic ventricular tachycardia in patients with coronary artery disease with or without healed myocardial infarction. *The American journal of cardiology*. 1994;74:1183-1186.

165. Armengol RE, Graff J, Baerman JM, Swiryn S. Lack of effectiveness of lidocaine for sustained, wide QRS complex tachycardia. *Annals of emergency medicine*. 1989;18:254-257.

166. Somberg JC, Bailin SJ, Haffajee CI, Paladino WP, Kerin NZ, Bridges D, Timar S, Molnar J, Investigators A-A. Intravenous lidocaine versus intravenous amiodarone (in a new aqueous formulation) for incessant ventricular tachycardia. *The American journal of cardiology*. 2002;90:853-859.

167. van der Ree MH, van Dussen L, Rosenberg N, Stolwijk N, van den Berg S, van der Wel V, Jacobs BA, Wilde AA, Hollak CE, Postema PG. Effectiveness and safety of mexiletine in patients at risk for (recurrent) ventricular arrhythmias: a systematic review. *EP Europace*. 2022;24:1809-1823.

168. Sapp JL, Wells GA, Parkash R, Stevenson WG, Blier L, Sarrazin J-F, Thibault B, Rivard L, Gula L, Leong-Sit P. Ventricular tachycardia ablation versus escalation of antiarrhythmic drugs. *New England Journal of Medicine*. 2016;375:111-121.

169. Echt DS, Liebson PR, Mitchell LB, Peters RW, Obias-Manno D, Barker AH, Arensberg D, Baker A, Friedman L, Greene HL. Mortality and morbidity in patients receiving encainide, flecainide, or placebo: the Cardiac Arrhythmia Suppression Trial. *New England journal of medicine*. 1991;324:781-788.

170. Raad M, Yogasundaram H, Oranefo J, Guandalini G, Markman T, Hyman M, Schaller R, Supple G, Deo R, Nazarian S. Class 1C antiarrhythmics for premature ventricular complex suppression in nonischemic cardiomyopathy with implantable cardioverter-defibrillators. *JACC Clinical Electrophysiology*. 2024;10:846-853.

171. Kotoulas S, Tsiachris D, Botis M, Kordalis A, Varvarousis D, Leventopoulos G, Kallergis E, Doundoulakis I, Poulimenos LE, Tsioufis K. Effect of Flecainide in Idiopathic Premature Ventricular Contractions and the Induced Cardiomyopathy—UNIFLECA: A

Single Arm, Non-Randomized Trial: Review of the Literature and Initial Results. *Journal of Personalized Medicine*. 2025;15:132.

172. Demir S, Gulsen K, Kepez A, Uslu A, Kup A, Celik M, Kanar BG, Yildirim C, Tulumen E, Akgun T. Predictors of positive response to beta-blockers for treatment of premature ventricular complexes. *Journal of electrocardiology*. 2022;70:50-55.

173. Baycan OF, Fidan S, Celik FB, Tatlisu MA, Ozyildirim S, Caliskan M. Comparison of Medical Treatments According to the Characteristics of Idiopathic Premature Ventricular Contractions: Beta-blockers or Calcium Channel Blockers? *Medeniyet Medical Journal*. 2023;38:32.

174. Tonet J, Frank R, Fontaine G, Grosgogeat Y. Efficacy and safety of low doses of beta-blocker agents combined with amiodarone in refractory ventricular tachycardia. *Pacing and Clinical Electrophysiology*. 1988;11:1984-1989.

175. Jiménez-Candil J, Hernández J, Martín A, Ruiz-Olgado M, Herrero J, Ledesma C, Moríñigo J, Martín-Luengo C. Influence of beta-blocker therapy on antitachycardia pacing effectiveness for monomorphic ventricular tachycardias occurring in implantable cardioverter-defibrillator patients: a dose-dependent effect. *Europace*. 2010;12:1231-1238.

176. Ceremuzynski L, Kleczar E, Krzeminska-Pakula M, Kuch J, Nartowicz E, Smielak-Korombel J, Dyduszynski A, Maciejewicz J, Zaleska T, Lazarczyk-Kedzia E. Effect of amiodarone on mortality after myocardial infarction: a double-blind, placebo-controlled, pilot study. *Journal of the American College of Cardiology*. 1992;20:1056-1062.

177. Julian D, Camm A, Frangin G, Janse M, Munoz A, Schwartz P, Simon Pft. Randomised trial of effect of amiodarone on mortality in patients with left-ventricular dysfunction after recent myocardial infarction: EMIAT. *The Lancet*. 1997;349:667-674.

178. Cairns JA, Connolly SJ, Roberts R, Gent M. Randomised trial of outcome after myocardial infarction in patients with frequent or repetitive ventricular premature depolarisations: CAMIAT. *The Lancet*. 1997;349:675-682.

179. Bokhari F, Newman D, Greene M, Korley V, Mangat I, Dorian P. Long-term comparison of the implantable cardioverter defibrillator versus amiodarone: eleven-year follow-up of a subset of patients in the Canadian Implantable Defibrillator Study (CIDS). *Circulation*. 2004;110:112-116.

180. Connolly SJ, Dorian P, Roberts RS, Gent M, Bailin S, Fain ES, Thorpe K, Champagne J, Talajic M, Coutu B. Comparison of β-blockers, amiodarone plus β-blockers, or sotalol for prevention of shocks from implantable cardioverter defibrillators: the OPTIC study: a randomized trial. *JAMA*. 2006;295:165-171.

181. Magidson O. Resection of post-myocardial infarction ventricular aneurysm for cardiac arrhythmia. *Chest*. 1969;56:211.

182. Josephson ME, Harken AH, Norowitz LN. Long-term results of endocardial resection for sustained ventricular tachycardia in coronary disease patients. *American heart journal*. 1982;104:51-57.

183. Scheinman MM, Morady F, Hess DS, Gonzalez R. Catheter-induced ablation of the atrioventricular junction to control refractory supraventricular arrhythmias. *JAMA*. 1982;248:851-855.

184. Gallagher JJ, Svenson RH, Kasell JH, German LD, Bardy GH, Broughton A, Critelli G. Catheter technique for closed-chest ablation of the atrioventricular conduction system: a therapeutic alternative for the treatment of refractory supraventricular tachycardia. *New England Journal of Medicine*. 1982;306:194-200.

185. Borggrefe M, Breithardt G, Podczeck A, Rohner D, Budde T, Martinez-Rubio A. Catheter ablation of ventricular tachycardia using defibrillator pulses: electrophysiological findings and long-term results. *European Heart Journal*. 1989;10:591-601.

186. Morady F. Radio-frequency ablation as treatment for cardiac arrhythmias. *New England Journal of Medicine*. 1999;340:534-544.

187. Latchamsetty R, Yokokawa M, Morady F, Kim HM, Mathew S, Tilz R, Kuck K-H, Nagashima K, Tedrow U, Stevenson WG. Multicenter outcomes for catheter ablation of idiopathic premature ventricular complexes. *JACC: Clinical Electrophysiology*. 2015;1:116-123.

188. Bogun F, Crawford T, Reich S, Koelling TM, Armstrong W, Good E, Jongnarangsin K, Marine JE, Chugh A, Pelosi F. Radiofrequency ablation of frequent, idiopathic premature ventricular complexes: comparison with a control group without intervention. *Heart rhythm*. 2007;4:863-867.

189. Yokokawa M, Good E, Crawford T, Chugh A, Pelosi Jr F, Latchamsetty R, Jongnarangsin K, Armstrong W, Ghanbari H, Oral H. Recovery from left ventricular dysfunction after ablation of frequent premature ventricular complexes. *Heart rhythm*. 2013;10:172-175.

190. Zang M, Zhang T, Mao J, Zhou S, He B. Beneficial effects of catheter ablation of frequent premature ventricular complexes on left ventricular function. *Heart*. 2014;100:787-793.

191. Hanson M, Futyma P, Bode W, Liang JJ, Tapia C, Adams C, Zarębski Ł, Wrzos A, Saenz L, Sadek M. Catheter ablation of intramural outflow tract premature ventricular complexes: a multicentre study. *Europace*. 2023;25:euad100.

192. Oomen A, Dekker L, Meijer A. Catheter ablation of symptomatic idiopathic ventricular arrhythmias: A five-year single-centre experience. *Netherlands Heart Journal*. 2018;26:210-216.

193. Pytkowski M, Maciag A, Jankowska A, Kowalik I, Kraska A, Farkowski MM, Golicki D, Szwed H. Quality of life improvement after radiofrequency catheter ablation of outfl ow tract ventricular arrhythmias in patients with structurally normal hearts. *Acta cardiologica*. 2012;67:153-159.

194. Ling Z, Liu Z, Su L, Zipunnikov V, Wu J, Du H, Woo K, Chen S, Zhong B, Lan X. Radiofrequency ablation versus antiarrhythmic medication for treatment of ventricular premature beats from the right ventricular outflow tract: prospective randomized study. *Circulation: Arrhythmia and Electrophysiology*. 2014;7:237-243.

195. Ghanbari H, Baser K, Yokokawa M, Stevenson W, Della Bella P, Vergara P, Deneke T, Kuck K-H, Kottkamp H, Fei S. Noninducibility in postinfarction ventricular tachycardia as an end point for ventricular tachycardia ablation and its effects on outcomes: a meta-analysis. *Circulation: Arrhythmia and Electrophysiology*. 2014;7:677-683.

196. Campbell T, Bennett RG, Garikapati K, Turnbull S, Bhaskaran A, De Silva K, Kumar S. Prognostic significance of extensive versus limited induction protocol during catheter ablation of scar-related ventricular tachycardia. *Journal of Cardiovascular Electrophysiology*. 2020;31:2909-2919.

197. Sipko J, Baranowski B, Bhargava M, Callahan TD, Dresing TJ, Higuchi K, Hussein AA, Kanj M, Lee J, Martin DO. Acute post-procedural inducibility is a poor predictor of clinical outcomes in high-risk patients (PAINESD> 17) undergoing scar-related ventricular tachycardia ablation. *EP Europace*. 2024;26:euae185.

198. Santangeli P, Higuchi K, Sroubek J. Ventricular tachycardia ablation endpoints: moving beyond noninducibility. *JACC: Clinical Electrophysiology*. 2024;10:981-999.

199. Bennett R, Turnbull S, Kotake Y, Campbell T, Kumar S. Ventricular arrhythmia burden as a marker of success following catheter ablation of ventricular arrhythmias in patients with structural heart disease. *Korean Circulation Journal*. 2021;51:455-468.

200. Stevenson WG, Wilber DJ, Natale A, Jackman WM, Marchlinski FE, Talbert T, Gonzalez MD, Worley SJ, Daoud EG, Hwang C. Irrigated radiofrequency catheter ablation guided by electroanatomic mapping for recurrent ventricular tachycardia after myocardial infarction: the multicenter thermocool ventricular tachycardia ablation trial. *Circulation*. 2008;118:2773-2782.

201. Reddy VY, Reynolds MR, Neuzil P, Richardson AW, Taborsky M, Jongnarangsin K, Kralovec S, Sediva L, Ruskin JN, Josephson ME. Prophylactic catheter ablation for the prevention of defibrillator therapy. *New England Journal of Medicine*. 2007;357:2657-2665.

202. Kuck K-H, Schaumann A, Eckardt L, Willems S, Ventura R, Delacrétaz E, Pitschner H-F, Kautzner J, Schumacher B, Hansen PS. Catheter ablation of stable ventricular tachycardia before defibrillator implantation in patients with coronary heart disease (VTACH): a multicentre randomised controlled trial. *The Lancet*. 2010;375:31-40.

203. AL-KHATIB SM, Daubert JP, Anstrom KJ, Daoud EG, Gonzalez M, Saba S, Jackson KP, Reece T, Gu J, Pokorney SD. Catheter ablation for ventricular tachycardia in patients with an implantable cardioverter defibrillator (CALYPSO) pilot trial. *Journal of cardiovascular electrophysiology*. 2015;26:151-157.

204. Kuck K-H, Tilz RR, Deneke T, Hoffmann BA, Ventura R, Hansen PS, Zarse M, Hohnloser SH, Kautzner J, Willems S. Impact of substrate modification by catheter ablation on implantable cardioverter–defibrillator interventions in patients with unstable ventricular arrhythmias and coronary artery disease: results from the multicenter randomized controlled SMS (Substrate Modification Study). *Circulation: Arrhythmia and Electrophysiology*. 2017;10:e004422.

205. Willems S, Tilz RR, Steven D, Kääb S, Wegscheider K, Gellér L, Meyer C, Heeger C-H, Metzner A, Sinner MF. Preventive or deferred ablation of ventricular tachycardia in patients with ischemic cardiomyopathy and implantable defibrillator (BERLIN VT) a multicenter randomized trial. *Circulation*. 2020;141:1057-1067.

206. Della Bella P, Baratto F, Vergara P, Bertocchi P, Santamaria M, Notarstefano P, Calò L, Orsida D, Tomasi L, Piacenti M. Does timing of ventricular tachycardia ablation affect prognosis in patients with an implantable cardioverter defibrillator? Results from the multicenter randomized PARTITA trial. *Circulation*. 2022;145:1829-1838.

207. Arenal Á, Ávila P, Jiménez-Candil J, Tercedor L, Calvo D, Arribas F, Fernández-Portales J, Merino JL, Hernández-Madrid A, Fernández-Avilés FJ. Substrate ablation vs antiarrhythmic drug therapy for symptomatic ventricular tachycardia. *Journal of the American College of Cardiology*. 2022;79:1441-1453.

208. Tung R, Xue Y, Chen M, Jiang C, Shatz DY, Besser SA, Hu H, Chung F-P, Nakahara S, Kim Y-H. First-line catheter ablation of monomorphic ventricular tachycardia in cardiomyopathy concurrent with defibrillator implantation: the PAUSE-SCD randomized trial. *Circulation*. 2022;145:1839-1849.

209. Sapp JL, Tang AS, Parkash R, Stevenson WG, Healey JS, Gula LJ, Nair GM, Essebag V, Rivard L, Roux J-F. Catheter ablation or antiarrhythmic drugs for ventricular tachycardia. *New England Journal of Medicine*. 2025;392:737-747.

210. Martinez BK, Baker WL, Konopka A, Giannelli D, Coleman CI, Kluger J, Cronin EM. Systematic review and meta-analysis of catheter ablation of ventricular tachycardia in ischemic heart disease. *Heart Rhythm*. 2020;17:e206-e219.

211. Lima da Silva G, Nunes-Ferreira A, Cortez-Dias N, de Sousa J, J. Pinto F, Caldeira D. Radiofrequency catheter ablation of ventricular tachycardia in ischemic heart disease in light of current practice: a systematic review and meta-analysis of randomized controlled trials. *Journal of Interventional Cardiac Electrophysiology*. 2020;59:603-616.

212. Reddy RK, Howard JP, Ahmad Y, Shun-Shin MJ, Simader FA, Miyazawa AA, Saleh K, Naraen A, Samways JW, Katritsis G. Catheter ablation for ventricular tachycardia after MI: a reconstructed individual patient data meta-analysis of randomised controlled trials. *Arrhythmia & Electrophysiology Review*. 2023;12:e26.

213. Virk SA, Kumar S. Catheter ablation of ventricular tachycardia in patients with structural heart disease: a meta-analysis. *JACC: Clinical Electrophysiology*. 2023;9:255-257.

214. Blandino A, Bianchi F, Frankel DS, Liang JJ, Mazzanti A, D'Ascenzo F, Masi AS, Grossi S, Musumeci G. Safety and efficacy of catheter ablation for ventricular tachycardia in elderly patients with structural heart disease: a systematic review and meta-analysis. *Journal of Interventional Cardiac Electrophysiology*. 2023;66:179-192.

215. Askarinejad A, Arya A, Zangiabadian M, Ghahramanipour Z, Hesami H, Farmani D, Ghanbari Mardasi K, Kohansal E, Haghjoo M. Catheter ablation as first-line treatment for ventricular tachycardia in patients with structural heart disease and preserved left

ventricular ejection fraction: a systematic review and meta-analysis. *Scientific Reports*. 2024;14:18536.

216. Prasitlumkum N, Navaravong L, Desai A, Desai D, Cheungpasitporn W, Rattanawong P, Bunch TJ, Jongnarangsin K, Chokesuwattanaskul R. Impact of early ventricular tachycardia ablation in patients with an implantable cardioverter-defibrillator: an updated systematic review and meta-analysis of randomized controlled trials. *Heart Rhythm*. 2022;19:2054-2061.

217. Tung R, Vaseghi M, Frankel DS, Vergara P, Di Biase L, Nagashima K, Yu R, Vangala S, Tseng C-H, Choi E-K. Freedom from recurrent ventricular tachycardia after catheter ablation is associated with improved survival in patients with structural heart disease: an International VT Ablation Center Collaborative Group study. *Heart rhythm*. 2015;12:1997-2007.

218. Ben-Haim SA, Osadchy D, Schuster I, Gepstein L, Hayam G, Josephson ME. Nonfluoroscopic, in vivo navigation and mapping technology. *Nature medicine*. 1996;2:1393-1395.

219. Kanawati J, De Silva K, Bhaskaran A, Turnbull S, Zhou J, Kotake Y, Kumar S, Campbell T. Intracardiac echocardiography techniques to identify ventricular arrhythmia substrate. *Heart Rhythm O2*. 2022;3:602-612.

220. Chery G, Khoshknab M, Nazarian S. Imaging to facilitate ventricular tachycardia ablation: intracardiac echocardiography, computed tomography, magnetic resonance, and positron emission tomography. *JACC: Clinical Electrophysiology*. 2024;10:2277-2292.

221. Stevenson WG, Soejima K. Recording techniques for clinical electrophysiology. *Journal of cardiovascular electrophysiology*. 2005;16:1017-1022.

222. Omara S, Glashan CA, Tofig BJ, Leenknegt L, Dierckx H, Panfilov AV, Beukers HK, van Waasbergen MH, Tao Q, Stevenson WG. Multisize electrode field-of-view: validation by high resolution gadolinium-enhanced cardiac magnetic resonance. *JACC: Clinical Electrophysiology*. 2024;10:637-650.

223. Luo S, Johnston P. A review of electrocardiogram filtering. *Journal of electrocardiology*. 2010;43:486-496.

224. Misra S, Zahid S, Prakosa A, Saju N, Tandri H, Berger RD, Marine JE, Calkins H, Zipunnikov V, Trayanova N. Field of view of mapping catheters quantified by electrogram associations with radius of myocardial attenuation on contrast-enhanced cardiac computed tomography. *Heart Rhythm*. 2018;15:1617-1625.

225. Takigawa M, Relan J, Martin R, Kim S, Kitamura T, Frontera A, Cheniti G, Vlachos K, Massoullié G, Martin CA. Effect of bipolar electrode orientation on local electrogram properties. *Heart Rhythm*. 2018;15:1853-1861.

226. de Bakker JM. Electrogram recording and analyzing techniques to optimize selection of target sites for ablation of cardiac arrhythmias. *Pacing and Clinical Electrophysiology*. 2019;42:1503-1516.

227. Vergara P, Trevisi N, Ricco A, Petracca F, Baratto F, Cireddu M, Bisceglia C, Maccabelli G, Della Bella P. Late potentials abolition as an additional technique for reduction of arrhythmia recurrence in scar related ventricular tachycardia ablation. *Journal of cardiovascular electrophysiology*. 2012;23:621-627.

228. Di Biase L, Santangeli P, Burkhardt DJ, Bai R, Mohanty P, Carbucicchio C, Dello Russo A, Casella M, Mohanty S, Pump A. Endo-epicardial homogenization of the scar versus

limited substrate ablation for the treatment of electrical storms in patients with ischemic cardiomyopathy. *Journal of the American College of Cardiology*. 2012;60:132-141.

229. Fernández-Armenta J, Penela D, Acosta J, Andreu D, Evertz R, Cabrera M, Korshunov V, Vassanelli F, Martínez M, Guasch E. Substrate modification or ventricular tachycardia induction, mapping, and ablation as the first step? A randomized study. *Heart Rhythm*. 2016;13:1589-1595.

230. Kumar S, Tedrow UB, Stevenson WG. Entrainment mapping. *Cardiac Electrophysiology Clinics*. 2017;9:55-69.

231. Tung R. Challenges and pitfalls of entrainment mapping of ventricular tachycardia: ten illustrative concepts. *Circulation: Arrhythmia and Electrophysiology*. 2017;10:e004560.

232. El Haddad M, Houben R, Stroobandt R, Van Heuverswyn F, Tavernier R, Duytschaever M. Novel algorithmic methods in mapping of atrial and ventricular tachycardia. *Circulation: Arrhythmia and Electrophysiology*. 2014;7:463-472.

233. De Chillou C, Groben L, Magnin-Poull I, Andronache M, Abbas MM, Zhang N, Abdelaal A, Ammar S, Sellal J-M, Schwartz J. Localizing the critical isthmus of postinfarct ventricular tachycardia: the value of pace-mapping during sinus rhythm. *Heart Rhythm*. 2014;11:175-181.

234. Guenancia C, Supple G, Sellal JM, Magnin-Poull I, Benali K, Hammache N, Echivard M, Marchlinski F, de Chillou C. How to use pace mapping for ventricular tachycardia ablation in postinfarct patients. *Journal of Cardiovascular Electrophysiology*. 2022;33:1801-1809.

235. Kotake Y, Bennett R, Silva KD, Bhaskaran A, Kanawati J, Turnbull S, Zhou J, Kumar S, Campbell T. Correlation of spatial patterns of endocardial pace mapping to underlying scar

topography in patients with scar-related ventricular tachycardia. *Journal of Cardiovascular Electrophysiology*. 2023;34:638-649.

236. Shinoda Y, Jameria ZA, Sahara N, Upadhyay GA, Liao Y, Martinez J, Katrapati P, Bai R, Zawaneh M, Weiss JP. Rate-Dependent Pacemap Matching in Scar-Related Ventricular Tachycardia: Impact of "TR Fusion" Phenomenon. *JACC: Clinical Electrophysiology*. 2024;10:2132-2144.

237. Nayyar S, Wilson L, Ganesan AN, Sullivan T, Kuklik P, Chapman D, Brooks AG, Mahajan R, Baumert M, Young GD, Sanders P, Roberts-Thomson KC. High-density mapping of ventricular scar: a comparison of ventricular tachycardia (VT) supporting channels with channels that do not support VT. *Circulation: Arrhythmia and Electrophysiology*. 2014;7:90-98.

238. Bennett R, Campbell T, Kotake Y, Turnbull S, Bhaskaran A, De Silva K, Lee G, Kalman J, Kumar S. Catheter ablation of idiopathic outflow tract ventricular arrhythmias with low intraprocedural burden guided by pace mapping. *Heart Rhythm O2*. 2021;2:355-364.

239. El Sherif N, Scherlag BJ, Lazzara R. Electroide cather recording during malignant ventricular arrythmia following experimental acute myocardial ischemia. Evidence for re-entry due to conduction delay and block in ischemic myocardium. *Circulation*. 1975;51:1003-1014.

240. Josephson ME, Horowitz LN, Farshidi A. Continuous local electrical activity. A mechanism of recurrent ventricular tachycardia. *Circulation*. 1978;57:659-665.

241. Fontaine G, Guiraudon G, Frank R, Fillette F, Tonet J, Grosgogeat Y. Correlations between latest delayed potentials in sinus rhythm and earliest activation during chronic ventricular

tachycardia. In: *Medical and surgical management of tachyarrhythmias*. Springer; 1980:138-154.

242. Klein H, Karp R, Kouchoukos N, Zorn Jr G, James T, Waldo A. Intraoperative electrophysiologic mapping of the ventricles during sinus rhythm in patients with a previous myocardial infarction. Identification of the electrophysiologic substrate of ventricular arrhythmias. *Circulation*. 1982;66:847-853.

243. Wiener I, Mindich B, Pitchon R. Determinants of ventricular tachycardia in patients with ventricular aneurysms: results of intraoperative epicardial and endocardial mapping. *Circulation*. 1982;65:856-861.

244. Di Biase L, Burkhardt JD, Lakkireddy D, Carbucicchio C, Mohanty S, Mohanty P, Trivedi C, Santangeli P, Bai R, Forleo G. Ablation of stable VTs versus substrate ablation in ischemic cardiomyopathy: the VISTA randomized multicenter trial. *Journal of the American College of Cardiology*. 2015;66:2872-2882.

245. Hutchinson MD, Gerstenfeld EP, Desjardins B, Bala R, Riley MP, Garcia FC, Dixit S, Lin D, Tzou WS, Cooper JM. Endocardial unipolar voltage mapping to detect epicardial ventricular tachycardia substrate in patients with nonischemic left ventricular cardiomyopathy. *Circulation: Arrhythmia and Electrophysiology*. 2011;4:49-55.

246. Polin GM, Haqqani H, Tzou W, Hutchinson MD, Garcia FC, Callans DJ, Zado ES, Marchlinski FE. Endocardial unipolar voltage mapping to identify epicardial substrate in arrhythmogenic right ventricular cardiomyopathy/dysplasia. *Heart Rhythm*. 2011;8:76-83. doi: 10.1016/j.hrthm.2010.09.088

247. Cano O, Hutchinson M, Lin D, Garcia F, Zado E, Bala R, Riley M, Cooper J, Dixit S, Gerstenfeld E. Electroanatomic substrate and ablation outcome for suspected epicardial

ventricular tachycardia in left ventricular nonischemic cardiomyopathy. *Journal of the American College of Cardiology*. 2009;54:799-808.

248. Tschabrunn CM, Roujol S, Dorman NC, Nezafat R, Josephson ME, Anter E. High-resolution mapping of ventricular scar: comparison between single and multielectrode catheters. *Circulation: Arrhythmia and Electrophysiology*. 2016;9:e003841.

249. Glashan CA, Tofig BJ, Tao Q, Blom SA, Sørensen JCH, Zeppenfeld K, Kristiansen SB. Whole heart histology: a method for the direct integration of histology with electrophysiological and imaging data. *JACC: Clinical Electrophysiology*. 2020;6:461-462.

250. Glashan CA, Tofig BJ, Beukers H, Tao Q, Blom SA, Villadsen PR, Lassen TR, de Riva M, Kristiansen SB, Zeppenfeld K. Multielectrode unipolar voltage mapping and electrogram morphology to identify post-infarct scar geometry: validation by histology. *JACC: Clinical Electrophysiology*. 2022;8:437-449.

251. Wijnmaalen AP, van der Geest RJ, van Huls van Taxis CF, Siebelink H-MJ, Kroft LJ, Bax JJ, Reiber JH, Schalij MJ, Zeppenfeld K. Head-to-head comparison of contrast-enhanced magnetic resonance imaging and electroanatomical voltage mapping to assess post-infarct scar characteristics in patients with ventricular tachycardias: real-time image integration and reversed registration. *European heart journal*. 2011;32:104-114.

252. Tung R, Kim S, Yagishita D, Vaseghi M, Ennis DB, Ouadah S, Ajijola OA, Bradfield JS, Mahapatra S, Finn P. Scar voltage threshold determination using ex vivo magnetic resonance imaging integration in a porcine infarct model: influence of interelectrode distances and three-dimensional spatial effects of scar. *Heart Rhythm*. 2016;13:1993-2002.

253. Sramko M, Abdel-Kafi S, van der Geest RJ, de Riva M, Glashan CA, Lamb HJ, Zeppenfeld K. New adjusted cutoffs for "normal" endocardial voltages in patients with post-infarct LV remodeling. *JACC: Clinical Electrophysiology*. 2019;5:1115-1126.

254. Campbell T, Bennett RG, Anderson RD, Davey C, O'Donohue AK, Schindeler A, De Silva K, Bhaskaran A, Turnbull S, Selvakumar D, Kotake Y, Hsu CJ, Chong JJH, Kizana E, Kumar S. Whole-Heart Histological and CMR Validation of Electroanatomic Mapping by Multielectrode Catheters in an Ovine Model. *JACC: Clinical Electrophysiology*. 2025.

255. De Bakker J, Van Capelle F, Janse MJ, Wilde A, Coronel R, Becker AE, Dingemans KP, Van Hemel NM, Hauer R. Reentry as a cause of ventricular tachycardia in patients with chronic ischemic heart disease: electrophysiologic and anatomic correlation. *Circulation*. 1988;77:589-606.

256. Arenal A, del Castillo S, Gonzalez-Torrecilla E, Atienza F, Ortiz M, Jimenez J, Puchol A, García J, Almendral J. Tachycardia-related channel in the scar tissue in patients with sustained monomorphic ventricular tachycardias: influence of the voltage scar definition. *Circulation*. 2004;110:2568-2574.

257. Hsia HH, Lin D, Sauer WH, Callans DJ, Marchlinski FE. Anatomic characterization of endocardial substrate for hemodynamically stable reentrant ventricular tachycardia: identification of endocardial conducting channels. *Heart Rhythm*. 2006;3:503-512.

258. Haqqani HM, Kalman JM, Roberts-Thomson KC, Balasubramaniam RN, Rosso R, Snowdon RL, Sparks PB, Vohra JK, Morton JB. Fundamental differences in electrophysiologic and electroanatomic substrate between ischemic cardiomyopathy patients with and without clinical ventricular tachycardia. *Journal of the American College of Cardiology*. 2009;54:166-173.

259. Berruezo A, Fernández-Armenta J, Andreu D, Penela D, Herczku C, Evertz R, Cipolletta L, Acosta J, Borràs R, Arbelo E. Scar dechanneling: new method for scar-related left ventricular tachycardia substrate ablation. *Circulation: Arrhythmia and Electrophysiology*. 2015;8:326-336.

260. Cassidy DM, Vassallo JA, Marchlinski FE, Buxton AE, Untereker WJ, Josephson ME. Endocardial mapping in humans in sinus rhythm with normal left ventricles: activation patterns and characteristics of electrograms. *Circulation*. 1984;70:37-42.

261. Dillon SM, Allessie MA, Ursell PC, Wit AL. Influences of anisotropic tissue structure on reentrant circuits in the epicardial border zone of subacute canine infarcts. *Circulation research*. 1988;63:182-206.

262. Ciaccio EJ, Tosti AC, Scheinman MM. Relationship between sinus rhythm activation and the reentrant ventricular tachycardia isthmus. *Circulation*. 2001;104:613-619.

263. Stevenson WG, Weiss JN, Wiener I, Rivitz SM, Nademanee K, Klitzner T, Yeatman L, Josephson M, Wohlgelernter D. Fractionated endocardial electrograms are associated with slow conduction in humans: evidence from pace-mapping. *Journal of the American College of Cardiology*. 1989;13:369-376.

264. Miller JM, Tyson GS, Hargrove III WC, Vassallo JA, Rosenthal ME, Josephson ME. Effect of subendocardial resection on sinus rhythm endocardial electrogram abnormalities. *Circulation*. 1995;91:2385-2391.

265. Bogun F, Good E, Reich S, Elmouchi D, Igic P, Lemola K, Tschopp D, Jongnarangsin K, Oral H, Chugh A. Isolated potentials during sinus rhythm and pace-mapping within scars as guides for ablation of post-infarction ventricular tachycardia. *Journal of the American College of Cardiology*. 2006;47:2013-2019.

266. Hsia HH, Lin D, Sauer WH, Callans DJ, Marchlinski FE. Relationship of late potentials to the ventricular tachycardia circuit defined by entrainment. *Journal of interventional cardiac electrophysiology*. 2009;26:21-29.

267. Harada T, Stevenson WG, Kocovic DZ, Friedman PL. Catheter ablation of ventricular tachycardia after myocardial infarction: relation of endocardial sinus rhythm late potentials to the reentry circuit. *Journal of the American College of Cardiology*. 1997;30:1015-1023.

268. Arenal A, Glez-Torrecilla E, Ortiz M, Villacastín J, Fdez-Portales J, Sousa E, del Castillo S, Perez de Isla L, Jimenez J, Almendral J. Ablation of electrograms with an isolated, delayed component as treatment of unmappable monomorphic ventricular tachycardias in patients with structural heart disease. *Journal of the American College of Cardiology*. 2003;41:81-92.

269. Al-Sheikhli J, Tran P, Siang R, Niespialowska-Steuden M, Mayer J, Dhanjal T. Functional Substrate Mapping: A New Frontier in the Treatment of Ventricular Tachycardia in Structural Heart Disease. *Arrhythmia & Electrophysiology Review*. 2024;13:e22.

270. Irie T, Yu R, Bradfield JS, Vaseghi M, Buch EF, Ajijola O, Macias C, Fujimura O, Mandapati R, Boyle NG, Shivkumar K, Tung R. Relationship between sinus rhythm late activation zones and critical sites for scar-related ventricular tachycardia: systematic analysis of isochronal late activation mapping. *Circulation: Arrhythmia and Electrophysiology*. 2015;8:390-399.

271. Aziz Z, Shatz D, Raiman M, Upadhyay GA, Beaser AD, Besser SA, Shatz NA, Fu Z, Jiang R, Nishimura T, Liao H, Nayak H, Tung R. Targeted ablation of ventricular tachycardia guided by wavefront discontinuities during sinus rhythm: a new functional substrate mapping strategy. *Circulation*. 2019;140:1383-1397.

272. Nishimura T, Shatz N, Weiss JP, Zawaneh M, Bai R, Beaser AD, Upadhyay GA, Aziz ZA, Nayak HM, Shatz DY, Miyazaki S, Goya M, Sasano T, Su W, Raiman M, Tung R. Identification of human ventricular tachycardia demarcated by fixed lines of conduction block in a 3-dimensional hyperboloid circuit. *Circulation*. 2023;148:1354-1367.

273. Maher TR, Freedman BL, Yang S, Locke AH, D'Angelo R, Galvao M, Buxton AE, Waks JW, d'Avila A. Targeting Wavefront Discontinuity Lines for Scar-Related Ventricular Tachycardia Ablation: A Novel Functional Substrate Ablation Approach. *Clinical Electrophysiology*. 2024;10:1255-1270.

274. Tonko JB, Chow A, Lambiase PD. High-density isochronal repolarization mapping and re-entry vulnerability estimation for scar-related ventricular tachycardia ablation: mechanistic basis, clinical application, and challenges. *EP Europace*. 2024;26:euae271.

275. Tonko JB, Chow A, Lozano C, Moreno J, Lambiase PD. Visualizing Reentry Vulnerable Targets During Scar-Related VT Ablation: A Novel Functional Substrate Mapping Approach Integrating Conduction and Repolarization Metrics. *Circulation: Arrhythmia and Electrophysiology*. 2024;17:e012915.

276. Anter E, Neuzil P, Reddy VY, Petru J, Park K-M, Sroubek J, Leshem E, Zimetbaum PJ, Buxton AE, Kleber AG. Ablation of reentry-vulnerable zones determined by left ventricular activation from multiple directions: a novel approach for ventricular tachycardia ablation: a multicenter study (PHYSIO-VT). *Circulation: Arrhythmia and Electrophysiology*. 2020;13:e008625.

277. Rossi P, Cauti FM, Niscola M, Calore F, Fanti V, Polselli M, Di Pastena A, Iaia L, Bianchi S. A novel Ventricular map of Electrograms DUration as a Method to identify areas of

slow conduction for ventricular tachycardia ablation: The VEDUM pilot study. *Heart Rhythm*. 2021;18:1253-1260.

278. Acosta J, Andreu D, Penela D, Cabrera M, Carlosena A, Korshunov V, Vassanelli F, Borras R, Martínez M, Fernández-Armenta J. Elucidation of hidden slow conduction by double ventricular extrastimuli: a method for further arrhythmic substrate identification in ventricular tachycardia ablation procedures. *EP Europace*. 2018;20:337-346.

279. de Riva M, Naruse Y, Ebert M, Androulakis AF, Tao Q, Watanabe M, Wijnmaalen AP, Venlet J, Brouwer C, Trines SA. Targeting the hidden substrate unmasked by right ventricular extrastimulation improves ventricular tachycardia ablation outcome after myocardial infarction. *JACC: Clinical Electrophysiology*. 2018;4:316-327.

280. Hawson J, Anderson RD, Das SK, Al-Kaisey A, Chieng D, Segan L, Watts T, Campbell T, Morton J, McLellan A, Sparks P, Lee A, Gerstenfled EP, Hsia HH, Voskoboinik A, Pathik B, Kumar S, Kistler PM, Kalman J, Lee G. Optimal annotation of local activation time in ventricular tachycardia substrate mapping. *JACC: Clinical Electrophysiology*. 2024;10:206-218.

281. Woods CE, Schricker AA, Nayak H, Hariharan R, Stevens B, Kwasnik A, Shatz N, Suchomel L, Moskovitz R, Salcedo J. Correlation between sinus rhythm deceleration zones and critical sites for localized reentrant atrial flutter: a retrospective multicenter analysis. *Heart Rhythm O2*. 2022;3:279-287.

282. Kuo M-J, Ton AN-K, Lo L-W, Lin Y-J, Chang S-L, Hu Y-F, Chung F-P, Tuan T-C, Chao T-F, Liao J-N. Abnormal conduction zone detected by isochronal late activation mapping accurately identifies the potential atrial substrate and predicts the atrial fibrillation ablation

outcome after pulmonary vein isolation. *Circulation: Arrhythmia and Electrophysiology*. 2023;16:e011149.

283. Maher TR, Freedman BL, Locke AH, Tracey M, Waks JW, Litmanovich D, d'Avila A. Correlation between functional substrate mapping and cardiac computed tomography–derived wall thinning for ventricular tachycardia ablation. *JACC: Clinical Electrophysiology*. 2023;9:1878-1889.

284. Vázquez-Calvo S, Casanovas JM, Garre P, Ferró E, Sánchez-Somonte P, Quinto L, Guasch E, Porta-Sanchez A, Tolosana JM, Borras R. Evolution of deceleration zones during ventricular tachycardia ablation and relation with cardiac magnetic resonance. *JACC: Clinical Electrophysiology*. 2023;9:779-789.

285. Guichard J-B, Regany-Closa M, Vázquez-Calvo S, Zazu B, Pellicer Sendra B, Serrano-Campaner J, Molero-Pereira S, Borràs R, Ortiz JT, Falzone PV. Substrate mapping for ventricular tachycardia ablation through high-density whole-chamber double extra stimuli: the S3 protocol. *JACC: Clinical Electrophysiology*. 2024;10:1534-1547.

286. Ciaccio EJ. Ventricular tachycardia duration and form are associated with electrical discontinuities bounding the core of the reentrant circuit. *Journal of cardiovascular electrophysiology*. 2005;16:646-654.

287. Ciaccio EJ, Coromilas J, Wan EY, Yarmohammadi H, Saluja DS, Biviano AB, Wit AL, Peters NS, Garan H. Slow uniform electrical activation during sinus rhythm is an indicator of reentrant VT isthmus location and orientation in an experimental model of myocardial infarction. *Computer Methods and Programs in Biomedicine*. 2020;196:105666.

288. Ciaccio EJ, Chow AW, Kaba RA, Davies DW, Segal OR, Peters NS. Detection of the diastolic pathway, circuit morphology, and inducibility of human postinfarction ventricular tachycardia from mapping in sinus rhythm. *Heart Rhythm*. 2008;5:981-991.

289. Lammers W, Kirchhof C, Bonke F, Allessie MA. Vulnerability of rabbit atrium to reentry by hypoxia. Role of inhomogeneity in conduction and wavelength. *American Journal of Physiology-Heart and Circulatory Physiology*. 1992;262:H47-H55.

290. Saumarez R, Slade A, Grace A, Sadoul N, Camm A, McKenna W. The significance of paced electrogram fractionation in hypertrophic cardiomyopathy: a prospective study. *Circulation*. 1995;91:2762-2768.

291. Porta-Sánchez A, Jackson N, Lukac P, Kristiansen SB, Nielsen JM, Gizurarson S, Massé S, Labos C, Viswanathan K, King B. Multicenter study of ischemic ventricular tachycardia ablation with decrement-evoked potential (DEEP) mapping with extra stimulus. *JACC: Clinical Electrophysiology*. 2018;4:307-315.

292. Bhaskaran A, Deshmukh T, Bennett R, Turnbull S, Campbell TG, Kotake Y, Selvakumar D, Barry MA, Lu J, Pearson L. Evolution of Substrate for Ventricular Arrhythmias Early Postinfarction: Insights From a Porcine Ischemia-Reperfusion Model. *JACC: Clinical Electrophysiology*. 2024;10:2158-2168.

293. Srinivasan NT, Garcia J, Schilling RJ, Ahsan S, Babu GG, Ang R, Dhinoja MB, Hunter RJ, Lowe M, Chow AW. Multicenter study of dynamic high-density functional substrate mapping improves identification of substrate targets for ischemic ventricular tachycardia ablation. *JACC: Clinical Electrophysiology*. 2020;6:1783-1793.

294. Callans DJ, Ren J-F, Michele J, Marchlinski FE, Dillon SM. Electroanatomic left ventricular mapping in the porcine model of healed anterior myocardial infarction:

correlation with intracardiac echocardiography and pathological analysis. *Circulation*. 1999;100:1744-1750.

295. Hussein A, Jimenez A, Ahmad G, Mesubi O, Klein T, Gurm G, Beck H, Shams O, See V, Saliaris A. Assessment of ventricular tachycardia scar substrate by intracardiac echocardiography. *Pacing and Clinical Electrophysiology*. 2014;37:412-421.

296. Denham N, Ding WY, Campbell T, Modi S, Luther V, Todd D, Kumar S, Agarwal S, Mahida S. UltraSOUND-based characterization of ventricular tachycardia SCAR and arrhythmogenic substrate: The SOUNDSCAR study. *Heart Rhythm*. 2024;21:45-53.

297. Deno DC, Balachandran R, Morgan D, Ahmad F, Massé S, Nanthakumar K. Orientation-independent catheter-based characterization of myocardial activation. *IEEE transactions on biomedical engineering*. 2016;64:1067-1077.

298. Massé S, Magtibay K, Jackson N, Asta J, Kusha M, Zhang B, Balachandran R, Radisic M, Deno DC, Nanthakumar K. Resolving myocardial activation with novel omnipolar electrograms. *Circulation: Arrhythmia and Electrophysiology*. 2016;9:e004107.

299. Ascione C, Kowalewski C, Bergonti M, Yokoyama M, Monaco C, Bouyer B, Chauvel R, Arnaud M, Buliard S, Tixier R. Omnipolar versus bipolar mapping to guide ventricular tachycardia ablation. *Heart Rhythm*. 2023;20:1370-1377.

300. Anter E, Brem O, Greenbaum L, Bubar ZP, Younis A, Yavin H, Yarnitsky J, Barkagan M. Multipolar electrograms: a new configuration that increases the measurement accuracy of intracardiac signals. *JACC: Clinical Electrophysiology*. 2024;10:1521-1533.

301. Payne JE, Woods C, Elshazly MB, Matthews A, Kroman A, Feng Z, Rabinkova A, Ghadban R, Dhakal B, Winterfield J. A novel automated peak frequency annotation

algorithm for identifying deceleration zones and ventricular tachycardia ablation sites. *Heart rhythm*. 2024;21:27-33.

302. Mayer J, Al-Sheikhli J, Niespialowska-Steuden M, Patchett I, Winter J, Siang R, Lellouche N, Manoharan K, Phan TT, Calvo JJ. Detailed analysis of electrogram peak frequency to guide ventricular tachycardia substrate mapping. *EP Europace*. 2024;26:euae253.

303. Cauti FM, Martini N, Fioravanti F, Tanese N, Magnocavallo M, Rampa L, Calore F, Scalisi G, Peretto G, Barengo A. Analysis of electrogram peak frequency during ventricular tachycardia ablation: insights into human tridimensional ventricular tachycardia circuits. *Heart Rhythm*. 2025;22:128-134.

304. Tonko JB, Lozano C, Moreno J, Chow A, Dhinoja M, Lambiase PD. Near-field detection and peak frequency metric for substrate and activation mapping of ventricular tachycardias in two-and three-dimensional circuits. *EP Europace*. 2024;26:euae154.

305. Hunt EB. *Artificial intelligence*. Academic Press; 2014.

306. Muthalaly RG, Evans RM. Applications of machine learning in cardiac electrophysiology. *Arrhythmia & Electrophysiology Review*. 2020;9:71.

307. Feeny AK, Chung MK, Madabhushi A, Attia ZI, Cikes M, Firouznia M, Friedman PA, Kalscheur MM, Kapa S, Narayan SM. Artificial intelligence and machine learning in arrhythmias and cardiac electrophysiology. *Circulation: Arrhythmia and Electrophysiology*. 2020;13:e007952.

308. Ng B, Nayyar S, Chauhan VS. The role of artificial intelligence and machine learning in clinical cardiac electrophysiology. *Canadian Journal of Cardiology*. 2022;38:246-258.

309. Kabra R, Israni S, Vijay B, Baru C, Mendu R, Fellman M, Sridhar A, Mason P, Cheung JW, DiBiase L. Emerging role of artificial intelligence in cardiac electrophysiology. *Cardiovascular Digital Health Journal*. 2022;3:263-275.

310. Svennberg E, Han JK, Caiani EG, Engelhardt S, Ernst S, Friedman P, Garcia R, Ghanbari H, Hindricks G, Man SH, et al. State of the Art of Artificial Intelligence in Clinical Electrophysiology in 2025. A Scientific Statement of the European Heart Rhythm Association (EHRA) of the ESC, the Heart Rhythm Society (HRS), and the ESC Working Group in e-Cardiology. *EP Europace*. 2025. doi: 10.1093/europace/euaf071

311. Attia ZI, Noseworthy PA, Lopez-Jimenez F, Asirvatham SJ, Deshmukh AJ, Gersh BJ, Carter RE, Yao X, Rabinstein AA, Erickson BJ. An artificial intelligence-enabled ECG algorithm for the identification of patients with atrial fibrillation during sinus rhythm: a retrospective analysis of outcome prediction. *The Lancet*. 2019;394:861-867.

312. Raghunath S, Ulloa Cerna AE, Jing L, VanMaanen DP, Stough J, Hartzel DN, Leader JB, Kirchner HL, Stumpe MC, Hafez A. Prediction of mortality from 12-lead electrocardiogram voltage data using a deep neural network. *Nature medicine*. 2020;26:886-891.

313. Yao X, Rushlow DR, Inselman JW, McCoy RG, Thacher TD, Behnken EM, Bernard ME, Rosas SL, Akfaly A, Misra A. Artificial intelligence–enabled electrocardiograms for identification of patients with low ejection fraction: a pragmatic, randomized clinical trial. *Nature medicine*. 2021;27:815-819.

314. Lampert J, Vaid A, Whang W, Koruth J, Miller MA, Langan M-N, Musikantow D, Turagam M, Maan A, Kawamura I. A Novel ECG-Based Deep Learning Algorithm to

Predict Cardiomyopathy in Patients With Premature Ventricular Complexes. *JACC: Clinical Electrophysiology*. 2023;9:1437-1451.

315. Ntoutsi E, Fafalios P, Gadiraju U, Iosifidis V, Nejdl W, Vidal ME, Ruggieri S, Turini F, Papadopoulos S, Krasanakis E. Bias in data-driven artificial intelligence systems—An introductory survey. *Wiley Interdisciplinary Reviews: Data Mining and Knowledge Discovery*. 2020;10:e1356.

316. Trayanova NA, Topol EJ. Deep learning a person's risk of sudden cardiac death. *The Lancet*. 2022;399:1933.

317. Popescu DM, Shade JK, Lai C, Aronis KN, Ouyang D, Moorthy MV, Cook NR, Lee DC, Kadish A, Albert CM, et al. Arrhythmic sudden death survival prediction using deep learning analysis of scarring in the heart. *Nature Cardiovascular Research*. 2022;1:334-343. doi: 10.1038/s44161-022-00041-9

318. Shade JK, Prakosa A, Popescu DM, Yu R, Okada DR, Chrispin J, Trayanova NA. Predicting risk of sudden cardiac death in patients with cardiac sarcoidosis using multimodality imaging and personalized heart modeling in a multivariable classifier. *Science Advances*. 2021;7:eabi8020.

319. Rogers AJ, Selvalingam A, Alhusseini MI, Krummen DE, Corrado C, Abuzaid F, Baykaner T, Meyer C, Clopton P, Giles W, et al. Machine Learned Cellular Phenotypes in Cardiomyopathy Predict Sudden Death. *Circulation Research*. 2021;128:172-184. doi: 10.1161/circresaha.120.317345

320. Yokokawa M, Liu T-Y, Yoshida K, Scott C, Hero A, Good E, Morady F, Bogun F. Automated analysis of the 12-lead electrocardiogram to identify the exit site of postinfarction ventricular tachycardia. *Heart rhythm*. 2012;9:330-334.

321. Sapp JL, Bar-Tal M, Howes AJ, Toma JE, El-Damaty A, Warren JW, MacInnis PJ, Zhou S, Horáček BM. Real-time localization of ventricular tachycardia origin from the 12-lead electrocardiogram. *JACC: Clinical Electrophysiology*. 2017;3:687-699.

322. Zhou S, AbdelWahab A, Horáček BM, MacInnis PJ, Warren JW, Davis JS, Elsokkari I, Lee DC, MacIntyre CJ, Parkash R. Prospective assessment of an automated intraprocedural 12-lead ECG-based system for localization of early left ventricular activation. *Circulation: Arrhythmia and Electrophysiology*. 2020;13:e008262.

323. Morellato J, Chik W, Barry M, Lu J, Thiagalingam A, Kovoor P, Pouliopoulos J. Quantitative spectral assessment of intracardiac electrogram characteristics associated with post infarct fibrosis and ventricular tachycardia. *PLoS One*. 2018;13:e0204997.

324. Whitaker J, Baum TE, Qian P, Prassl AJ, Plank G, Blankstein R, Cochet H, Sauer WH, Bishop MJ, Tedrow U. Frequency Domain Analysis of Endocardial Electrograms for Detection of Nontransmural Myocardial Fibrosis in Nonischemic Cardiomyopathy. *JACC: Clinical Electrophysiology*. 2023;9:923-935.

325. Ntagiantas K, Pignatelli E, Peters NS, Cantwell CD, Chowdhury RA, Bharath AA. Estimation of fibre architecture and scar in myocardial tissue using electrograms: an in-silico study. *Biomedical Signal Processing and Control*. 2024;89:105746.

326. Saeed M, Bremerich J, Wendland MF, Wyttenbach R, Weinmann HJ, Higgins CB. Reperfused myocardial infarction as seen with use of necrosis-specific versus standard extracellular MR contrast media in rats. *Radiology*. 1999;213:247-257. doi: 10.1148/radiology.213.1.r99se30247

327. Saeed M, Lund G, Wendland MF, Bremerich J, Weinmann H, Higgins CB. Magnetic resonance characterization of the peri-infarction zone of reperfused myocardial infarction

with necrosis-specific and extracellular nonspecific contrast media. *Circulation*. 2001;103:871-876. doi: 10.1161/01.cir.103.6.871

328. Bello D, Fieno DS, Kim RJ, Pereles FS, Passman R, Song G, Kadish AH, Goldberger JJ. Infarct morphology identifies patients with substrate for sustained ventricular tachycardia. *Journal of the American College of Cardiology*. 2005;45:1104-1108. doi: 10.1016/j.jacc.2004.12.057

329. Yan AT, Shayne AJ, Brown KA, Gupta SN, Chan CW, Luu TM, Di Carli MF, Reynolds HG, Stevenson WG, Kwong RY. Characterization of the peri-infarct zone by contrast-enhanced cardiac magnetic resonance imaging is a powerful predictor of post–myocardial infarction mortality. *Circulation*. 2006;114:32-39.

330. Kim RJ, Fieno DS, Parrish TB, Harris K, Chen E-L, Simonetti O, Bundy J, Finn JP, Klocke FJ, Judd RM. Relationship of MRI delayed contrast enhancement to irreversible injury, infarct age, and contractile function. *Circulation*. 1999;100:1992-2002.

331. Wagner A, Mahrholdt H, Holly TA, Elliott MD, Regenfus M, Parker M, Klocke FJ, Bonow RO, Kim RJ, Judd RM. Contrast-enhanced MRI and routine single photon emission computed tomography (SPECT) perfusion imaging for detection of subendocardial myocardial infarcts: an imaging study. *The Lancet*. 2003;361:374-379.

332. Fieno DS, Kim RJ, Chen E-L, Lomasney JW, Klocke FJ, Judd RM. Contrast-enhanced magnetic resonance imaging of myocardium at risk: distinction between reversible and irreversible injury throughout infarct healing. *Journal of the American College of Cardiology*. 2000;36:1985-1991.

333. Mesubi O, Ego-Osuala K, Jeudy J, Purtilo J, Synowski S, Abutaleb A, Niekoop M, Abdulghani M, Asoglu R, See V. Differences in quantitative assessment of myocardial scar

and gray zone by LGE-CMR imaging using established gray zone protocols. *The international journal of cardiovascular imaging*. 2015;31:359-368.

334. Beek AM, Bondarenko O, Afsharzada F, van Rossum AC. Quantification of late gadolinium enhanced CMR in viability assessment in chronic ischemic heart disease: a comparison to functional outcome. *Journal of Cardiovascular Magnetic Resonance*. 2009;11:6.

335. Pop M, Ghugre NR, Ramanan V, Morikawa L, Stanisz G, Dick AJ, Wright GA. Quantification of fibrosis in infarcted swine hearts by ex vivo late gadolinium-enhancement and diffusion-weighted MRI methods. *Physics in Medicine and Biology*. 2013;58:5009-5028. doi: 10.1088/0031-9155/58/15/5009

336. Ashikaga H, Sasano T, Dong J, Zviman MM, Evers R, Hopenfeld B, Castro V, Helm RH, Dickfeld T, Nazarian S. Magnetic resonance–based anatomical analysis of scar-related ventricular tachycardia: implications for catheter ablation. *Circulation research*. 2007;101:939-947.

337. Faga V, Dallaglio PD, Claver E, Rodriguez-García J, San Antonio R, Rodriguez M, Payan C, Comin-Colet J, Anguera I, Di Marco A. Variations in threshold values for border zone and dense scar produce significant changes in scar parameters obtained by ADAS-3D. *Heart Rhythm*. 2025;22:106-117.

338. Fernández-Armenta J, Berruezo A, Andreu D, Camara O, Silva E, Serra L, Barbarito V, Carotenutto L, Evertz R, Ortiz-Pérez JT. Three-dimensional architecture of scar and conducting channels based on high resolution ce-CMR: insights for ventricular tachycardia ablation. *Circulation: Arrhythmia and Electrophysiology*. 2013;6:528-537.

339. Andreu D, Penela D, Acosta J, Fernández-Armenta J, Perea RJ, Soto-Iglesias D, de Caralt TM, Ortiz-Perez JT, Prat-González S, Borràs R. Cardiac magnetic resonance–aided scar dechanneling: influence on acute and long-term outcomes. *Heart rhythm*. 2017;14:1121-1128.

340. Soto-Iglesias D, Penela D, Jáuregui B, Acosta J, Fernández-Armenta J, Linhart M, Zucchelli G, Syrovnev V, Zaraket F, Terés C. Cardiac magnetic resonance-guided ventricular tachycardia substrate ablation. *JACC: Clinical Electrophysiology*. 2020;6:436-447.

341. Cochet H, Komatsu Y, Sacher F, Jadidi AS, Scherr D, Riffaud M, Derval N, Shah A, Roten L, Pascale P. Integration of merged delayed-enhanced magnetic resonance imaging and multidetector computed tomography for the guidance of ventricular tachycardia ablation: a pilot study. *Journal of cardiovascular electrophysiology*. 2013;24:419-426.

342. Yamashita S, Sacher F, Mahida S, Berte B, Lim HS, Komatsu Y, Amraoui S, Denis A, Derval N, Laurent F. Image integration to guide catheter ablation in scar-related ventricular tachycardia. *Journal of Cardiovascular Electrophysiology*. 2016;27:699-708.

343. Roca-Luque I, Van Breukelen A, Alarcon F, Garre P, Tolosana JM, Borras R, Sanchez P, Zaraket F, Doltra A, Ortiz-Perez JT. Ventricular scar channel entrances identified by new wideband cardiac magnetic resonance sequence to guide ventricular tachycardia ablation in patients with cardiac defibrillators. *EP Europace*. 2020;22:598-606.

344. Lilli A, Parollo M, Mazzocchetti L, De Sensi F, Rossi A, Notarstefano P, Santoro A, Aquaro GD, Cresti A, Lapira F. Ventricular tachycardia ablation guided or aided by scar characterization with cardiac magnetic resonance: rationale and design of VOYAGE study. *BMC Cardiovascular Disorders*. 2022;22:169.

345. Miller CA, Naish JH, Bishop P, Coutts G, Clark D, Zhao S, Ray SG, Yonan N, Williams SG, Flett AS. Comprehensive validation of cardiovascular magnetic resonance techniques for the assessment of myocardial extracellular volume. *Circulation: Cardiovascular Imaging*. 2013;6:373-383.

346. Chen Z, Sohal M, Voigt T, Sammut E, Tobon-Gomez C, Child N, Jackson T, Shetty A, Bostock J, Cooklin M. Myocardial tissue characterization by cardiac magnetic resonance imaging using T1 mapping predicts ventricular arrhythmia in ischemic and non–ischemic cardiomyopathy patients with implantable cardioverter-defibrillators. *Heart Rhythm*. 2015;12:792-801.

347. Nakamori S, Dohi K, Ishida M, Goto Y, Imanaka-Yoshida K, Omori T, Goto I, Kumagai N, Fujimoto N, Ichikawa Y. Native T1 mapping and extracellular volume mapping for the assessment of diffuse myocardial fibrosis in dilated cardiomyopathy. *JACC: Cardiovascular Imaging*. 2018;11:48-59.

348. Sramko M, Abdel-Kafi S, Wijnmaalen AP, Tao Q, van der Geest RJ, Lamb HJ, Zeppenfeld K. Head-to-head comparison of T1 mapping and electroanatomical voltage mapping in patients with ventricular arrhythmias. *JACC: Clinical Electrophysiology*. 2023;9:740-748.

349. Tian J, Jeudy J, Smith MF, Jimenez A, Yin X, Bruce PA, Lei P, Turgeman A, Abbo A, Shekhar R. Three-dimensional contrast-enhanced multidetector CT for anatomic, dynamic, and perfusion characterization of abnormal myocardium to guide ventricular tachycardia ablations. *Circulation: Arrhythmia and Electrophysiology*. 2010;3:496-504.

350. Komatsu Y, Cochet H, Jadidi A, Sacher F, Shah A, Derval N, Scherr D, Pascale P, Roten L, Denis A. Regional myocardial wall thinning at multidetector computed tomography correlates to arrhythmogenic substrate in postinfarction ventricular tachycardia:

assessment of structural and electrical substrate. *Circulation: Arrhythmia and Electrophysiology*. 2013;6:342-350.

351. Jáuregui B, Soto-Iglesias D, Zucchelli G, Penela D, Ordóñez A, Terés C, Chauca A, Acosta J, Fernández-Armenta J, Linhart M. Arrhythmogenic substrate detection in chronic ischaemic patients undergoing ventricular tachycardia ablation using multidetector cardiac computed tomography: compared evaluation with cardiac magnetic resonance. *EP Europace*. 2021;23:82-90.

352. Cedilnik N, Pop M, Duchateau J, Sacher F, Jaïs P, Cochet H, Sermesant M. Efficient patient-specific simulations of ventricular tachycardia based on computed tomography-defined wall thickness heterogeneity. *JACC: Clinical Electrophysiology*. 2023;9:2507-2519.

353. Marchesseau S, Seneviratna A, Sjöholm AT, Qin DL, Ho JX, Hausenloy DJ, Townsend DW, Richards AM, Totman JJ, Chan MY. Hybrid PET/CT and PET/MRI imaging of vulnerable coronary plaque and myocardial scar tissue in acute myocardial infarction. *Journal of Nuclear Cardiology*. 2018;25:2001-2011.

354. Youssef G, Leung E, Mylonas I, Nery P, Williams K, Wisenberg G, Gulenchyn KY, Dekemp RA, DaSilva J, Birnie D. The use of 18F-FDG PET in the diagnosis of cardiac sarcoidosis: a systematic review and metaanalysis including the Ontario experience. *Journal of nuclear medicine*. 2012;53:241-248.

355. Van der Bijl P, Knuuti J, Delgado V, Bax JJ. Cardiac sympathetic innervation imaging with PET radiotracers. *Current Cardiology Reports*. 2021;23:1-9.

356. Ghzally Y, Imanli H, Smith M, Mahat J, Chen W, Jimenez A, Sawan MA, Abdelmegid MA-KF, Abd el Rahman Helmy H, Demitry S. Metabolic scar assessment with18F-FDG

PET: correlation to ischemic ventricular tachycardia substrate and successful ablation sites. *Journal of Nuclear Medicine*. 2021;62:1591-1598.

357. Matos CD, Romero JE, Steiger NA. Biophysics of Radiofrequency Ablation for Cardiac Arrhythmias: A Current Review. *Current Treatment Options in Cardiovascular Medicine*. 2024;26:221-231.

358. Tanner H, Hindricks G, Volkmer M, Furniss S, Kühlkamp V, Lacroix D, De Chillou C, Almendral J, Caponi D, KUCK KH. Catheter ablation of recurrent scar-related ventricular tachycardia using electroanatomical mapping and irrigated ablation technology: results of the prospective multicenter Euro-VT-study. *Journal of cardiovascular electrophysiology*. 2010;21:47-53.

359. Bennett R, Campbell T, Byth K, Turnbull S, Kumar S. Catheter ablation using half-normal saline and dextrose irrigation in an ovine ventricular model. *JACC: Clinical Electrophysiology*. 2021;7:1229-1239.

360. Nguyen DT, Gerstenfeld EP, Tzou WS, Jurgens PT, Zheng L, Schuller J, Zipse M, Sauer WH. Radiofrequency ablation using an open irrigated electrode cooled with half-normal saline. *JACC: Clinical Electrophysiology*. 2017;3:1103-1110.

361. Hasegawa K, Yoneda ZT, Powers EM, Tokutake K, Kurata M, Richardson TD, Montgomery JA, Shen S, Estrada JC, Saavedra PJ. Safety of ventricular arrhythmia radiofrequency ablation with half-normal saline irrigation. *Europace*. 2024;26:euae018.

362. Yang J, Liang J, Shirai Y, Muser D, Garcia FC, Callans DJ, Marchlinski FE, Santangeli P. Outcomes of simultaneous unipolar radiofrequency catheter ablation for intramural septal ventricular tachycardia in nonischemic cardiomyopathy. *Heart Rhythm*. 2019;16:863-870.

363. Koruth JS, Dukkipati S, Miller MA, Neuzil P, d'Avila A, Reddy VY. Bipolar irrigated radiofrequency ablation: a therapeutic option for refractory intramural atrial and ventricular tachycardia circuits. *Heart Rhythm*. 2012;9:1932-1941.

364. Nguyen DT, Zheng L, Zipse MM, Borne RT, Tzou WS, Fleeman B, Sauer WH. Bipolar radiofrequency ablation creates different lesion characteristics compared to simultaneous unipolar ablation. *Journal of Cardiovascular Electrophysiology*. 2019;30:2960-2967.

365. Della Bella P, Peretto G, Paglino G, Bisceglia C, Radinovic A, Sala S, Baratto F, Limite LR, Cireddu M, Marzi A. Bipolar radiofrequency ablation for ventricular tachycardias originating from the interventricular septum: safety and efficacy in a pilot cohort study. *Heart Rhythm*. 2020;17:2111-2118.

366. Sapp JL, Beeckler C, Pike R, Parkash R, Gray CJ, Zeppenfeld K, Kuriachan V, Stevenson WG. Initial human feasibility of infusion needle catheter ablation for refractory ventricular tachycardia. *Circulation*. 2013;128:2289-2295.

367. Dukkipati SR, Nakamura T, Nakajima I, Oates C, Narui R, Tanigawa S, Sljapic T, Whang W, Koruth JS, Choudry S. Intramural needle ablation for refractory premature ventricular contractions. *Circulation: Arrhythmia and Electrophysiology*. 2022;15:e010020.

368. Tedrow UB, Kurata M, Kawamura I, Batnyam U, Dukkipati S, Nakamura T, Tanigawa S, Fuji A, Richardson TD, Kanagasundram AN. Worldwide experience with an irrigated needle catheter for ablation of refractory ventricular arrhythmias. *JACC: Clinical Electrophysiology*. 2023;9:1475-1486.

369. Im SI, Higuchi S, Lee A, Stillson C, Buck E, Morrow B, Schenider K, Speltz M, Gerstenfeld EP. Pulsed field ablation of left ventricular myocardium in a swine infarct model. *JACC: Clinical Electrophysiology*. 2022;8:722-731.

370. Kawamura I, Reddy VY, Santos-Gallego CG, Wang BJ, Chaudhry HW, Buck ED, Mavroudis G, Jerrell S, Schneider CW, Speltz M. Electrophysiology, pathology, and imaging of pulsed field ablation of scarred and healthy ventricles in swine. *Circulation: Arrhythmia and Electrophysiology*. 2023;16:e011369.

371. Livia C, Sugrue A, Witt T, Polkinghorne MD, Maor E, Kapa S, Lehmann HI, DeSimone CV, Behfar A, Asirvatham SJ. Elimination of Purkinje fibers by electroporation reduces ventricular fibrillation vulnerability. *Journal of the American Heart Association*. 2018;7:e009070.

372. Nies M, Watanabe K, Kawamura I, Santos-Gallego CG, Reddy VY, Koruth JS. A Preclinical Study of Pulsed Field Ablation of" Difficult" Ventricular Targets: Intracavitary Mobile Structures, Interventricular Septum and Left Ventricular Free Wall. *Circulation: Arrhythmia and Electrophysiology*. 2024.

373. Askarinejad A, Kohansal E, Sabahizadeh A, Hesami H, Adimi S, Haghjoo M. Pulsed-Field Ablation in Management of Ventricular Tachycardia: A Systematic Review of Case Reports and Clinical Outcomes. *Clinical Cardiology*. 2024;47:e70018.

374. Loo Jr BW, Soltys SG, Wang L, Lo A, Fahimian BP, Iagaru A, Norton L, Shan X, Gardner E, Fogarty T. Stereotactic ablative radiotherapy for the treatment of refractory cardiac ventricular arrhythmia. *Circulation: Arrhythmia and Electrophysiology*. 2015;8:748-750.

375. Cuculich PS, Schill MR, Kashani R, Mutic S, Lang A, Cooper D, Faddis M, Gleva M, Noheria A, Smith TW. Noninvasive cardiac radiation for ablation of ventricular tachycardia. *New England Journal of Medicine*. 2017;377:2325-2336.

376. Robinson CG, Samson PP, Moore KM, Hugo GD, Knutson N, Mutic S, Goddu SM, Lang A, Cooper DH, Faddis M. Phase I/II trial of electrophysiology-guided noninvasive cardiac radioablation for ventricular tachycardia. *Circulation*. 2019;139:313-321.

377. Robinson C, Samson P, Moore K, Hugo G, Knutson N, Mutic S, Goddu S, Cooper D, Faddis M, Noheria A. Longer term results from a phase I/II study of EP-guided Noninvasive Cardiac Radioablation for Treatment of Ventricular Tachycardia (ENCORE-VT). *International Journal of Radiation Oncology, Biology, Physics*. 2019;105:682.

378. Neuwirth R, Cvek J, Knybel L, Jiravsky O, Molenda L, Kodaj M, Fiala M, Peichl P, Feltl D, Januška J. Stereotactic radiosurgery for ablation of ventricular tachycardia. *EP Europace*. 2019;21:1088-1095.

379. Marinelli A, Giaj Levra N, Trachanas K, Costa A, Sicignano G, Cuccia F, Corso M, Alongi F, Molon G. Stereotactic ablative body radiotherapy of ventricular tachycardia. Single italian centre experience. *EP Europace*. 2022;24:euac053. 362.

380. Peichl P, Haskova J, Wichterle D, Neuwirth R, Jiravsky O, Cvek J, Knybel L, Sramko M, Kautzner J. Stereotactic body radiotherapy for refractory ventricular tachycardia: the overall czech experience. *EP Europace*. 2022;24:euac053. 368.

381. van der Ree MH, Dieleman EM, Visser J, Planken RN, Boekholdt SM, de Bruin-Bon RH, Rasch CR, Hoeksema WF, de Jong RM, Kemme MJ. Non-invasive stereotactic arrhythmia radiotherapy for ventricular tachycardia: results of the prospective STARNL-1 trial. *EP Europace*. 2023:euad020.

382. Das SK, Ryan T, Panettieri V, Hawson J, Lim T, Hardcastle N, Chang D, Goodall SK, Anderson RD, Kalman J. Stereotactic Arrhythmia Radioablation (STAR) for refractory ventricular tachycardia–the initial Australian experience. *Heart Rhythm*. 2025.

383. Marcus GM. Evaluation and management of premature ventricular complexes. *Circulation*. 2020;141:1404-1418.

384. Von Rotz M, Aeschbacher S, Bossard M, Schoen T, Blum S, Schneider S, Estis J, Todd J, Risch M, Risch L. Risk factors for premature ventricular contractions in young and healthy adults. *Heart*. 2017;103:702-707.

385. Cha Y-M, Lee GK, Klarich KW, Grogan M. Premature ventricular contraction-induced cardiomyopathy: a treatable condition. *Circulation: Arrhythmia and Electrophysiology*. 2012;5:229-236.

386. Latchamsetty R, Bogun F. Premature ventricular complex ablation in structural heart disease. *Cardiac electrophysiology clinics*. 2017;9:133-140.

387. Noda T, Shimizu W, Taguchi A, Aiba T, Satomi K, Suyama K, Kurita T, Aihara N, Kamakura S. Malignant entity of idiopathic ventricular fibrillation and polymorphic ventricular tachycardia initiated by premature extrasystoles originating from the right ventricular outflow tract. *Journal of the American College of Cardiology*. 2005;46:1288-1294.

388. Hoogendijk MG, Géczy T, Yap S-C, Szili-Torok T. Pathophysiological mechanisms of premature ventricular complexes. *Frontiers in Physiology*. 2020;11:406.

389. Tanaka Y, Rahmutula D, Duggirala S, Nazer B, Fang Q, Olgin J, Sievers R, Gerstenfeld EP. Diffuse fibrosis leads to a decrease in unipolar voltage: Validation in a swine model of premature ventricular contraction–induced cardiomyopathy. *Heart Rhythm*. 2016;13:547-554.

390. Walters TE, Rahmutula D, Szilagyi J, Alhede C, Sievers R, Fang Q, Olgin J, Gerstenfeld EP. Left ventricular dyssynchrony predicts the cardiomyopathy associated with premature

ventricular contractions. *Journal of the American College of Cardiology*. 2018;72:2870-2882.

391. Wang Y, Eltit JM, Kaszala K, Tan A, Jiang M, Zhang M, Tseng G-N, Huizar JF. Cellular mechanism of premature ventricular contraction–induced cardiomyopathy. *Heart Rhythm*. 2014;11:2064-2072.

392. Bänsch D, Oyang F, Antz M, Arentz T, Weber R, Val-Mejias JE, Ernst S, Kuck K-H. Successful catheter ablation of electrical storm after myocardial infarction. *Circulation*. 2003;108:3011-3016.

393. Bogun F, Crawford T, Chalfoun N, Kuhne M, Sarrazin JF, Wells D, Good E, Jongnarangsin K, Oral H, Chugh A. Relationship of frequent postinfarction premature ventricular complexes to the reentry circuit of scar-related ventricular tachycardia. *Heart Rhythm*. 2008;5:367-374.

394. Muser D, Santangeli P, Castro SA, Casado Arroyo R, Maeda S, Benhayon DA, Liuba I, Liang JJ, Sadek MM, Chahal A. Risk stratification of patients with apparently idiopathic premature ventricular contractions: a multicenter international CMR registry. *JACC: Clinical Electrophysiology*. 2020;6:722-735.

395. Dukes JW, Dewland TA, Vittinghoff E, Mandyam MC, Heckbert SR, Siscovick DS, Stein PK, Psaty BM, Sotoodehnia N, Gottdiener JS. Ventricular ectopy as a predictor of heart failure and death. *Journal of the American College of Cardiology*. 2015;66:101-109.

396. Munoz FDC, Syed FF, Noheria A, Cha Y-M, Friedman PA, Hammill SC, Munger TM, Venkatachalam K, Shen W-K, Packer DL. Characteristics of premature ventricular complexes as correlates of reduced left ventricular systolic function: study of the burden,

duration, coupling interval, morphology and site of origin of PVCs. *Journal of cardiovascular electrophysiology*. 2011;22:791-798.

397. Pol LC, Deyell MW, Frankel DS, Benhayon D, Squara F, Chik W, Kohari M, Deo R, Marchlinski FE. Ventricular premature depolarization QRS duration as a new marker of risk for the development of ventricular premature depolarization–induced cardiomyopathy. *Heart rhythm*. 2014;11:299-306.

398. Scorza R, Jonsson M, Friberg L, Rosenqvist M, Frykman V. Prognostic implication of premature ventricular contractions in patients without structural heart disease. *EP Europace*. 2023;25:517-525.

399. DeBacker G, Jacobs D, Prineas R, Crow R, Vilandre J, Kennedy H, Blackburn H. Ventricular premature contractions: a randomized non-drug intervention trial in normal men. *Circulation*. 1979;59:762-769.

400. Kim E-j, Hoffmann TJ, Nah G, Vittinghoff E, Delling F, Marcus GM. Coffee consumption and incident tachyarrhythmias: reported behavior, mendelian randomization, and their interactions. *JAMA internal medicine*. 2021;181:1185-1193.

401. Tang JK, Andrade JG, Hawkins NM, Laksman ZW, Krahn AD, Bennett MT, Heilbron B, Chakrabarti S, Yeung-Lai-Wah JA, Deyell MW. Effectiveness of medical therapy for treatment of idiopathic frequent premature ventricular complexes. *Journal of Cardiovascular Electrophysiology*. 2021;32:2246-2253.

402. Cronin EM, Bogun FM, Maury P, Peichl P, Chen M, Namboodiri N, Aguinaga L, Leite LR, Al-Khatib SM, Anter E, et al. 2019 HRS/EHRA/APHRS/LAHRS expert consensus statement on catheter ablation of ventricular arrhythmias. *EP Europace*. 2019. doi: 10.1093/europace/euz132

403. Rohatgi A. WebPlotDigitizer (v5.2). https://automeris.io.

404. Sterne JA, Savović J, Page MJ, Elbers RG, Blencowe NS, Boutron I, Cates CJ, Cheng H-Y, Corbett MS, Eldridge SM. RoB 2: a revised tool for assessing risk of bias in randomised trials. *BMJ*. 2019;366.

405. Sterne JA, Hernán MA, Reeves BC, Savović J, Berkman ND, Viswanathan M, Henry D, Altman DG, Ansari MT, Boutron I. ROBINS-I: a tool for assessing risk of bias in non-randomised studies of interventions. *BMJ*. 2016;355.

406. Stec S, Sikorska A, Zaborska B, Kryński T, Szymot J, Kułakowski P. Benign symptomatic premature ventricular complexes: short− and long− term efficacy of antiarrhythmic drugs and radiofrequency ablation. *Polish Heart Journal (Kardiologia Polska)*. 2012;70:351-358.

407. Fang Y, Wen C, Yang L, Zhang X, Chu W, Zeng C. Radiofrequency ablation can reverse the structural remodeling caused by frequent premature ventricular contractions originating from the right ventricular outflow tract even in a "normal heart". *Clinics (Sao Paulo)*. 2013;68:1312-1317.

408. Zhong L, Lee Y-H, Huang X-M, Asirvatham SJ, Shen W-K, Friedman PA, Hodge DO, Slusser JP, Song Z-Y, Packer DL. Relative efficacy of catheter ablation vs antiarrhythmic drugs in treating premature ventricular contractions: a single-center retrospective study. *Heart rhythm*. 2014;11:187-193.

409. Yang M, Zhong L, Lee Y-H, Vaidya VR, Asirvatham SJ, Ackerman MJ, Pislaru SV, Suri RM, Slusser JP, Hodge DO. Ventricular premature contraction associated with mitral valve prolapse. *International journal of cardiology*. 2016;221:1144-1149.

410. Haanschoten DM, Vernooy K, Beukema RJ, Szili-Torok T, Ter Bekke RMA, Khan M, De Jong JSSG, Otten AM, Adiyaman A, Smit JJJ, et al. Elimination of Benign Ventricular Premature Beats or Ventricular Tachycardia with Catheter Ablation versus Two Different Optimal Antiarrhythmic Drug Treatment Regimens (Sotalol or Verapamil/Flecainide). *Cardiology (Switzerland)*. 2020;145:795-801. doi: http://dx.doi.org/10.1159/000509661

411. Prospective Assessment of Premature Ventricular Contractions Suppression in Cardiomyopathy(PAPS). https://ClinicalTrials.gov/show/NCT03228823.

412. Catheter Ablation Versus Amiodarone for Therapy of Premature Ventricular Contractions in Patients With Structural Heart Disease (CAT-PVC). https://clinicaltrials.gov/study/NCT02924285

413. Catheter Ablation Versus Antiarrhythmic Drugs for Outflow Tract Ventricular ARrhythmias (AVATAR). https://www.clinicaltrials.gov/study/NCT01780311

414. Hayashi T, Liang JJ, Shirai Y, Kuo L, Muser D, Kubala M, Kumareswaran R, Arkles JS, Garcia FC, Supple GE. Trends in successful ablation sites and outcomes of ablation for idiopathic outflow tract ventricular arrhythmias. *JACC: Clinical Electrophysiology*. 2020;6:221-230.

415. Voskoboinik A, Hadjis A, Alhede C, Im SI, Park H, Moss J, Marcus GM, Hsia H, Lee B, Tseng Z. Predictors of adverse outcome in patients with frequent premature ventricular complexes: the ABC-VT risk score. *Heart Rhythm*. 2020;17:1066-1074.

416. Wang J-s, Shen Y-g, Yin R-p, Thapa S, Peng Y-p, Ji K-t, Liao L-m, Lin J-f, Xue Y-j. The safety of catheter ablation for premature ventricular contractions in patients without structural heart disease. *BMC cardiovascular disorders*. 2018;18:1-6.

417. Lee AK, Andrade J, Hawkins NM, Alexander G, Bennett MT, Chakrabarti S, Laksman ZW, Krahn A, Yeung-Lai-Wah JA, Deyell MW. Outcomes of untreated frequent premature ventricular complexes with normal left ventricular function. *Heart*. 2019;105:1408-1413.

418. van Huls van Taxis CF, Piers SR, de Riva Silva M, Dekkers OM, Pijnappels DA, Schalij MJ, Wijnmaalen AP, Zeppenfeld K. Fatigue as presenting symptom and a high burden of premature ventricular contractions are independently associated with increased ventricular wall stress in patients with normal left ventricular function. *Circulation: Arrhythmia and Electrophysiology*. 2015;8:1452-1459.

419. Wijnmaalen AP, Delgado V, Schalij MJ, van Taxis CFvH, Holman ER, Bax JJ, Zeppenfeld K. Beneficial effects of catheter ablation on left ventricular and right ventricular function in patients with frequent premature ventricular contractions and preserved ejection fraction. *Heart*. 2010;96:1275-1280.

420. Rivera S, Tomas L, Ricapito MdlP, Nicolas V, Reinoso M, Caro M, Mondragon I, Albina G, Giniger A, Scazzuso F. Updated results on catheter ablation of ventricular arrhythmias arising from the papillary muscles of the left ventricle. *Journal of Arrhythmia*. 2019;35:99-108.

421. Proietti R, Rivera S, Dussault C, Essebag V, Bernier ML, Ayala-Paredes F, Badra-Verdu M, Roux J-F. Intracardiac echo-facilitated 3D electroanatomical mapping of ventricular arrhythmias from the papillary muscles: assessing the 'fourth dimension'during ablation. *EP Europace*. 2017;19:21-28.

422. Haanschoten DM, Vernooy K, Beukema RJ, Szili-Torok T, ter Bekke R, Khan M, de Jong JS, Otten AM, Adiyaman A, Smit JJJ. Elimination of benign ventricular premature beats or ventricular tachycardia with catheter ablation versus two different optimal

antiarrhythmic drug treatment regimens (sotalol or verapamil/flecainide). *Cardiology*. 2020;145:795-801.

423. Santangeli P, Muser D, Zado ES, Magnani S, Khetpal S, Hutchinson MD, Supple G, Frankel DS, Garcia FC, Bala R, et al. Acute hemodynamic decompensation during catheter ablation of scar-related ventricular tachycardia: incidence, predictors, and impact on mortality. *Circ Arrhythm Electrophysiol*. 2015;8:68-75. doi: 10.1161/CIRCEP.114.002155

424. Josephson ME, Anter E. Substrate Mapping for Ventricular Tachycardia: Assumptions and Misconceptions. *JACC: Clinical Electrophysiology*. 2015;1:341-352. doi: 10.1016/j.jacep.2015.09.001

425. Sramko M, Abdel-Kafi S, van der Geest RJ, de Riva M, Glashan CA, Lamb HJ, Zeppenfeld K. New Adjusted Cutoffs for "Normal" Endocardial Voltages in Patients With Post-Infarct LV Remodeling. *JACC: Clinical Electrophysiology*. 2019;5:1115-1126. doi: 10.1016/j.jacep.2019.07.007

426. Glashan CA, Tofig BJ, Tao Q, Blom SA, Jongbloed MRM, Nielsen JC, Lukac P, Kristiansen SB, Zeppenfeld K. Multisize Electrodes for Substrate Identification in Ischemic Cardiomyopathy: Validation by Integration of Whole Heart Histology. *JACC: Clinical Electrophysiology*. 2019;5:1130-1140. doi: 10.1016/j.jacep.2019.06.004

427. Aziz Z, Shatz D, Raiman M, Upadhyay GA, Beaser AD, Besser SA, Shatz NA, Fu Z, Jiang R, Nishimura T, et al. Targeted Ablation of Ventricular Tachycardia Guided by Wavefront Discontinuities During Sinus Rhythm: A New Functional Substrate Mapping Strategy. *Circulation*. 2019;140:1383-1397. doi: 10.1161/CIRCULATIONAHA.119.042423

428. Wolf M, Sacher F, Cochet H, Kitamura T, Takigawa M, Yamashita S, Vlachos K, Cheniti G, Frontera A, Martin R, et al. Long-Term Outcome of Substrate Modification in Ablation

of Post-Myocardial Infarction Ventricular Tachycardia. *Circulation: Arrhythmia and Electrophysiology*. 2018;11:e005635. doi: 10.1161/CIRCEP.117.005635

429. Vázquez-Calvo S, Casanovas JM, Garre P, Ferró E, Sánchez-Somonte P, Quinto L, Guasch E, Porta-Sanchez A, Tolosana JM, Borras R. Evolution of Deceleration Zones During Ventricular Tachycardia Ablation and Relation With Cardiac Magnetic Resonance. *JACC: Clinical Electrophysiology*. 2023.

430. Pouliopoulos J, Chik WW, Kanthan A, Sivagangabalan G, Barry MA, Fahmy PN, Midekin C, Lu J, Kizana E, Thomas SP, et al. Intramyocardial adiposity after myocardial infarction: new implications of a substrate for ventricular tachycardia. *Circulation*. 2013;128:2296-2308. doi: 10.1161/CIRCULATIONAHA.113.002238

431. Sanchez-Somonte P, Garre P, Vazquez-Calvo S, Quinto L, Borras R, Prat S, Ortiz-Perez JT, Steghofer M, Figueras IVRM, Guasch E, et al. Scar conducting channel characterization to predict arrhythmogenicity during ventricular tachycardia ablation. *EP Europace*. 2023;25:989-999. doi: 10.1093/europace/euac257

432. Bhagirath P, Campos FO, Costa CM, Wilde AAM, Prassl AJ, Neic A, Plank G, Rinaldi CA, Gotte MJW, Bishop MJ. Predicting arrhythmia recurrence following catheter ablation for ventricular tachycardia using late gadolinium enhancement magnetic resonance imaging: Implications of varying scar ranges. *Heart Rhythm*. 2022;19:1604-1610. doi: 10.1016/j.hrthm.2022.05.021

433. Jais P, Maury P, Khairy P, Sacher F, Nault I, Komatsu Y, Hocini M, Forclaz A, Jadidi AS, Weerasooryia R, et al. Elimination of local abnormal ventricular activities: a new end point for substrate modification in patients with scar-related ventricular tachycardia. *Circulation*. 2012;125:2184-2196. doi: 10.1161/CIRCULATIONAHA.111.043216

434. Healing IITI. Contrast-enhanced magnetic resonance imaging of myocardium at risk. *Journal of the American College of Cardiology*. 2000;36.

435. Sanchez-Somonte P, Quinto L, Garre P, Zaraket F, Alarcon F, Borras R, Caixal G, Vazquez S, Prat S, Ortiz-Perez JT, et al. Scar channels in cardiac magnetic resonance to predict appropriate therapies in primary prevention. *Heart Rhythm*. 2021;18:1336-1343. doi: 10.1016/j.hrthm.2021.04.017

436. Falasconi G, Penela D, Soto-Iglesias D, Francia P, Teres C, Viveros D, Bellido A, Alderete J, Meca-Santamaria J, Franco P, et al. Preventive substrate ablation in chronic post-myocardial infarction patients with high-risk scar characteristics for ventricular arrhythmias: rationale and design of PREVENT-VT study. *Journal of Interventional Cardiac Electrophysiology*. 2023;66:39-47. doi: 10.1007/s10840-022-01392-w

437. Fernandes GC, Fernandes A, Cardoso R, Penalver J, Knijnik L, Mitrani RD, Myerburg RJ, Goldberger JJ. Association of SGLT2 inhibitors with arrhythmias and sudden cardiac death in patients with type 2 diabetes or heart failure: A meta-analysis of 34 randomized controlled trials. *Heart Rhythm*. 2021;18:1098-1105. doi: 10.1016/j.hrthm.2021.03.028

438. Hsia HH, Lin D, Sauer WH, Callans DJ, Marchlinski FE. Anatomic characterization of endocardial substrate for hemodynamically stable reentrant ventricular tachycardia: identification of endocardial conducting channels. *Heart Rhythm*. 2006;3:503-512. doi: 10.1016/j.hrthm.2006.01.015

439. Sung E, Prakosa A, Zhou S, Berger RD, Chrispin J, Nazarian S, Trayanova NA. Fat infiltration in the infarcted heart as a paradigm for ventricular arrhythmias. *Nature Cardiovascular Research*. 2022;1:933-945. doi: 10.1038/s44161-022-00133-6

440. Mayr A, Klug G, Reindl M, Lechner I, Tiller C, Holzknecht M, Pamminger M, Troger F, Schocke M, Bauer A, et al. Evolution of Myocardial Tissue Injury: A CMR Study Over a Decade After STEMI. *JACC: Cardiovascular Imaging*. 2022;15:1030-1042. doi: 10.1016/j.jcmg.2022.02.010

441. Dhanjal TS, Lellouche N, von Ruhland CJ, Abehsira G, Edwards DH, Dubois-Randé J-L, Moschonas K, Teiger E, Williams AJ, George CH. Massive accumulation of myofibroblasts in the critical isthmus is associated with ventricular tachycardia inducibility in post-infarct swine heart. *JACC: Clinical Electrophysiology*. 2017;3:703-714.

442. Valderrábano M, Fuentes Rojas SC, Lador A, Patel A, Schurmann PA, Tapias C, Rodríguez D, Carlos Sáenz L, Malahfji M, Shah DJ. Substrate ablation by multivein, multiballoon coronary venous ethanol for refractory ventricular tachycardia in structural heart disease. *Circulation*. 2022;146:1644-1656.

443. Fernandez-Armenta J, Berruezo A, Andreu D, Camara O, Silva E, Serra L, Barbarito V, Carotenutto L, Evertz R, Ortiz-Perez JT, et al. Three-dimensional architecture of scar and conducting channels based on high resolution ce-CMR: insights for ventricular tachycardia ablation. *Circulation: Arrhythmia and Electrophysiology*. 2013;6:528-537. doi: 10.1161/CIRCEP.113.000264

444. Burton RA, Lee P, Casero R, Garny A, Siedlecka U, Schneider JE, Kohl P, Grau V. Three-dimensional histology: tools and application to quantitative assessment of cell-type distribution in rabbit heart. *EP Europace*. 2014;16:iv86-iv95.

445. Glashan CA, Tofig BJ, Beukers H, Tao Q, Blom SA, Villadsen PR, Lassen TR, de Riva M, Kristiansen SB, Zeppenfeld K. Multielectrode Unipolar Voltage Mapping and

Electrogram Morphology to Identify Post-Infarct Scar Geometry: Validation by Histology. *JACC: Clinical Electrophysiology*. 2022;8:437-449. doi: 10.1016/j.jacep.2021.11.012

446. Glashan CA, Beukers HK, Tofig BJ, Tao Q, Blom S, Mertens B, Kristiansen SB, Zeppenfeld K. Mini-, micro-, and conventional electrodes: an in vivo electrophysiology and ex vivo histology head-to-head comparison. *JACC: Clinical Electrophysiology*. 2021;7:197-205.

447. Burger JC, Hopman LH, Kemme MJ, Hoeksema W, Takx RA, Ventura RMFI, Campos FO, Plank G, Planken RN, Allaart CP. Optimizing ventricular tachycardia ablation through imaging-based assessment of arrhythmic substrate: A comprehensive review and roadmap for the future. *Heart Rhythm O2*. 2024;5:561.

448. Yamashita S, Cochet H, Sacher F, Mahida S, Berte B, Hooks D, Sellal J-M, Al Jefairi N, Frontera A, Komatsu Y. Impact of new technologies and approaches for post–myocardial infarction ventricular tachycardia ablation during long-term follow-up. *Circulation: Arrhythmia and Electrophysiology*. 2016;9:e003901.

449. De Silva K, Campbell T, Bennett RG, Anderson RD, Davey C, O'Donohue AK, Schindeler A, Turnbull S, Selvakumar D, Bhaskaran A. Whole-Heart Histological and Electroanatomic Assessment of Postinfarction Cardiac Magnetic Resonance Imaging Scar and Conducting Channels. *Circulation: Arrhythmia and Electrophysiology*. 2024;17:e012922.

450. Huang K, Bennett RG, Campbell T, Lee V, Turnbull S, Chik WW, El-Sokkari I, Hallani H, Dieleman J, Kruit N. Early catheter ablation versus initial medical therapy for ventricular tachycardia storm. *Circulation: Arrhythmia and Electrophysiology*. 2022;15:e011129.

451. Stevenson WG, Sager PT, Natterson PD, Saxon LA, Middlekauff HR, Wiener I. Relation of pace mapping QRS configuration and conduction delay to ventricular tachycardia reentry circuits in human infarct scars. *Journal of the American College of Cardiology*. 1995;26:481-488.

452. Hanaki Y, Komatsu Y, Nogami A, Kowase S, Kurosaki K, Sekiguchi Y, Aonuma K, Ieda M. Combined endo-and epicardial pace-mapping to localize ventricular tachycardia isthmus in ischaemic and non-ischaemic cardiomyopathy. *EP Europace*. 2022;24:587-597.

453. Desjardins B, Crawford T, Good E, Oral H, Chugh A, Pelosi F, Morady F, Bogun F. Infarct architecture and characteristics on delayed enhanced magnetic resonance imaging and electroanatomic mapping in patients with postinfarction ventricular arrhythmia. *Heart rhythm*. 2009;6:644-651.

454. Andreu D, Ortiz-Perez JT, Boussy T, Fernandez-Armenta J, de Caralt TM, Perea RJ, Prat-Gonzalez S, Mont L, Brugada J, Berruezo A. Usefulness of contrast-enhanced cardiac magnetic resonance in identifying the ventricular arrhythmia substrate and the approach needed for ablation. *European heart journal*. 2014;35:1316-1326.

455. Andreu D, Ortiz-Perez JT, Fernandez-Armenta J, Guiu E, Acosta J, Prat-Gonzalez S, De Caralt TM, Perea RJ, Garrido C, Mont L. 3D delayed-enhanced magnetic resonance sequences improve conducting channel delineation prior to ventricular tachycardia ablation. *EP Europace*. 2015;17:938-945.

456. Sasaki T, Miller CF, Hansford R, Yang J, Caffo BS, Zviman MM, Henrikson CA, Marine JE, Spragg D, Cheng A. Myocardial Structural Associations With Local Electrograms: A Study of Postinfarct Ventricular Tachycardia Pathophysiology and Magnetic Resonance–

Based Noninvasive Mapping. *Circulation: Arrhythmia and Electrophysiology*. 2012;5:1081-1090.

457. Chawla NV, Bowyer KW, Hall LO, Kegelmeyer WP. SMOTE: synthetic minority over-sampling technique. *Journal of artificial intelligence research*. 2002;16:321-357.

458. Christ M, Braun N, Neuffer J, Kempa-Liehr AW. Time series feature extraction on basis of scalable hypothesis tests (tsfresh–a python package). *Neurocomputing*. 2018;307:72-77.

459. Yu L, Liu H. Feature selection for high-dimensional data: A fast correlation-based filter solution. Paper/Poster presented at: Proceedings of the 20th international conference on machine learning (ICML-03); 2003

460. Ismail Fawaz H, Lucas B, Forestier G, Pelletier C, Schmidt DF, Weber J, Webb GI, Idoumghar L, Muller P-A, Petitjean F. Inceptiontime: Finding alexnet for time series classification. *Data Mining and Knowledge Discovery*. 2020;34:1936-1962.

461. Campos B, Jauregui ME, Marchlinski FE, Dixit S, Gerstenfeld EP. Use of a novel fragmentation map to identify the substrate for ventricular tachycardia in postinfarction cardiomyopathy. *Heart Rhythm*. 2015;12:95-103.

462. Hu B, Chen Y, Keogh E. Time series classification under more realistic assumptions. Paper/Poster presented at: Proceedings of the 2013 SIAM international conference on data mining; 2013

463. Orini M, Graham AJ, Srinivasan NT, Campos FO, Hanson BM, Chow A, Hunter RJ, Schilling RJ, Finlay M, Earley MJ. Evaluation of the reentry vulnerability index to predict ventricular tachycardia circuits using high-density contact mapping. *Heart rhythm*. 2020;17:576-583.

464. De Silva K, Campbell T, Bennett RG, Anderson RD, Davey C, O'Donohue AK, Schindeler A, Turnbull S, Selvakumar D, Bhaskaran A. Whole-Heart Histological and Electroanatomic Assessment of Postinfarction Cardiac Magnetic Resonance Imaging Scar and Conducting Channels. *Circulation: Arrhythmia and Electrophysiology*. 2024:e012922.

465. Takigawa M, Sacher F, Martin C, Cheniti G, Duchateau J, Pambrun T, Derval N, Cochet H, Hocini M, Yamamoto T. Impact of filter configurations on bipolar EGMs: An optimal filter setting for identifying VT substrates. *Journal of Cardiovascular Electrophysiology*. 2023;34:1708-1717.

466. Starreveld R, Knops P, Roos-Serote M, Kik C, Bogers AJ, Brundel BJ, de Groot NM. The impact of filter settings on morphology of unipolar fibrillation potentials. *Journal of cardiovascular translational research*. 2020;13:953-964.

467. Whitaker J, Batnyam U, Kapur S, Sauer WH, Tedrow U. Safety and efficacy of cryoablation for right ventricular moderator band–papillary muscle complex ventricular arrhythmias. *JACC: Clinical Electrophysiology*. 2022;8:857-868.

468. Huntrakul A, Yokokawa M, Ghannam M, Liang J, Patel S, Cochet H, Latchamsetty R, Jongnarangsin K, Morady F, Bogun F. Implications of the anatomy of papillary muscle connections for mapping and ablation of focal ventricular arrhythmias. *Heart Rhythm*. 2023;20:1445-1454.

469. Yamada T, Yoshida N, Litovsky SH, Itoh T, Doppalapudi H, Kay GN. Idiopathic ventricular arrhythmias originating from the infundibular muscles: prevalence, electrocardiographic and electrophysiological characteristics, and outcome of catheter ablation. *Circulation: Arrhythmia and Electrophysiology*. 2018;11:e005749.

470. Crawford T, Mueller G, Good E, Jongnarangsin K, Chugh A, Pelosi Jr F, Ebinger M, Oral H, Morady F, Bogun F. Ventricular arrhythmias originating from papillary muscles in the right ventricle. *Heart rhythm*. 2010;7:725-730.

471. Rivera S, Ricapito MdlP, Tomas L, Parodi J, Bardera Molina G, Banega R, Bueti P, Orosco A, Reinoso M, Caro M. Results of cryoenergy and radiofrequency-based catheter ablation for treating ventricular arrhythmias arising from the papillary muscles of the left ventricle, guided by intracardiac echocardiography and image integration. *Circulation: Arrhythmia and Electrophysiology*. 2016;9:e003874.

472. Gordon JP, Liang JJ, Pathak RK, Zado ES, Garcia FC, Hutchinson MD, Santangeli P, Schaller RD, Frankel DS, Marchlinski FE. Percutaneous cryoablation for papillary muscle ventricular arrhythmias after failed radiofrequency catheter ablation. *Journal of cardiovascular electrophysiology*. 2018;29:1654-1663.

473. Chinitz JS, Sedaghat D, Harding M, Darge A, Epstein LM, John R. Adjuvant use of a cryoballoon to facilitate ablation of premature ventricular contraction–triggered ventricular fibrillation originating from the moderator band. *HeartRhythm Case Reports*. 2019;5:578-581.

474. Peichl P, Bulava A, Wichterle D, Schlosser F, Stojadinović P, Borišincová E, Štiavnický P, Hašková J, Kautzner J. Efficacy and safety of focal pulsed-field ablation for ventricular arrhythmias: two-centre experience. *EP Europace*. 2024;26:euae192.

475. Della Rocca DG, Cespón-Fernández M, Keelani A, Raffa S, Pannone L, Almorad A, Ströker E, Borisov G, Bala G, Sieira J. Focal pulsed field ablation for premature ventricular contractions: a Multicenter experience. *Circulation: Arrhythmia and Electrophysiology*. 2024;17:e012826.

476. Ruwald MH, Johannessen A, Worck R, Hansen ML, Haugdal M, Hansen J. Feasibility and mid-term effectiveness of focal pulsed field ablation for ventricular arrhythmias. *Heart Rhythm*. 2025.

477. Muthu P, Prajapati P, Vemulapalli H, Rodriguez-Riascos JF, Raman A, Srivathsan K. Ablation of premature ventricular complexes originating from papillary muscle using pulsed field energy: the first in USA experience. *Heart rhythm*. 2024.

478. Vasquez N, Chrispin J. Successful ablation of premature ventricular complexes arising from the posteromedial papillary muscle using Pulse Field Ablation. *HeartRhythm Case Reports*. 2025.

479. Lozano-Granero C, Hirokami J, Franco E, Matía-Francés R, Schmidt B, Hernández-Madrid A, Zamorano Gómez JL, Moreno J, Chun J. Case series of ventricular tachycardia ablation with pulsed-field ablation: pushing technology further (into the ventricle). *JACC: Clinical Electrophysiology*. 2023;9:1990-1994.

480. Adragão P, Matos D, Carmo P, Costa FM, Ramos S. Pulsed-field ablation vs radiofrequency ablation for ventricular tachycardia: First in-human case of histologic lesion analysis. *Heart Rhythm*. 2023;20:1395-1398.

481. Yavin HD, Higuchi K, Sroubek J, Younis A, Zilberman I, Anter E. Pulsed-field ablation in ventricular myocardium using a focal catheter: the impact of application repetition on lesion dimensions. *Circulation: Arrhythmia and Electrophysiology*. 2021;14:e010375.

482. Verma A, Asivatham SJ, Deneke T, Castellvi Q, Neal RE. Primer on pulsed electrical field ablation: understanding the benefits and limitations. *Circulation: Arrhythmia and Electrophysiology*. 2021;14:e010086.

483. Mitchell LB, Pineda EA, Titus JL, Bartosch PM, Benditt DG. Sudden death in patients with implantable cardioverter defibrillators: the importance of post-shock electromechanical dissociation. *Journal of the American College of Cardiology*. 2002;39:1323-1328.

484. Kumar S, Romero J, Mehta NK, Fujii A, Kapur S, Baldinger SH, Barbhaiya CR, Koplan BA, John RM, Epstein LM. Long-term outcomes after catheter ablation of ventricular tachycardia in patients with and without structural heart disease. *Heart Rhythm*. 2016;13:1957-1963.

485. Tokuda M, Kojodjojo P, Tung S, Tedrow UB, Nof E, Inada K, Koplan BA, Michaud GF, John RM, Epstein LM. Acute failure of catheter ablation for ventricular tachycardia due to structural heart disease: causes and significance. *Journal of the American Heart Association*. 2013;2:e000072.

486. Stiles MK, Fauchier L, Morillo CA, Wilkoff BL. 2019 HRS/EHRA/APHRS/LAHRS focused update to 2015 expert consensus statement on optimal implantable cardioverter-defibrillator programming and testing. *EP Europace*. 2019;21:1442-1443.

487. Al-Khatib SM, Stevenson WG, Ackerman MJ, Gillis AM, Bryant WJ, Hlatky MA, Callans DJ, Granger CB, Curtis AB, Hammill SC, et al. 2017 AHA/ACC/HRS Guideline for Management of Patients With Ventricular Arrhythmias and the Prevention of Sudden Cardiac Death: Executive Summary: A Report of the American College of Cardiology/American Heart Association Task Force on Clinical Practice Guidelines and the Heart Rhythm Society. *Heart Rhythm*. 2017. doi: 10.1016/j.hrthm.2017.10.035

488. Kumar S, Sivagangabalan G, Zaman S, West EB, Narayan A, Thiagalingam A, Kovoor P. Electrophysiology-guided defibrillator implantation early after ST-elevation myocardial infarction. *Heart Rhythm*. 2010;7:1589-1597. doi: 10.1016/j.hrthm.2010.07.019

489. Marchlinski FE, Zado E, Dixit S, Gerstenfeld E, Callans DJ, Hsia H, Lin D, Nayak H, Russo A, Pulliam W. Electroanatomic substrate and outcome of catheter ablative therapy for ventricular tachycardia in setting of right ventricular cardiomyopathy. *Circulation*. 2004;110:2293-2298. doi: 10.1161/01.CIR.0000145154.02436.90

490. Aliot EM, Stevenson WG, Almendral-Garrote JM, Bogun F, Calkins CH, Delacretaz E, Della Bella P, Hindricks G, Jais P, Josephson ME, et al. EHRA/HRS Expert Consensus on Catheter Ablation of Ventricular Arrhythmias: developed in a partnership with the European Heart Rhythm Association (EHRA), a Registered Branch of the European Society of Cardiology (ESC), and the Heart Rhythm Society (HRS); in collaboration with the American College of Cardiology (ACC) and the American Heart Association (AHA). *Heart Rhythm*. 2009;6:886-933. doi: 10.1016/j.hrthm.2009.04.030

491. Gianni C, Rivera D, Burkhardt JD, Pollard B, Gardner E, Maguire P, Zei PC, Natale A, Al-Ahmad A. Stereotactic arrhythmia radioablation for refractory scar-related ventricular tachycardia. *Heart Rhythm*. 2020;17:1241-1248.

492. Haskova J, Peichl P, Šramko M, Cvek J, Knybel L, Jiravský O, Neuwirth R, Kautzner J. Case report: repeated stereotactic radiotherapy of recurrent ventricular tachycardia: reasons, feasibility, and safety. *Frontiers in Cardiovascular Medicine*. 2022;9.